THE UNIVERSITY OF CALGARY

Optimizing the Estimation Procedure in INS/GPS Integration for Kinematic Applications

By

Ahmed H. Mohamed

A DISSERTATION
SUBMITTED TO THE FACULTY OF GRADUATE STUDIES
IN PARTIAL FULFILLMENT OF THE REQUIREMENTS FOR THE
DEGREE OF DOCTOR OF PHILOSOPHY

DEPARTMENT OF GEOMATICS ENGINEERING
CALGARY, ALBERTA
APRIL, 1999

ABSTRACT

Conventional Kalman filtering has been the widely used and accepted procedure for integrating the inertial navigation systems (INS) with the global positioning system (GPS). In this respect, two main application areas are of interest to geomatics, direct georeferencing of imagery from mobile multi-sensor systems and estimating the anomalous gravity field by airborne gravity systems. In both cases, a conventional Kalman filter designed with a fixed estimation algorithm is used to fuse the INS and GPS streams of information. In such applications, the estimation environment is not always fixed. In a changing environment, imperfect a priori information and insufficient estimation time will affect the obtained accuracy of the integrated INS/GPS system if a fixed filter formulation is used. An adaptive filtering formulation, therefore, tackles the problem of imperfect a priori information and provides better tracking of the filter states.

In this research, an adaptive Kalman filtering approach is developed, analyzed, and proposed to replace the fixed (conventional) Kalman filtering approach for the INS/GPS integrated system. The adaptivity of the estimation procedure is carried out through the use of the measurement innovation sequence as piece-wise stationary process inside an estimation window to estimate either or both of the system noise matrix, Q or/and the measurement noise covariance matrix, R. In this dissertation, the performance of each of the two filters in kinematic environment is studied. Besides the flexibility it provides, the proposed adaptive approach has shown that an improvement of 10%-15% (rms) can be achieved to an airborne gravity system, and, in normal flight environments, an improvement of the attitude estimation by 20% (rms) could be achieved.

GPS positioning accuracy directly represents the positioning accuracy of the INS/GPS integrated system. It also indirectly enhances the attitude accuracy through the coupling effect between the filter states. Since the phase observable delivers the best possible GPS positioning information, its initial integer cycle ambiguity must be correctly resolved. It provides robustness and strength to the overall integrated system accuracy and reliability. A new method is developed in this research to resolve the GPS phase ambiguity using the so-called whitening filter. The method is discussed in this dissertation where it proved successful for short baselines and fair satellite coverage.

ACKNOWLEDGMENTS

My first and foremost gratitude is due to Allah, the one who guided me to His path and to the light of faith through His messenger Mohamed <peace be upon him>.

I am grateful to Dr. Klaus-Peter Schwarz, my supervisor, who persevered with amazing tolerance and good disposition all through my research endeavors. His exceptional foresight, without losing focus of the bigger picture, his immeasurable and sagacious contribution brought about the direction to this work. I cannot thank him enough - this work would not have been possible without his guidance and continuous support. Dr. J.A.R. Blais and Dr. W. Teskey, on my supervisory committee, are thanked for their guidance throughout the course of my research work. Dr. A. Sesay and Dr. B. Mercer, members of the examining committee, are thanked for reading this dissertation and for their feedback. It is a privilege to be associated with such exemplary advisors.

I have also benefited from a wealth of technical information and insight from the stimulating and invaluable discussions with the members of the Department of Geomatics Engineering. In particular, my close friends and work-colleagues, H. Kinawi, M. Mostafa, J. Skaloud, A. Bruton, and C. Amlacher are thanked for their help in the fieldwork and the fruitful discussions I had with them. I also appreciate the help and support of the office staff at the Department of Geomatics Engineering.

Through my life, my loving parents, Fahima and Hassan, were the best teachers I've ever had. You taught me to respect others. You sure can take the whole credit for much of what I am today. Without you, this work would have never seen light. My very thoughtful brother, Mahmoud, and my loving sisters, Aziza, Amal, and Abeer, have been a constant source of support and inspiration. I am also fortunate to have a loving father and mother in-law, El-Nabawy and Fatima. To all of you, I owe much, much more than words can express.

Finally, to my sweet and loving wife, my better half, Amira, to my beloved son and special friend, Yousif, whom I still owe lots of fun hours, and to my sweet little daughter, the hilarious pumpkin, Mariam, who stood by me, supported me, and believed in me - you kept me going through it all. Words will never say how grateful I am.

To my better half, my dear loving wife,
Amira.
You stood by me, encouraged me,
and enlightened my life.
Words will never say how grateful I am.

TABLE OF CONTENTS

LIST OF FIGURES

LIST OF SYMBOLS*

* *some symbols have been repeatedly used in different context to indicate different meaning.*

∇ ..... blunder vector
' ..... minute of arc
" ..... second of arc
° ..... degree of arc
% ..... percentage
Ξ ..... Attitude
Ψ ..... receiver-satellite vector space angle of original position
Ψ' ..... receiver-satellite vector space angle of shifted position
a ..... ambiguity vector
A ..... matrix; ambiguity design matrix
b ..... baseline vector; measurement bias
B ..... matrix; geometry design matrix
c ..... speed of light
C_{DOP} ..... DOP cofactor matrix
cor ..... correlation coefficient
cov ..... covariance
C_r ..... residual covariance matrix
C_x ..... state covariance matrix
$C_{\Delta x}$ ..... state correction covariance matrix
C_v ..... innovation covariance matrix
d ..... desired response
D ..... diagonal matrix
d_{ion} ..... ionosphere signal delay
dT ..... receiver clock offset
dt ..... satellite clock offset
d_{trop} ..... troposphere signal delay
$d\rho$ ..... satellite orbital error
e ..... natural exponent; random error; measurement random noise
E ..... east direction; error norm
E_c ..... Eötvös correction
f ..... probability density function; specific force
F ..... probability distribution function ; dynamics matrix;
..... specific force matrix; Fisher test parameter
F_0 ..... Fisher test threshold
f_c ..... cut-off frequency
g ..... Earth's mean gravity acceleration; number of ambiguities;
..... measurement redundancy number
G ..... measurement redundancy matrix
h ..... height
H ..... measurement design matrix
H_a ..... statistical test alternative hypothesis
H_o ..... statistical test null hypothesis

I ..... the Identity matrix
k ..... epoch number
K ..... gain factor/matrix
l ..... inertial measurement
L ..... lag; unitary lower triangular matrix; inertial observable
m ..... number of measurements; statistical average (mean)
M ..... time average
MDE ..... minimally detectable error
n ..... number of states; norm; random noise
N ..... initial carrier ambiguity; moving window size; normal distribution
..... north direction; sensor axes misalignment matrix
p ..... number of baseline components; position variable
P ..... probability; state estimate covariance matrix
PSD ..... Power Spectral Density
q ..... system (process) noise density
Q ..... system (process) noise covariance matrix
r ..... measurement residual
R ... Earth's mean radius; attitude (rotation) matrix; measurement noise covariance matrix
R_1 ..... ellipsoidal radius of curvature in the prime-vertical direction
R_2 ..... ellipsoidal radius of curvature in the meridian direction
R^p ..... real number space of size p
s ..... useful signal; Laplace parameter
S ..... scale factor
t ..... time parameter; local test statistics
T ..... time period; global test statistics; transformation matrix
T_{ph} ..... phugoid motion period
t_v ..... validation time
u ..... up direction; an element in matrix U
U ..... unitary upper triangular matrix
v ..... vector; measurement random noise; velocity variable
V ..... velocity matrix
var ..... variance
w ..... white noise; system (process) noise
w_o ..... expected shift in the mean
x ..... state vector; system (filter) input; random event; coordinate
x' ..... normalized random event
X ..... random variable
x_0 ..... state initial value
y ..... random event; system (filter) output; coordinate
Y ..... random variable
z ..... measurement
Z^g ..... integer number space of size g
$\Delta\Psi$ ..... receiver-satellite vector space angle difference
Δx ..... state correction vector
Φ ..... transition matrix; observed GPS carrier phase

P ..... power spectral density
Ω ..... rotation matrix
α ..... adaptive parameter
β ..... correlation length
γ ..... attenuation factor
χ^2 ..... Chi-squared distribution
δ ..... Dirac delta function; non-central parameter of the normal distribution
δp ..... position error
δv ..... velocity error
$\delta\omega$ ..... rotation error
ε ..... attitude error
ε_o ..... leveling (tilt) attitude error
ε_u ..... azimuth misalignment attitude error
$\varepsilon_{\Phi mult}$ ..... carrier phase signal multipath
$\varepsilon_{\Phi noise}$ ..... carrier phase signal noise
ϕ ..... latitude
γ ..... normal gravity
λ ..... carrier wavelength
λ^2 ..... non-central parameter of the Chi-squared distribution
μ^2 ..... second moment
ν ..... measurement innovation; Schuler frequency
ν' ..... modified Schuler frequency
π ..... the ratio of the circumference of a circle to the diameter
θ ..... body rate
ρ ..... correlation coefficient; geometric spatial distance
σ ..... standard deviation; covariance
σ^2 ..... variance
τ ..... time offset
ω ..... frequency parameter
ω_e ..... Earth's rotation rate
§ ..... section

(-) ..... state before update (prediction)
(+) ..... state after update (filtering)
$\nabla\Delta$ ..... double differencing
∂ ..... partial difference/derivative
$\bar{}$ (*overbar*) ..... whitened variable
$\breve{}$ (inverted *hat*) ..... adjusted value
$\dot{}$ (*dot*) ..... first derivative
$\ddot{}$ (double *dot*) ..... second derivative
$\hat{}$ (*hat*) ..... estimated value
$\tilde{}$ (tilde) ..... provisional value
$'$ (*dash*) ..... normalization
^{n} (*power*) ..... power n
^{T} ..... transposition
subscript ..... designated variable
subscript ..... original frame
subscript subscript ..... designated variables
subscript subscript ..... to-from frames
superscript ..... designated system
superscript ..... reference frame
| ..... conditioning
|.| ..... determinant
||.|| ..... norm
C ..... covariance matrix
d ..... difference/derivative
e ..... the natural base
E ..... mathematical expectation
f ..... function
G ..... function
ij ..... matrix row and column position
j ..... counter
ln ..... the natural logarithm
P ..... probability
tr ..... matrix trace
udu ..... upper-diagonal-upper matrix factorization
Δ ..... difference
Π ..... product
Σ ..... summation
δ ..... perturbation

#df ..... number of degrees of freedom
2D ..... two dimensional
2min ..... second minimum
3D ..... three dimensional
accel ..... accelerometer
ADOP ..... Ambiguity Dilution Of Precision
AKF ..... Adaptive Kalman Filter
arcmin ..... minute of circular arc
arcsec ..... second of circular arc
ATM ..... Ambiguity Transformation Matrix
AZ ..... Azimuth
c ..... camera coordinate frame
C/C++ ..... computer programming language
CKF ..... Conventional Kalman Filter
cm ..... centimeter
code ..... GPS pseudo-range code
corr ..... correction
cov ..... covariance
DGPS ..... Differential Global Positioning System
diag ..... diagonal
DOP ..... Dilution Of Precision
DOP_w ..... Dilution Of Precision after whitening
ECEF ..... Earth-Centered Earth-Fixed coordinate frame
Eq. ..... Equation
FARA ..... Fast Ambiguity Resolution Approach
FASF ..... Fast Ambiguity Search Filter
FFT ..... Fast Fourier Transform
Fig. ..... Figure
GM ..... first-order Gauss-Markov
GM1 ..... first-order Gauss-Markov
GPS ..... Global Positioning System
GUPT ..... GPS UpdaTe
gyro ..... gyroscope
h ..... hour of time
HPF ..... High Pass Filter
Hz ..... Hertz (cycle per second)
IAE ..... Innovation-based Adaptive Estimation
IMU ..... Inertial Measuring Unit
INLP ..... Integer Non-Linear Programming method
ino ..... innovation
INS ..... Inertial Navigation System
INS/GPS ..... integrated System of INS and GPS
ion ..... ionosphere

KF ..... Kalman Filter
KINADA ..... KINematic ADAptive Kalman filter processor
KINGSPAD..... KINematic Geodetic System for Position and Attitude Determination
KINWHITE ..... KINematic and WHITEning Kalman filter processor
km ..... kilometer
L1 ..... GPS L1 signal/observable
L1-norm ..... L1-norm space
L2 ..... GPS L2 signal/observable
L2-norm ..... L2-norm space
LAMBDA ..... Least squares AMBiguity Decorrelation Adjustment
LDL ..... Lower Diagonal Lower matrix factorization
LL ..... Local Level coordinate frame
LPF ..... Low Pass Filter
LREF-III ..... Honeywell inertial navigation system
LS ..... Least Squares
LSS ..... Least-Squares-Search method
LTN 90-100 ..... Litton inertial navigation system
max ..... maximum
MDE ..... Minimally Detectable Error
mGal ..... milliGal (10^{-5} m/s^2)
min ..... minimum
ML ..... Maximum Likelihood
mm ..... millimeter
MMAE ..... Multiple Model-based Adaptive Estimation
mrad ..... milliradian
msec ..... millisecond
mult ..... multipath
nmiph ..... nautical mile per hour
OTF ..... On The Fly
OTFWhite ..... OTF ambiguity resolution technique using the whitening filter
PDF ..... Probability Density Function
PDF ..... Probability Distribution Function
PDOP..... Position Dilution Of Precision
phase ..... GPS carrier phase
ppm ..... part per million
PSD ..... Power Spectral Density
QMF ..... Quadratic Mirror Function
res ..... residual
RLS ..... Recursive Least Squares
RMS ..... Root Mean Squared error
RMSE ..... Root Mean Squared Error
s ..... second of time
SA ..... GPS Selective Availability
sat ..... satellite
sec ..... second of time
TM ..... Transverse Mercator projection system

trop ..... troposphere
UDU ..... Upper Diagonal Upper matrix factorization
UTM ..... Universal Transverse Mercator projection system
vs. ..... versus
WGS84 ..... World Geodetic System of 1984
win ..... window
WL ..... GPS Wide Lane observable
ZUPT ..... Zero velocity UpdaTe
μm ..... micrometer

Operational Inertial Frame - i-frame

origin : at the center of mass of the Earth

x-axis : pointing towards the mean equinoctial colure

y-axis : being orthogonal to the two other axes to complete a right-handed frame

z-axis : being parallel to the mean spin axis of the Earth

Body Frame - b-frame (measurement)

origin : at center of accel proof masses

x-axis : pointing left for right-handed systems and right for left-handed systems

y-axis : pointing forward (direction of motion)

z-axis : pointing upward

Local-level Frame - l-frame (navigation)

origin : at topocenter; coincide with sensor frame origin

x-axis : completing a right-handed orthogonal frame

y-axis : pointing towards geodetic north

z-axis : pointing outwards orthogonal to a reference ellipsoid

Earth-fixed Frame - e-frame (geocentric)

origin : at the center of mass of the Earth

x-axis : pointing towards the mean meridian of Greenwich

y-axis : completing a right-handed orthogonal frame

z-axis : parallel to the mean spin axis of the Earth

Camera Frame - c-frame (imagery)

origin : at camera perspective center

x-axis : completing a right-handed orthogonal frame

y-axis : pointing forward

z-axis : pointing upward

1. INTRODUCTION

In this chapter, background information on the formulation of the INS/GPS integrated system estimation problem is given. The problem of optimizing the estimation procedure of the INS/GPS integrated system is stated. Adaptive Kalman filtering and GPS phase ambiguity resolution are proposed as vehicles to the optimization problem. Research objectives, the contribution of the research, and the dissertation outline are given.

1.1 Background and Problem Statement

When surveying systems based on the principle of inertial navigation were developed in the early 1970's for military agencies, and became available to non-military users in 1975, Kalman filtering was the main vehicle to carry out the sequential processing of data. After a short period of testing, it was almost immediately employed in geodetic work, where it proved quite successful [Babbage 1977, Schwarz 1983]. The main focus was then on two major application areas: efficient control of point positioning from moving vehicles and precise interpolation of the anomalous gravity vector. Both tasks could be solved with a Kalman filter processing the inertial system output at zero velocity update points (ZUPTs) in a semi-kinematic mode. However, during the 1980's, major changes have taken place, which were driven by the rapid development of GPS and the increased use of strapdown inertial systems. GPS, with its continuous updates, has freed inertial techniques from the need for zero velocity updates and has thus considerably extended their kinematic functionality. The use of the Kalman filter with the integrated INS/GPS has, since then, gained greater importance.

The progress of the INS/GPS integration during the last two decades can be identified as: evolution of the integration concept and development of production systems that make use of the integrated system. In the former, the development of new algorithms, see e.g. [Wei and Schwarz, 1990a] and the development of the integrated

system itself, see e.g. [Liu 1992, Schwarz and Zhang, 1994, Zhang 1995] characterizes the evolution. The production systems that make use of the integrated INS/GPS system are either mobile multi-sensor systems or airborne gravity systems.

Mobile multi-sensor systems, land-based or airborne, use INS/GPS as a means for positioning and orientation to directly georeference the production system, see e.g., [Schwarz et al., 1993a, El-Sheimy et al., 1995, Mostafa et al. 1997]. In this case, high frequency trajectory information becomes highly important; the attitude (orientation) information is especially critical. Tracking of such information requires high data rate and an efficient algorithm capable of preserving high frequency trajectory information content. In the airborne gravity systems, however, acceleration information derived from both GPS and INS is used to recover gravity, see e.g. [Wei and Schwarz, 1995, Schwarz and Glennie 1997]. High frequency trajectory information becomes critical for short wavelength resolution of the gravity field especially in situations where higher interpolation is required, e.g. trajectory turns.

In the process of adapting the original integration concept to the growing number of applications, the concept has grown in leaps and bounds and contains contributions from many individuals. In this process, the use of a conventional filter designed with a fixed estimation algorithm in mind was dominant. In the meantime, the subject of adaptive filters has matured to the point where it has become an important part of statistical signal processing. The use of an adaptive filter offers an attractive solution to the integration problem as it usually provides a significant improvement in performance over the fixed filter. Furthermore, the use of adaptive filters provides new signal processing capabilities that would not be available otherwise [Haykin 1996].

The fixed integration formulation has shown success in fulfilling the accuracy requirements of many kinematic applications. However, it was not fully successful in other applications especially with medium accuracy INS systems like the LTN 90-100. In some cases, it did not fulfill the accuracy requirements at all times; in others, it did not fulfill them all the time. In the first case, it was not a suitable system for applications that require accuracy better than ten centimeter like engineering and cadastral applications. In

the second case, it was not a one hundred percent reliable system especially in situations like bad geometric satellite coverage or loss of lock, see [Schwarz et al., 1993a] for accuracy requirements.

It can be seen from the Kalman filter basic formula (Eq. (1.1)), that at estimation epoch k, the estimate of the INS/GPS filter after update, $\hat{x}_k(+)$, is dependant on the INS system model through the predicted state, $\hat{x}_k(-)$, the GPS update measurement through the measurement innovation, v_k, and on the system noise and measurement noise a priori statistical information through the filter weighting (gain) matrix, K_k

$$\hat{x}_k(+) = \hat{x}_k(-) + K_k v_k . \tag{1.1}$$

Therefore, the problem of achieving better performance (reliability and accuracy) of INS/GPS systems can be divided into a modeling problem and an estimation problem. While the modeling problem is concerned with developing better error models that more accurately describe the INS/GPS system, the estimation problem is concerned with achieving better trajectory and sensor error estimates through the proper use of the available process and measurement information. From the estimation viewpoint, the optimality of conventional Kalman filter requires, in principle, good a priori knowledge about the process and infinite (or sufficiently long) estimation time or data length [Kalman 1960, Gelb 1974, Brown and Hwang, 1992]. These criteria have limited the applicability of the Kalman filter in the case of INS/GPS systems, both conceptually and practically.

From the conceptual point of view, good a priori information, because it is difficult to obtain, depends on factors such as the type of application and the process dynamics. The insufficiently known a priori filter statistics will on the one hand reduce the precision of the estimated states or introduce biases to their estimates (robustness). On the other hand, wrong a priori information will lead to practical divergence of the filter. From the implementation point of view, estimation time is always finite and, in some cases, not all filter states can be estimated; this applies specifically to the filter weak observable

components. Limited data length will not only invalidate the optimality criterion of the Kalman filter, but also will, in many cases, have the practical problem that the weak observable components of the filter cannot be estimated, e.g. accelerometer bias and gyro drift. Through the coupling effect, these weak observable components directly affect the quality with which the main components of the filter (position, velocity, and attitude) can be estimated.

In kinematic applications, the estimation environment of the integrated system is not always fixed but changing. In a changing estimation environment, imperfect a priori information and finite data length will affect the obtained accuracy of the integrated INS/GPS system if a fixed filter formulation is used. This implies that there is a major drawback in using a fixed filter designed by conventional methods in this case. An adaptive filtering formulation, therefore, tackles the problem of imperfect a priori information and may provide a significant improvement in performance over the fixed filter through the filter learning process based on the innovation sequence [Mehra 1970, 1971]. In this case, perfect knowledge of a priori information is only of secondary importance because the new measurement and process covariance matrices are adapted according to the filter learning history. This requires frequent adaptation of the integration. The fixed estimation formulation should, therefore, be replaced by an adaptive estimation formulation to suit the changing integration environment. It can be expected that with adaptive estimation of the integrated system, better performance can be achieved.

As seen from Eq. (1.1), optimizing the estimation procedure of the INS/GPS integrated system requires the measurement update to the Kalman filter to be of the highest accuracy possible. Quality of GPS position and velocity directly represent the positioning accuracy of the integrated system. They, also, indirectly enhance the attitude accuracy of the integrated system through the updates and the interaction (coupling) of the attitude and the position and velocity states of the filter. Since phase observables deliver the best possible GPS navigation information, their initial integer cycle

ambiguities must be resolved correctly because they provide robustness to the GPS observables and strength to the overall accuracy and reliability of the integrated system.

Over the last decade various methods for ambiguity resolution have been proposed. In these methods, the ambiguity is either resolved in the measurement domain where a search is employed to locate the correct ambiguity set through statistical testing, see e.g. [Hatch 1990], or in the position domain (code-guided) where a precise pre-determined receiver position is required to search a physical space for the correct receiver position, see e.g. [Almgren 1998]. The latter requires receivers that have low noise level, while the former usually employ complicated search algorithms. Over short baselines, however, the residual errors in the double differenced GPS observable don't exceed half the phase observable wavelength [Parkinson and Spilker, 1996]. After a few observations, the float ambiguity estimate becomes very close to the integer ambiguity. A space projection method, like the integer whitening filter, reduces the data noise and allows a reliable estimation over a shorter observation time. Therefore, the integer whitening filter provides an algorithm for the problem of GPS ambiguity resolution on the fly over short baselines which does not require a search, is easy to understand, simple to implement, applicable in real time, economic for hardware, and, of course, is reliable.

1.2 Research Objectives

The main objective of this research is to optimize the estimation procedure of the INS/GPS integrated system by replacing the conventional Kalman filtering formulation of the integration by an adaptive one. The adaptive formulation is superior to the conventional one as it provides a means to accommodate irregular situations. This, in return, enhances the reliability and accuracy of the INS/GPS integrated system providing improved accuracy and reliability in kinematic applications. The GPS phase ambiguity resolution algorithm is also revisited and a new simple technique is developed.

To achieve the goals of this research, the following are identified:

1. investigate an alternative to conventional Kalman filtering, in general, and in formulating the INS/GPS integration, in particular, and then develop and implement an adaptive Kalman filter for the INS/GPS integrated system
2. analyze the performance of the developed adaptive Kalman filter against the conventional Kalman filter for kinematic applications
3. develop an efficient and simplified approach to the GPS phase ambiguity resolution problem for short baselines.

1.3 Author's Contribution

In this dissertation, the adaptive Kalman filter is introduced as an alternative to the widely used conventional Kalman filter for application in an integrated INS/GPS. A thorough analysis of the developed method is carried out for different kinematic applications to show the effectiveness and suitability of the adaptive technique. It is shown that the adaptive filter is not only more convenient and relaxes the requirement on the a priori statistical information, but also outperforms the conventional filter. It, therefore, has potential for kinematic applications requiring high reliability and accuracy.

A new method for GPS phase ambiguity resolution is also introduced in this dissertation. The efficiency of the method stems from the fact that it requires only one transformation step and no search. The method proved very efficient for short baselines over short observation periods. A thorough analysis of the method is given with details on the transformation used.

1.4 Dissertation Outline

In Chapter 2, a general overview of the dynamic processes is given. Stationary and non-stationary processes are outlined. The treatment of the non-stationary process as a piece-wise stationary is discussed for the case of innovation-based adaptive Kalman filtering.

Chapter 3 covers the Kalman filtering theory and implementation for the INS/GPS integrated system. The problem of the integrated system is discussed and its Kalman filtering formulation is outlined. Details of the INS/GPS Kalman filter structure are also discussed. The role of the a priori statistical information and its effect on the filter formulation is given. Adaptive filtering methods, in general, and those useful for application in Geomatics and Navigation are discussed.

The development of an innovation-based adaptive Kalman filter for the INS/GPS integrated system is documented in Chapter 4. A discussion of the appropriateness of the maximum likelihood approach as opposed to the least squares approach is outlined. The maximum likelihood derivation of the filter is then given in details. Special cases where the filter system noise covariance and/or the measurement noise covariance matrices are adapted are derived. Whitening of the innovation sequence via the float-whitening filter is also discussed.

In Chapter 5, a preliminary analysis of the developed adaptive Kalman filter is carried out through simulation studies. Various performance parameters are used to analyze the performance of the developed adaptive filter and compare it to the conventional filter.

Introduced in Chapter 6 is a new method for GPS phase ambiguity resolution on the fly, the OTFWhite method. The problem of GPS phase ambiguity resolution is first discussed. The solution of the ambiguity problem through transforming the problem from the original space to a space that is easier to analyze is then discussed. Geometric and precision implications are also discussed.

Field tests, results, and analysis pertaining to the developed OTF ambiguity resolution technique are covered in Chapter 7. Investigations of the new method and its applicability for short baselines are also discussed in this chapter.

In Chapter 8, four different types of testing are outlined. The first test is carried out in a well-controlled environment to test the overall performance of the developed adaptive Kalman filter. The second test is a field flight test similar to the simulated flight

test to support the simulation studies. The third and fourth are flight tests covering the two most demanding INS/GPS applications, direct georeferencing and gravity systems. The first flight test is carried out in an attitude-controlled environment, while the second is flown over an area of well-known ground gravity field. Results and analysis of the developed adaptive filter is carried out on the field tests and presented in this chapter.

Finally, Chapter 9 summarizes the work done in this research and draws conclusions from it. It also gives recommendations for further developments in the same field.

2.
DYNAMICS OF ERROR PROCESSES

In this chapter, fundamental characteristics of random variables and processes are outlined. The concept of stationary random process is discussed. The treatment of non-stationary random process as a piece-wise stationary process in adaptive estimation is given. Standard references such as [Papoulis 1965, Gelb 1974, Maybeck 1982, Yaglom 1987, Brown and Hwang, 1992] are used extensively in this chapter.

2.1 Random Variables and Random Processes

Random (or stochastic) events are the very first object of study in the theory of probability. Their importance in geomatics lies in the interaction with the estimation theory. There can not be a fair treatment of the estimation theory, especially adaptive estimation, without the proper treatment of the random events. Random variables are characterized by their distribution functions which require statistics, which can be derived from experiments, in order for it to be defined.

Random variables are the outcome of random experiments. These random variables take on values at random according to their probability distribution (or density) functions. What is observed of a random variable are some of its realizations. Because of their nature, measurement and system (or process) errors that cannot be modeled take the form of random variables. It is this property of the error behavior that makes the estimation of the trajectory in the case of INS/GPS kinematic applications to deal with random processes.

If X is a random variable, then the occurrence of the values of X which is less than a fixed number x is a random event. The probability distribution function of x, F(x), is defined as

$$F(x) = P(X<x). \tag{2.1}$$

where P represents probability. In probability theory, a random variable is considered given if its distribution function is known; this will become evidently clear in the discussion of the special case of the Gaussian distribution. It is clear that not every function can be a distribution function. The condition for a function to be a distribution function is that it should be a monotone non-decreasing function of x, i.e.

$$\begin{aligned} &F(x+a)-F(x)\geq 0, \\ &\lim_{x\to-\infty} F(x)=0, \qquad \text{for } a>0 \\ &\lim_{x\to\infty} F(x)=1. \end{aligned} \tag{2.2}$$

For continuous random variables, the probability distribution function can be represented by its derivative, the probability density function f(x), where

$$f(x)=\frac{dF(x)}{dx}. \tag{2.3}$$

It is evident from Eq.(2.3) that the distribution function can be computed once the density function is known, i.e.

$$F(x)=\int_{-\infty}^{x} f(x')dx'. \tag{2.4}$$

The condition in Eq.(2.2) is then rewritten in terms of the density function as

$$\int_{-\infty}^{\infty} f(x)dx=1, \qquad f(x)>0 \text{ for all } x. \tag{2.5}$$

One very important probability distribution/density function, in geomatics, is the normal (or Gaussian) distribution/density function. The importance of this distribution stems from the following facts:

1. the distribution is totally defined by only two statistics, namely, the mean and the variance of the random variable
2. according to the central limit theorem, if the random phenomenon we observe is generated as the sum of effects of many independent infinitesimal random phenomena, then the distribution of the observed phenomenon approaches a Gaussian distribution as more random effects are summed, regardless of the distribution of each individual phenomenon [Maybeck 1982]. Therefore, the Gaussian distribution has engineering importance because it provides adequate modeling of random phenomena observed empirically. In [Papoulis 1965], it was shown that three uniformly distributed random variables convolve together to a very good approximation of a Gaussian distribution.

Figs. (2.1a) and (2.1b) show a schematic plot of the normal distribution and density functions, respectively.

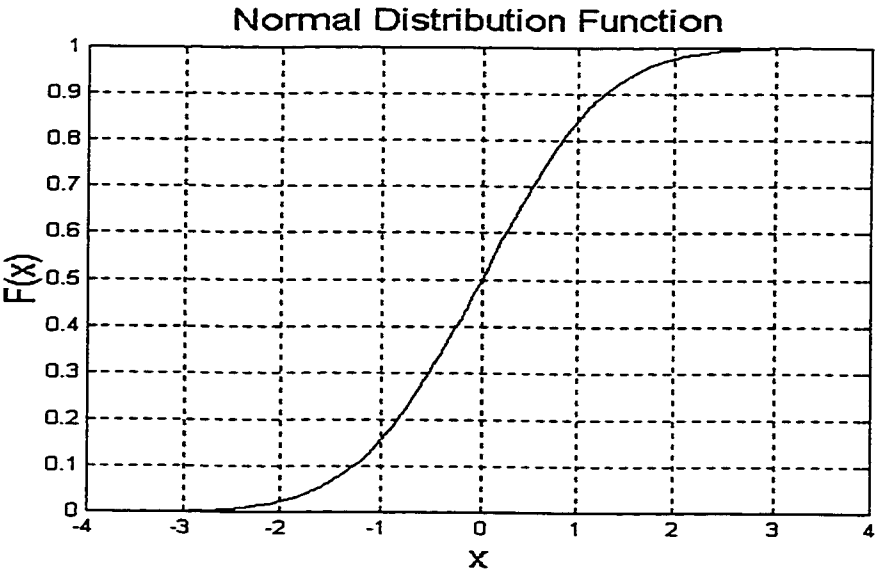

Fig. (2.1a) : Normal Distribution Function

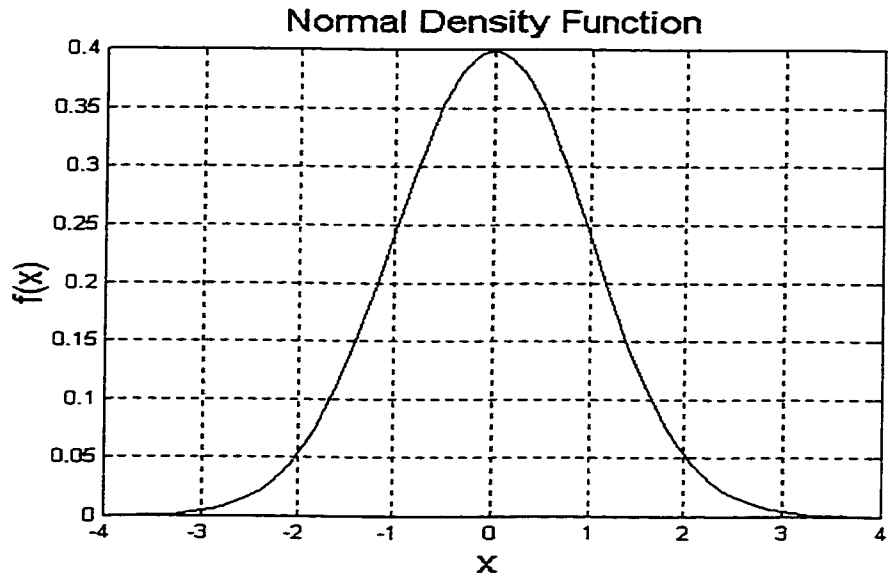

Fig.(2.1b) : Normal Density Function

The probability density function of the normal distribution is

$$f(x) = \frac{1}{\sqrt{2\pi\sigma_x^2}} e^{-\frac{x'^2}{2}}, \tag{2.6}$$

where, $x' = \frac{(x - m_x)}{\sigma_x}$ is the normalized variable and m_x and σ_x will be defined in the following. The two *statistics* required to define a uni-variate normal distribution of a random variable are the mean and the variance. The *mean value* of a random variable X, and consequently of its distribution, is defined as

$$m_x = E[X] = \int_{-\infty}^{\infty} x f(x) dx . \tag{2.7}$$

The mean value is the first moment, μ_x, of the random variable. It is also the mathematical expectation of the random variable which tends to the average observation, in a probabilistic sense, as the number of observations increases.

The *variance* of a random variable is the mean squared deviation of the random variable from its mean; it is defined as

$$\operatorname{var} X = \sigma_x^2 = E[(X - m_x)^2] = \int_{-\infty}^{\infty} (x - m_x)^2 f(x)dx . \tag{2.8}$$

It is evident from Eq.(2.8) that the variance of a random variable is *not* its second moment (mean squared values), μ_x^2. Expanding Eq.(2.8), it can be seen that the variance of a random variable deviates from its second moment by the squared value of the mean of the random variable, i.e.

$$\sigma_x^2 = E[x^2] - (E[x])^2 = \mu_x^2 - m_x^2 . \tag{2.9}$$

The mean squared value and the variance are equal for zero-mean random variables, however. It should be noted that the above definitions of the mean value and the variance are also valid for discrete data; in this case, the integral will be replaced by the averaging summation.

In geomatics, one is usually concerned with more than one random variable. In this case, a multidimensional (or multivariate) distribution is used. In addition to the above mentioned two statistics, a third statistic is required to define the multivariate model, the covariance. The *covariance* is the partial indication of the degree by which one random variable is related to another. It is defined as the expectation of the product of the two random variables after their means have been subtracted,

$$\begin{aligned} \operatorname{cov} XY = \sigma_{xy} &= E[(X - m_x)(Y - m_y)] \\ &= \int_{-\infty}^{\infty} \int_{-\infty}^{\infty} (x - m_x)(y - m_y) f(x, y)dxdy . \end{aligned} \tag{2.10}$$

Again, the covariance of two random variables is *not* the first moment of their product, but is related to it as follows

$$\sigma_{xy} = \mu_{xy} - m_x m_y . \tag{2.11}$$

A more convenient representation of the relationship between two random variables is given by the *correlation* coefficient. It is the covariance of the two variables normalized by the square root of their variances (standard deviations), and is expressed as

$$\mathrm{corXY} = \rho_{xy} = \frac{\sigma_{xy}}{\sigma_x \sigma_y} = \frac{\mu_{xy} - m_x m_y}{\sigma_x \sigma_y} . \tag{2.12}$$

The range of possible values of the correlation coefficient ρ is restricted by the inequality

$$-1 \le \rho \le 1 . \tag{2.13}$$

The previous expression is a rephrasing of the Schwarz inequality

$$|\sigma_{xy}| \le \sigma_x \sigma_y , \tag{2.14}$$

which defines the relationship between the covariance of two random variables and their variances. The probability density function of the bi-variate normal distribution is

$$f(x,y) = \frac{1}{\sqrt{(1-\rho_{xy}^2)(2\pi)^2 \sigma_x^2 \sigma_y^2}} e^{-\left[\frac{x'^2 - 2\rho_{xy} x'y' + y'^2}{2(1-\rho_{xy}^2)}\right]} \tag{2.15}$$

where, x' and y' are the normalized variables.

Two random variables are said to be *statistically uncorrelated* if their correlation coefficient vanishes, i.e. $\rho_{xy} = 0$. They are said to be *linearly independent* if their joint distribution can be expressed as a product of their individual distributions, i.e. f(x,y) = f(x) f(y). In case of a normal distribution, the statistical non-correlatedness implies linear

independence. This is evident from Eq.(2.15) by substituting $\rho = 0$, one can express f(x,y) as a product of f(x) and f(y).

The correlation coefficient can also be used between two different time epochs of the same variable; in this case, it is called auto-correlation or auto-covariance coefficient. In general, *the auto-covariance* takes the form

$$\begin{aligned} \operatorname{cov} X(t_1)X(t_2) &= \sigma_{x(t_1)x(t_2)} = E[(X(t_1)-m_{x(t_1)})(X(t_2)-m_{x(t_2)})] \\ &= \int_{-\infty}^{\infty}\int_{-\infty}^{\infty}(x(t_1)-m_{x(t_1)})(x(t_2)-m_{x(t_2)})f(x(t_1),x(t_2))dx_1dx_2 \end{aligned} \tag{2.16}$$

If the normalized variables are used instead, the *auto-correlation* can be defined as

$$\begin{aligned} \operatorname{cor} X(t_1)X(t_2) &= \rho_{x(t_1)x(t_2)} = E[X'(t_1)X'(t_2)] \\ &= \int_{-\infty}^{\infty}\int_{-\infty}^{\infty}x'(t_1)x'(t_2)f(x(t_1),x(t_2))dx_1dx_2 \end{aligned} \tag{2.17}$$

In case two different variables at two different time instants are of interest, *cross-covariance* and *cross-correlation* coefficients are defined. Eqs.(2.16) and (2.17) are then used with one of the X's replaced by Y to represent the second variable.

The extension of the concept of random variable in time-space is the random function or random process. *A Random Process* can be thought of as a collection, or ensemble, of functions of time. The value of the observed member of the ensemble at a particular time is a random variable. As it is computed at different time instants, the correlation coefficient can be replaced by the correlation function for a random process. Substituting $t_2 = t_1 + \tau$, an *auto-correlation* function can be defined as

$$\operatorname{cor} XX(\tau) = \rho_{xx}(\tau) = E[x(t_1)x(t_1+\tau)], \tag{2.18}$$

and the *cross-correlation* function as

$$\mathrm{corXY}(\tau) = \rho_{xy}(\tau) = \mathrm{E}[x(t_1)y(t_1+\tau)]. \tag{2.19}$$

It should be noted, that for discrete processes, the previous definitions are also valid. The difference is that sequences, rather than processes, are used.

2.2 Stationarity

A *stationary process* is a process whose statistical properties are invariant in time, in a probabilistic sense. It follows that the probability distribution function of the process remains the same when shifted along the time axis. In other words, the first probability distribution for the process, $F(x_1,t_1)$, is independent of the time of observation, t_1. For the distribution function to remain independent of the time of observation, the first and second moments of the process, and consequently the mean value and the variance, should also be independent of the time of observation. They may take different values at random as time elapses, but stay independent of the absolute time of observation. A random process satisfying this condition is called a stationary random process in the strict sense or *strictly stationary*.

The previous definition of stationarity requires the estimation of the distribution function for the estimation of the process itself; this is a typical Bayesian approach. In practice, however, the strict stationarity condition is very difficult to fulfill. If Gaussian distributions are of concern, as is the case in most geomatics applications, wide-sense stationarity suffices. And, consequently, a more simplified approach to the estimation problem can be taken.

A random process is said to be stationary in the wide sense or *widely stationary* if its mean value remains constant, its mean-squared value is finite, and its correlation function is independent of the absolute time of observation, t_1 or t_2, but still dependent on the difference between them $\tau = t_2 - t_1$. In this case, Eqs.(2.18) and (2.19) are used to define the correlation functions. Since the Gaussian distribution of a random process is completely defined by the process mean value, m, and its correlation function, $\rho(\tau)$, the

concept of stationarity in the wide sense and in the strict sense are exactly the same for Gaussian random processes.

The correlation function of a stationary random process is a positive definite function. It follows, that the following conditions hold

$$\rho_{xx}(0) > 0$$

$$|\rho_{xx}(-\tau)| = \rho_{xx}(\tau) \tag{2.20}$$

$$|\rho_{xx}(\tau)| \leq \rho_{xx}(0).$$

One important stationary correlation function widely used in geomatics and in INS/GPS integrated systems is the correlation function of a first-order Gauss-Markov process. The process is generated by passing white noise, w(t), through a simple first-order lag filter, as shown in Fig.(2.2).

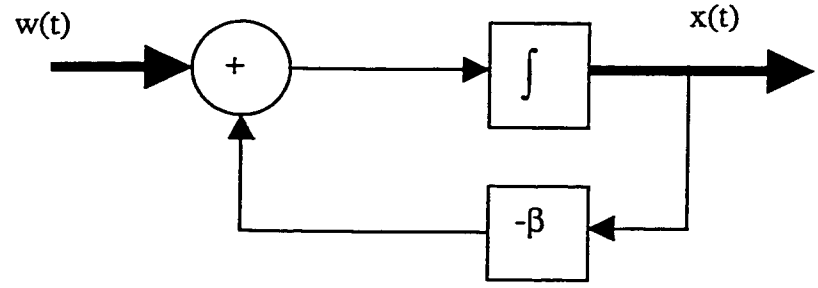

Fig.(2.2) : First-order Gauss-Markov Process

The state-space representation of this process (system) takes the form of the following first-order differential equation

$$\dot{x}(t) = -\beta x(t) + w(t), \tag{2.21}$$

where, β is the correlation length (the reciprocal of the correlation time at 1/e point). Solving the above differential equation and evaluating Eq.(2.18), the correlation function of the process is

$$\rho_{xx}(\tau) = \sigma_0^2 e^{-\beta|\tau|} + m^2, \tag{2.22}$$

where m is the process mean value, and σ_o is the square root of its mean squared value (its power) at time zero. The probability distribution for the process $x(t_k)$ is dependent only on the value at one point immediately in the past, $x(t_{k-1})$, i.e.

$$F[x(t_k) \mid x(t_{k-1}),\ldots x(t_1)] = F[x(t_k) \mid x(t_{k-1})]. \tag{2.23}$$

The Fourier transform of the auto-correlation function, $\rho_{xx}(\tau)$, is the power spectral density function of the process, which is defined as

$$P(\omega) = \frac{2\beta\sigma_0^2}{\beta^2 + \omega^2}, \tag{2.24}$$

where, ω represents the frequency parameter. Figs(2.3a) and (2.3b) show a schematic plot of the first-order Gauss-Markov auto-correlation and spectral density functions.

2.3 Piece-wise stationarity and Adaptive Estimation

Stationarity is an idealization of the real world. Under stationarity, it is assumed that the random process is defined for all values of time t, and has precisely identical properties for all t. In other words, stationarity refers to a state of statistical equilibrium or steady state. In reality, there is a state of transition before the process goes to steady state. The transient state is obviously dependent on the choice of the process initial conditions and is non-stationary in nature. A similar state, as the transient state, can also occur when

the process dynamics change. In both cases, the validity of the process stationarity assumption becomes questionable.

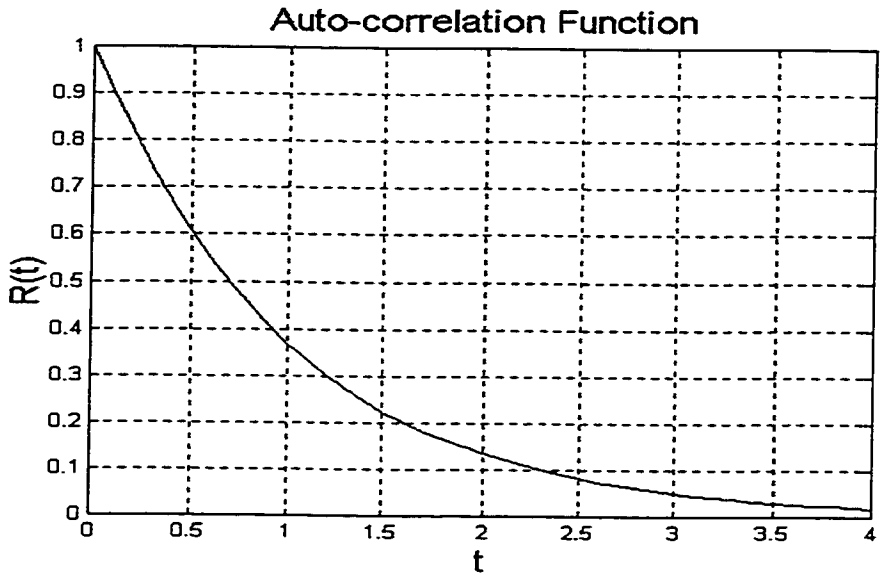

Fig.(2.3a) : First-order Gauss-Markov Auto-correlation Function

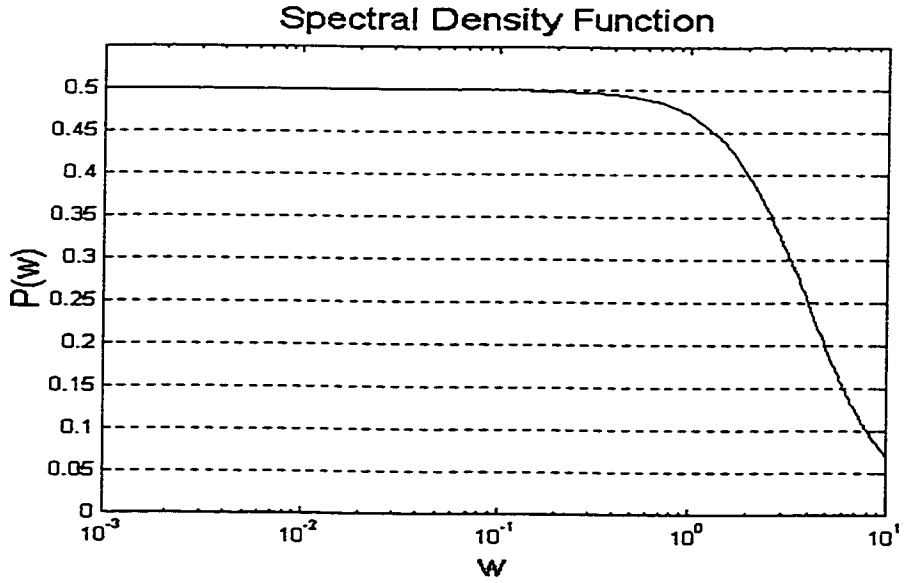

Fig.(2.3b) : First-order Gauss-Markov Spectral Density Function

Brownian motion or random walk is a non-stationary random process. Its mean squared value grows unbounded as time increases. Many navigation sensors partially

display random walk behavior. Inertial sensors, such as gyroscopes and accelerometers, usually are characterized by random walk effects. A microscopic observation of the random walk shows clearly the non-stationary nature of the process. However, there is still something resembling stationarity involved in the microscopic observation. The set of increments of the random walk process X(t) during consecutive and equal time intervals, i.e., the set of random variables

$$N_k X \equiv X((k+1)N) \rightarrow X(kN), \tag{2.25}$$

where, k is a counter and N is an arbitrary fixed number describing the sample size, form a stationary random sequence. In other words, the random walk, and in effect a non-stationary process can be considered stationary within small time intervals.

Ergodicity is one further concept associated with random processes. A process is claimed ergodic if any statistic calculated by averaging over all members of the ensemble at a fixed time can also be calculated by averaging over all time on a single representative member of the ensemble. For a stationary random process X,

$$M_x \rightarrow m_x \text{ for all } T \tag{2.26}$$

under the condition that

$$E[(M_x - m_x)^2] \rightarrow 0 \text{ as } T \rightarrow \infty, \tag{2.27}$$

where, M_x is the time average of the process X, corresponding to the time period T. This last condition is understood in the mean square sense. It is clear that an ergodic process satisfying this condition guarantees any desirable degree of accuracy, provided the observation time is chosen long enough, and stems from a single realization of the process. It follows, that the statistics for an ergodic stationary random process can be calculated by time averaging as follows

$$\mu_x^{(i)} = M_x^{(i)} = \lim_{T\to\infty} \frac{1}{2T} \int_{-T}^{T} x^{(i)}(t)dt, \tag{2.28}$$

and the auto-correlation function by

$$\rho_{xx}(\tau) = \lim_{T\to\infty} \frac{1}{2T} \int_{-T}^{T} x(t)x(t+\tau)dt. \tag{2.29}$$

With this heuristically motivated approach, one can treat non-stationary processes as piece-wise stationary ones in an adaptive fashion and obtain satisfactory results. The trade-off will always be the size of window used against the process dynamics. For more details on the subject of random variables and stationarity, one may refer to the numerous statistical books especially those taking the estimation problem viewpoint such as [Papoulis 1965, Gelb 1974, Maybeck 1982, Yaglom 1987, Brown and Hwang, 1992].

3. INS/GPS KALMAN FILTERING

In this chapter, the integration of INS and GPS will be discussed from the estimation viewpoint. The error characterization of the integrated system will be given first and the conventional as well as the adaptive estimation approaches will then be discussed. The contents of this chapter is considered as background material and, therefore, extensive use of standard references is made.

3.1 INS/GPS Integration

The integration of Inertial Navigation Systems (INS) with the Global Positioning System (GPS) has become widely accepted as a full kinematic solution of the navigation problem. The complementary nature of the two systems gives rise to the increasing use of the integrated system. In georeferencing applications, GPS provides the positioning component, while INS gives the attitude component and fills the gaps between the GPS updates. In airborne gravimetry, both data streams are used simultaneously to estimate the gravity disturbance.

3.1.1 Error characteristics of the GPS phase observables

For an INS/GPS integrated system, GPS is responsible for the update measurement. It provides three different observables, namely, pseudo code, carrier phase, and Doppler (or phase rate) observables. For precise kinematic applications, however, carrier phase observables are generally used. The carrier phase observation equation can be written as [Wells et al. 1987, Hoffmann-Wellenhof et al. 1992, Parkinson and Spilker, 1996, Lachapelle 1998]

$$\Phi = \rho + d\rho + c(dt - dT) + \lambda N - d_{ion} + d_{trop} + \varepsilon_{\Phi mult} + \varepsilon_{\Phi noise}, \qquad (3.1)$$

where,

Φ : observed carrier phase (measurement)

ρ : geometric spatial distance between the receiver and the satellite (observable)

$d\rho$: satellite orbital error (nominal and ε-error due to Selective Availability)

c : speed of light

dt : satellite clock offset (nominal and δ-error due to Selective Availability)

dT : receiver clock offset

λ : carrier wavelength

N : initial carrier ambiguity

d_{ion} : ionospheric signal delay

d_{trop} : tropospheric signal delay

$\varepsilon_{\Phi mult}$: carrier phase signal multipath

$\varepsilon_{\Phi noise}$: carrier phase signal noise.

Errors contributing to the phase observable in single point positioning mode (SPP) are due to satellite orbital perturbations and clock bias, receiver clock bias and measurement noise, signal delay through the ionosphere, the troposphere, signal multipath, and due to the intentional denial of full GPS system accuracy to non-authorized users, the so-called Selective Availability or SA. Table (3.1) summarizes typical values for these errors [Wells et al 1987, Parkinson and Spilker, 1996, Lachapelle 1998]. Because the errors incurred in SPP mode cannot meet the accuracy requirements, SPP mode is not suitable for precise applications.

Table (3.1) : Typical SPP GPS Phase Range Measurement Errors

Error Source	**Typical Error [m]**
Nominal Orbital Perturbation	5 - 30
Nominal Satellite Clock Bias	up to 300,000
SA (Orbital & Clock)	0 - 100
Ionospheric Delay	2 - 150
Tropospheric Delay	2 - 30
Signal Multipath	< 0.05
Receiver Clock Bias	10 - unlimited
Receiver Measurement Noise	< 0.005

To eliminate or reduce measurement errors, differential observables are used. In real-time kinematic applications, single differencing between receivers is often used to reduce measurement errors and eliminate satellite clock error. It, however, does not eliminate the receiver clock error. Since the receiver clock drifts over time, a new receiver clock term has to be modeled for each observation epoch. The estimation of the receiver clock term requires precise modeling which is not always achievable, especially for quartz clocks commonly used in GPS receivers. In precise kinematic applications, double differencing is often used to eliminate receiver and satellite clock errors and reduce the correlated measurement errors. Double differencing is carried out by differencing between receivers and between satellites at the same observation epoch. The double differenced phase observation equation takes the form [ibid.]

$$\nabla\Delta\Phi = \nabla\Delta\rho + \nabla\Delta d\rho + \lambda\nabla\Delta N - \nabla\Delta d_{ion} + \nabla\Delta d_{trop} + \varepsilon_{\nabla\Delta\Phi mult} + \varepsilon_{\nabla\Delta\Phi noise}, \tag{3.2}$$

where $\nabla\Delta$ represents the double differencing operator.

In the double differenced observable, the receiver and satellite clock offsets are eliminated, the correlated measurement errors are reduced, but the phase signal noise is amplified. The phase noise is a function of the receiver tracking bandwidth. It is usually within one percent of the phase signal wavelength [Lachapelle 1998, Parkinson and Spilker 1996]. For the GPS L1 signal, the phase noise corresponds to about 2 millimeters (1 σ), which will double after double differencing [ibid.].

Due to the high geometric correlation of range measurements between the receivers and the satellite over short baselines, the *orbital error* is considerably reduced by differencing. The relative position error resulting from the remaining orbital error, with Selective Availability (SA) on, is well below one part per million [ibid.]. For a baseline of 20 kilometer length, the maximum expected range error due to $\delta\rho$ is 20 millimeters with a relatively long wavelength (slow variation).

50 percent of the *Ionospheric delay* can be removed by using the broadcast Klobuchar model [Klobuchar 1991]. Based on the dispersiveness of the ionosphere, ionospheric delay can be determined and subsequently totally eliminated by combining L1 and L2 phase observations of a dual frequency receiver. This combination, however, is not recommended for short baselines as it results in a 3 times noisier observable than the double differenced one [Lachapelle et al, 1987, Langley 1993]. It also destroys the integer nature of the phase ambiguity of the resulting observable. For short baselines, the ionospheric delay is spatially and temporally correlated; the spatial correlation is found to be 200 km up to 1000 km, and the temporal correlation ranges from 2 to 50 minutes under disturbed and normal conditions, respectively [Wild et al, 1990]. This means that the major part of the ionospheric delay is removed by differencing. The remaining part of the ionospheric delay is normally less than 10 percent of the signal wavelength [Lachapelle et al, 1992] or about 1 to 2 ppm of the baseline length [Lachapelle 1998]. For instance, for a double differenced L1 phase observable over a 10 km baseline, the maximum expected residual ionospheric delay is 20 millimeters.

The *troposphere*, a non-disperse medium, delays both L1 and L2 signals identically and consequently cannot be removed by dual frequency receivers. It shows a maximum effect at the horizon and minimum at the zenith. Up to 90 percent of the tropospheric delay is due to the so-called dry component and the rest is due to the so-called wet component. The dry component can be predicted with high accuracy using empirical models [Wells et al, 1986, Lachapelle 1998]. The wet component, however, requires either meteorological data and a model or measurements from water vapor radiometers to be accurately determined. On the other hand, for short baselines, the tropospheric residual error almost completely disappears by using double differenced measurements and rarely exceeds 10 millimeters for land-based applications [ibid.]. However, for airborne applications, where the height separation between the master station and the rover can easily reach a kilometer, a refined tropospheric model becomes important [Seeber 1993].

Multipath is totally uncorrelated between stations and therefore cannot be removed by differencing. However, at the same station, the multipath signature repeats itself every

sidereal day because of the repeated satellite-receiver geometry. The phase multipath cannot exceed quarter wavelength, i.e. 50 millimeters for L1 observations [Braasch 1998]. Temporal correlation between 1 to 20 minutes have been reported depending on the observation site [El-Rabbany 1996]. Multipath is considered the limiting factor when ambiguities are to be resolved within a few epochs. Modern receivers usually employ multipath mitigation techniques to reject the reflected signal. In general, multipath has less effect on kinematic applications than on static ones.

The variation of the antenna phase (or physical) center from its electronic center, to which the position is referred, introduces another source of range error. This is particularly important for kinematic applications, where the GPS antenna keeps moving most of the time. In modern GPS antennas, however, the phase center is usually defined to sub-millimeter accuracy [Seeber 1993].

In order to achieve high accuracy with phase observations, the double differenced ambiguities need to be resolved to their correct values. Double differencing introduces additional complexity to the ambiguity resolution by increasing the mutual correlation of the phase observables [El-Rabbany 1994]. An ambiguity which has been incorrectly fixed by one cycle (19 cm for L1 signal), introduces a 19 cm of error in the range and propagates into the baseline solution depending on the receiver-satellite geometry. Table (3.2) summarizes typical values for the phase measurement errors incurred in double differenced mode [Wells et al 1987, Seeber 1993, Parkinson and Spilker, 1996, Lachapelle 1998]. A schematic plot of the spectrum of the errors in the double differenced GPS mode is shown in Fig. (3.1), see [Schwarz et al., 1993c] for more details.

Velocity information is derived from GPS Doppler or phase rate observables. Double differenced Doppler observables display similar error characteristics as of the phase observable. In general, they are less sensitive to orbital and atmospheric effects. They are not subject to cycle slips and have no initial ambiguity. The noise level of the double differenced Doppler observable for modern geodetic GPS receivers is usually below 10 mm/s [Lachapelle 1998].

Table (3.2) : Typical DDGPS Phase Range Measurement Errors

Error Source	Relative Error [ppm]	Typical Error* [m]
Orbital Perturbation (Nominal + SA)	< 1	< 0.02
Ionospheric Delay	1-2	0.02-0.04
Tropospheric Delay	0.3**- 3***	0.01-0.06
Signal Multipath	< 0.05	0-0.05
Measurement Noise	< 0.01	0.002-0.01

*Baseline Length = 20 km, **Land-based, ***Airborne.

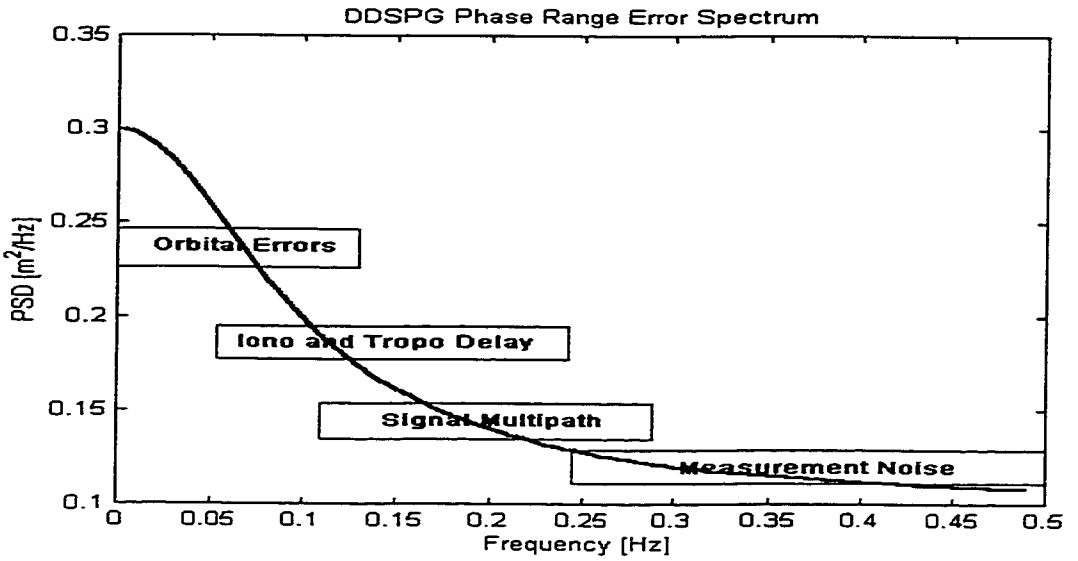

Fig. (3.1) : Spectrum of Phase Errors in Double Differenced GPS Mode

3.1.2 Error characteristics of the inertial observables

Within the integrated system, the inertial navigation system (INS) plays the role of the interpolator between updates (short-term positioning component), and provides attitude information. The INS system comprises two types of inertial sensors, accelerometers which measure incremental linear velocities and gyroscopes which measure incremental angular velocities. In order to show the general characteristics of the inertial navigation system, simplified models will be used in the following.

At the sensor level, an inertial measurement can be described in a simplified form as follows [Savage 1983],

$$l = L + b_l + S_l l + N_l l + \varepsilon_l , \tag{3.3}$$

where,

l : inertial measurement (specific force or angular velocity)

L : inertial observable (specific force or angular velocity)

b_l : measurement bias

S_l : diagonal matrix of measurement scale factors

N_l : skew symmetric matrix representing sensor axes misalignment

ε_l : measurement random noise.

The measurement *bias* is usually defined as a constant bias in the accelerometer or the gyroscope. This means that the derived velocity errors and attitude errors are linear with time. Both biases are the result of the manufacturing imperfection of the sensors. The bias value is determined by calibrating the system in lab or field tests. Measurements are then compensated for the estimated bias. In actuality, these biases are never completely constant. Their time-variable part is modeled as stochastic noise.

The *scale factor* is the ratio between the sensor input and output. It depends on the system dynamics and the temperature variation. Under normal operational condition and relatively low dynamics, the scale factor remains constant. In high dynamics, however, it becomes a function of the dynamics itself. Scale factors are usually determined by lab calibration of the system; in some cases, field calibration is also used [Salychev 1998].

Axes *misalignment* is the result of mounting imperfections of the sensors inside the system. It results in a non-orthogonality of the axes that define the inertial coordinate system. As a result, each axis is affected by the other two axes of the triad. In kinematic applications, the misalignment effect becomes of less significance if frequent maneuvers occur. In this case, the misalignment error changes in a random manner that permits lumping it among the random errors. However, if a strapdown system is mounted in an aircraft that flies in a straight line, the misalignment error effect will be systematic.

The previously discussed errors represent systematic effects of the sensors that can be deterministically modeled and removed from the measurements. On the other hand, the inertial measurement *noise* represents the effects that cannot be deterministically modeled and are time variable, such as bias instability, dynamics dependence and white noise. Noise represents the overall uncertainty in the sensor model. These remaining errors are characterized by quasi-systematic and random types of behavior [Schwarz 1986]. They are often modeled as first-order Gauss-Markov or random walk processes with model parameters derived from lab experiments. The stochastic model is used to represent the remaining error effects after the systematic sensor errors have been removed by deterministic models and lab or field calibrations.

Various error sources contribute to the behavior of the errors of the inertial navigation system. They are due to sensor errors, initial navigation errors, vehicle dynamics, and the mechanization used. The local-level frame will be used for the mechanization of the inertial navigation system in this study. In this specific mechanization, the inertial navigation system can be looked at to have two horizontal channels and a vertical channel. For each channel, a position error, a velocity error and an attitude error are modeled; 9 all together for the three channels, the so-called the 9 Benson inertial navigation errors [Benson 1975, Maybeck 1997]. The simplified INS error model in Appendix A will be our vehicle to the following discussion.

In a *horizontal channel*, position, velocity, and leveling errors grow systematically but are bounded by the Schuler envelope, cf. Eqs. (A.10), (A.12), (A.13). The reason for the systematic error growth is the fact that navigation parameters (position, velocity, and attitude) are the outcome of integrating incremental linear velocity and angular velocity corrupted measurements with time; the sensor and initial errors are also integrated and contribute to the systematic navigation errors. The reason for the Schuler envelope in a horizontal channel is the interaction between the attitude errors and the velocity errors in the model, the $g\varepsilon$ and $\delta v/R$ terms in Eq. (A.4). Because it is integrated twice, position error is linearly dependant on time which causes the position to drift. For a navigation-grade INS, like the one simulated in appendix A, a Schuler envelope of 20" for the

leveling error, an envelope of 1 m/s for the velocity error, and an envelope of 1 km with a drift rate of 0.3 m/s for the position error are expected.

In the vertic*al channel*, position error is quadratic dependant on time while velocity error is linearly dependant on time; they both drift away as observation time elapses, cf. Eqs. (A.15, A.16). Because of the interaction between the azimuth misalignment (the vertical attitude error) with the horizontal velocity, the azimuth error grows systematically but is bounded by the Schuler envelope. It, however, has linear dependence on time which causes it to drift, cf. Eq. (A.18). For a navigation-grade INS, a Schuler envelope of 20" with a drift rate of about 0.002"/s for the azimuth error is expected. Velocity error and position error have no Schuler envelopes and they drift are expected to drift with a rate of 10^{-4} m/s^2 for velocity error and almost half this value plus 0.005 m/s for position error for the same navigation-grade INS.

Short-term error characteristics of the navigation errors is due to the propagation of the inertial sensors noise in the navigation parameters. Through the integration process, the measurement noise is reduced, resulting in smooth position, velocity, and attitude parameters. Under optimal dynamic conditions, like lab conditions, a navigation-grade INS is capable of a short-term position accuracy of better than 1 mm, velocity accuracy of about 1 mm/s, and attitude accuracy of about 3" after all Schuler-type errors have been eliminated [Schwarz and Wei, 1995b, Schwarz et al, 1993c]. The spectrum of the freely navigating inertial system is characterized by the Schuler frequency in the low-frequency band and by white noise in the high-frequency band as illustrated in Fig. (3.2).

3.1.3 The complementary nature of the INS system and the GPS system

From the discussion of §3.1.1 and §3.1.2, and that in Appendix A, the following can be concluded:

- GPS has long-term stability with a homogeneous accuracy
- The double differenced GPS measurement errors are mostly of high frequency nature and occupy a wideband in the high frequency spectrum

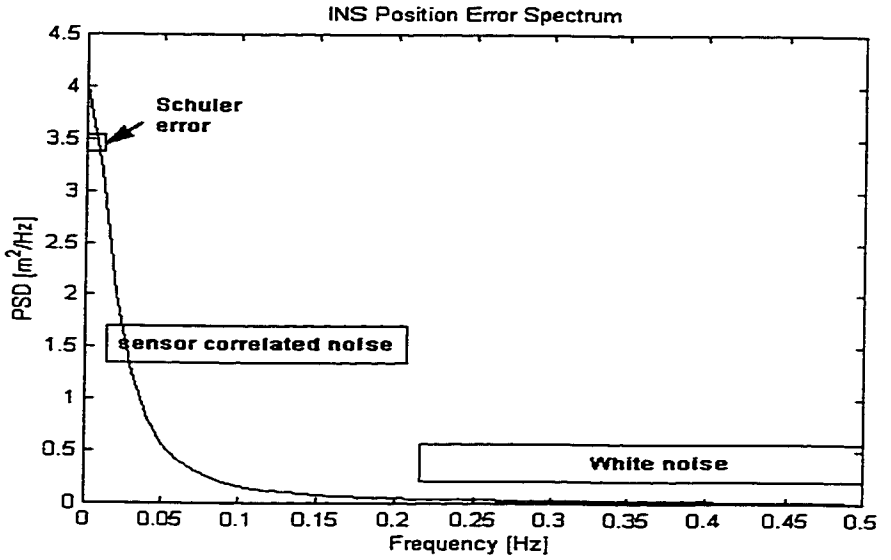

Fig. (3.2) : Spectrum of INS Position Error

- residual atmospheric, orbital, and multipath GPS errors occupy a rather wideband in the medium to low frequency spectrum (60 - 3000 s)
- the short-term stability of the INS system is excellent with high navigation accuracy
- INS stand-alone positioning accuracy deteriorates very rapidly with time
- navigation errors of the two INS horizontal channels are bounded by the Schuler envelope
- position and velocity drift away in the vertical channel, while azimuth, besides being drifting, is also bounded by the Schuler envelope
- INS Schuler-type errors occupy a narrow bandwidth in the low frequency spectrum (5000 s)
- the quasi-systematic errors of the INS system have a narrow bandwidth in the medium to low frequency spectrum

Therefore, for modeling the INS/GPS integrated system, the following assumptions can be made:

- For short baseline, where residual non-white errors can be neglected, GPS errors are white noise with flat spectrum
- INS Schuler-type errors are highly systematic and predictable in nature
- INS non-Schuler-type quasi-systematic errors are not predictable and need external aiding

Hence, in the estimation filter design, the following is assumed:

- DGPS errors are modeled as white noise
- INS Schuler-type errors are systematic and modeled according to their respective error models
- INS non-Schuler quasi-systematic errors are modeled as first-order Gauss-Markov processes, with the short-term errors modeled as white noise

It is, then, clear that the global positioning system and the inertial navigation system complement each other. On one hand, INS needs the long-term stability of GPS to have a handle on its non-predictable quasi-systematic errors. On the other hand, INS short-term highly-accurate positioning and attitude information provides trajectory interpolation between GPS updates. INS, also, fills between GPS signal outages and helps it recover after loss of lock, for short periods.

3.1.4 Error characteristics of the INS/GPS integrated system

The integration of the INS and GPS systems, makes the error spectra of the two data streams to overlap. GPS provides position and velocity information which are used to update INS through an integration filter, a Kalman filter. With frequent GPS updates, the error spectra of the navigation parameters of the integrated system change from that of the freely navigating INS system. Position and velocity error spectra of the integrated system become characterized by the error spectra of the GPS position and velocity errors because they are directly observable components of the filter. The Schuler loop configuration of the position and velocity errors of the INS horizontal channels is

destroyed. Attitude errors of the integrated system, however, retain a modified Schuler loop configuration because they are coupled with velocity errors, the term $g\varepsilon$ in Eq. (A.4). The coupling effect shows up in the INS/GPS Kalman filter through the gain matrix. In other words, the modified Schuler frequency of the INS/GPS attitude errors, ν', is a function of the original Schuler frequency, ν, and the respective attitude-velocity gain factor, K, and takes the form $\nu'=(\nu^2+K^2)^{0.5}$ [Schwarz and Wei, 1995b].

3.2 Kalman Filtering of the INS/GPS Integrated System

The Kalman filtering approach to the integration of inertial and GPS data is discussed in the following with special emphasis on the gain matrix and the innovation sequence.

3.2.1 INS/GPS complementary filtering

The discussion in §3.1 revealed the complementary nature of the errors of the INS and GPS systems. It is, therefore, natural to use linear complementary filtering (as opposed to quadratic complementary filtering, e.g. QMF) as an optimal integration technique of the two systems. In complementary filtering two filters are in use, one to pass high frequencies and its complement which passes low frequencies. For such a combination, where the transfer function of the high-pass filter (HPF) is denoted by $G_1(s)$, and the one of the low-pass filter (LPF) is denoted by $G_2(s)$, the two filters must have the following properties [Brown and Hwang, 1992, Levy 1996, Merhav 1996]:

$$\begin{aligned} &\lim_{s\to 0} G_1(s) = 0, \\ &\lim_{s\to \infty} G_2(s) = 0, \\ &G_1(s) + G_2(s) = 1, \end{aligned} \tag{3.4}$$

where s is the Laplace parameter and refers to the frequency domain.

In the INS/GPS complementary filtering setup, the same quantity, x, is measured twice, once by INS with a systematic low frequency error (e_1), and once by GPS with a high frequency noise (e_2). Fig. (3.3) below shows a schematic illustration of the situation.

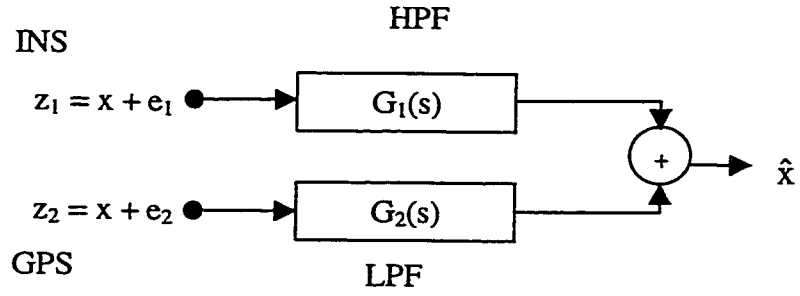

Fig. (3.3) : Complementary Filtering of INS/GPS Data

Denoting the gain of the LPF by G(s), the gain of the HPF becomes 1-G(s), and the filtered signal takes the form

$$\hat{x}(s) = x(s) + (1 - G(s))e_1(s) + G(s)e_2(s). \tag{3.5}$$

Eq. (3.5) shows that the INS narrow band error, e_1, is blocked by the HPF, 1-G(s), and the GPS wide band error, e_2, is low-pass filtered by G(s). This setup is equivalent to a differencing and feed-forward complementary filtering as in Fig. (3.4).

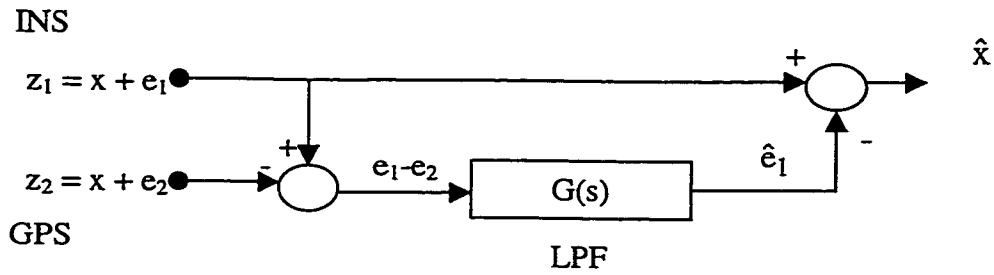

Fig. (3.4) : Feed-forward Complementary Filtering of INS/GPS Data

It will be shown later that the complementary filtering setup is equivalent to the INS/GPS Kalman filter used in this research.

3.2.2 Measurement and dynamics models

At the INS/GPS Kalman filter where both streams of information are fused, both measurement and dynamics models interact. The *measurement model* in a generic form is

$$z = H x + v \tag{3.6}$$

where,

z : filter measurements

x : filter states

H : measurement design matrix

v : measurement noise.

In the case of the INS/GPS error filter formulation, it results by differencing the INS navigation information from that of the GPS [KINGSPAD 1994]

$$\begin{aligned} z &= X^{INS} - X^{GPS} \\ &= (X + \delta x + n^{INS}) - (X + n^{GPS}) \\ &= \delta x - e_z \end{aligned} \tag{3.7}$$

where,

X : navigation information

δx : INS navigation error state vector

$e_z = n^{INS} - n^{GPS}$: measurement model noise.

The *dynamics model* comprises two types of error states, the navigation error states which result from mechanizing the INS in the computational frame and the sensor error states. The former are a function of the vehicle dynamics and the Earth's rotation and gravity field. The dynamics model takes the following generic form

$$\dot{x}_k = F x_k + w_k, \tag{3.8}$$

where,

$\dot{x}$: the time derivative of x at epoch k

F : the dynamics matrix

w : the process noise.

In a local-level frame, it takes the form [Schwarz and Wei, 1994]

$$\begin{aligned}
\delta\dot{p}^l &= \delta v^l \\
\delta\dot{v}^l &= -F^l\varepsilon^l + R_b^l b_A - (2\Omega_{ie}^l + \Omega_{el}^l)\delta v^l + V^l(2\delta\omega_{ie}^l + \delta\omega_{el}^l) + \delta\gamma^l \\
\dot{\varepsilon}^l &= -\Omega_{il}^l\varepsilon^l - \delta\omega_{il}^l + R_b^l b_G
\end{aligned} \tag{3.9}$$

where,

the superscripts* b, l, e : represent the body (measurement), local-level (navigation), and earth-fixed (geocentric) frames

δp, δv, ε : position, velocity, and attitude INS errors

F, V, R_b : matrices describing specific force (measured), vehicle velocity and attitude

Ω_{ie}, Ω_{il}, Ω_{el}, $\delta\omega_{ie}$, $\delta\omega_{il}$, $\delta\omega_{el}$: Earth's rotation, local-level-to-inertial, and local-level-to-earth frame rotation rates and their respective errors

b_A, b_G : accelerometer and gyro biases

$\delta\gamma$: normal gravity error.

Appendix A gives a simplified form of this system of differential equations. Details of the mechanization in different computational frames and the derivation of the dynamics matrix can be found in [Britting 1974, Schwarz and Wei, 1994].

3.2.3 Structure of the INS/GPS integration Kalman filter

Data processing, in the developed INS/GPS filtering algorithm, is divided into two stages. In the first stage, GPS data is filtered in a local filter and a local best estimate of the positioning information is sought. The GPS local estimate is then fused with the INS data in a master filter to obtain the best global estimate of the filter state vector [Wei and Schwarz, 1990]. Advantages of this approach are a flexible combination of GPS and INS

* For simplicity, when the superscript is omitted, it is assumed to be 'l', the local-level frame.

and higher processing speed because two smaller parallel Kalman filters replace one large Kalman filter [Schwarz and Wei, 1994]. A disadvantage is that covariance information from the GPS filter is required for an optimal solution, otherwise the solution will be sub-optimal. One limitation of this approach for GPS/INS integration is that at least four satellites are required to provide acceptable GPS update for the INS. The general structure of the used filter is shown in Fig. (3.5) below.

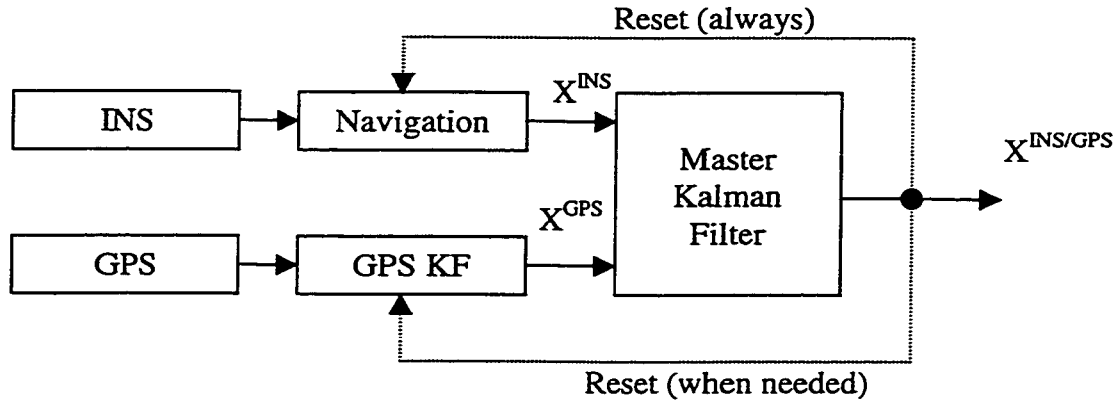

Fig. (3.5) : INS/GPS Kalman Filter Structure

The main integration procedure and the master Kalman filter are shown in Fig. (3.6) below.

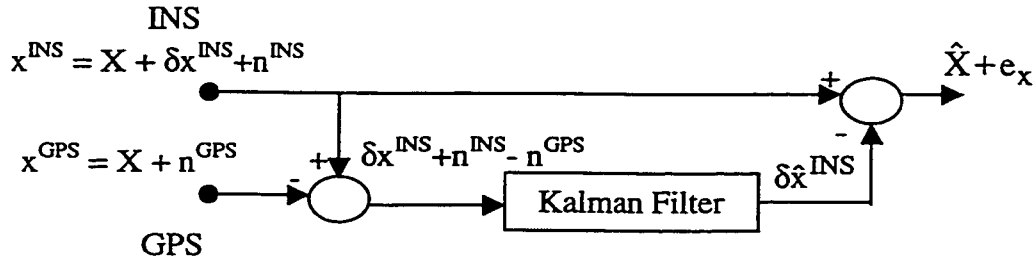

Fig. (3.6) : INS/GPS Integration Procedure and Master Kalman Filter

In Fig. (3.5) above, a GPS reset is required when carrier phase cycle slips occur. While the INS reset happens all the time because it prevents the navigation errors from growing beyond the limit where the linearity assumption of the Kalman filtering still

valid. It closes the error growth estimation loop in an extended Kalman filter formulation fashion. The Kalman filter estimation model takes the form

$$\dot{x}_k = Fx_k + K_k(z_k - Hx_k) \tag{3.10}$$

in continuous time, and in discrete time as

$$x_k = \Phi x_{k-1} + K_k(z_k - H\Phi x_{k-1}) \tag{3.11}$$

where F is the dynamics matrix and Φ is the transition matrix. More discussion on the INS/GPS Kalman filter structure can be found in [Wei and Schwarz, 1990], and details of the filter used in this research is found in [KINGSPAD 1994].

The mathematical equivalence of the structures of the complementary and the INS/GPS Kalman filters of Figs. (3.4) and (3.5) is given in [Merhav 1996]. In the following, a brief description of this mathematical argument will be given. According to Eq. (3.7), the two streams of navigation information from the INS mechanization and the GPS Kalman filter output are differenced, where the low frequency component common to both systems, X in Eq. (3.7), is attenuated, i.e. the signal is high-pass filtered. The remaining errors are essentially the noise and quasi-systematic errors of the INS system with wavelength shorter than the high-pass filter and the GPS Kalman filter estimation noise. Since a Kalman filter is essentially a low-pass filter [Hammada 1996], the high-frequency error (noise) of the mixed INS/GPS measurement is attenuated when it passes through the master Kalman filter. Therefore, the Kalman filter in the INS/GPS Kalman filter structure (Fig. (3.6)) has the role of the low-pass filter of the complementary filter (Fig. (3.4)). The estimate of the filter in this structure (the LPF in the complementary filter structure) is then feedback to the INS system navigation output to adjust it. It closes the estimation loop and results in the adjusted navigation information.

3.2.4 Kalman gain

The two issues central to the integration Kalman filter, considering error state integration formulation, are the gain matrix and the measurement (innovation) sequence; the latter will be discussed in the next section. To understand the meaning of the gain matrix, let H in Eq. (B.25) be equal to the identity matrix, i.e. the elements of the state vector are directly measured. Further, assume that the matrix R is diagonal. In this particular case, each element of the gain matrix, K_k, at epoch k, is essentially the ratio between the statistical uncertainties (variances) in the state estimate error and the measurement noise, i.e. (Eq. (B.25))

$$K_k = \frac{\sigma_x^2}{\sigma_z^2}. \tag{3.12}$$

Eq.(3.12) states that the gain factor can be interpreted heuristically as a signal to noise ratio [Maybeck 1996]. If the measurement noise σ_z^2 is large and the state estimate error σ_x^2 is small, the gain will be small and consequently, the changes in the state estimates will be small; the opposite is also true.

The gain of a state that is not directly observed in the filter, e.g. an attitude state when only position and velocity are observed, is a function of its degree of correlation with the measurement state. For a diagonal measurement matrix and a direct measurement design matrix with ones and zeros, such as the case of the INS/GPS integrated system, the indirect state gain takes the form

$$K_{xx_z} = \frac{\sigma_{xx_z}}{\sigma_z^2}, \tag{3.13}$$

where, σ_{xxz} is the covariance between the unobserved state, x, e.g. attitude, and the observed state, x_z, e.g. velocity, through the measurement, z. The gain, in this case, can also be interpreted as a signal to noise ratio. However, only the part of this ratio that is

transferred through the correlation coefficient will contribute to the gain. In other words, the gain of a directly observed state can be thought of as a signal to noise ratio that is completely transferred with a complete correlation, i.e. a correlation of 1.

Another insight can be gained by looking at Eq. (B.21) when, again, H is set to identity. In this case, the gain at epoch k is related to the measurement noise variance σ_z^2 and the initial state variance σ_o^2 as follows [Gelb 1974, Salychev 1994]:

$$K_k = \frac{\sigma_o^2}{k\sigma_o^2 + \sigma_z^2} = \frac{1}{k + \frac{\sigma_z^2}{\sigma_o^2}} = \frac{\frac{\sigma_o^2}{\sigma_z^2}}{1 + k\frac{\sigma_o^2}{\sigma_z^2}}. \tag{3.14}$$

If our a priori knowledge about the initial state is poorer than the information provided by the update measurement, i.e. $\sigma_o >> \sigma_z$, each new update measurement will provide vital information to the filter. Sufficiently large estimation time, however, is needed for the gain to reach steady state, i.e. the transition stage will be quite long. On the other hand, when $\sigma_o << \sigma_z$, the transition stage will be shorter because the new information provided by the update measurement does not add much to our knowledge about the initial state.

In reality, no system model is perfect. When the system process noise matrix, Q, is added to the stochastic model, the gain is obtained as follows:

$$K_k = \frac{\sigma_o^2 + q_x^2}{k\sigma_o^2 + kq_x^2 + \sigma_z^2} = \frac{1 + \frac{\sigma_o^2}{q_x^2}}{k + k\frac{\sigma_o^2}{q_x^2} + \frac{\sigma_z^2}{q_x^2}}. \tag{3.15}$$

Again, if our certainty in the dynamics model is poor relative to our a priori knowledge of the initial state and the quality of the update measurement, i.e. $q_x >> \sigma_o$ and $q_x >> \sigma_z$, a large estimation time will be needed until the gain reaches steady state. However, when our trust in the dynamics model is high, i.e. when the process noise is small relative to the

measurement noise, the a priori information about the initial state, q_x can be ignored in Eq. (3.15) and the analysis carried out on Eq. (3.14) can be applied.

The above equations and the general formulation in Appendix B for the gain matrix show a major drawback of the conventional Kalman filter formulation where the measurement noise covariance matrix, R, and the system noise covariance matrix, Q, are kept constant. At steady state, the filter gain remains constant regardless of the changes in the system dynamics or the update measurement quality. This problem is solved by arranging for the variation of R and/or Q in an adaptive manner; this will be discussed in details later.

3.2.5 Kalman filter innovation sequence and the filter learning history

The other central issue of the integration Kalman filter is the measurement innovation sequence. In principle, the innovation (new information) sequence at different instants is uncorrelated. At the current time k, the new observation does not really provide completely new information because some of the information is obtained by prediction from previous filter states. Hence, the innovation sequence represents the information content in the new observation and is considered as the most relevant source of information for the filter adaptation [Kailath 1972, 1981]. In the Kalman filter error state formulation, however, the prediction step is not needed and the difference between the INS and GPS measurements represents the innovation sequence, see the discussion at the end of Appendix B. In fact, both the innovation sequence and the measurement sequence contain the same statistical information and are equivalent as far as linear operations are concerned [Mehra 1970].

Based on Eq. (B.19), the innovation sequence can be expressed as follows

$$v_k = e_{z_k} - He_{x_k} . \tag{3.16}$$

The above equation shows clearly that the innovation sequence contains information about the system error, e_x, and the measurement error, e_z. Both the system and the

measurement errors are assumed to be Gaussian and white. This property is transferred to the resulting innovation sequence because of the linear operation in Eq. (3.16). In other words, the innovation sequence is also a Gaussian white sequence provided that the filter is optimal. In fact, this property of the innovation sequence is used to check the optimality of the Kalman filter [ibid.]. On the other hand, observing the innovation sequence during the evolution of the estimation process is like observing the learning history of the filter. In other words, the innovation sequence contains the necessary information about the filter error propagation [ibid.]. This last property makes the innovation sequence a very good candidate for filter self tuning or adaptation. This will be discussed in detail in the next chapter.

3.2.6 Kalman filter bandwidth

The Kalman filter estimate in the continuous time domain is given by Eq. (3.10) and is repeated here for convenience

$$\dot{\hat{x}}(t) = F\hat{x}(t) + K(z(t) - H\hat{x}(t)),$$

$$\text{or, } \dot{\hat{x}}(t) + (KH - F)\hat{x}(t) = Kz(t).$$

The frequency-domain representation of the above system (differential equation) is given by its Laplace transform as follows

$$(sI + (KH - F))\hat{x}(s) = Kz(s), \tag{3.17}$$

where, t is the time-domain (time) parameter, and s is the frequency-domain (Laplace) parameter. Therefore, the frequency-domain representation of the transfer function of the Kalman filter (the ratio between the output and input of the filter) is computed as follows

$$H(s) = \frac{\hat{x}(s)}{z(s)} = \frac{K}{sI + (KH - F)}. \tag{3.18}$$

Eq. (3.18) represents a transfer function for a low-pass filter. As discussed in §3.2.1 and §3.2.3, the Kalman filter plays the role of a low-pass filter in the INS/GPS complementary filter structure. Therefore, the Kalman filter bandwidth or cut-off frequency, ω_c (the frequency at which the transfer function becomes half its maximum value), can be computed as follows

$$\omega_c = KH - F. \tag{3.19}$$

It is clear, from the above equation, that the error model dynamics, the measurement model design, and the filter gain determine the bandwidth of the Kalman filter. Since, in the case of the INS/GPS filter structure discussed in §3.2.3, both of the error model dynamics matrix and the measurement model design matrix are time-invariant, only the Kalman gain matrix has the major effect in determining the filter bandwidth. In other words, one can use the two terms, the Kalman filter bandwidth and the Kalman filter gain, interchangeably to mean the same thing. Since the filter gain can be interpreted as a signal to noise ratio, the Kalman filter bandwidth can be seen to change with the quality of the update measurement, i.e. the better the quality of the update measurement, lower variance, the bigger the filter gain and the larger the bandwidth of the filter will be.

3.3 A priori Information and its Role in INS/GPS Kalman Filtering

To start off the Kalman filter, a priori information needs to be known. While dynamics and measurement models provide the deterministic information required by the filter, the filter stochastic a priori information is provided by the a priori covariance matrices of the parameters of the models. In addition to the system transition matrix, Φ, and the measurement design matrix, H, four other information quantities are required to start off the filter, namely, the initial state vector, x_o, the initial state error covariance matrix, P_o, the measurement noise covariance matrix, R, and, the system noise covariance

matrix, Q. At epoch k, the a priori information errors propagate into the Kalman filter and results in the following state estimation error [Salychev 1998]

$$e_{x_k} = e_{x_0} \prod_{i=1}^{k} (A_i \Phi) + \sum_{j=0}^{k-2} \{ e_{x\,k-j-1} A_{k-j} \prod_{i=1}^{j} (A_i \Phi) \} - \sum_{j=0}^{k-1} \{ K_{k-j} e_{z\,k-j} \prod_{i=1}^{j} (A_i \Phi) \}, \tag{3.20}$$

where, $A_i = I - K_{k+1-i} H_k$ is always smaller than identity. Consequently, the product, $\Pi(A_i \Phi)$, decreases with time and acts as an attenuation factor in the above expression. It shows that the Kalman filter is a stable filter with decreasing bounded errors. For an optimal filter state estimate, the filter, eventually, attenuates the initial state errors, e_{xo}. It also smoothes the effect of the system errors, e_x, and that of the measurement errors, e_z, through the averaging process, Σ.

A priori information about the *initial state vector, xo*, is of secondary importance to the Kalman filter algorithm; it has no influence on the filter output at steady state and only determines the start of the transition stage of the filter before the filter reaches steady state. In fact, Kalman filter optimality is not affected by the choice of the initial state value [Gelb 1974]. In the case of INS/GPS error state formulation, the initial state vector of the navigation parameters is of no influence because it is reset to zero at the start of every estimation cycle after the navigation parameters have been corrected in the closed loop. They are usually initialized to zero. However, due to their slow variation and their weak observability in the filter, the accelerometer and gyro bias initial states are important. Their initial values are determined in lab calibration tests by observing their average values in a stationary situation.

The *initial state error covariance matrix, Po*, characterizes the uncertainty in the initial state value. It plays a role in the transition stage of the filter, but has no role once the filter reaches steady state. A large value of Po allows for tolerance in the variation of the state vector at the transition stage. A very large value of P_o, however, means large uncertainty in the initial state and is essentially telling the filter to ignore that value.

Again, in the case of INS/GPS error state formulation, the P_0 value of the navigation parameters is of little importance, while those of the accelerometer and gyro biases are important. Their values are determined in lab calibration tests by observing their variances in a stationary situation.

The *measurement noise covariance matrix*, *R*, is of great importance to the optimality and significance of the Kalman filter output. It describes how well the measurement model is and how good the measurements are. The shortcoming of the mathematical model is usually due to either non-modeling, mismodeling, or ignoring one of the non-white (colored or correlated) measurement errors. This type of error propagates in the Kalman filter algorithm through the measurement covariance matrix and results in a state covariance that is more optimistic than reality. In effect, the non-whiteness of the measurement errors, which contradicts one of the Kalman filter assumptions, results in a sub-optimal behavior of the filter. The other part of the measurement error is due to noise. Usually, one can get an estimate of the measurement covariance matrix by observing raw measurements in a stationary situation. Recall that in the case of the INS/GPS Kalman filter, the measurement is the difference between the navigation output of the GPS filter and the INS navigation resulting from mechanizing the accelerometer and gyro measurements in the computational frame. In this case, the GPS filter covariance matrix is used as measurement covariance matrix of the INS/GPS filter.

If the accelerometers and gyros of the INS system exhibit no noise and the process can be described (modeled) deterministically with absolute accuracy, the *system noise covariance matrix*, *Q*, can be simply set to zero. A 15-state INS model is just a simplified version of the truth model which may contain more than one hundred states [Maybeck 1997]. Sensors always exhibit noise; no sensor manufacturing is perfect. Consequently, the role of the Q matrix, in the Kalman filter, is to define the width of the uncertainty tube after each prediction step. In other words, it defines to what extent prediction should be trusted. A large value of Q essentially enlarges the uncertainty tube and results in a noisy estimate. A smaller Q, on the other hand, results in a smoother estimate, that may,

however, be biased. Although the Kalman filter does not restrict a certain value of Q to guarantee optimality [Gelb 1974], a correct value of Q is critical for achieving practically sound results. The correct value of Q depends on factors such as system dynamics and sensor noise level. In order to numerically calculate Q, the integral of Eq. (B.4) need to be evaluated over the sampling period. For that to happen, the system noise spectral density, P, has to be known. Recall from Chapter Two that the spectral density of a process is the Fourier transform of its auto-correlation function. The raw output of the INS accelerometers and gyros are observed and the auto-correlation function is calculated against pre-determined time lags. The data points of the auto-correlation function are then fitted to a first-order Gauss-Markov model, and the model parameters, namely, the process noise power σ_0^2 and the process correlation length β, are determined. The power spectral density of the process, P, can then be calculated using [Gelb 1974]

$$P = 2\beta\sigma_0^2. \tag{3.21}$$

The evaluation of the integral can be done numerically. For sufficiently small sampling intervals, the integral can be approximated by its first-order term, i.e.

$$Q = PT \tag{3.22}$$

or, its second-order terms

$$Q = [P + \Phi P \Phi^T]\frac{T}{2}. \tag{3.23}$$

In case the sampling period is not small enough for the above approximation, it can be subdivided into smaller intervals, δT, and Q can be updated recursively as follows [Brown and Hwang, 1992]

$$Q_i = \Phi Q_{i-1} \Phi^T + \Delta Q, \tag{3.24}$$

where, ΔQ and Φ are calculated according to the interval δT and the initial Q_o could be set to zero.

The measurement noise covariance matrix and the system noise covariance matrix are important to the optimality of the Kalman filtering algorithm. Their mutual interaction with the state covariance can be clearly observed through Eq. (B.24) which in the scalar case takes the form

$$\frac{1}{\sigma^2_{x(+)}} = \frac{1}{\sigma^2_{x(-)}} + \frac{1}{\sigma^2_z}, \tag{3.25}$$

which is called the propagation of information equation (as opposed to error propagation) [Levy 1996]. It is clear from the previous equation that the updated state is better than the predicted state by the amount of information added by the update measurement. The predicted state covariance is affected by the Q matrix, while the update measurement covariance is R. They both determine the quality of the estimated state. They both are vital to the Kalman filter algorithm and in order to get practically sound results, they both should be set to the values that reflect the actual situation.

3.3.1 INS/GPS non-stationarity and its effect on filter formulation

The conventional Kalman filter algorithm, after a transition stage, goes in a steady state mode where it stops paying attention to new measurements. The filter does so because it either overweighs its prediction, Q problem, or underestimates new measurements, R problem, or both. The result of such filter behavior is an unrealistic estimation of the gain and state covariance and, consequently, filter divergence [Gelb 1974]. In other words, the filter precision becomes unreliable. On the other hand, non-stationarity of the process, which is not accounted for in the filter formulation, adds another dimension to the filter divergence problem. When actual process changes occur, incorrectly estimated gain results in an incorrect state estimate. In other words, the filter estimate, in this case, becomes biased.

To get meaningful (reliable) filter precision, the filter gain needs to be correctly estimated. One way of getting realistic estimates of the gain is to account for changes in the filter's current measurement. An overweight of the gain can be calculated and added to the regular Kalman gain based on weighting the filter residuals. The state estimate and its covariance matrix can then be corrected accordingly [Schmidt 1970]. Another approach to tackle the problem is to use a moving window to weight past measurements and correct the gain accordingly; this is called age weighting [Miller 1971]. One manner of accomplishing this is to pump up the measurement covariance matrix, R, with an empirically derived exponential weighting function of predefined window size [ibid.]. These two methods for practically non-diverging Kalman filters, though sound, are not rigorous. The adaptive Kalman filtering approach, however, tackles the same problem and is rigorous at the same time [Mehra 1970, Maybeck 1982].

3.4 Adaptive Filtering

In conventional Wiener (or least squares) filtering, a priori information about the statistics of the processed data is required. The difference between some desired response and the actual filter output is minimized, in a mean-square sense. Optimality of the filter output is defined by this minimization process. Wiener filtering requires the input signal to be stationary and results in constant filter taps or coefficients. If the a priori statistical information is unavailable or the input signal is non-stationary, conventional Wiener filter theory cannot be applied. In such situations, adaptive filtering methods provide a solution to the filtering optimization problem. A wide variety of recursive algorithms have been developed for the operation of linear adaptive filters. The choice of one algorithm over another is determined by factors such as the rate of convergence, misadjustment, tracking, robustness, computational requirements, structure, and numerical properties [Haykin 1996]. On the other hand, the three types of filter structures that distinguish themselves in the context of finite memory adaptive filtering are the transversal filter, the lattice predictor, and the systolic array, see [ibid.] for an extensive discussion of adaptive filter theory.

The four basic classes of adaptive filtering applications are: system identification, inverse modeling, prediction, and interference canceling [ibid.]. In the first two applications, the adaptive filter is used to provide a linear model that represents the best fit, in some sense, to either an unknown system or an unknown noisy system; these two applications are beyond the scope of this research and will not be pursued further. In the prediction application, the adaptive filter is to provide the best prediction, in some sense, of the present value of a random signal. Among others, the conventional Kalman filter falls in this category. In fact, the Kalman filter provides the general framework for deriving all of the known algorithms that constitute the recursive least-squares family of adaptive filters [Sayed and Kailath, 1994]. The final class of applications is interference canceling where the adaptive filter is used to cancel unknown interference contained in a primary signal with the cancellation being optimized in some sense.

Other than Kalman filtering, the other class of application that is of interest to this research in adaptive filtering is interference canceling. The concept of adaptive filtering for interference canceling is illustrated in Fig. (3.7) below

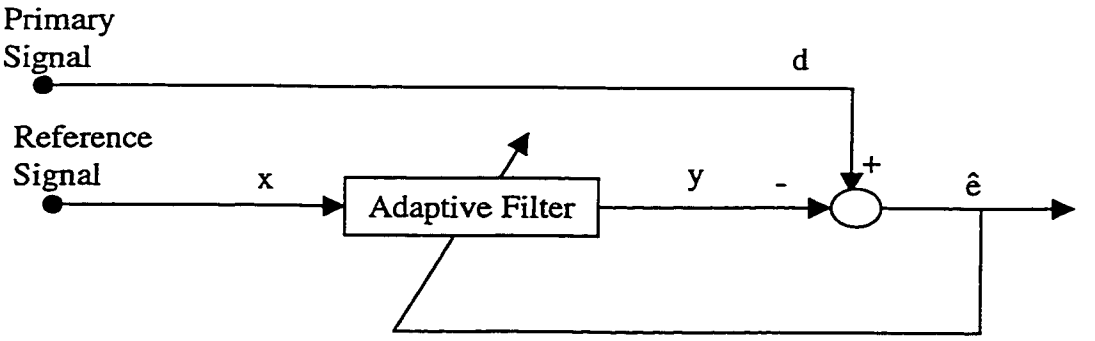

Fig. (3.7) : Concept of Adaptive Filtering

where, x is the filter input, y is the output of the adaptive filter, and $d = s + n$, is the desired response, for which s is the useful signal and n is noise; $e = d - y = s + n - y$, is the estimation error (system output).

In this structure, the primary signal serves as the desired response of the adaptive filter. It has, in addition to the noise, a weak or essentially undetectable information-

bearing (useful) signal component. A reference signal, derived from another source, is employed as the input to the filter. The noise of the reference signal is correlated with the noise of the primary signal while it should be uncorrelated with the primary signal information-bearing component. The error signal at the system output is feedback into the adaptive filter to train it and adjust its tap weights [ibid.]. Ideally, minimizing the error signal in some statistical sense, should result in an error signal very close to the useful signal in the primary signal. In other words, the job of the filter is to output a signal, y, that has the same interference noise characteristics, n, and cancels its effect.

3.4.1 Adaptive filtering applications in geomatics

Two main application areas are distinguished in the context of navigation with INS/GPS systems: direct georeferencing of imaging systems from moving vehicles and precise estimation of the anomalous gravity field. In the first application area, where typically INS and GPS are used as navigational sensors to aid a mapping system, a model-based estimation technique is used. In this case, navigation information from both sensors is integrated, usually at the position level, for optimal georeferencing of the imaging sensor. For instance, in mobile multi-sensor systems, where position and attitude information is of primary interest, a model-based filtering technique is required [Schwarz 1998]. In the second application area, however, acceleration from both INS and GPS is required to precisely estimate the anomalous gravity field. In such a situation, non-model based filtering methods become of primary interest. For instance, in an airborne gravimetry system, however, where acceleration is of primary interest, non-model based filtering techniques may outperform a model-based approach [Hammada 1996]. They also can be used as an aid to a model-based technique to assist reducing the measurement noise, see e.g. [Bruton 1997, Bruton and Schwarz, 1997].

Some of the available adaptive filtering methods are possible candidates for geomatics applications, some are not. For instance, methods targeting system identification and inverse modeling problems are excluded because of the different nature of the application. Model-based and non-model-based adaptive estimation methods are

appealing to the geomatics field. Two application areas are identified: interference canceling and prediction.

Interference canceling, as described previously, cannot stand alone as a solution for the navigation problem. It is, however, most appealing to the problem of noise reduction at the navigation sensor measurement level. For instance, in [Zhang 1997] an adaptive noise canceling method is used to model GPS clock drift and track the changes in an aided GPS augmented vehicular navigation system. In [Bruton and Schwarz, 1997] an adaptive noise canceler is used to reduce GPS acceleration noise for an airborne gravity system.

For the prediction problem, the Kalman filter provides the general framework for deriving the known algorithms that constitute the recursive least-squares family of adaptive filters [Sayed and Kailath, 1994]. In other words, one can consider the conventional Kalman filter as the fundamental tool for solving the prediction/filtering problem in an adaptive manner. All the other adaptive least squares filtering methods are subsets of the Kalman filtering [ibid.]. That is probably the major reason for using the Kalman filter in the navigation community, see the extensive literature about Kalman filtering and its applications in navigation. Adaptive Kalman filtering, on the other hand, adds another dimension to the concept of adaptivity in the transition stage by allowing for adaptivity of the whole estimation process.

3.5 Adaptive Kalman Filtering

In the context of adaptive Kalman filtering, the uncertain parameters that need to be adapted may be part of the system model through the state transition matrix Φ, of the measurement model through the design matrix H, or of the filter statistical information through the covariance matrices R and/or Q. The first two cases are more likely to occur in problems where system design/identification or inverse modeling is of concern. In this research, it is assumed that the INS/GPS system model used is sufficient for the intended

applications. Therefore, adaptive Kalman filtering throughout this research is restricted to adapting the filter covariance matrices R and/or Q.

3.5.1 Approaches to adaptive Kalman filtering

The two major approaches to adaptive Kalman filtering are multiple model adaptive estimation (MMAE) and innovation-based adaptive estimation (IAE). They both share the same concept of utilizing the new information in the innovation (or residual) sequence but differ in their implementation. The innovation sequence v_k at epoch k in the Kalman filter algorithm is the difference between the real measurement z_k received by the filter and its predicted value $z_k(-)$, see Appendix B for formulas. At the current time k, the new measurement z_k does not really provide completely new information because some of the information is obtained by prediction from previous filter states. Hence, the innovation sequence represents the information content in the new measurement and is considered as the most relevant source of information for the filter adaptation, see [Genin 1970, Kailath 1972 and 1981] for a more detailed discussion of the innovation sequence and its use in linear filter theory.

In the context of Adaptive Kalman filtering, the innovation sequence is used to derive the measurement weights either through multiple models, the MMAE approach, or the R and/or Q covariance matrices, the IAE approach. It is, however, preferable in estimation problems to derive the second moment information about the measurement from an independent source. The independent second-moment information guarantees the unbiasedness of the estimation scheme. In practice, an independent source of information is not always available and one usually opt for procedures like the two described in the following two sections. The cost is a high likelihood of getting a biased solution. In general, that is not a problem as long as one is aware of the possible consequences of a biased solution.

3.5.1.1 Multiple model adaptive estimation

In the multiple model adaptive estimation (or parallel-filter) approach , a bank of Kalman filters runs in parallel [Magill 1965, Maybeck 1989, Brown and Hwang, 1992, White 1996, Gary and Maybeck 1996, White et al.1996] or with a gating algorithm [Chaer et al, 1997] under different models for the statistical filter information matrices, i.e. the process noise matrix Q and/or the update measurement noise matrix R. The structure of each filter in the bank of filters is depicted in Fig. (3.8) and the final estimate of the bank-of-filters is explained in Fig. (3.9).

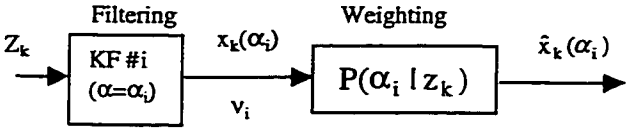

Fig. (3.8): The Estimate of the ith Filter in the MMAE

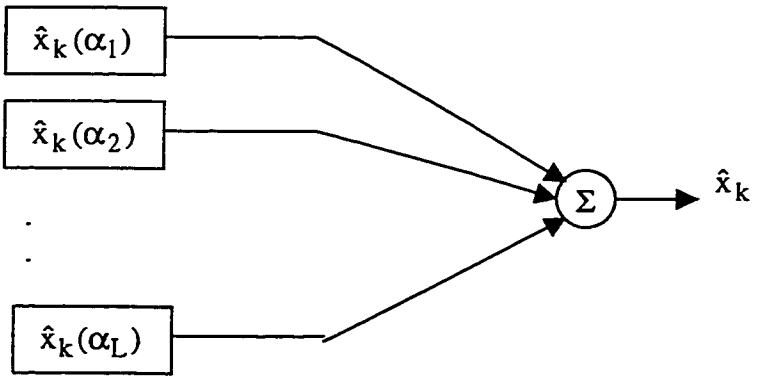

Fig. (3.9): The Estimate of the Bank of Filters in the MMAE

In every run, each filter of the bank will have its own estimate $\hat{x}_k(\alpha_i)$. At the first epoch, the bank of filters receives the first measurement z_o, and the $P(z_o|\alpha_i)$ distribution is computed for each permissible α_i. At each recursive step the adaptive filter does three things:

1. Firstly, each filter in the bank-of-filters computes its own estimate, which is hypothesized on its own model,
2. Secondly, the system computes the a posteriori probabilities for each of the hypotheses,
3. Finally, the scheme forms the adaptive optimal estimate of x as a weighted sum of the estimates produced by each of the individual Kalman filters as

$$\hat{x}_k = \sum_{i=1}^{L} \hat{x}_k(\alpha_i) P(\alpha_i \mid z_k), \tag{3.26}$$

where $P(\alpha_i|z_k)$ is the weight of the i^{th} filter when measurements z_k up to epoch k are available; α_i is an unknown random variable with known statistical distribution $P(\alpha_i)$, which drives the adaptive process of the filter, and L is the total number of filters used.

As measurements evolve with time, the adaptive scheme learns which of the filters is the correct one, and its weight factor approaches unity while the others are going to zero. The bank of filters accomplishes this, in effect, by looking at the sums of the weighted squared measurement innovations or residuals. The estimate of the filter with the smallest sum receives the highest weight and, in effect, prevails.

In the MMAE approach, the fact that a bank of filters are required to run in parallel adds considerably to the computational complexity of the INS/GPS integration algorithm. Even with a gating technique, the algorithm will need to process different statistical models for every estimation epoch. Therefore, the MMAE approach is not suitable for formulating the INS/GPS adaptive integration navigation problem for the geomatics applications. It is, however, successfully used in tracking problems where two parallel filters run simultaneously in a yes/no fashion [Girgis and Brown, 1985, White 1996, Gary and Maybeck 1996, White et al.1996].

3.5.1.2 Innovation-based adaptive estimation

In the innovation-based adaptive estimation (IAE) approach [Mehra 1970, 1971, Kailath 1972, Maybeck 1982, Salychev 1994], the covariance matrices R_k and Q_k themselves are adapted as measurements evolve with time. Based on the whiteness of the filter innovation sequence, the filter statistical information matrices are adapted as follows:

$$\hat{R}_k = \hat{C}_{v_k} - H_k P_{k(-)} H_k^T \tag{3.27}$$

and

$$\hat{Q}_k = K_k \hat{C}_{v_k} K_k^T \tag{3.28}$$

where $P_k(-)$ and K_k are the state covariance matrix before update and the gain matrix, respectively. Knowing the innovation sequence, one can compute the innovation covariance matrix, $\hat{C}_{v_k}$, at epoch k, through averaging inside a moving estimation window of size N as follows

$$\hat{C}_{v_k} = \frac{1}{N} \sum_{j=j_0}^{k} v_j v_j^T , \tag{3.29}$$

where $j_0 = k-N+1$ is the first epoch inside the estimation window. In order to account for such an adaptive approach in the Kalman filter algorithm, an additional block for computing the innovation covariance matrix and both Q and R has to be added as shown in Fig. (3.10). Details of this approach will be discussed in the next chapter.

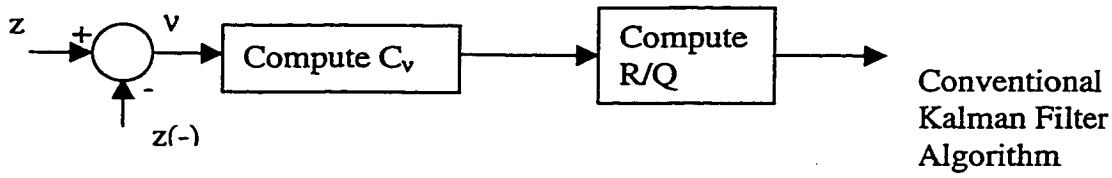

Fig. (3.10): The Innovation Process in the IAE Algorithm

Besides its simplicity, the IAE approach adds little computational complexity to the INS/GPS integration algorithm. Based on many computer runs of different INS/GPS data sets, the time added for the computation of the adaptive blocks in the IAE approach does not exceed 5% of the original processing time of the conventional Kalman filter. When compared to the time required to run parallel filters simultaneously in the MMAE approach, considerable computational time saving is achieved with the IAE. Therefore, IAE is chosen as the adaptive approach to formulating the INS/GPS integration problem in this research.

In some real-time applications where computation time is a major concern, one might opt for approximating the R and/or Q models according to the expected dynamics of the trajectory. For instance, in trajectories which have straight lines and curves, one might derive simple models for R and/or Q for each case and apply the appropriate models according to the trajectory situation. If such a simplification does not add to the overall performance of the adaptive Kalman filter, it is always recommended to use the on-line epoch-by-epoch adaptive solution described above as it guarantees a better automatic solution over the simplified models. On the other hand, if on-line (real-time) processing of the data is not needed and post-mission processing is possible, backward smoothing is recommended. It will correct the problem of overweighing parts of the trajectory over others, e.g. when changing from a straight line segment to a curve. If optimal smoothing is used, the adaptive Kalman filter is not expected to considerably outperform the conventional Kalman filter because the information gained by the AKF will, generally, be substituted by backward smoothing in case of the CKF. Since this research is only concerned with real-time applications, backward smoothing is not pursued in this dissertation.

3.5.2 Adaptive Kalman filtering vs. adaptive filtering

Although adaptive filtering and adaptive Kalman filtering handle the navigation problem in a similar manner, they are different in the way they define and implement adaptivity. Given the fact that recursive least squares (RLS) adaptive filter is a subset of

the more general framework of Kalman filters, there still are some important differences between the two approaches. Adaptivity in the context of RLS filtering affects mostly the transition stage of the filter. The RLS adaptive filter looks for the optimal filter tap weights in the transition stage (learning stage) by minimizing the mean square error of the filter. Once the tap weights reach their optimal value, the filter has reached steady state, and the adaptive stage is finished. This is similar to what happens in conventional Kalman filtering. The adaptive Kalman filter, on the other hand, differs from the conventional adaptive filter in the sense that adaptivity never stops as long as dynamics or measurement statistics change. Both the conventional Kalman filter (and consequently RLS adaptive filters) and the adaptive Kalman filter tune the filter estimate by looking at the state estimation error. In addition, the adaptive Kalman filter use the innovation sequence to further tune the filter estimate based on real-world changes. This makes the filter alert to change the filter gain (tap weights) even after the filter reaches steady state.

Estimation problems (as opposed to prediction problems) in conventional adaptive filters require another source of information to exist in addition to the original signal in order to provide the filter with the training sequence. The training sequence is a key element in adaptive filtering in that it is the means by which the filter adjusts its tap weights in the transition stage. Kalman filtering has this property as it has two sources of information, one being the system and the other being the measurement. The filter gain changes to reflect the uncertainty in each information stream until the filter reaches steady state. Adaptive Kalman filtering takes this property a step further by utilizing the two information streams through the innovation sequence and allowing the filter gain to change at all times. It is, however, possible to relate the adaptive Kalman filter algorithm to an interference canceler. In both cases, two sources of information do exist where the correlated component of the two signals is attenuated and the information-bearing component passes.

3.5.3 Adaptive Kalman filtering in geomatics and its limitations

The conventional Kalman filter has been used in geomatics for decades as an estimation tool. The algorithm has proved successful in many application areas where navigation sensors like GPS and INS are used. The use of adaptive Kalman filtering in geomatics, however, has not been given much attention, yet. Nevertheless, some uses of the adaptive Kalman filtering algorithm in geomatics exist. In [Wang et al 1997] an IAE algorithm based on the adaptation of the measurement covariance matrix, R, is proposed to improve the reliability of the GPS phase ambiguity resolution. At the University of Calgary, a full-scale IAE for INS/GPS systems is developed and is used in estimating the trajectory for mobile georeferencing and airborne gravimetry systems [Mohamed and Schwarz, 1999]. Many possible uses of the adaptive Kalman filtering algorithm in geomatics remain to be explored, however.

There is no method without some limitations. Two practical aspects are of interest to the applicability of adaptive Kalman filtering in geomatics applications. The first is the add-on computational complexity the adaptive algorithm adds to the conventional algorithm. The MMAE method using a bank of parallel filters is a point in case, the numerical work becomes so heavy that it will rarely be considered for geomatics applications. Even a gating algorithm like the one proposed in [Chaer et al., 1997] requires considerable numerical work for more than two models. Therefore, the MMAE algorithm can be used only for preliminary investigations but not for final developments. The IAE algorithm, with the addition of the two blocks for estimating R and/or Q, complicates the conventional Kalman filter algorithm. Also, off-line covariance propagation is not possible within the adaptive Kalman filter algorithm because of its dependency on the innovation sequence which is dependant on the external measurements. For high-order INS/GPS systems of practical interest, the proposed algorithm is computationally heavy and may not be efficient as well [Gelb 1974, White et al, 1996].

Another major limitation to the applicability of the algorithm in its standard form, is due to the possible existence of blunders in the measurements. Blunders change the

information content of the innovation sequence and distort its distribution. Tracking a faulty measurement will result in a divergent estimate. This problem can be solved by using a blunder detection and identification block before the application of the new update measurement. One efficient technique for doing that is a L1-norm blunder detection and identification methods. In this case, the L2-norm based reliable adaptive Kalman filter is integrated with a robust L1-norm technique for the proper detection and identification of blunders and hence a reliable and robust filter estimate [Mohamed 1996, 1997].

A key issue to the success of adaptive filtering techniques, in general, is the ability to track high-frequency information in the signal. In other words, adaptive Kalman filtering should preserve the high-frequency information of the useful signal [Salychev 1998]. In cases where smoothing of the filter output is required to enhance accuracy, as in INS/GPS airborne gravimetry, the high-frequency content gained by adaptive filtering will be lost by the smoothing effect. In such situations adaptive Kalman filtering offers little advantage over conventional methods especially at coarse resolutions.

4. DEVELOPMENT OF AN INNOVATION-BASED ADAPTIVE KALMAN FILTER

In this chapter, the detailed development of an innovation-based adaptive Kalman filter for an integrated INS/GPS system is given. The developed adaptive Kalman filter is based on the maximum likelihood (ML) criterion for the proper choice of the filter weights and hence the filter gain. Cases discussed include tuning either the system noise covariance matrix Q, the update measurement noise covariance matrix R or both of them. Analysis of the developed filter for an integrated INS/GPS system is given.

4.1 Maximum Likelihood Estimation

Adaptive Kalman Filtering is one of the cases which is not a simple extension of conventional least-squares (LS) estimation, widely used in geomatics engineering and in many other engineering fields. One reason is that LS aims at estimating and modifying the first moment information, the mean, while in adaptive Kalman filtering the adaptation of the second moment information, the covariance, is also of interest. As discussed in §3.4, conventional Kalman filter can be classified among the adaptive techniques based on its property of sequentially modifying the covariance matrix of the filter states, P, which corresponds to an adaptation of the filter tap weights according to the Wiener theory; this classification will not be used in the following. By adaptive, we mean, imposing conditions under which the statistical information matrices R and/or Q, which are considered constant in the conventional Kalman filter, are estimated via the available new information in the filter innovation sequence.

Both LS and ML aim at maximizing the PDF of the measurements conditioned on the adaptive parameter, see Eq. (4.1). Least squares only considers the variation of the innovation, v, but not the variation of its covariance matrix, C_v, with respect to the adaptive variable. In other words, LS ignores the term $\ln|C_v|$ in Eq. (4.3). This term is very crucial to the adaptivity of the filter statistical matrices. For this reason, the formulas

are derived in the Maximum Likelihood (ML) setting which is more suitable for the problem formulation.

Also, the suitability of the ML technique for the adaptive Kalman filtering problem stems from the fact that for the case of independently and identically distributed measurements, an unbiased estimate with finite covariance can always be found through the ML method such that no other unbiased estimate with a lower covariance exists [Cramér 1946]. The other attractive property of the ML estimate is its uniqueness and its consistency. Uniqueness, the first property, means that the ML formulation will result in one solution, consistency, on the other hand, means that the ML estimate converges, in a probabilistic sense, to the true value of the variable as the number of sample data grows without bound. The ML estimate, however, will in general be biased for small sample sizes. In general, it will provide the unique attainable estimate with minimum variance under the existence of sufficient statistics. On the other hand, LS not only suffers severe analytical difficulties when handling this problem, but also will, in general, result in a biased estimate for small sample sizes, as well. The sample size puts additional restrictions on the choice of the estimation window size that will be discussed later, see e.g. [Cramér 1946, Maybeck 1982] for more details.

4.2 Derivation of the ML Adaptive Kalman Filter

In this development, the specific case of a fixed-length memory (windowing) filter will be considered. In addition, the covariance matrices containing the statistics are to be adapted and not the filter states. Therefore, the *underlying assumptions* of the ML adaptive Kalman filtering problem are:

1. the filter states x are independent of the adaptive parameters α, i.e., $\partial x/\partial \alpha = 0$
2. the filter transition matrix Φ and the measurement design matrix H are time invariant and independent of α

3. the innovation sequence is a white and ergodic sequence within the estimation window
4. the innovation/residual covariance matrix C_v/C_r (through v/r) is the key to adaptation and hence is the α-dependant parameter.

Further, it will be assumed that the data is Gaussian distributed, refer to the discussion in §2.1 about the central limit theory for this assumption.

4.2.1 ML equation for the adaptive Kalman filter

Following the derivation in [Mohamed and Schwarz, 1999], the probability density function of the measurements conditioned on the adaptive parameter α at the specific epoch k is

$$P_{(z|\alpha)_k} = \frac{1}{\sqrt{(2\pi)^m \, | C_{v_k} |}} e^{-\frac{1}{2} v_k^T C_{v_k}^{-1} v_k}, \tag{4.1}$$

where,

m : the number of measurements,

|.| : the determinant operator,

e : the natural base.

To simplify the above equation, its logarithmic form

$$\ln P_{(z|\alpha)_k} = -\frac{1}{2}\{m * \ln(2\pi) + \ln(| C_{v_k} |) + v_k^T C_{v_k}^{-1} v_k\}, \tag{4.2}$$

will be considered. Multiplying both sided of Eq. (4.2) by –2 and neglecting the constant term (which is merely a shift of the distribution), one gets

$$E = \ln(| C_{v_k} |) + v_k^T C_{v_k}^{-1} v_k . \tag{4.3}$$

Note that due to the multiplication by a negative number, maximization of the PDF becomes minimization of its linearized form (the generalized error norm).

For a fixed-length memory filter, the innovation sequence will only be considered inside a window of size N and all innovations inside the estimation window will be summed. The ML condition, in this case, becomes

$$E = \sum_{j=j_0}^{k} \ln |C_{v_j}| + \sum_{j=j_0}^{k} v_j^T C_{v_j}^{-1} v_j = \min. \tag{4.4}$$

It is worth mentioning here that 'k' in the above formula represents the epoch number at which estimation takes place, while 'j' is the moving counter inside the estimation window and j_0 is its initial value, where $j_0 = k\text{-}N+1$.

In conventional least squares, only the second term of Eq. (4.4) is considered which corresponds to the error norm in the L2-norm space. Minimizing that norm with respect to the state vector will result in the optimal state estimate, see e.g. [Sorenson 1970, Swerling 1971, Kailath 1972, 1974] for a discussion of the least squares method. This, however, is different for Eq. (4.4). The covariance matrix of the innovation sequence C_v, not the innovation sequence itself, is dependent on the adaptive parameter 'α', and is the key to adaptation. So, in terms of C_v, the above formula represents a condition for the decision to choose the error weight not the state optimal estimate. In other words, while the LS problem aims at finding the smallest error norm according to a predefined measurement and system error weight, the above ML problem aims at finding the weight that will result in the smallest error norm. This means that the adaptive estimation of the weight is complementary to the state estimation.

The above formula, then, describes the best estimate as the one that has the maximum likelihood based on the adaptive parameter 'α'. To do so, matrix differential calculus will be used to obtain the derivative of Eq. (4.4) with respect to α at the current time k,

$$\partial E/\partial \alpha_k = 0,$$

which results in

$$\sum_{j=j_0}^{k} [\mathrm{tr}\{C_{v_j}^{-1} \frac{\partial C_{v_j}}{\partial \alpha_k}\} - v_j^T C_{v_j}^{-1} \frac{\partial C_{v_j}}{\partial \alpha_k} C_{v_j}^{-1} v_j] = 0, \tag{4.5}$$

where 'tr' is the matrix trace operator. Note that the following two relations from matrix differential calculus [Maybeck 1972, Rogers 1980] have been used to obtain the above formula,

$$\frac{\partial \ln |A|}{\partial x} = \frac{1}{|A|} \frac{\partial |A|}{\partial x} = \mathrm{tr}\{A^{-1} \frac{\partial A}{\partial x}\}$$

$$\frac{\partial A^{-1}}{\partial x} = -A^{-1} \frac{\partial A}{\partial x} A^{-1}.$$

Also, the following relation from matrix calculus will be used,

$$v^T A^T B A v = \mathrm{tr}(A v v^T A^T B),$$

where, v is a vector, and A and B are square matrices.

Eq. (4.5) shows that the problem of adaptive Kalman filtering is reduced to the problem of determining C_v and its partial derivative with respect to the adaptive parameter α. Since there is little interest in C_v itself, but rather in the measurement noise covariance matrix R and the system noise covariance matrix Q, the following substitution will be made (consult Appendix B, Eq. (B.20))

$$C_{v_k} = R_k + H_k P_k(-) H_k^T. \tag{4.6}$$

The partial derivative of Eq. (4.6) with respect to α yields

$$\frac{\partial C_{\nu_k}}{\partial \alpha_k} = \frac{\partial R_k}{\partial \alpha_k} + H_k \frac{\partial P_k(-)}{\partial \alpha_k} H_k^T . \tag{4.7}$$

It is also known that

$$P_k(-) = \Phi P_{k-1}(+)\Phi^T + Q_k , \tag{4.8}$$

which after differentiation with respect to α yields

$$\frac{\partial P_k(-)}{\partial \alpha_k} = \Phi \frac{\partial P_{k-1}(+)}{\partial \alpha_k} \Phi^T + \frac{\partial Q_k}{\partial \alpha_k} . \tag{4.9}$$

Assuming that the process inside the estimation window is essentially in steady state , the first term can be neglected and Eq.(4.9) can be rewritten as

$$\frac{\partial P_k(-)}{\partial \alpha_k} = \frac{\partial Q_k}{\partial \alpha_k} \tag{4.10}$$

Substituting Eq. (4.10) into Eq. (4.7) results in

$$\frac{\partial C_{\nu_k}}{\partial \alpha_k} = \frac{\partial R_k}{\partial \alpha_k} + H_k \frac{\partial Q_{k-1}}{\partial \alpha_k} H_k^T . \tag{4.11}$$

Now, substitute Eq. (4.11) into Eq. (4.5) and expand it. The resulting expression, Eq. (4.12), is the *ML equation for the adaptive Kalman filter*,

$$\boxed{\sum_{j=j_0}^{k} \mathrm{tr}\{[C_{\nu_j}^{-1} - C_{\nu_j}^{-1} \nu_j \nu_j^T C_{\nu_j}^{-1}][\frac{\partial R_j}{\partial \alpha_k} + H_j \frac{\partial Q_{j-1}}{\partial \alpha_k} H_j^T]\} = 0} \tag{4.12}$$

The number of equations in Eq. (4.12) is equal to the number of update measurements 'm', sufficient to estimate a new value for the covariance matrix of the

innovation sequence, C_v and hence adapt either R or Q or both of them based on the adaptive parameter 'α'. To do this, the partial derivative matrices of R and Q with respect to the adaptive parameter 'α' must be known. Also, the design matrix H and the innovation sequence 'v' must be known.

It is worth noting that a similar expression, in terms of the residual sequence, can be reached if the residual sequence not the innovation sequence is used in the first place in Eq. (4.1), consult Appendix B for the definitions of both the innovation and the residual sequences. The result would be

$$\boxed{\sum_{j=j_0}^{k} \mathrm{tr}\{[C_{r_j}^{-1} - C_{r_j}^{-1} r_j r_j^T C_{r_j}^{-1}][\frac{\partial R_j}{\partial \alpha_k} + H_j \frac{\partial Q_{j-1}}{\partial \alpha_k} H_j^T]\} = 0} \qquad (4.13)$$

where,

r : the filter measurement residual sequence,

C_r : the residual sequence covariance matrix.

4.2.2 Adapting the measurement noise covariance matrix (R-Only)

In order to obtain an explicit expression for R, it is assumed that Q is completely known and independent of α. The case of $\alpha_i = R_{ii}$, will be considered, where i is the matrix row or column index; i.e. the adaptive parameters are the variances of the update measurements. This is a situation of practical interest. In this specific case, the ML equation for the adaptive Kalman filter, Eq. (4.12), reduces to

$$\sum_{j=j_0}^{k} \mathrm{tr}\{[C_{v_j}^{-1} - C_{v_j}^{-1} v_j v_j^T C_{v_j}^{-1}][I+0]\} = 0, \qquad C_{v_j}^{-1} \neq 0$$

which after expansion and taking $C_{v_j}^{-1}$ as a common factor on both sides becomes

$$\sum_{j=j_0}^{k} \mathrm{tr}\{C_{v_j}^{-1}[C_{v_j} - v_j v_j^T]C_{v_j}^{-1}\} = 0. \tag{4.14}$$

The above formula only vanishes when the expression in the inner brackets vanishes, because the covariance matrix of the innovation sequence is assumed positive definite. Assuming an ergodic innovation sequence inside the estimation window, the expression for the estimated covariance matrix of the innovation sequence is

$$\hat{C}_{v_k} = \frac{1}{N}\sum_{j=j_0}^{k} v_j v_j^T . \tag{4.15}$$

Substituting the estimated C_{vk} from Eq. (4.15) into Eq. (4.6), the *innovation-based adaptive estimate of R* is

$$\hat{R}_k = \hat{C}_{v_k} - H_k P_{k(-)} H_k^T \tag{4.16}$$

A numerically stable expression for the measurement noise covariance matrix using the residual sequence instead of the innovation sequence can also be derived. Using Eq. (4.13) and applying the same conditions as above, the estimated covariance matrix of the residual sequence can be computed as follows:

$$\hat{C}_{r_k} = \frac{1}{N}\sum_{j=j_0}^{k} r_j r_j^T . \tag{4.17}$$

The residual sequence, r_k, can also be computed from the innovation sequence, v_k, as follows (see Appendix B)

$$r_k = R_k C_{vk}^{-1} v_k \tag{4.18}$$

and hence, using the law of propagation of covariance, its covariance matrix is

$$C_{r_k} = R_k C_{vk}^{-1} R_k . \tag{4.19}$$

Also, from Kalman filtering theory,

$$P_k(-)H_k^T C_{vk}^{-1} = P_k(+)H_k^T R_k^{-1} . \tag{4.20}$$

Re-arrange terms in Eq. (4.6) to get

$$H_k P_k(-)H_k^T = C_{v_k} - R_k . \tag{4.21}$$

Pre-multiply both sides of Eq. (4.20) by H and substitute Eq. (4.21) into it, to get

$$(C_{vk} - R_k)C_{vk}^{-1} = H_k P_k(+)H_k^T R_k^{-1} . \tag{4.22}$$

Now, pre-multiply both sides of Eq. (4.22) by R and re-arrange the terms, to get

$$R_k C_{vk}^{-1} R_k = R_k - H_k P_k(+)H_k^T . \tag{4.23}$$

Equating Eq. (4.23) with Eq. (4.19), the *residual-based 'R' matrix* is

$$\hat{R}_k = \hat{C}_{r_k} + H_k P_k(+)H_k^T . \tag{4.24}$$

4.2.3 Adapting the system noise covariance matrix (Q-Only)

The same strategy used for R can also be used to obtain an estimate for Q. In Eq. (4.12), R will be considered as known and independent of 'α', i.e. its partial derivative with respect to it vanishes. Taking '$\alpha_i = Q_{ii}$', i.e. adapting the variances of the system noise matrix, Eq. (4.12) reduces to

$$\begin{matrix} \sum_{j=j_0}^{k} \mathrm{tr}\{H_j^T[C_{v_j}^{-1} - C_{v_j}^{-1} v_j v_j^T C_{v_j}^{-1}]H_j\} = \\ \sum_{j=j_0}^{k} \mathrm{tr}\{H_j^T C_{v_j}^{-1} H_j - H_j^T C_{v_j}^{-1} v_j v_j^T C_{v_j}^{-1} H_j\} = 0 \end{matrix}, \tag{4.25}$$

which projects the problem from the measurement space to the state space. The number of equations in Eq. (4.25) is equal to the number of states 'n' and can be used to estimate a new value of the projection of the innovation covariance matrix into the state space, i.e. $H^T C_v H$.

Using the expression for the Kalman gain matrix K_k (see Appendix B), and pre-multiplying both sides by the inverse of $P_{k(-)}$, the following expression can be deduced,

$$H_k^T C_{v_k}^{-1} = P_k^{-1}(-) K_k . \tag{4.26}$$

Substituting this expression into Eq. (4.25), one gets

$$\sum_{j=j_0}^{k} \mathrm{tr}\{P_j^{-1}(-) K_j H_j - P_j^{-1}(-) K_j v_j v_j^T K_j^T P_j^{-1}(-)\} = 0, \tag{4.27}$$

which can be further re-arranged to

$$\sum_{j=j_0}^{k} \mathrm{tr}\{P_j^{-1}(-)[K_j H_j P_j(-) - K_j v_j v_j^T K_j^T] P_j^{-1}(-)\} = 0, \tag{4.28}$$

which is similar to the expression in Eq. (4.14) but given in the state space rather than in the measurement space. Again, because the covariance matrix of the predicted states P(-) is positive definite, Eq. (4.28) only vanishes when

$$\sum_{j=j_0}^{k} \mathrm{tr}\{K_j H_j P_j(-) - K_j v_j v_j^T K_j^T\} = 0. \tag{4.29}$$

Thus, KHP(-) can be expressed by

$$\begin{aligned} K_k H_k P_k(-) &= \frac{1}{N}\sum_{j=j_0}^{k} K_k v_j v_j^T K_k^T \\ &= K_k\left(\frac{1}{N}\sum_{j=j_0}^{k} v_j v_j^T\right)K_k^T \\ &= K_k \hat{C}_{v_k} K_k^T \end{aligned} \tag{4.30}$$

From Kalman filtering theory, we have

$$\begin{aligned} K_k H_k P_k(-) &= P_k(-) - P_k(+) \\ &= \Phi P_{k-1}(+)\Phi^T + Q_k - P_k(+)' \end{aligned} \tag{4.31}$$

which when substituted into Eq. (4.30) results in an expression for the *adaptive covariance matrix of the system noise Q* of the form

$$\hat{Q}_k = K_k \hat{C}_{v_k} K_k^T + P_k(+) - \Phi P_{k-1}(+)\Phi^T. \tag{4.32}$$

Using the substitution,

$$\Delta x_k = K_k v_k, \tag{4.33}$$

a similar expression of the *adaptive covariance matrix of the system noise Q* is obtained

$$\begin{aligned} \hat{Q}_k &= \frac{1}{N}\sum_{j=j_0}^{k} \Delta x_j \Delta x_j^T + P_k(+) - \Phi P_{k-1}(+)\Phi^T \\ &= \hat{C}_{\Delta x_k} + P_k(+) - \Phi P_{k-1}(+)\Phi^T \end{aligned} \tag{4.34}$$

where,

Δx : the state correction sequence (the difference between the state before and after update) and is computed by $\Delta x_k = \hat{x}_k(+) - \hat{x}_k(-)$.

The adaptive covariance matrix of the system noise Q (Eq. (4.32) or Eq. (4.34)) can be approximated by

$$\hat{Q}_k \cong \hat{C}_{\Delta x_k} \cong \frac{1}{N} \sum_{j=j_0}^{k} \Delta x_j \Delta x_j^T \cong K_k \hat{C}_{vk} K_k^T, \tag{4.35}$$

in case the change in the state error covariance matrix 'P' can be neglected. Due to the approximations taking place in the estimation of Q, its estimate is inferior to that of R.

4.2.4 Adapting the covariance matrices for measurement noise and system noise (R and Q) simultaneously

In this case, both R and Q will be dependent on 'α' at the same time. We will consider the case where the variances of the system noise matrix Q_{ii} and the variances of the measurement noise matrix R_{ii} are equal to the adaptive parameter 'α'. In that case, Eq. (4.12) reduces to

$$\sum_{j=j_0}^{k} \mathrm{tr}\{[C_{v_j}^{-1} - C_{v_j}^{-1} v_j v_j^T C_{v_j}^{-1}][I + H_j H_j^T]\} = 0, \tag{4.36}$$

which represents a general case for adapting both of R and Q.

Adapting the Measurement Noise Covariance Matrix (R)

Re-arrange terms in Eq. (4.36) above, to get

$$\sum_{j=j_0}^{k} \mathrm{tr}\{C_{v_j}^{-1}[C_{v_j} - v_j v_j^T][I + H_j H_j^T] C_{v_j}^{-1}\} = 0. \tag{4.37}$$

The term $(I+HH^T)$ is positive definite because it is a sum of a quadratic term and the identity matrix. Hence, Eq. (4.37) only vanishes when the term C_v-vv^T vanishes

which leads to the same condition for adapting R-only. Therefore, the estimate of the innovation sequence covariance matrix in Eq. (4.15) will again be used here. Further, the expression for R based on the innovation sequence is given by Eq. (4.16) and that based on the residual sequence by Eq. (4.24).

Adapting the System Noise Covariance Matrix (Q)

To project Eq. (4.36) onto the state space, expand it as follows

$$\sum_{j=j_0}^{k} \mathrm{tr}\{[C_{v_j}^{-1} - C_{v_j}^{-1} v_j v_j^T C_{v_j}^{-1}] + [H_j^T C_{v_j}^{-1} H_j - H_j^T C_{v_j}^{-1} v_j v_j^T C_{v_j}^{-1} H_j]\} = 0 . \tag{4.38}$$

The estimated covariance matrix of the innovation sequence is calculated using Eq. (4.15). In this case, the first term in square brackets of Eq. (4.38) vanishes and the whole expression collapses to the case of Q-only adaptation, viz.,

$$\sum_{j=j_0}^{k} \mathrm{tr}\{0 + H_j^T C_{v_j}^{-1} H_j - H_j^T C_{v_j}^{-1} v_j v_j^T C_{v_j}^{-1} H_j\} = 0 . \tag{4.39}$$

Therefore, Eqs. (4.32), (4.34), and (4.35) can be used to adaptively estimate Q. It is worth noting here that although the same equations for adapting R-only and Q-only are used in the case of simultaneously adapting R and Q, numerical difficulties can be encountered in real data. Because of the approximations made, care has to be taken in the choice of the adaptive filter parameters such as the averaging moving window size.

To account for such an adaptive approach in the Kalman filter algorithm, an additional estimation block has to be added. Firstly, the covariance matrix of the innovation sequence has to be estimated and then R and/or Q will be estimated afterwards as shown in Fig. (3.8). Numerous results can be reached for the expressions for R and Q

based on the assumptions to be made for the adaptive parameters. For instance, one can assume the full matrix to be variable. In this case, the variances as well as the covariances will be estimated. On the other extreme, one can assume same variance for the matrix entries with no or same covariances. The choice of the adaptive parameters of the covariance matrix depends on the application. In this study, the cases of a diagonal matrix and full matrix are investigated.

4.3 Innovation Sequence Whitening

A necessary and sufficient condition for the optimality of a Kalman filter is that the innovation sequence be white [Mehra 1970, 1972]. When the measurement noise and the system noise are white sequences, the resulting innovation sequence is a white sequence because it results from a linear operation that does not change the nature of the original contributors. There are situations, however, where non-white errors propagate into either the measurement or the system noise, or both. In these situations, and to satisfy the requirement of the adaptive Kalman filter, the innovation sequence will need to be whitened through a process called whitening.

Whitening is a transformation process that projects the problem described by the model

$$z = H x + e \tag{4.40}$$

from its original space into another space where the model error is white. This is accomplished by factorizing the covariance matrix of the model noise, C_e, using a matrix factorization method. The condition for the whitening process to be successful is that the resulting matrix from the factorization be a square root (or normalized square root) of the model noise matrix [Bierman 1977]. Since the model error covariance matrix, used in geomatics applications in general and in INS/GPS systems in particular, is positive definite, a UDU (or LDL) factorization method will result in the required matrix. Other

transformations are also applicable in this context, for a discussion about the use of Givens transformations see [Bierman 1977, Blais 1985].

4.3.1 The float whitening filter

For the model described above, whitening starts by factorizing the covariance matrix as follows

$$C_e = U\,D\,U^T \tag{4.41}$$

where U is a unitary upper triangular matrix, and D is a diagonal matrix. By pre-multiplying both sides of the model equation (4.40) by U^{-1}, one gets

$$U^{-1}z = U^{-1}Hx + U^{-1}e \tag{4.42}$$

or in compact form:

$$\bar{z} = \bar{H}x + \bar{e} \tag{4.43}$$

where, $\bar{z} = U^{-1}z$ and $\bar{H} = U^{-1}H$, which are the transformed model equations. It is worth noting that the model parameter 'x' is unchanged after whitening which means that whitening does not change the problem in the parameter space. The whitening transformation is non-orthogonal and results in transformed (whitened) measurements that are uncorrelated, because

$$\begin{aligned} C_{\bar{e}} &= E[\bar{e}\bar{e}^T] = E[U^{-1}ee^TU^{-T}] \\ &= U^{-1}E[ee^T]U^{-T} = U^{-1}C_eU^{-T} = D \end{aligned}, \tag{4.44}$$

the resulting whitened covariance matrix is diagonal. It can, also, be proven that the whitened model noise variances are equal to or less than their counterparts before whitening. Another inference associated with whitening is that there is no loss of generality in assuming that the model errors are uncorrelated and normalized because it is

always possible to transform the current model, which might have non-white noise, and construct a model with white noise.

4.3.2 Statistical test for whiteness of the innovation sequence

The condition for optimality of the Kalman filter can be tested statistically by using the whiteness property of the innovation sequence [Mehra 1970]. The auto-correlation function of a white sequence is a Dirac delta function at zero lag and its Fourier transform is constant representing equal spectral densities at all frequencies. In practice, it is not easy to get an exact Dirac delta for the auto-correlation function or a constant spectral density in the frequency domain. As an accepted procedure in practice, the auto-correlation function is approximated by a Gaussian distribution symmetrical at zero lag. The innovation sequence will be considered white if the derived auto-correlation fits the Gaussian distribution within boundary limits of 1.96σ (95% probability) or 3σ (99.6% probability). Based on the ergodic property of the innovation sequence, v_k at epoch k, an estimate of its auto-correlation function at lag L is

$$\begin{aligned}\hat{P}_L &= E[v_k v_{k-L}^T] \\ &= \frac{1}{N}\sum_{k=L}^{N} v_k v_{k-L}^T\end{aligned}, \tag{4.45}$$

where N is the estimation window size. Estimates of the normalized auto-correlation coefficients ρ_L, are obtained as follows

$$\hat{\rho}_{ij_L} = \frac{\hat{P}_{ij_L}}{\sqrt{\hat{P}_{ii_0}\hat{P}_{jj_0}}} \tag{4.46}$$

where, i,j : row and column indices of the auto-correlation matrix.

Of special interest here are the diagonal elements of the auto-correlation function,

$$\hat{\rho}_{ii_L} = \frac{\hat{P}_{ii_L}}{\hat{P}_{ii_0}} \tag{4.47}$$

which represent the auto-correlation of the same innovation element.

For a large enough estimation window, the variance of the resulting distribution can be calculated from that of the individual elements by dividing over the sample size N. This is equivalent to calculating the variance of the mean value from that of a single observation. In this case, the variance of the estimated unbiased auto-correlation function is

$$\sigma^2_{\hat{P}_{ii_L}} = \frac{1}{N}\hat{P}_{ii0} \tag{4.48}$$

and that of the estimated normalized auto-correlation coefficient is

$$\sigma^2_{\hat{\rho}_{ii_L}} = \frac{1}{N} \tag{4.49}$$

where $\hat{\rho}_{ii0} = 1$ is embedded in the right hand side of the above formula. Using the above formulae, the 95% confidence bounds at different lags L are $\pm 1.96\sqrt{\frac{\hat{P}_{ii_0}}{N}}$ for the estimated auto-correlation function diagonal elements and $\pm 1.96\sqrt{\frac{1}{N}}$ for the estimated normalized auto-correlation coefficients [Mehra 1970]. If the estimated auto-correlation elements at different lags L lie within the confidence bounds, the innovation sequence is said to be white and the Kalman filter is optimal. In case more than 5% of them lie outside the confidence bounds, the filter is declared sub-optimal and the innovation sequence is non-white and need to be whitened as discussed in §4.3.1.

4.3.3 Statistical test for blunders in the innovation sequence

The previous test (whiteness statistical test) measures the existence of correlation between the innovations between epochs inside the estimation window. On the other hand, update measurement blunders, mostly due to GPS cycle slips, propagate into the filter and spoil the assumption of a Gaussian distribution of the innovation sequence. Both conventional and adaptive methods are affected alike by blunders. The actual covariances deviate from the estimated covariances and the filter estimate becomes unreliable and will not be robust. To robustify the filter estimate, three approaches are commonly used to assist dealing with blunders. The first approach is to first detect and eliminate blunders and then apply conventional estimation methods on blunder-free data [Baarda 1968]. The second approach is to apply a robust estimation procedure to derive a blunder-free robust solution [Kubik 1983]. The third approach is to deal with blunders within the context of a robust estimation method like the L1-norm method and then process blunder-free data by an L2-norm method, see e.g. [Mohamed 1996] for a hybrid norm algorithm. The first approach is rather simple and appealing in many applications. However, it does not have the ability to detect the existence of multiple blunders. The second approach has the advantage that blunders are estimated to their correct sizes but the technique does not lead to a unique solution and the overall efficiency of the robust solution is inferior to an L2-norm solution when blunder-free data are used. The third approach is advantageous in detecting blunders and providing robust and reliable solutions. However, combined norm algorithms demand high computational power and are usually not applicable on line. For post-mission processing of INS/GPS data, the third approach is recommended, while for on-line processing the first approach is the choice.

In order to check the existence of innovation blunders at epoch 'k' , a global test statistic 'T_k' is set as follows [Koch 1988]:

$$H_o: E[v_k] = 0,$$
$$H_a: E[v_k] = \nabla_k$$

$$T_k = v_k^T C_{v_k}^{-1} v_k \mid H_o \sim \chi^2(m_k,0) \qquad (4.50)$$
$$\mid H_a \sim \chi^2(m_k,\lambda_k^2)$$

where,

H_o, H_a : null and alternative hypotheses, respectively,

∇_k : suspected blunder vector at epoch k,

m_k : number of innovations at the same epoch,

χ^2 : Chi-squared distribution,

λ_k^2 : non-central parameter of the Chi-squared distribution.

In a one-sided test on the basis of 99.99% confidence for the case of 8 innovations, the upper limit value of T_k is 0.46, see tables in [Mikhail and Ackerman 1976]. The non-central parameter of the innovation Chi-squared distribution is calculated as follows:

$$\lambda_k^2 = \nabla_k^T C_v^{-1} \nabla_k \qquad (4.51)$$

Once the global test statistic indicates the existence of innovation blunders, a local test is carried out to locate the failure. The hypothesis for the local test statistic 't_i' for innovation number 'i' at the specified epoch 'k' is as follows [Koch 1988]:

$$H_o: E[v_i] = 0,$$
$$H_a: E[v_i] = \nabla_i$$
$$t_i = \frac{v_i}{\sigma_{v_i}} \qquad \mid H_o \sim N(0,1) \qquad (4.52)$$
$$\mid H_a \sim N(\delta_i,1)$$

where,

∇_i : suspected blunder in innovation number 'i',

σ_{vi} : standard error of innovation number 'i',

N : normal distribution,

δ_i : non-central parameter of the innovation normal distribution.

In a one-sided test on the basis of 99.99% confidence, the limit value for t_i is 3.9, see tables in [Mikhail and Ackerman 1976]. The non-central parameter of the innovation normal distribution is computed as follows:

$$\delta_i = \frac{\nabla_i}{\sigma_i}. \tag{4.53}$$

Blunders smaller than the minimally detectable error (MDE) disappear in the filter errors. The MDE for innovation number 'i' is computed as follows:

$$MDE_i = \sigma_{v_i} \sqrt{\frac{w_o}{g_i}} \tag{4.54}$$

where,

σ_{vi} : standard error of measurement number 'i',

w_o : expected shift (bias) in the innovation mean value,

g_i : redundancy number of measurement number 'i'.

The expected shift (bias) in the innovation mean value is calculated as the sum of two normal distribution values at the specified significance and weakness levels. For a test significance level of 5% (probability of rejecting good observation) and weakness level of 25% (probability of accepting bad observation), $w_o^2 = (1.5)^2$, see tables in [Mikhail and Ackerman 1976]. The redundancy number of measurement number 'i' is calculated as follows:

$$g_i = \frac{\sigma_{v_i}^2}{\sigma_{v_i}^2}, \tag{4.55}$$

where the total redundancy matrix is

$$G = C_v R^{-1} = C_v C_v^{-1}. \tag{4.56}$$

Redundancy numbers are smaller than one since innovation variances (σ_v^2) are generally smaller than measurement variances (σ_v^2). For perfect filtering ($g_i = 1$), the MDE is equal to 1.5 times the measurement standard error under the aforementioned significance and weakness levels of the test. Hence, innovation blunders greater than $1.5\sigma_v$ can be detected. Measurements with innovations greater than $3.9\sigma_v$ will be declared erroneous and rejected. It is worth noting here that the previous statistical tests can also be carried out on the residual sequence in exactly the same way.

4.3.4 Whitening procedure

The innovation sequence used to adaptively estimate measurement and/or system noise covariance matrices is assumed blunder-free, with Gaussian distribution and white noise characteristics. The developed optimized adaptive Kalman filter has a whitening block. The role of the whitening block is to ensure the whiteness and Gaussianess of the innovation sequence. It checks for the existence of blunders and isolates faulty innovations using global and local test statistics as described in the previous section. It then checks for the whiteness of the innovation sequence between epochs inside the estimation window according to the test described in §4.3.2. Fig. (4.1) below illustrates the whitening procedure used in the developed optimized INS/GPS adaptive Kalman filter.

It should be noted that the whitening block described here is not meant to be a quality control block for the developed INS/GPS integrated system. It is merely a procedure to ensure the appropriateness of the innovation sequence to do the adaptive filtering job, ensure filter tractability, and alleviate filter divergence. For quality control issues in integrated systems the interested reader is directed to literature such as [Teunissen 1990, McBurney 1990, Wei et al. 1990, Gao 1992].

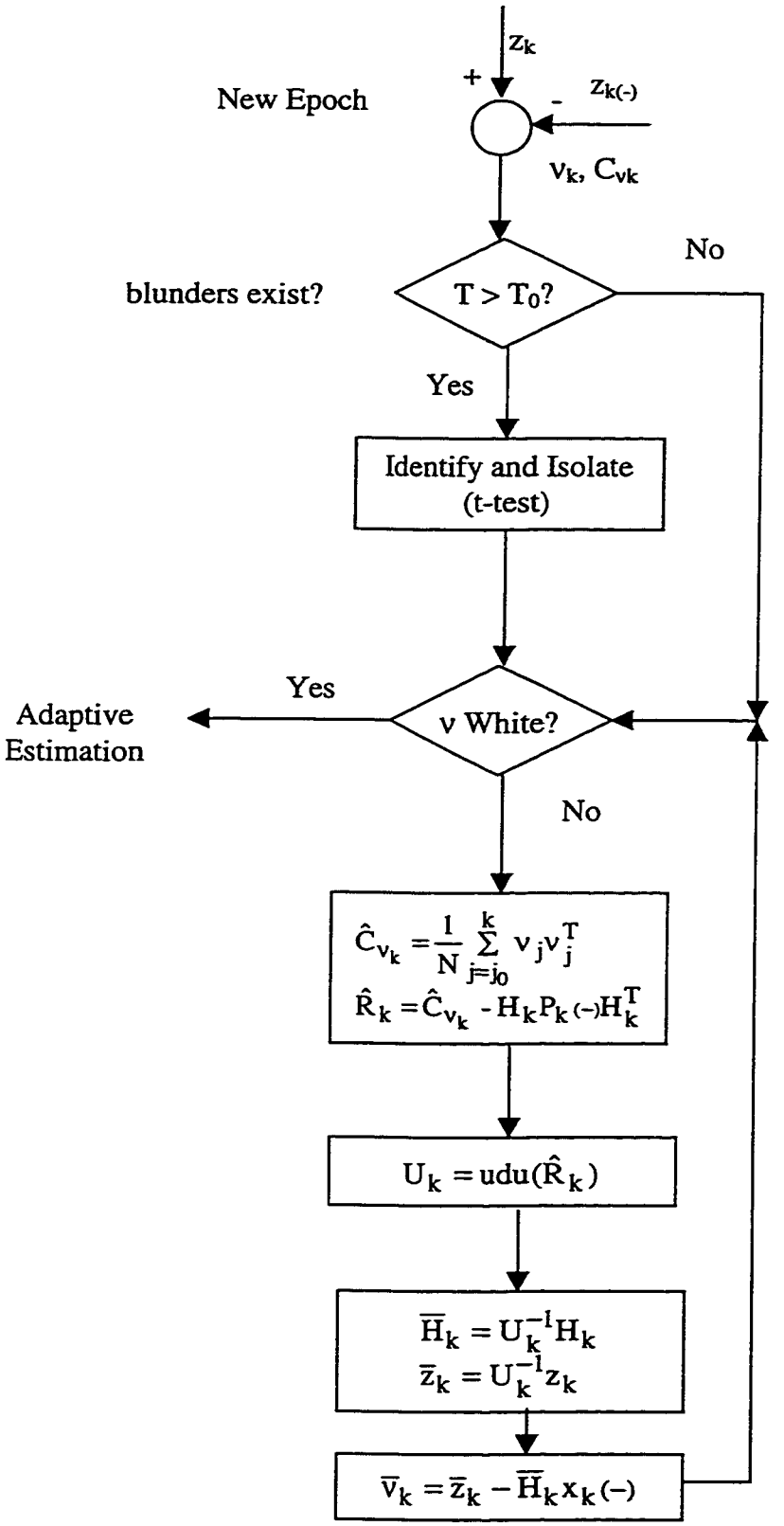

Fig. (4.1) : Whitening Procedure in KINADA

4.4 Adaptive Kalman Filtering of the INS/GPS Integrated System

The developed adaptive Kalman filter, along with the conventional Kalman filter, are both implemented in a software package called KINADA, a derivative of KINGSPAD. KINADA is a modular package written in C/C++ computer language. It includes modules to adaptively filter INS/GPS data. It also includes modules to whiten the innovation sequence before it is used in the adaptive estimation procedure. Below is a description of the developed adaptive Kalman filter as implemented in the KINADA package.

4.4.1 Structure of the INS/GPS adaptive extended Kalman filter

The structure of the INS/GPS conventional Kalman filter is discussed in §3.2.3. The structure of the innovation-based adaptive Kalman filter resembles that of the conventional Kalman filter; the difference, however, is in the use of the innovation sequence. While in the conventional Kalman filter, the innovation sequence plays a role in updating the state estimate through the system update step, it is used in the adaptive filter to update both the state estimate and the filter statistical information. It constitutes the major distinctive feature of the adaptive Kalman filter algorithm. Indeed, the general structure of the adaptive Kalman filter follows the use of the innovation sequence.

The two building blocks of the developed adaptive algorithm are the parameter estimation block (first moment) and the covariance matrix estimation block (second moment). The first estimation block, the parameter estimation block, resembles that of the conventional Kalman filter. It uses the output of the second building block, the covariance matrices, and runs a conventional Kalman filter algorithm to propagate the filter state and its covariance. The covariance building block, on the other hand, updates the measurement noise and the system noise covariance matrices when a new measurement, and hence a new innovation, becomes available. Fig. (4.2) illustrates the general structure of the developed INS/GPS adaptive integration procedure.

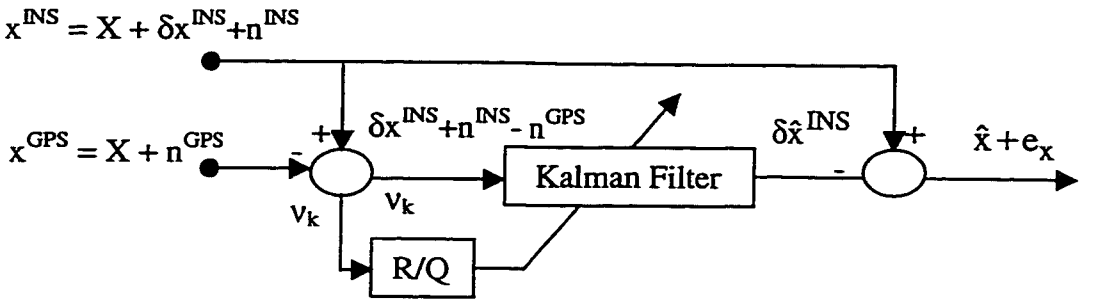

Fig. (4.2) : INS/GPS Adaptive Integration Procedure

In the conventional INS/GPS extended Kalman filter structure, the innovation, v, is used once in the 'Kalman Filter' block, see Fig. (3.4). In the adaptive structure, however, it is also used in an adaptive manner as shown in Fig. (4.2). Notice also that, in the extended Kalman filter error formulation, the time update cycle disappears and the full update measurement represents the innovation, see Appendix B (Eq. (B.30)).

The role of the 'Kalman Filter' in Fig. (4.2) is to suppress GPS and INS noise and estimate δx^{INS}, the INS correction term. The first step, the suppression of noise, is done automatically by the Kalman filter through low-pass filtering of both streams of INS and GPS data, see §3.2.1 for a discussion about INS/GPS complementary (LPF/HPF) filtering. The estimation of the filter state, δx^{INS}, is given through a weighting process between both streams of information, the INS data and the GPS data. The additional adaptive block helps mainly in the weighting step. The filter weighting and the filter state estimate are, now, based on the current innovation. The covariance propagation in the adaptive Kalman filter depends on the newly available measurement which robustify the estimated covariance of the filter state estimate. Filter divergence becomes less likely than in the conventional case. When undetected non-white and non-Gaussian errors exist in the measurements they show up in the innovation and consequently in the covariance propagation indicating an unstable condition; this does not happen in the conventional Kalman filter. Consequently, the weighting process in the adaptive filter is more likely to be correct and the change in the filter states become more tractable, i.e. high frequency filter state changes are more likely estimable than in the case of the conventional filter.

The structure of the algorithm of the developed adaptive Kalman filter is shown in Fig. (4.3) below; specific parameters of the developed adaptive Kalman filter will be discussed later.

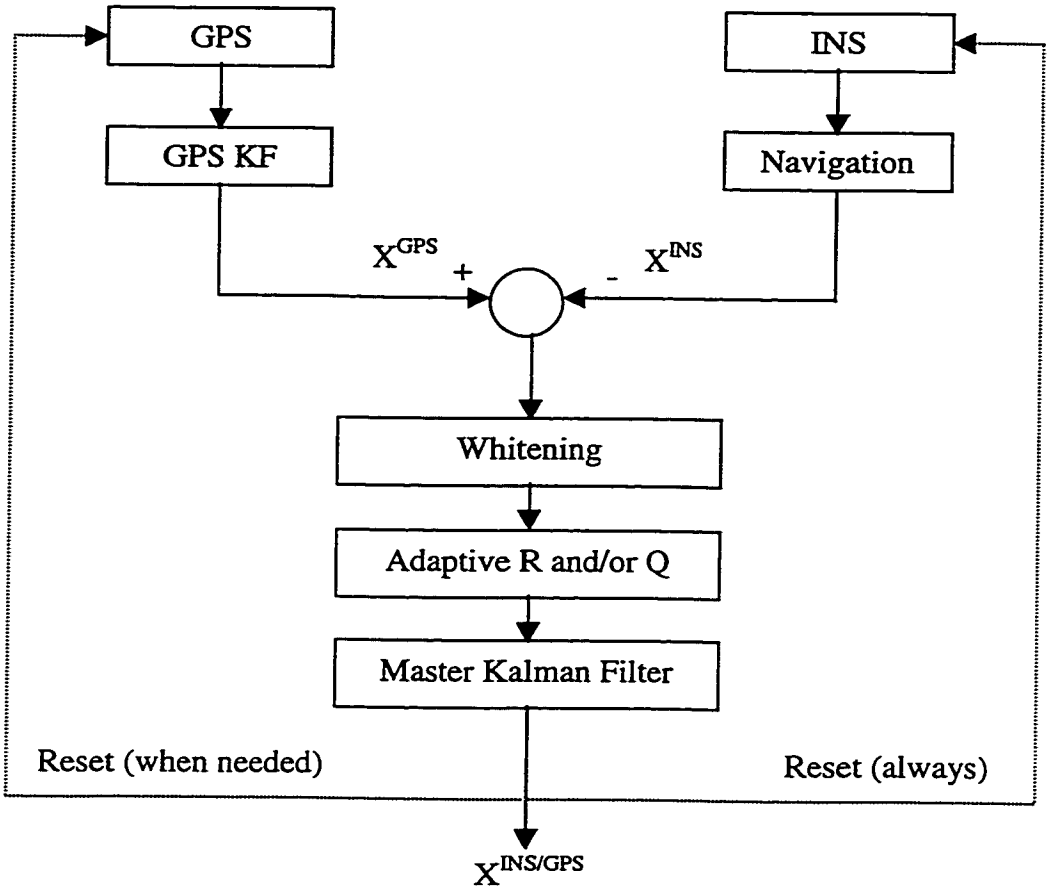

Fig. (4.3) : INS/GPS Adaptive Kalman Filter Structure

4.4.2 Estimation window size

The moving window inside which the innovation sequence is assumed stationary and ergodic is called the estimation window. It plays an important role in the adaptive estimation procedure because it provides the limits to the tractability of the adaptive algorithm. The smaller the estimation window size, the better the tractability and sensitivity to dynamic changes of the filter. However, small estimation windows result in small sample sizes and the filter becomes more vulnerable to biasedness and divergence.

The ML estimate, in general, will be biased for small sample sizes [Cramér 1946]. The larger the estimation window, the less likely is a biased estimate. However, the large estimation window, beyond the filter bandwidth, reduces the ability of the algorithm to correctly trace short-term changes of the trajectory, e.g. turns. A window of the size of the data length is essentially converting the adaptive filter into a conventional filter, since adaptation will take place only once. Therefore, a trade-off between the biasedness and the tractability of the estimate according to the application at hand should be taken into account. In addition, the proper choice of the window size depends very much on the trajectory dynamics.

Divergence occurs when the number of equations required to estimate the unknown adaptive parameters is smaller than the number of unknowns themselves. The following three cases lead to destabilization of the filter and to the problem of filter divergence in practice :

1. A window size smaller than the number of update measurements when adapting R,
2. A window size smaller than the number of filter states when adapting Q,
3. A window size smaller than the sum of update measurements and filter states when adapting both R and Q simultaneously.

4.4.3 The filter learning history and its gain

In conventional Kalman filtering, the filter learning history can be observed through the filter innovation sequence. The filter covariance propagation can be carried out off line because it is independent of actual measurements. Optimality of the Kalman filter algorithm is based on the second moment information (covariance matrices). Also, the filter gain is a function of the covariance propagation of the measurement and system models. It can happen that the innovation learning history shows a situation that is not reflected in the covariance propagation, as for instance dynamics or geometry change. The filter covariance, in this case, will not reflect the actual accuracy and the filter is said to be diverged.

In contrast, in adaptive Kalman filtering, the innovation learning history is reflected in the covariance propagation. Consequently, the first moment information of the filter is consistent with the second moment information. Changes in the measurement and/or system sequences are reflected in the innovation sequence and will propagate into the filter covariance. The result is a more realistic filter gain and better observability of the filter state components. To show the reflection of the innovation sequence on the filter gain, let us consider a scalar case. In this case, the gain of the conventional Kalman filter is

$$K_k = \frac{\sigma_x^2}{\sigma_v^2}. \tag{4.57}$$

The gain of the adaptive Kalman filter with R adaptation based on the innovation sequence is

$$K_k = \frac{\sigma_x^2}{v_k^2 - \sigma_x^2}, \tag{4.58}$$

and with R adaptation based on the residual sequence is

$$K_k = \frac{\sigma_x^2}{r_k^2 + \sigma_x^2}, \tag{4.59}$$

while that for Q adaptation is

$$K_k = \frac{\sigma_o^2 + K_k^2 v_k^2}{\sigma_v^2}, \tag{4.60}$$

and that for R and Q simultaneous adaptation is

$$K_k = \frac{\sigma_o^2 + K_k^2 v_k^2}{v_k^2 - \sigma_o^2}. \tag{4.61}$$

Eqs. (4.58 - 4.61) show clearly the dependence of the gain on the actual size of the innovation and the filter state variance. It is clear that the gain learning history is connected to the innovation learning history. In other words, the filter will never lock on a fixed gain and stop responding to the outside world. The adaptive Kalman filter response to changes is more reflective than that of the conventional Kalman filter, see Fig. (4.4).

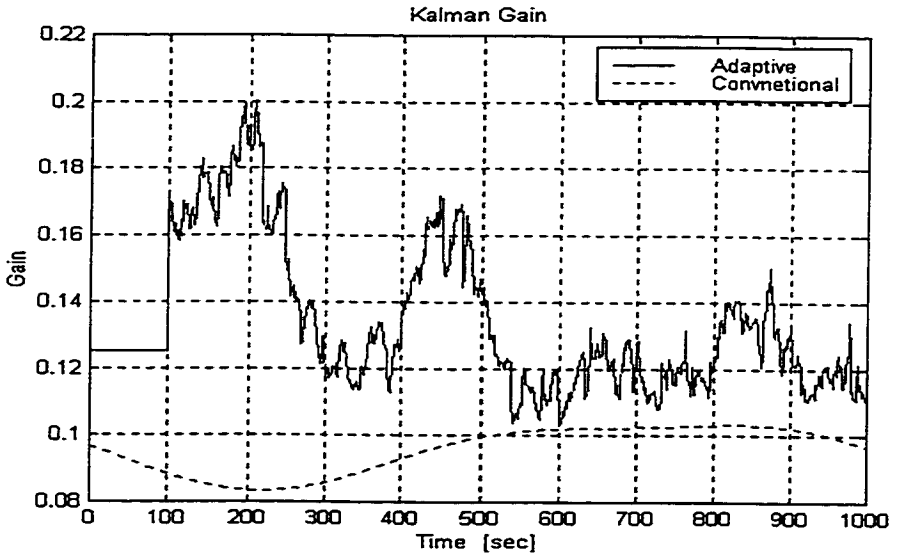

Fig. (4.4) : Kalman Filter Gain - AKF vs. CKF

In the adaptive scheme, the smaller the averaging window size, the higher the response to frequency changes in the filter gain and the higher the vulnerability of the filter to singularity situations. It is worth mentioning here that the same conclusion can be reached for the filter state estimation error and its covariance. While the steady-state covariance of the state is characterized by a flat pattern indicating a stabilized situation in

the case of a conventional Kalman filter, the pattern is dynamics dependant in the case of adaptive Kalman filter as is the filter gain. This means that the filter performance is expected to be superior to that of the conventional Kalman filter in tracing trajectory changes but also more subject to filter instabilities and thus filter artifacts in the trajectory.

4.4.4 Constant Q and/or R vs. adaptive Q and/or R

In the INS/GPS integrated system, R represents the uncertainty in the GPS update measurement and Q represents the uncertainty in the INS system and its model. Constant values for these two parameters, as in the case of conventional Kalman filter, gives little chance to track changes. For instance, many geodetic GPS receivers change their tracking bandwidth based on the experienced dynamics in order to ensure tractability of the GPS signal. According to [Parkinson and Spilker 1996], the GPS receiver tracking frequency rate may deviate from its nominal value, which causes an increase in the measurement noise, R. In a strapdown INS system, gyroscopes and accelerometers are strapped down to the vehicle where it experiences all kind of dynamics the vehicle experiences; the system noise, Q, should reflect such dynamics changes in its parameters.

In conventional Kalman filtering, the constant measurement and system covariance matrices result in a smoothed gain, state estimate, and state covariance. In adaptive Kalman filtering, however, the pattern of changes of the covariance matrices follow the pattern of changes in the innovation sequence which is excited by dynamics changes. In a scalar case, for instance, the estimated variance of the measurement noise takes the form

$$\hat{\sigma}^2_{z_k} = v_k^2 - \sigma_x^2, \tag{4.62}$$

and that for the system noise takes the form

$$\hat{q}_k^2 = K_k^2 v_k^2. \tag{4.63}$$

Figs. (4.5) and (4.6) below illustrate the above equations. Both figures show clearly how the dynamics in the innovation sequence is transferred to the estimated measurement and system noise. The pattern of each of them is similar to that of the innovation sequence inside the averaging moving window and that of the filter gain and filter state error covariance. It is completely different from the smooth pattern characterizing constant R or Q. The multi-dimensional case is no different from the scalar case, except for the interaction between the different elements of the respective matrices.

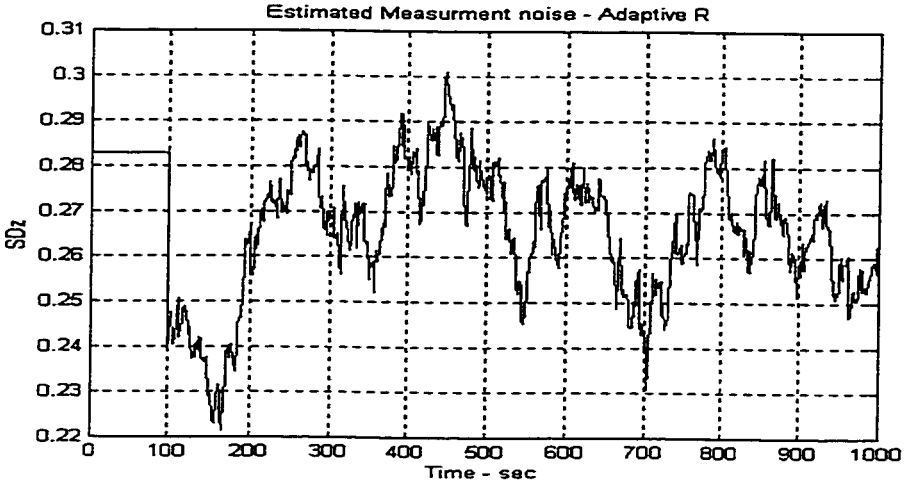

Fig. (4.5) : Kalman Filter Estimated Measurement Noise - AKF

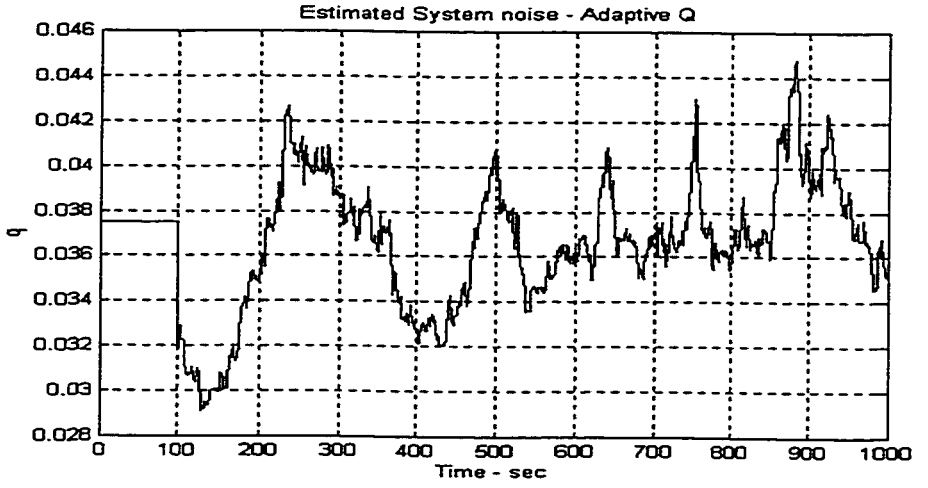

Fig. (4.6) : Kalman Filter Estimated System Noise - AKF

4.4.5 Sensitivity analysis of adaptive Kalman filtering

Eq. (3.20) shows the inherent stability of the conventional Kalman filter. The attenuation factor, I-KH, plays an important role in stabilizing the filter in steady state, at epoch k. In the scalar case where H = 1, the attenuation factor takes the form

$$\gamma_k = 1 - K_k . \tag{4.64}$$

This factor can be used to check both the stability of the filter and the positive definiteness of its state covariance matrix. In the scalar case, the condition for the filter *stability* is

$$\gamma_k < 1, \tag{4.65}$$

which guarantees the decay of the state error. For the *positiveness* of the state variance, however, the following condition must hold

$$\gamma_k > 0. \tag{4.66}$$

Both of the previous two conditions specify the range of values the gain factor can take as

$$0 < K_k < 1. \tag{4.67}$$

In order to show the stability and positiveness of the conventional Kalman filter for the scalar case, the attenuation factor is computed based on Eq. (3.14) for the gain as follows

$$\gamma_k = \frac{\sigma_v^2 + (k-1)\sigma_o^2}{\sigma_v^2 + k\sigma_o^2}. \tag{4.68}$$

Eq. (4.68) shows clearly that

$$0 < \gamma_k < 1,$$

at all epochs of the conventional Kalman filter. In the transition stage, i.e. for small k, γ_k is closer to zero while it approaches one as the time epoch k approaches infinity.

In the following, the stability and positiveness of the adaptive Kalman filter for the different adaptations will be studied.

Innovation-based R-only

In this case, the attenuation factor can be computed based on Eq. (4.58) as follows

$$\gamma_k = \frac{v^2 - 2\sigma_x^2}{v^2 - \sigma_x^2}. \tag{4.69}$$

It is clear that the filter stability is guaranteed in this case because $\gamma_k < 1$ always. Positiveness of the state variance, however, is subject to the condition

$$0.5 < \frac{\sigma_x^2}{v^2} < 1, \tag{4.70}$$

where singularity of the filter solution can occur outside this range. If one can use v^2 to represent the quality of the update measurement, Eq. (4.70), then, suggests that the signal to noise ratio should be within 0.5 and 1 for this specific filtering procedure to yield optimal results.

Residual-based R-only

Based on Eq. (4.59), the attenuation factor, in this case, can be computed as follows

$$\gamma_k = \frac{r^2}{r^2 + \sigma_x^2}. \tag{4.71}$$

which guarantees filter stability and state variance positiveness at all epochs because $0 < \gamma_k < 1$ always. The R only adaptation based on the residual sequence is, then, expected to be numerically more robust than that based on the innovation sequence.

Q-only

Eq. (4.60) contains the gain factor twice, once on each side, resulting in a quadratic equation in K_k, which when solved results in the following attenuation factor

$$\gamma_k = \frac{1}{2v^2}[2v^2 - \sigma_v^2 - \sqrt{\sigma_v^4 - 4\sigma_o^2 v^2}], \tag{4.72}$$

which guarantees filter stability because $\gamma_k < 1$ always. It is, however, required that

$$\frac{\sigma_o^2 v^2}{\sigma_v^4} < 0.25, \tag{4.73}$$

in order for the state variance to be positive. In an ideal filtering procedure, one can assume that $v^2 = \sigma_v^2$, and the condition above reduces to

$$\frac{\sigma_o^2}{\sigma_v^2} < 0.25. \tag{4.74}$$

The condition in Eq. (4.74) refers to the choice of the signal to noise ratio at the beginning of the filtering procedure and suggests that one should not start with a very low signal to noise ratio for the filter to achieve positive state variance at steady state when using Q-only adaptation.

R and Q simultaneously

Here also a quadratic equation is obtained for the gain factor based on Eq. (4.61), from which the attenuation factor is computed as follows

$$\gamma_k = \frac{1}{2v^2}[v^2 + \sigma_o^2 - \sqrt{\sigma_o^4 - 6\sigma_o^2 v^2 + v^4}]. \tag{4.75}$$

From Eq. (4.75),

$$\gamma_k > 1 \tag{4.76}$$

always, indicating an unstable filtering procedures at all epochs. The state variance positiveness is, however, guaranteed at all epochs under the condition

$$\frac{\sigma_o^2}{v^2} < 5.83, \tag{4.77}$$

i.e. a signal to noise ratio greater than 5.83 is needed for this filtering procedure to yield positive state variance. In general, the simultaneous adaptation of R and Q will result in an unstable filtering procedure and should, therefore, be avoided.

It should be noted that the proof provided in this section is only true for the one element state vector and should not be considered as a general proof for the sensitivity of the adaptive Kalman filtering procedure. Numerical studies for the different adaptation cases will be carried out in Chapter Eight where real data and a full-scale state vector are used to further analyze the sensitivity of the adaptive Kalman filtering procedure.

5. ADAPTIVE KALMAN FILTER PERFORMANCE ANALYSIS

In this chapter, a computer simulation is presented and analyzed, where the performance of the adaptive Kalman filter (AKF) is compared to that of the conventional Kalman filter (CKF). The objective of this simulation is to show the behavior of the conventional and the adaptive Kalman filter states in a general way.

5.1 Trajectory and Model Description

A system similar to the GPS/INS used in the field tests is simulated, see Appendix D for specifications. The simulated INS is a navigation-grade system with a position error growth of one nautical mile per hour. The DGPS system consists of two geodetic GPS receivers providing differential phase and Doppler measurements. Only short baselines are considered in the simulation and therefore spatially correlated GPS errors do not greatly affect the obtained accuracy and can generally be ignored; the effect of the ignored errors is taken into account by amplifying the GPS white noise level.

The filter consists of 9 navigation states (position, velocity, attitude), 3 gyro bias states, and 3 accelerometer bias states. The biases are modeled as first-order Gauss-Markov processes. The local-level frame is used for the INS navigation mechanization. The navigation error model simulated is similar to the one used in KINGSPAD, see [KINGSPAD 1994] for details of the model. The simulated measurements are the differences between the position and the velocity derived from both the INS system and the GPS system, as follows

$$z = x^{INS} - x^{GPS} \tag{5.1}$$

where,

x^{INS} : INS measurement (position, velocity)

x^{GPS} : GPS measurement (position, velocity).

Trajectory geometry and dynamics are provided in the form of data series of the different navigation parameters. To show the behavior of the conventional and adaptive filter states for both straight lines and turns under dynamical changes, an L-shaped aircraft trajectory is simulated. Details of the simulation are shown in Table (5.1) and Fig. (5.1) below. Take-off is simulated with changes in the pitch parameter, while the maneuver at the turn is simulated with changes in the roll and azimuth parameters.

The underlying statistical assumptions of the simulation are as follows:

- GPS errors are white noise with standard deviations for position $\sigma_{pGPS} = 0.1$ m and for velocity $\sigma_{vGPS} = 0.05$ m/s^2
- INS noise for position is $\sigma_{pINS} = 0.1$ m and for velocity $\sigma_{vINS} = 0.005$ m/s^2
- INS initial misalignment leveling error $\varepsilon_o = 5''$, and azimuth error $\varepsilon_u = 3.5'$
- accelerometer bias is a first-order Gauss-Markov model of value $b_{Ao} = 20$ mGal, correlation time $\beta_A = 4$ h, , and power spectral density $p_A = 2$ mGal/$\sqrt{h}$
- gyro bias is a first-order Gauss-Markov model of value $b_{Go} = 0.01°$/h, correlation time $\beta_A = 4$ h, and power spectral density $p_A = 0.001°/\sqrt{h}$

Table (5.1) : Dynamics of Simulation Trajectory

Segment	Time [sec]	L [km]	Height [km]	Vel. [m/s]	Acc. [m/s^2]	Curv. [km]	Roll [deg]	pitch [deg]	Az. [deg]	Remark
A-A1	0-100	3.5	1.2	0-100	1	straight	0	0	0	taxiing
A1-B	100-300	19.0	1.2-4.4	95	0	straight	0	15	0	take-off
B-C	300-360	5.3	4.4-4.45	95-100	2.5	3.4	15	0	0-270	turn
C-D	360-470	11.0	4.45	100	0	straight	0	0	270	fly

5.2 Filter Performance Analysis

Different aspects pertaining to the performance of the AKF and the CKF are discussed in the following. The purpose is to analyze the behavior of both filters during the estimation process.

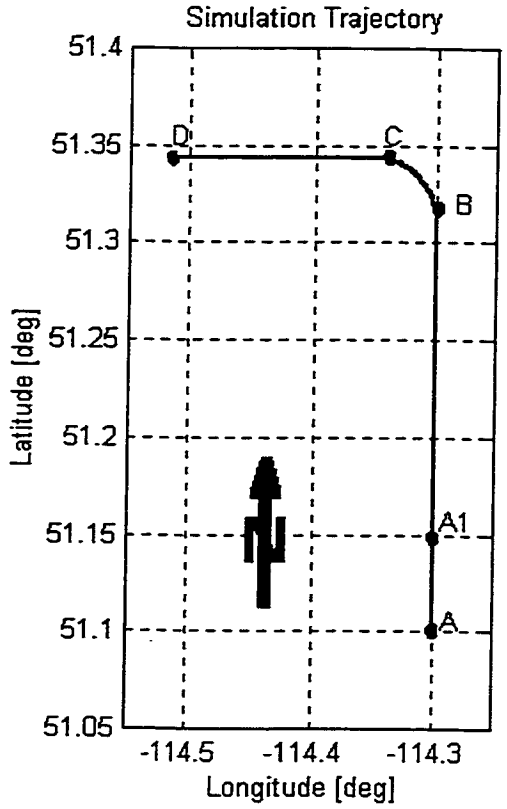

Fig. (5.1) : Simulation Trajectory

5.2.1 Kalman gain

As discussed in §3.2.6, the Kalman filter gain determines the filter bandwidth. For a stationary dynamics matrix and fixed gain (at steady state), the bandwidth of the Kalman filter stays unchanged. This fact is depicted in Fig. (5.2), where the dotted line represents the conventional case with almost constant gain (bandwidth). The change in the adaptive Kalman filter bandwidth with dynamics can be seen in the filter gain change. Fig. (5.2) shows that dynamics changes like that during take off and at turns are reflected in the gain of the adaptive case, the solid line. The change in the filter gain is a result of adapting Q only while R was kept unchanged. It is clear that at periods of benign dynamics or constant velocity, the gain from the conventional filter and that from the

adaptive filter are almost matched, see the period after take-off and before the turn in Fig.(5.2). The change in the gain affects the state estimation as will be discussed in the following section.

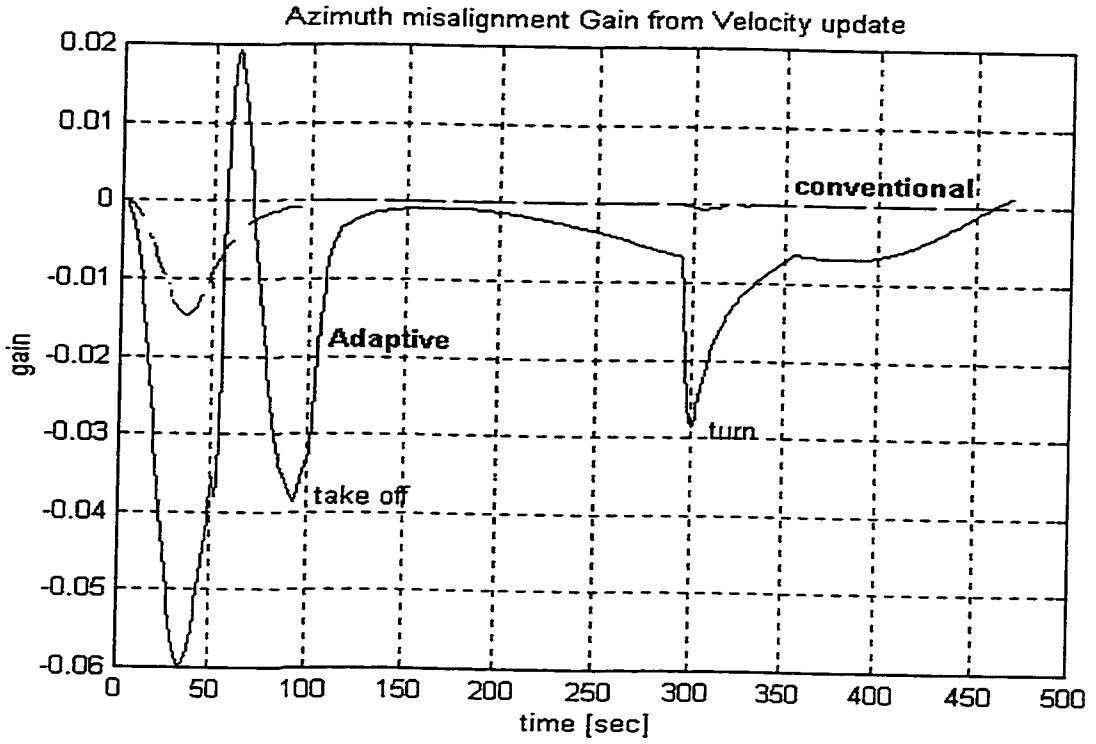

Fig. (5.2) : Kalman Gain of Azimuth Misalignment from Velocity Update (Simulation) - CKF vs. AKF

5.2.2 Filter state estimation

Position and velocity states are directly observable components in the INS/GPS Kalman filter. Their precision is directly linked to the precision of the update measurements obtained from GPS. Attitude states, however, are less observable and more critical for kinematic applications such as image direct georeferencing. Leveling errors of the horizontal channels are better observable than azimuth misalignment [Schwarz and Wei, 1995b]. While leveling errors are directly linked to velocity errors through the vertical gravity acceleration 'g' and hence can benefit from a velocity update, see Eq.

(A.4) in Appendix A, azimuth misalignment has no[1] direct link to velocity updates and can hardly profit from GPS updates.

Leveling errors and azimuth misalignment errors develop in different manners with time. For leveling errors, Eq. (A.13) shows that the gyro drift and the accelerometer bias are modulated by the Schuler frequency (through sinusoidal waves) which result in bounded errors. On the other hand, Eq. (A.18) shows that, in addition to being modulated with the Schuler frequency, the gyro drift error affects the azimuth misalignment through a linear time-dependant term which causes the azimuth misalignment to drift. It also shows that the effect of the gyro drift on the azimuth misalignment can be one order of magnitude higher than the effect of the accelerometer bias, e.g. 50" for gyro drift as opposed to 5" for accelerometer bias after a complete Schuler cycle for a navigation-grade INS. Effects of initial velocity errors and leveling errors on azimuth misalignment are almost negligible. Thus, the estimation of the azimuth misalignment state and the gyro drift state is critical in the Kalman filter estimation process. Therefore, the estimation of the azimuth misalignment and gyro drift states in both cases of the CKF and the AKF will be the main focus of the analysis in this simulation.

Fig. (5.3a) and (5.3b) depict the estimation of the Z-gyro drift state in both cases, the CKF and the AKF. For the adaptive case presented here, comparable results were obtained when adapting Q-only and R-only; results shown below are from Q-only with a 20 epoch window size. Because both filters handle dynamical changes differently, their estimates are different. For instance, in the case of CKF, the jump in the gyro drift state estimate, Fig. (5.3a), occurring around epoch 300, is due to the maneuver (segment B-C in Table 5.1). Because the gyro drift state and the azimuth misalignment state cannot be separated in the INS/GPS Kalman filter model, the filter treats both states as one state

---

[1] In fact, there is a weak link between the azimuth misalignment and the velocity update through the vehicle horizontal acceleration and indirectly through the leveling states. The vehicle horizontal acceleration is usually much smaller than the vertical gravity acceleration, g, and hence was ignored in the simplified formulation in Appendix A.

until dynamical changes occur to de-couple them. The acceleration (2.5 m/s^2 linear and 0° to 15° angular) at the maneuver, along with the velocity update, caused the CKF to de-couple the two states resulting in a change in their estimates, see also Fig. (5.4a) below. Another example of the de-coupling of the filter states in the CKF case after dynamical changes occurred around epoch 100 at take off. In this case, the jump occurred in the azimuth misalignment estimate while the gyro drift estimate maintained an estimate that is closer to the true value. Except for some response to dynamical changes at transition and after take-off where pitch changes occur, the estimate of the conventional filter is fairly smooth, see Fig. (5.4a).

As discussed before, the Kalman filter bandwidth is mainly affected by changes in the filter gain. AKF changes its gain and consequently its bandwidth with dynamical changes. For a weak observable component such as the gyro drift, the gain from measurement updates is very close to zero. Therefore, in the AKF, the change of the filter bandwidth, and consequently of the state estimate, is expected to be small. Fig. (5.3b) shows this situation for the estimate of the gyro drift state in the AKF case. Except for changes at the transition stage, the estimate is almost following the first-order Gauss-Markov model of four hours correlation time without interacting with the navigation states. The azimuth misalignment state, on the other hand, has a relatively larger gain, and the dynamical changes are apparent in its estimate, see Fig. (5.4b). The estimate jumps that happened in the CKF case did not happen in the AKF case, see Fig. (5.3b). While the conventional Kalman filter kept almost constant bandwidth, especially after transition to steady state, the adaptive Kalman filter kept changing its bandwidth to reflect changes in the dynamics. The estimate of the azimuth misalignment state of the adaptive filter, is noisier, especially at the take-off period, see Fig. (5.4b). The change in the bandwidth of the adaptive filter is due to the fact that the update gains are based on the innovations (corrections). In Fig. (5.4b), for instance, dynamics changes at take-off result in large innovations which, in turn, result in large value of the Q matrix (process noise) and noisier states. The states are less noisy at flight height because small innovations are encountered and hence Q remains small.

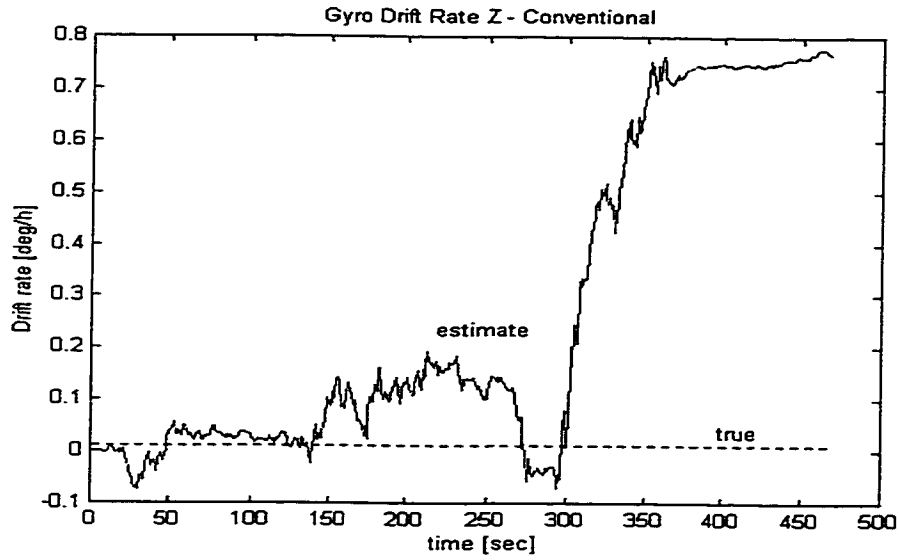

Fig. (5.3a) : Z-Gyro Drift State Estimate (Simulation) - CKF

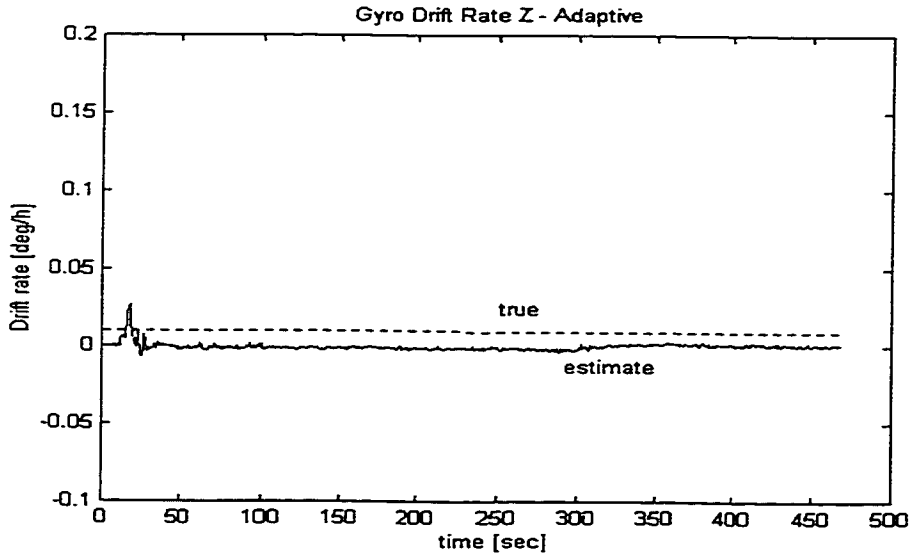

Fig. (5.3b) : Z-Gyro Drift State Estimate (Simulation) - AKF

5.2.3 Effect of the moving averaging window size on state estimation

The size of the moving window over which the process is considered stationary and ergodic has an impact on the adaptive filter performance. The smaller the window size is

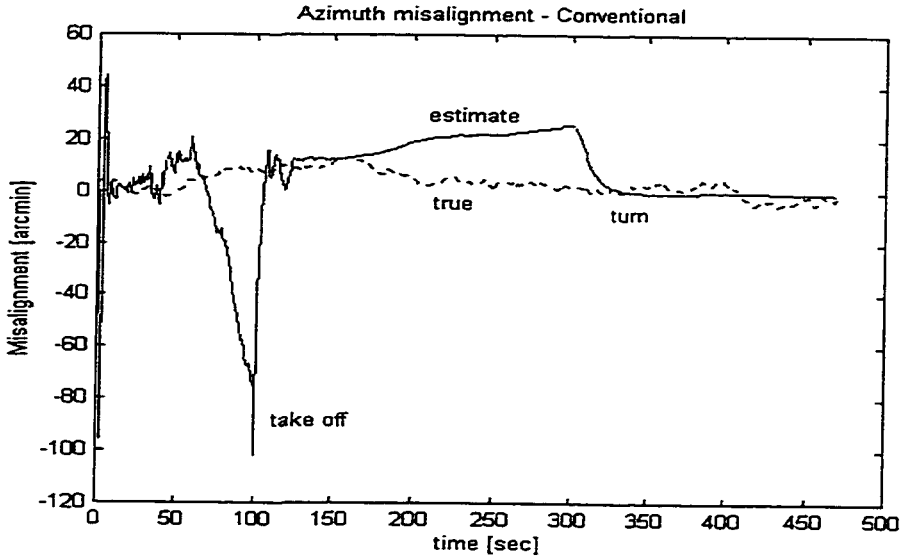

Fig. (5.4a) : Azimuth Misalignment State Estimate (Simulation) - CKF

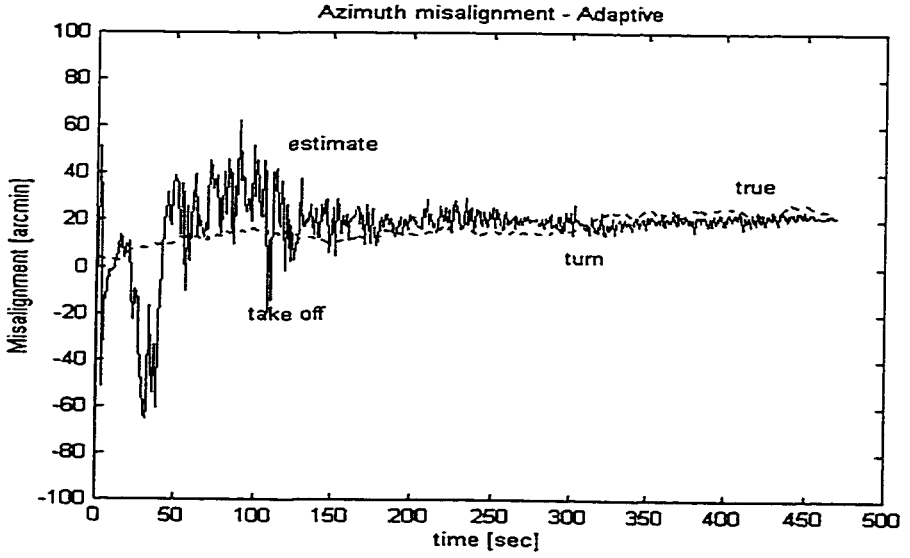

Fig. (5.4b) : Azimuth Misalignment State Estimate (Simulation) - AKF

the faster the changes that can be captured by the adaptive filter. Fig. (5.5) shows the effect of the window size on the azimuth misalignment gain from the velocity update of the simulated trajectory. A window size of the same length as the update interval of one epoch is essentially changing the gain with every update. It results in the largest response at turns and keeps changing with the changes of the dynamics. On the other side, a

relatively large window size of 100 epochs results in the slowest response and is close to the conventional filter response. A window size of 20 epochs, which is slightly larger than the number of the filter states, 15, provides an average response. The 20 epoch window size, in this case, is neither responding too slowly as the 100 epoch window nor too fast as the one epoch window.

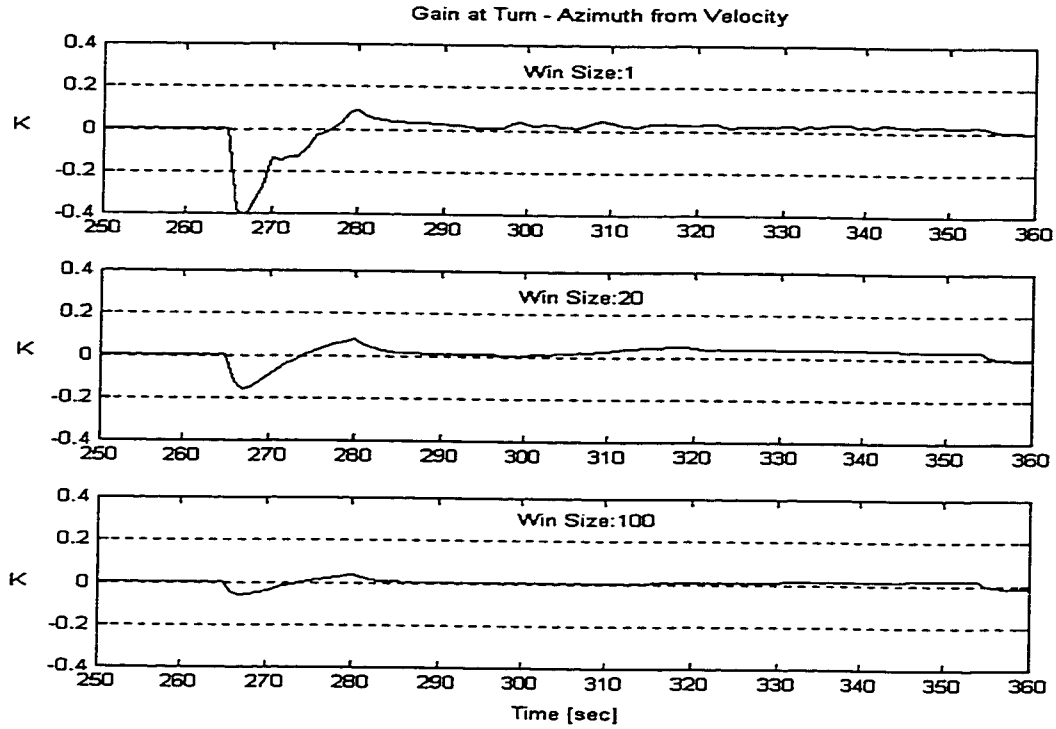

Fig. (5.5) : Effect of the Window Size on the Filter Gain at a Turn (Simulation) - AKF

There are situations where the filter performance degrades when the window size is not chosen correctly. Fig. (5.6) shows the azimuth misalignment state estimate as compared to the true value for the three different window sizes. The filter used in this case has 15 states indicating that 15 unknowns are encountered for adapting the Q matrix (diagonal case). The estimate in the case of the 100 epoch window size, which is close to the conventional filter, responds slowly to the dynamics changes and maintains an almost constant and biased estimate. On the other hand, the estimate of the one epoch window size has direct response to dynamics resulting in a divergent estimate at the turn. Taking into account the fact that 15 unknowns are required in this specific case, the solution

resulting from a one-epoch window size cannot be accepted. The estimate of the 20 epoch window size, which is a little larger than the number of unknowns, provides a trade-off solution. It neither diverges too much like the one-epoch solution nor does it result in a biased solution like the 100 epoch solution.

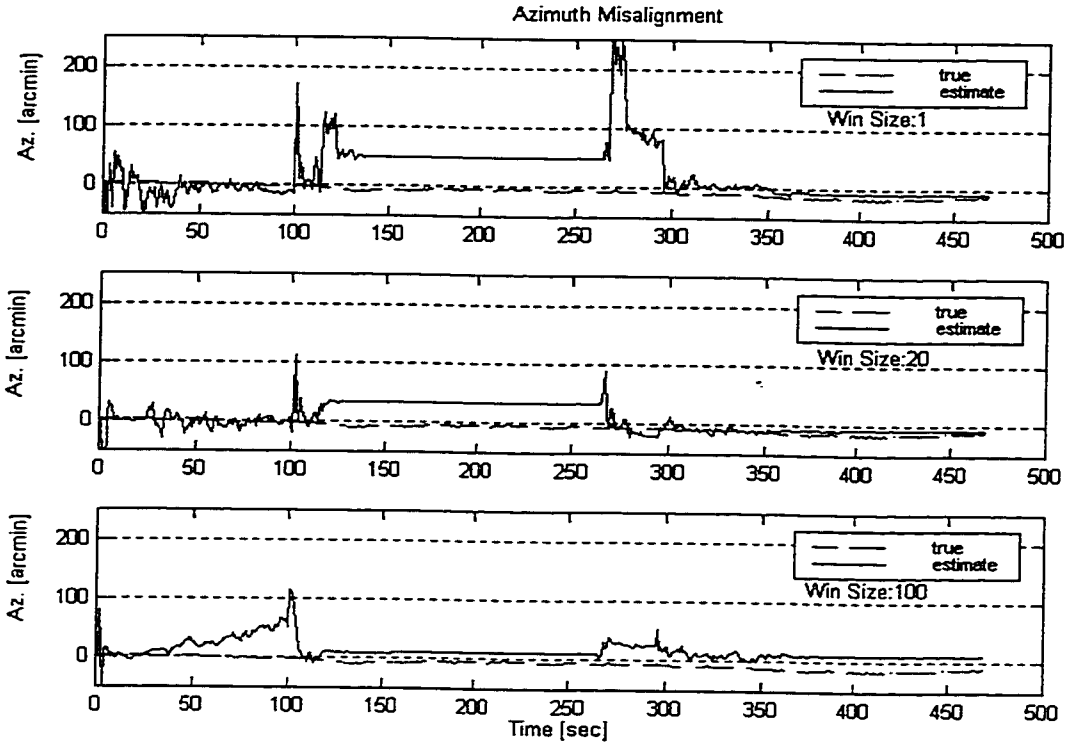

Fig. (5.6):Effect of Window Size on the Azimuth Misalignment Estimate (Simulation)-AKF

5.2.4 Innovation sequence properties

Because the innovation sequence is a very important element in adaptive Kalman filter theory, its properties will be discussed in this section. Fig. (5.7) depicts a kinematic velocity innovation sequence, while Fig. (5.8) depicts its auto-correlation coefficient at different lags. Both figures are used to indicate the whiteness property of the innovation sequence and hence the optimality of the adaptive Kalman filter. It is worth mentioning that the innovation sequence of the same parameter resulting from the conventional Kalman filter was also white indicating that both filters share the whiteness property. Fig.

(5.9) depicts the distribution of the innovation sequence which, in this case, show a Gaussian behavior. For 95% confidence and 20 degrees of freedom, the critical χ^2 threshold is 10.9. The computed goodness of fit factor for the velocity innovation is 8.6, which indicates that the velocity innovation distribution, in this case, can be assumed Gaussian.

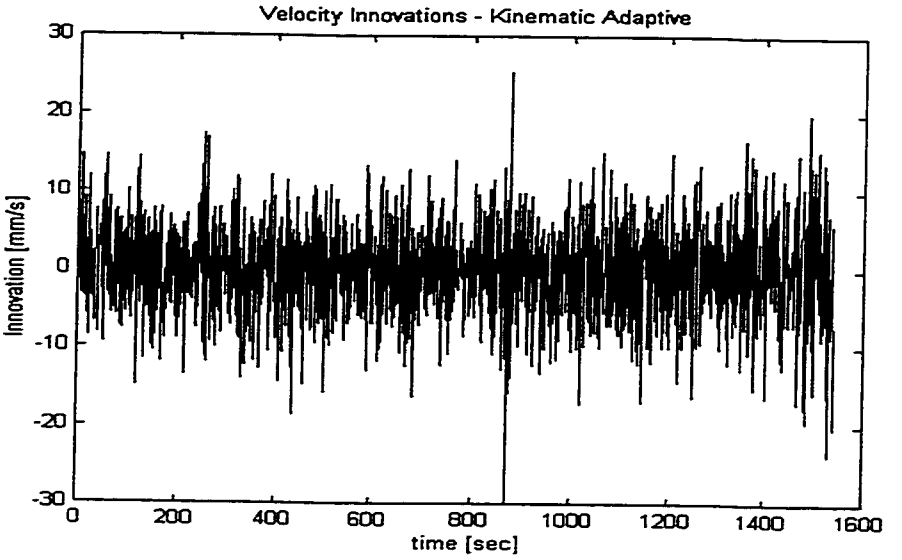

Fig. (5.7) : Velocity Whitened Innovation Sequence (Simulation) - AKF

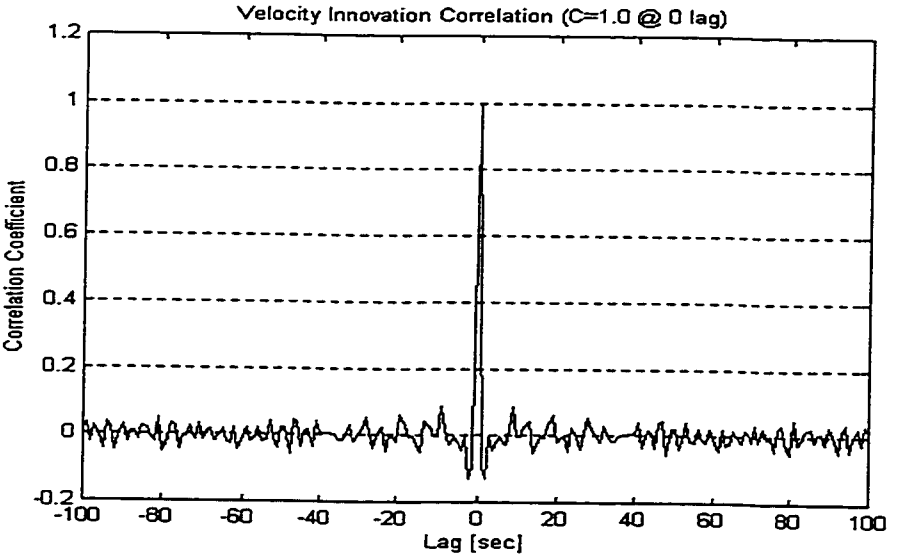

Fig. (5.8) : Velocity Innovation Sequence Auto-correlation (Simulation) - Whiteness of AKF

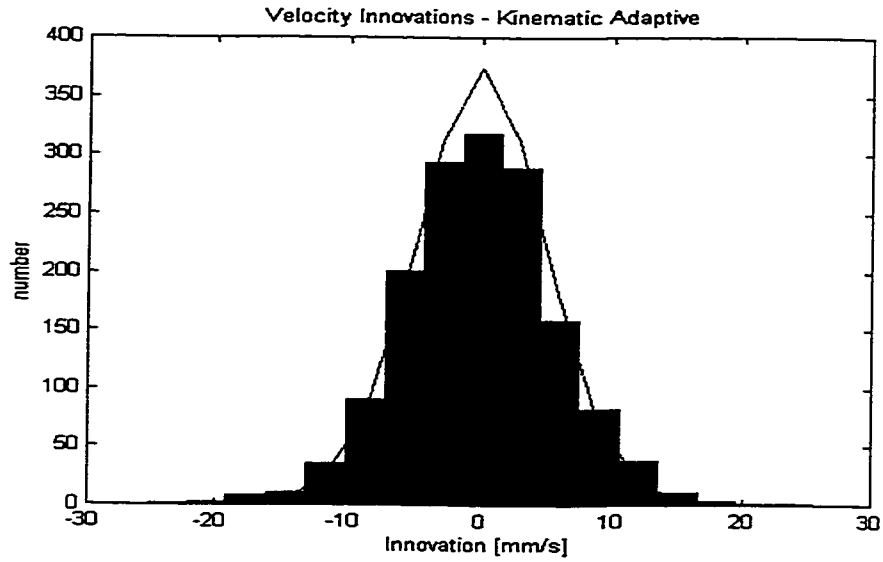

Fig. (5.9): Velocity Innovation Sequence Distribution (Simulation) - Gaussianess of AKF

5.2.5 Innovation sequence whitening

The purpose of this section is to give a practical example on how the whitening procedure is applied inside the KINADA software. As described in Chapter Four, float whitening is based on a 'udu' matrix factorization of the innovation correlation matrix. It is applied when the correlation test shows that the innovation sequence is non-white. The correlation test (or whiteness statistical test) described in §4.2.2 ensures that the innovation sequence has a maximum correlation of one at zero lag and almost zero correlation at all other lags. This test can be approximated by the goodness of fit test for the Gaussian distribution. It approximates the Dirac impulse at zero lag by a narrow Gaussian distribution. In the INS/GPS filter, and with position and velocity updates available, this test has to be applied to six different innovations.

Figs. (5.10a) and (5.10b) illustrate the auto-correlation coefficient computed for the position innovation in the INS/GPS Kalman filter. Fig. (5.10a) shows the auto-correlation coefficient for the original innovation sequence inside a 100 epoch window, while Fig. (5.10b) shows the auto-correlation coefficient for the same innovation sequence after applying the float whitening procedure described in §4.2.1. Correlation coefficients at

lags other than zero exist in the original innovation sequence shown in Fig. (5.10a), while they disappear after whitening. While theoretically they should disappear, the coefficients around the zero lag in Fig. (5.10b) demonstrate the practical limitations of the float whitening filter.

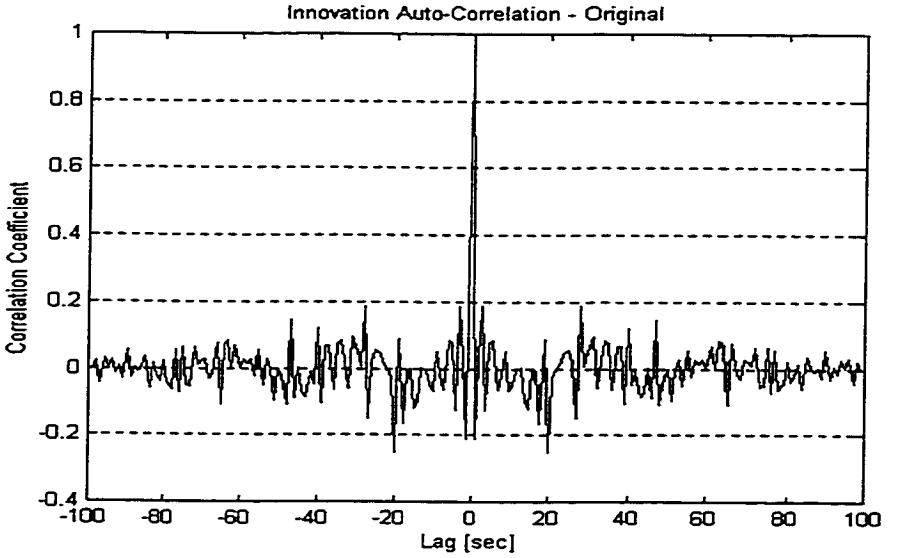

Fig. (5.10a) : Innovation Auto-correlation (Simulation) - Original

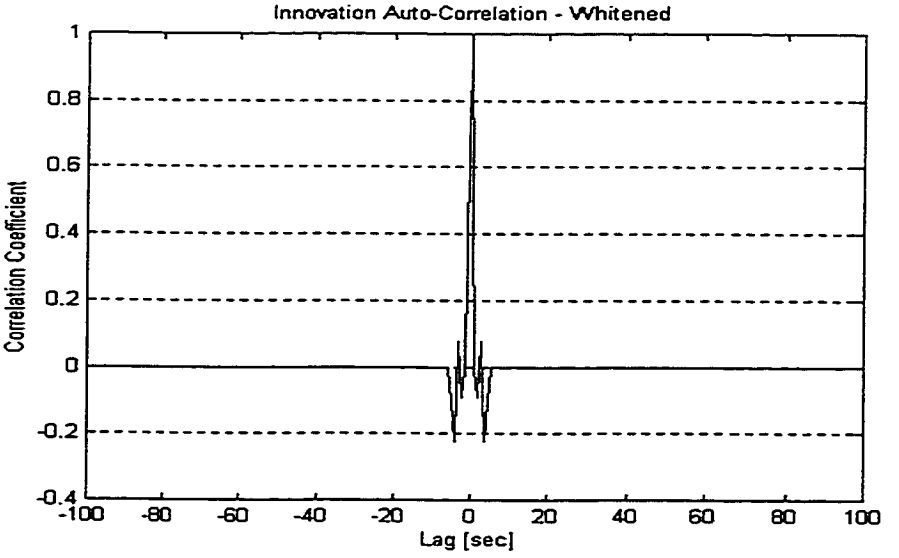

Fig. (5.10b) : Innovation Auto-correlation (Simulation) - Whitened

5.2.6 Estimation of R and Q

The changes in the estimated measurement noise covariance matrix and the estimated system noise covariance matrix reflect the behavior of the AKF. Fig. (5.11) below depicts the estimated measurement noise covariance matrix, R, when window sizes of 10, 20, 50, and 100 seconds are used. In this specific test, the noise standard deviation of the velocity measurement update is considered. The conventional Kalman filter value used for the velocity measurement standard deviation is 0.05 m/s. In Fig. (5.11), the value of the velocity measurement standard deviation in the adaptive filter fluctuates around 0.05 m/s, the assigned standard deviation for the conventional filter. The rate of fluctuation increases as the window size decreases. While the 10 second window size estimate is rather noisy, the 100 seconds window size estimate is the smoothest and closest to the average value.

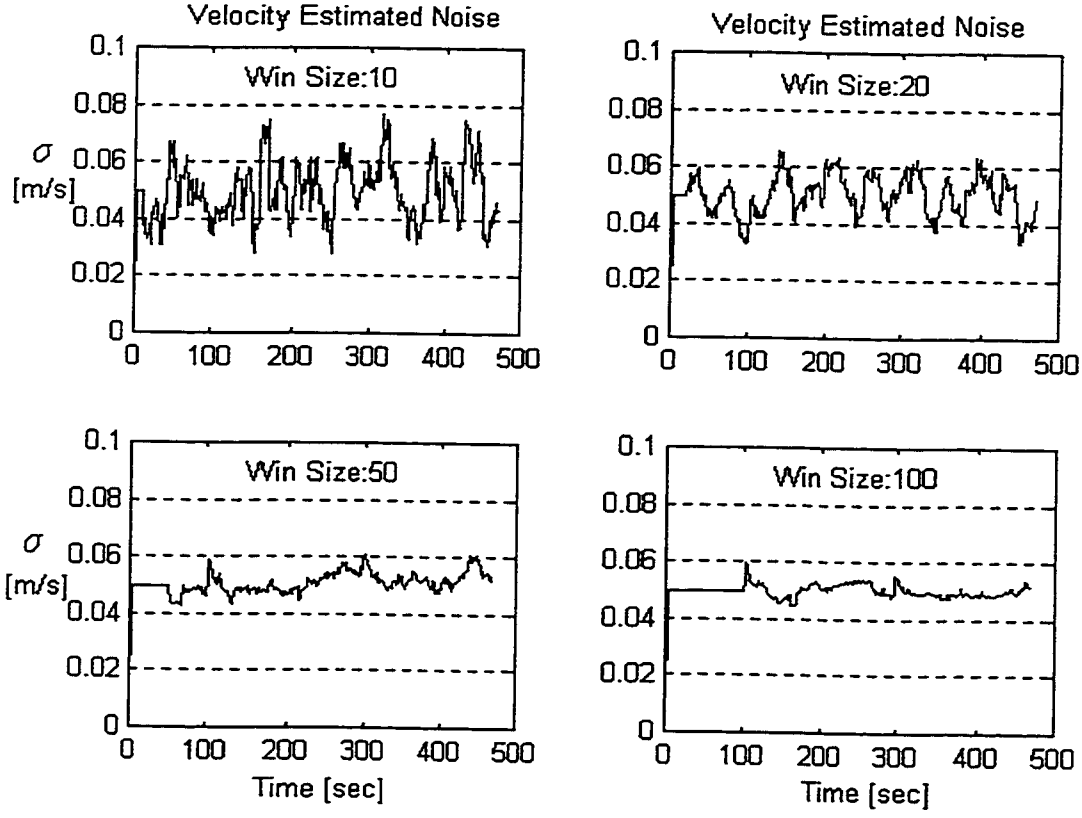

Fig. (5.11) : Changes in the Estimated R vs. Window Size (Simulation) - AKF

The changes in the Q matrix, on the other hand, seem to follow geometrical and dynamical changes in the trajectory more than the changes in the R matrix, see Fig. (5.12) below. This can be explained in light of Eqs. (4.24) and (4.34). The estimate of the Q matrix directly include the 'Δx' parameters which are not directly linked to R. The changes in the 'Δx' parameter reflect changes occurring in the trajectory. Although the window size clearly has an effect on the estimate of the Q matrix, it is not as apparent as in the estimate of the R matrix. For instance, the 10 second and 20 second window size estimate are very close to one another in the Q estimate, while they are quite different in the case of the R estimate; the same also applies to the 50 second and 100 second estimates. The estimate of R is based on a white sequence, the innovation sequence, that defines the estimate variance envelope.

At take-off and at the turn, there is a widening of the uncertainty tube of the system noise Q to allow for fast dynamical changes. This property makes the adaptive filter favorable in high dynamics situations. The uncertainty in the system (or process) model varies along the trajectory and this is reflected by the Q matrix. While the filter bandwidth (or uncertainty tube) reaches a value of 40-50 arcsec for the noise of the azimuth misalignment state, for instance at take off and at turns, it stays at the level of a few arcseconds in the straight line segment with constant velocity between epochs 150 to 250 seconds. There is a clear disadvantage of using large window sizes of 50 seconds or 100 second in this case, because the trajectory changes are not directly reflected.

5.2.7 Diagonal vs. full R and Q

The purpose of this section is to compare the adaptive Kalman filter performance when full R or Q matrices are used as opposed to the performance when the off-diagonal elements of the estimated R or Q matrices are ignored and only the diagonal elements are considered. When a full R or Q matrices are to be estimated, the number of adaptive unknowns increase and the complexity of the adaptive estimation procedure increases.

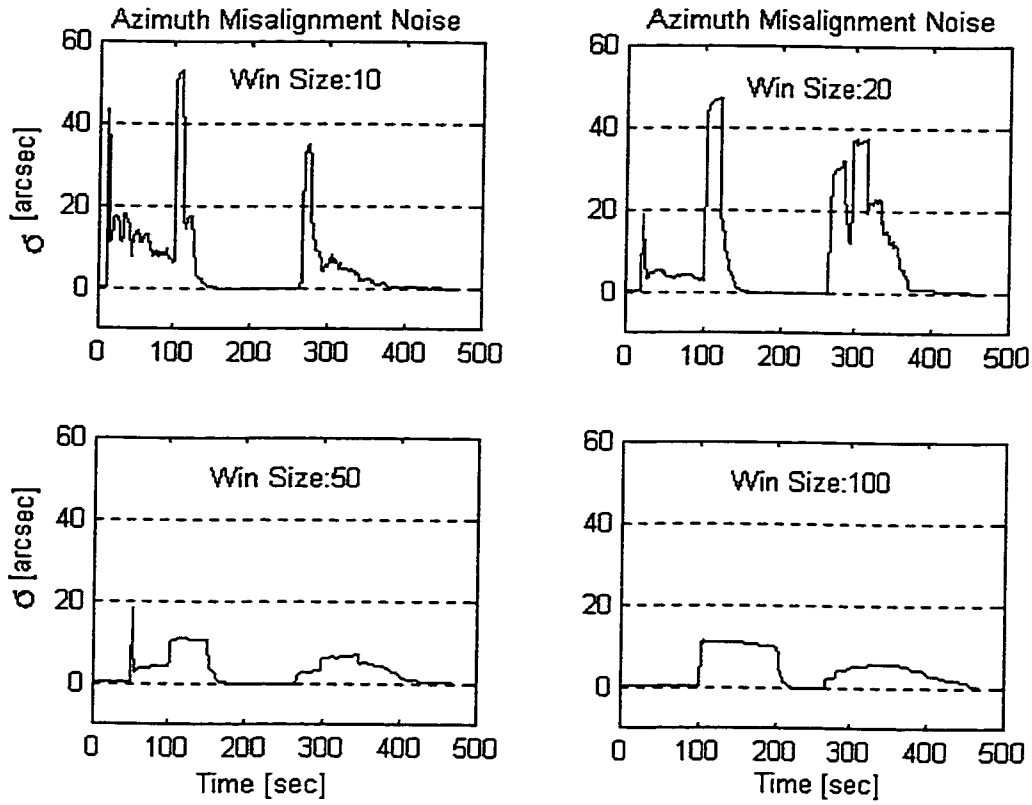

Fig. (5.12) : Changes in the Estimated Q vs. Window Size (Simulation) - AKF

Fig. (5.13) illustrates the correlation coefficient obtained from the estimated full R matrix when using different window sizes. The correlation coefficient chosen for this discussion is between the GPS update measurements for latitude and longitude in the INS/GPS adaptive Kalman filter; the rest of the correlation coefficients between the position and velocity update measurements followed more or less the same pattern. The figure shows clearly that as the averaging window size increases, the estimated correlation coefficient decreases. In fact, this was to be expected because of the whiteness property of the innovation sequence upon which the estimated R matrix is based. The choice of a very large window size would mean an almost diagonal estimated R matrix. A conventional Kalman filter can be thought of as an adaptive filter with a very large averaging window, i.e. a window of the size of the whole data span. In light of this fact, one can justify the use of a diagonal R matrix in the case of a conventional Kalman filter. Moreover, the performance of the filter in estimating the states, x, and their covariance,

P, is almost the same as for a diagonal R. So, one could come to the conclusion that the neglect of the off-diagonal elements of the R matrix has little practical effect on Kalman filter performance, although including the off-diagonal elements of the covariance matrix is theoretically appealing. The same conclusion also applies to the adaptive Kalman filter because the algorithm applied after adapting R and/or Q is the same as that of the conventional Kalman filter.

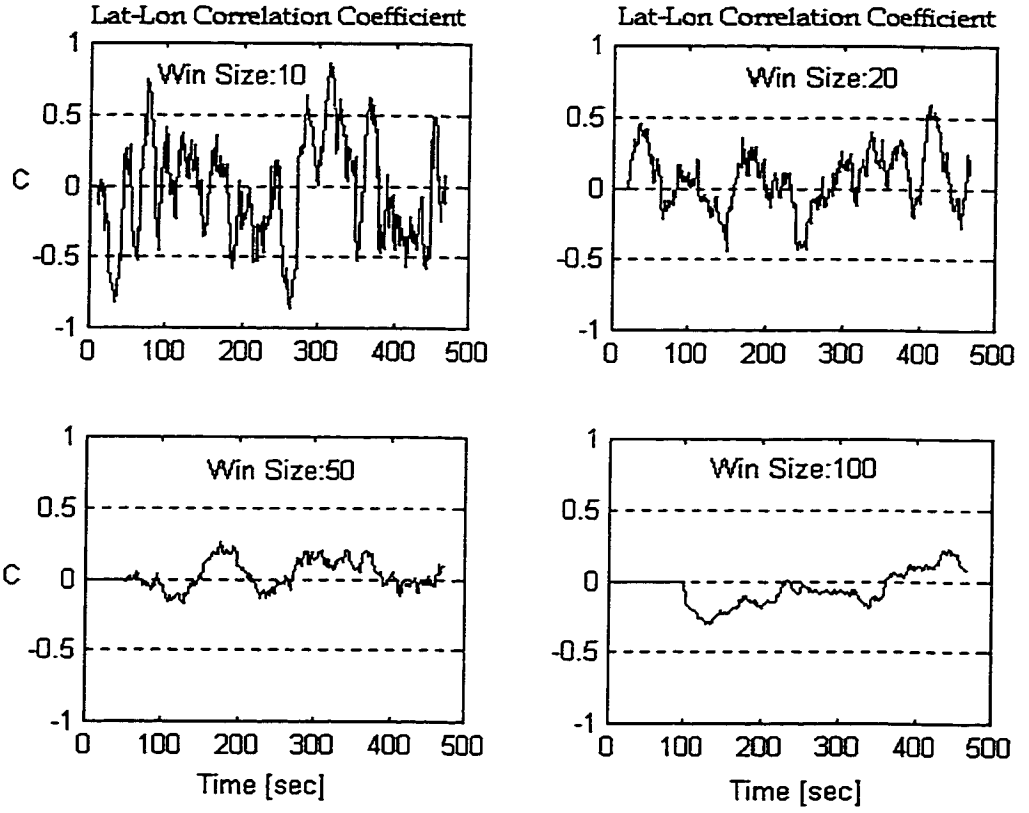

Fig. (5.13) : Correlation Coefficient vs. Window Size (Simulation) - AKF Full R

The conclusion obtained from the analysis of a full R matrix vs. a diagonal R matrix, applies also to the case of a full Q matrix vs. a diagonal Q matrix. It was found that, as the averaging window size increases, the correlation between the filter states in the Q matrix decreases. Also, the performance of the adaptive Kalman filter when a full Q is used is pretty much the same as its performance when a diagonal Q is used. For instance, Fig. (5.14) below illustrates the azimuth misalignment state when a full Q is

used. Fig. (5.4b) illustrates the same state for a diagonal Q. There is little difference between the two cases. Thus there is no real need to use a full matrix Q when a diagonal Q does the job.

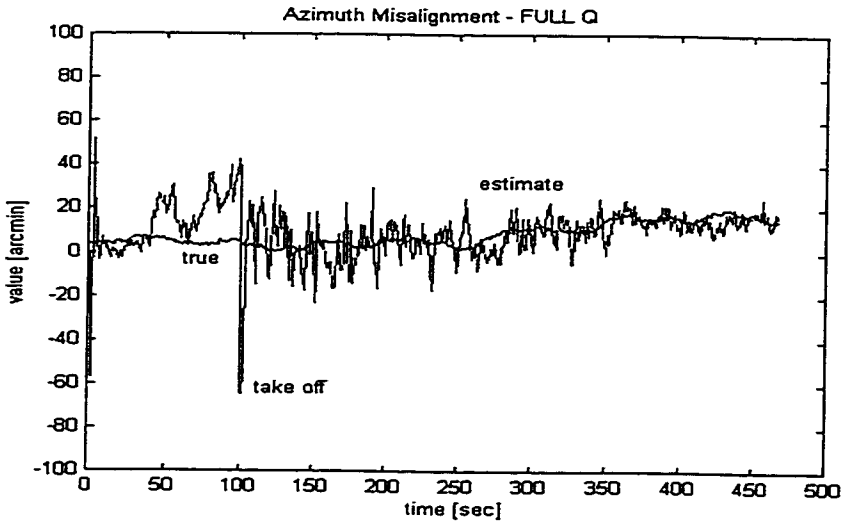

Fig. (5.14) : Azimuth Misalignment State Estimate (Simulation) - AKF Full Q

5.2.8 Tuning the state covariance matrix P

In conventional Kalman filtering, once the filter reaches steady state, the estimate of the state covariance matrix reaches a constant value. It only fluctuates in the transition stage until it reaches the steady-state stage and locks onto it. This, however, is not the case with the adaptive Kalman filter. Since the process is not assumed stationary, changes to the state estimates and to their covariance are expected. Fig. (5.15) shows that the estimate of the position state variance, after transition, fluctuates around the decaying average that would have been accomplished by the conventional filter. There is a clear reflection of the dynamics during the take-off (around epoch 100) and the turn (around epoch 300) on the estimated variance. This change in the estimated position variance reflects reality because one would not trust a position estimate at take-off as one would do with a position estimate in benign dynamics.

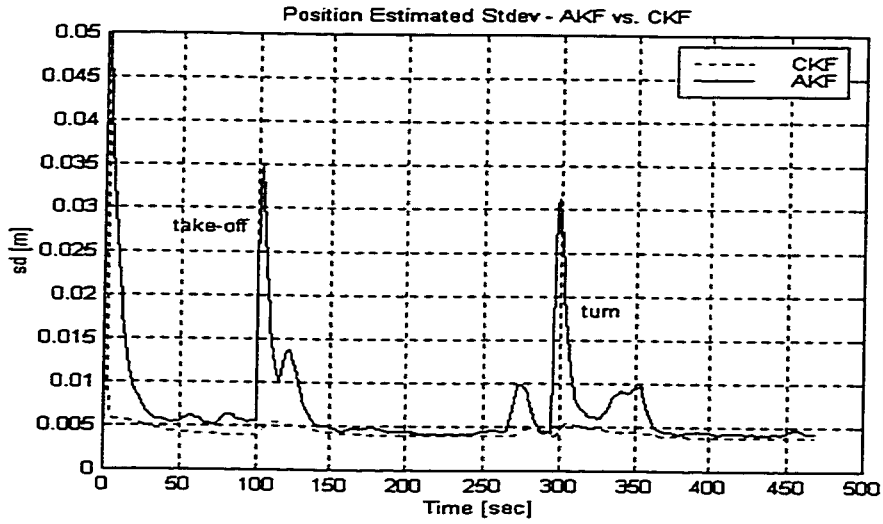

Fig. (5.15) : The Estimated State Covariance P (Simulation) - AKF vs. CKF

As it was discussed in §4.4.5, the R and Q simultaneous adaptation leads to an unstable and divergent filter estimate. Fig. (5.16) below depicts the estimated variance for the position state when adapting R and Q simultaneously. Although the filter kept a positive variance, it diverged to a value almost one order of magnitude higher than that resulting from R-only or Q-only adaptation, compare with the result in Fig. (5.15) above. It, therefore, asserts the analytical analysis of §4.4.5. It also confirms the conclusion of the non-suitability of the R&Q simultaneous adaptation, in general.

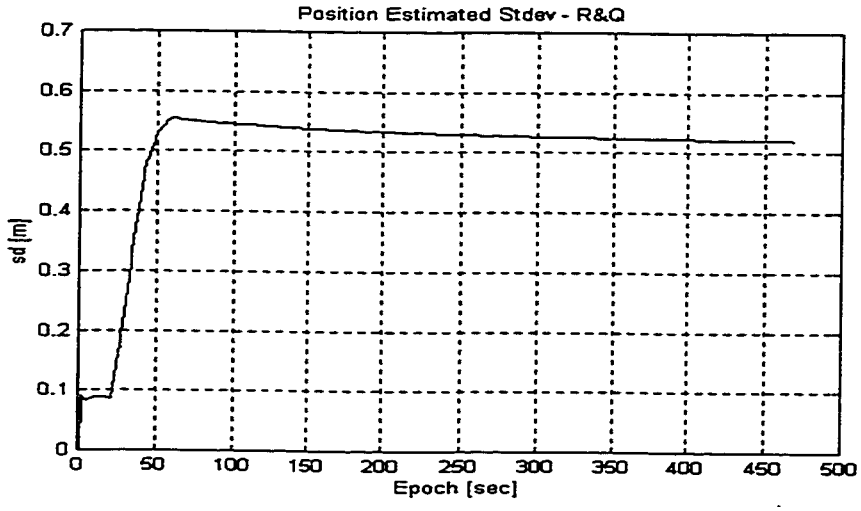

Fig. (5.16) : The Estimated State Covariance P (Simulation) - AKF (R&Q)

6.
GPS AMBIGUITY RESOLUTION USING THE INTEGER WHITENING FILTER

The high accuracy of the integrated INS/GPS system is a function of both INS and GPS. To obtain high GPS accuracy, the phase ambiguity has to be resolved to its correct value. The problem of GPS phase ambiguity resolution is discussed in this chapter. A simple and economical , yet efficient, solution to this problem is outlined. The solution is based on a factorization and transformation method to decorrelate the highly correlated double difference phase ambiguities and round to the nearest integer, a method called OTFWhite. Precision as well as geometric implications of the method are discussed.

6.1 The Problem of GPS Phase Ambiguity Resolution On The Fly

Highly precise GPS position estimates can only be attained when the ambiguities of the carrier phase observations are resolved to their correct integer values. A simple technique to resolve the integer carrier phase ambiguity is the use of long observation periods over which receiver-satellite geometry changes and an ambiguity float solution asymptotically approaches the correct integer one. These long periods of observation assure a better (more precise) float estimate and, in effect, a decorrelated ambiguity set. Over short observation times, however, the same effect can be obtained by applying a whitening filter. The role of the whitening filter is to decorrelate the ambiguities and improve the precision of their estimates. The whitening process also plays a role in the required change in the receiver-satellite geometry. Both effects are essential to the ambiguity resolution process.

6.1.1 Methods of ambiguity resolution On The Fly

Over the last decade various methods for ambiguity resolution have been proposed. In these methods, the ambiguity is either resolved in the measurement domain or resolved in the position domain. In the latter, the ambiguity resolution takes place based on a

precise pre-determined receiver position. In the measurement domain, however, the ambiguity is resolved in the ambiguity space. The two main approaches to resolving the ambiguity in the ambiguity space are the code-guided and the phase-only techniques. The code-guided technique requires receivers that have a low noise level and high multipath mitigation characteristics, see e.g. [Almgren 1998]. The phase-only resolution technique employs either a search method or a space-projection method or both. The phase-only resolution technique will be discussed here.

In the search method, a float estimate of the phase ambiguity is first obtained and a search space is formed around it. A search algorithm is then employed to find the correct ambiguity set that the residual distribution is peaked at. Examples of the techniques that use search algorithms are: the Least-Squares-Search method [Hatch 1990], the ambiguity covariance methods like the FARA [Frei and Beutler 1990], and the FASF [Chen and Lachapelle 1994], the genetic algorithms [Li 1995], and the Integer Non-Linear Programming method [Wei and Schwarz 1995]. Comparative studies of most of these methods can be found in [Hatch and Euler 1994, Hein and Werner 1995].

The power of the search techniques stems from their ability to reject incorrect ambiguity candidates. The aim of the search algorithms, therefore, is that after the rejection procedure, it is left with two acceptable candidates. A test is then performed to accept the best candidate. The search technique is widely used and has been implemented in different ways. However, the available algorithms that use a search technique, are rather complicated and often not easily understood. The direct search which is simple and easily understood, on the other hand, is time consuming and inefficient. In addition, the search techniques lack the ability to utilize the information content of the float estimate because the float estimate in the search techniques is considered as a starting point not as a goal in itself. In other words, none of the search techniques attempts to directly or indirectly improve the quality of the float estimate.

The space-projection technique, on the other hand, relies on the quality of the float ambiguity estimate. In this technique, the whole estimation problem is projected onto another space that is easier to analyze. As a consequence of this special projection, the

ambiguity float estimate becomes more precise, the ambiguity set decorrelates, and the receiver-satellite mutual positional vectors geometry changes. These three effects accelerate the ambiguity resolution process. The whitening filter, through an iterative matrix factorization procedure, is an example of a space-projection technique for resolving the integer ambiguity over short baselines [Mohamed and Schwarz, 1998]. LAMBDA (Least squares AMBiguity Decorrelation Adjustment) is an example of an algorithm that combines a space-projection technique with a search technique in one algorithm. The space projection (transformation) in the LAMBDA algorithm is carried out through consecutive Gaussian transformations. The search is combined with a conditional least squares adjustment and is based on sequential least-squares estimation, see [Teunissen 1994, Rizos and Han 1995, Jonge and Tiberius 1996] for details.

6.1.2 OTF requirements

In the process of resolving the integer ambiguity, the float ambiguity estimate is a real-value representation of the integer ambiguity at the time the ambiguities are decorrelated and have reached a steady-state condition with high precision. This implies that in order to resolve the integer carrier phase ambiguity, a precise float estimate of the ambiguity is needed. This can be achieved either by enlarging the observation period over which receiver-satellite geometry changes and the estimate of the float ambiguity becomes more precise, or by obtaining the same effect through a process like whitening which reduces the data noise and allows a reliable estimation over a shorter observation time.

For short baselines and with space projection, a sophisticated search is not needed and, in effect, complicates the algorithm. Therefore, the problem of GPS ambiguity resolution on the fly over short baselines can be solved with simple space-projection technique and no search. The sought algorithm, which does not require a search, is easy to understand, simple to implement, applicable in real time, economic for hardware implementation, and, of course, is reliable for short baselines. The algorithm can be part of a Kalman filtering algorithm used in the solution of the kinematic modeling.

6.1.3 Ambiguity resolution using a Kalman filter algorithm

In kinematic positioning, the problem of integer ambiguity resolution is embedded in the process of estimating a GPS-based vehicle trajectory. The estimation of the float solution starts by using the observation model:

$$z = B\,b + A\,a + e_z \tag{6.1}$$

or in more compact form,

$$z = H\,x + e_z \tag{6.2}$$

where,

z : 'm' measurement vector

b : 'p' baseline component vector

B : 'mxp' geometry design matrix

a : 'g' ambiguity bias vector

A : 'mxg' ambiguity design matrix

e_z : 'm' measurement error vector

H : 'mxn' measurement design matrix, [B A]

x : 'n' (p+g) parameter (state) vector, $[\,b\ a\,]^T$.

The a priori stochastic information necessary to perform an L2-norm algorithm is:

C_{ez} : 'mxm' covariance matrix of measurement errors

C_b : 'pxp' covariance matrix of baseline components

C_a : 'gxg' covariance matrix of ambiguities.

The criterion for solving this problem is to minimize the norm of the errors in the L2-norm space, $\min \| e \|^2$, i.e. $\min_{b,a} \| z - Bb - Aa \|^2_{C_z^{-1}}$, with $b \in R^p$ and $a \in Z^g$, where R represents the real-number space and Z represents the integer number space, and C_z^{-1} having the stochastic information on z. The solution of this optimization problem requires two steps, first, the solution of the navigation problem and estimation of a float

ambiguity, and, second, the estimation of the integer ambiguity and correction of the navigation solution.

Step 1: ***Estimation of the Float Ambiguity***

The above formulation of the problem can be solved using a standard Kalman filter algorithm, see Fig. (B.2). In case the a priori stochastic information about the parameters 'a' and 'b' is not available, the filter starts the update cycle with zero matrices for P_{xo}^{-1} in the inverse Kalman filter setup (sometimes called Bayes filtering or information filtering). This special case is the most common; a more general solution, however, is always available through this algorithm once the a priori information has been obtained. The result of this step is the estimation of the baseline components along with a float estimate of the integer ambiguities which takes the form:

$$\hat{x}(+) = \begin{bmatrix} \hat{b} \\ \hat{a} \end{bmatrix} = \begin{bmatrix} B^T R^{-1} B B^T + B^T R^{-1} A A^T \\ A^T R^{-1} B B^T + A^T R^{-1} A A^T \end{bmatrix}^{-1} R^{-1} z. \tag{6.3}$$

The precision of $\hat{x}(+)$ is:

$$P(+) = \begin{bmatrix} C_{\hat{b}} & C_{\hat{b}\hat{a}} \\ C_{\hat{a}\hat{b}} & C_{\hat{a}} \end{bmatrix} = \begin{bmatrix} B^T R^{-1} B & B^T R^{-1} A \\ A^T R^{-1} B & A^T R^{-1} A \end{bmatrix}^{-1}. \tag{6.4}$$

The precision of the float estimate depends on the errors contaminating the observations. As discussed in Chapter 3, with double differenced GPS phase observations, clock errors disappear. Also, over short baselines, the remaining contamination through the atmospheric and orbital errors is fairly small due to their spatial correlation. What remains after double differencing are residual spatially correlated errors, receiver noise and multipath effects. At this point, if one gets a highly precise float estimate, rounding to the nearest integer should in the case of a short baseline lead to the correct integer ambiguity set. Unfortunately, the float estimate

obtained by this method is not precise enough, especially for short observation periods. This is due to the effect of both the unmodeled and spatially correlated errors and signal multipath. In addition, double differencing causes the double differenced ambiguities to become highly correlated, especially at the first few observation epochs. Thus, a second step is required for the estimation of the integer ambiguity.

Step 2: ***Solution of the Baseline based on the Integer Ambiguity***

Once a float solution '$\hat{a}$' has been obtained, a second estimation step can take place. The criterion for solving the second problem can be set in the L2-norm space as $\min_{a} \| \hat{a} - a \|^2_{C^{-1}_{\hat{a}}}$, where $a \in Z^g$, and $C^{-1}_{\hat{a}}$ the estimated ambiguity covariance matrix from step 1. The result of this step is the estimation of the integer ambiguity; the estimation of the integer ambiguity will be discussed in §6.2.

Once the correct integer ambiguity is known, it can be backward substituted into the original problem and the baseline components can be solved for. It is also possible to use the correctly estimated (fixed) integer ambiguity set as a deterministic update measurement to the filter and calculate the updated baseline components as follows

$$\breve{b} = \hat{b} - C_{\hat{b}\hat{a}} C^{-1}_{\hat{a}} (\breve{a} - \hat{a}), \tag{6.5}$$

and their precision as:

$$C_{\breve{b}} = C_{\hat{b}} - C_{\hat{b}\hat{a}} C^{-1}_{\hat{a}} C_{\hat{b}\hat{a}}, \tag{6.6}$$

where, $\breve{b}$ is the updated baseline solution. It is, however, more appropriate in most cases to consider the estimated (fixed) integer ambiguity set as a stochastic variable rather than a deterministic one. In this case, the ambiguity covariance matrix is not set to zero in the update equation of the Kalman filter, but to a value that represents the receiver-satellite

configuration at hand. By so doing, the baseline component estimation becomes more realistic.

6.1.4 Ambiguity testing

When resolving the ambiguity using the whitening filter technique, one of two approaches can be taken to decide upon the correct ambiguity set. In the first approach, one considers the closest integer to the float solution as the correct ambiguity at the time the largest ambiguity variance is smaller than a pre-specified value; a χ^2 test can be used to decide on the smallness of the ambiguity variance in this case. In the second approach, in order to make the selected fixed ambiguity set more reliable, a number of ambiguity candidates are used. These candidates are normally chosen to be close to the float solution and, in general, the higher the precision of the float solution, the smaller the number of possible integer candidates. The closest integer to the float solution is a very good initial candidate and indeed, in most cases, leads to the correct integer solution. The last statement is true when the ambiguity variance is small enough (smaller than a pre-specified χ^2 value) and the iterative integer whitening process completely whitens the ambiguity; due to the restriction of having integer ambiguity transformation matrix, the factorization whitening process, most of the time, does not result in fully decorrelating the ambiguities. Because the previous two conditions are not always given, other candidates are required. The upper and lower integer bounds of the float solution are possible candidates.

For all possible ambiguity integer candidates, the norms of the residuals are calculated either in the measurement space or in the ambiguity space. In either space, the smallest norm (best candidate) and the second smallest norm (second best) are chosen for testing. Because of the nature of their estimation procedure and in order to be able to apply statistical testing, the ambiguity residuals are assumed to have random distribution. Since both norms represent a sum of squares of random errors, their values and the ratio between them should theoretically follow a χ^2 distribution and Fisher distribution,

respectively. The χ^2 and Fisher percentiles (thresholds), for a certain test significance level, depend on the number of degrees of freedom of the problem, i.e. the number of available satellites for a given baseline. Hence, the algorithm should be designed in such a way that these values can be defined by the user or are variable parameters with an expert lookup table. Typical values for the two threshold parameters are 30 to 20 and 1.2 to 2.5, respectively, for a satellite coverage of 9 to 5, with good to fair geometry (PDOP). In order to check against abrupt changes, it is good to have a validation (or verification) time, a time over which the ratio of the second norm to the best norm is greater than the threshold. This time is usually chosen to be greater than one epoch and is typically between 5 to 30 epochs. Fig. (6.1) summarizes the previous discussion and gives a schematic description of the procedure used in the developed software, KINWHITE.

From a geometrical point of view, baselines of a few hundred kilometers are considered short in the context of satellite positioning for points on the Earth. Due to the effect of the unmodeled atmospheric errors, however, a hundred kilometer baseline is considered long in the context of baseline estimation and ambiguity resolution. The definition of a short baseline, therefore, involves more than a distance in space. The most important two factors affecting the short baseline definition are the number of satellites used and their configuration, i.e. their PDOP factor. Based on these two factors, a χ^2 threshold can be set to specify the distance after which the ambiguity resolution using the whitening filter becomes not reliable and hence an additional search is recommended. When using numerical results with dual frequency receivers, baselines of 30 to 40 km can be considered as short for a satellite coverage of 6 to 8, a PDOP factor between 3 to 2, and a χ^2 of approximately 25 under a 0.1 percent test significance level.

6.2 The Integer Whitening Filter

Whitening is a factorization process used to project a sequence of data from one space to another [Bierman 1977]. It is used to obtain a decorrelated version of a data set by projecting it onto another space that is simpler to analyze. In the context of adaptive

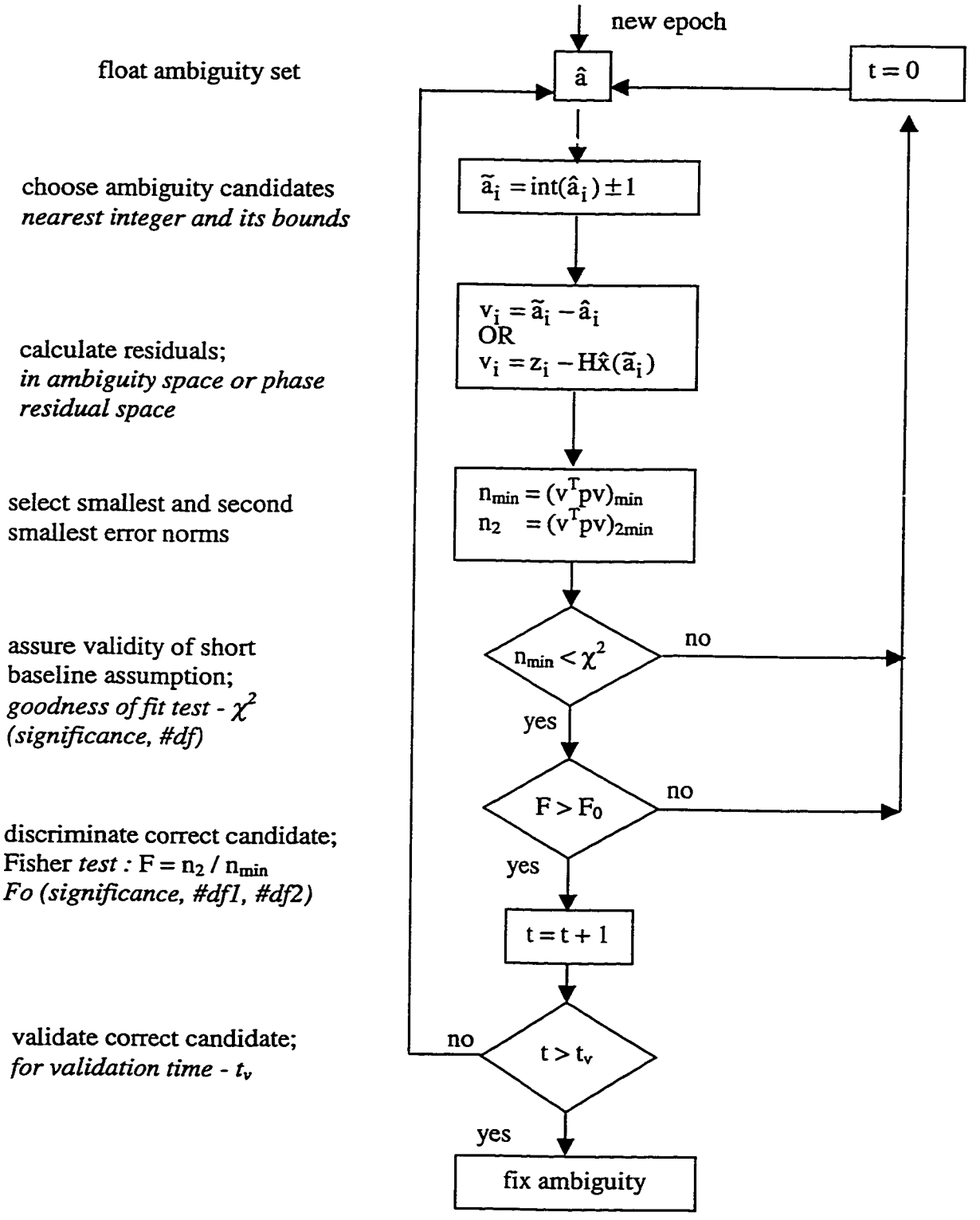

Fig. (6.1): Statistical Testing of Ambiguity Fix in KINWHITE

Kalman filtering, as described in Chapter Four, the whitening filter, in its float version, is used to decorrelate the innovation sequence used to fine-tune (adapt) the statistical information of the filter according to the system dynamics. In the context of ambiguity resolution, however, whitening is used in its integer version to decorrelate the highly correlated GPS carrier phase ambiguities over short observation periods. It also results in pseudo-observations with lower noise.

6.2.1 Ambiguity transformation and its requirements

Whitening is a transformation process that projects the problem described by the observation model of Eq. (6.2) from its original space into another space which is simpler to analyze. This is accomplished by factorizing the update measurement covariance matrix as follows:

$$C_e = U\,D\,U^T \tag{6.7}$$

where U is an upper triangular matrix and D is a diagonal matrix. By pre-multiplying both sides of Eq. (6.2) by U^{-1}, one gets

$$U^{-1}z = U^{-1}Hx + U^{-1}e \tag{6.8}$$

or in compact form

$$\bar{z} = \bar{H}x + \bar{e} \tag{6.9}$$

which is the transformed observation equation using the same state vector 'x'. The transformation is non-orthogonal and results in transformed (whitened) measurements that are uncorrelated, because

$$\begin{aligned} C_{\bar{e}} &= E(\bar{e}\bar{e}^T) = E(U^{-1}ee^TU^{-T}) \\ &= U^{-1}E(ee^T)U^{-T} = U^{-1}C_eU^{-T} = D. \end{aligned} \tag{6.10}$$

There are, however, conditions on the choice of the Ambiguity Transformation Matrix (ATM):

- Firstly, since the ambiguity transformation process should not alter the integer nature of the ambiguity parameters, the 'ATM' should only contain integer entries,
- Secondly, in order to assure a two-way transformation between the original space and the white space, the whitened and the original ambiguity covariance matrices should have equal volumes (determinants).

Since the ATM, in the general case, is a float matrix, the first condition constrains the degree of success of the filter to decorrelate the ambiguities. On the other hand, the second condition usually results in a higher precision for the entries.

6.2.2 Iterative integer whitening

To carry out the integer whitening process, a one step whitening is not possible because of the integer constraint on the ATM entries. To overcome this constraint and get a covariance matrix of the whitened observations which is close to a diagonal, an iterative procedure is needed which is shown in Fig. (6.2) below.

After passing the identity check in step number 7, the whitening (transformation) integer matrix is calculated as follows

$$T^{-1} = \prod_{k}^{l} \bar{L}_i^{-1} \bar{U}_i^{-1} \tag{6.11}$$

where Π is the product symbol and k is the number of iterations. It is worth mentioning here that the product in the previous equation showed up because the substitution of the factored matrices should yield the original matrix as follows:

$$C_e = \bar{L}_k^{-1}\bar{U}_k^{-1}\bar{L}_{k-1}^{-1}\bar{U}_{k-1}^{-1}...\bar{L}_1^{-1}\bar{U}_1^{-1}\bar{C}_e\bar{L}_1^{-T}\bar{U}_1^{-T}...\bar{L}_{k-1}^{-T}\bar{U}_{k-1}^{-T}\bar{L}_k^{-T}\bar{U}_k^{-T}. \tag{6.12}$$

Starting with C_e, do an upper triangular factorization and get a first real-value approximation, say U_1.

Round all elements of U_1 to their nearest integers

Whiten (transform) the covariance matrix C_e after rounding

Factor the previously whitened covariance matrix, but this time use a lower triangular (ldl) factorization, get L_1.

Round all elements of L_1 to their nearest integers

Re-whiten the covariance matrix $\overline{C}_e$ after rounding

Check whether $\overline{L}_1$ is identity (re-iterate if not)

whitening completed

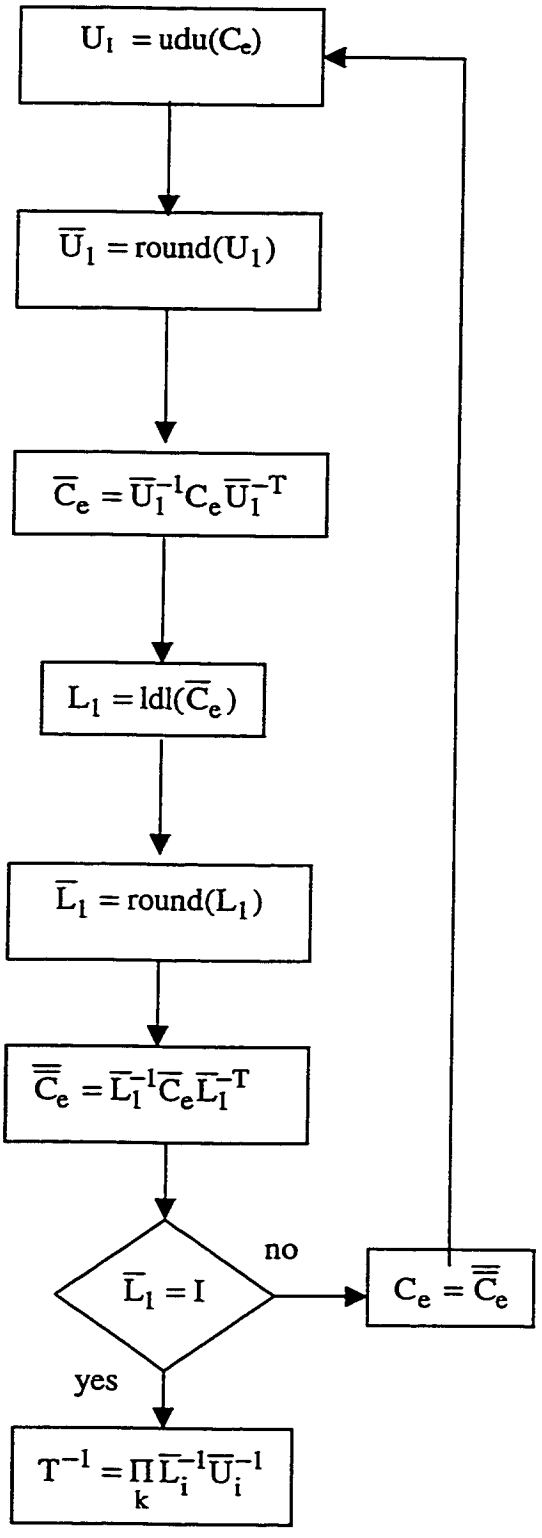

Fig. (6.2): Iterative Integer Whitening Procedure

The whitened ambiguities and their covariance matrix are calculated as:

$$\bar{a} = T^{-1}a, \tag{6.13}$$

and

$$C_{\bar{a}} = T^{-1}C_a T^{-T}, \tag{6.14}$$

respectively; see Appendix C for the Matlab® implementation of this algorithm.

The degree of success of the whitening process, with the integer constraint applied, can be measured by the decorrelation number. The decorrelation number is the square root of the determinant of the whitened observation correlation matrix:

$$\bar{r}_{\bar{a}} = \sqrt{|\rho_{\bar{a}}|}, \tag{6.15}$$

where

$$\rho_{\bar{a}} = \sqrt{[\mathrm{diag}(C_{\bar{a}})]^{-1}}\, C_{\bar{a}} \sqrt{[\mathrm{diag}(C_{\bar{a}})]^{-1}}. \tag{6.16}$$

The closer this number is to one, the more successful the iterative integer whitening is. In the case of short baselines, this happens in the first few epochs of observation when using the whitening filter. In this case, the decorrelation number varies between 0.9 to 0.98 for satellite coverage between 5 to 8.

When comparing the whitening filter to the LAMBDA method, the similarities are in the factorization of the covariance matrix, while the differences are in the approach to integer ambiguity resolution. The LAMBDA method combines three essential elements to obtain a general solution to the integer ambiguity problem; they are: a Gaussian transformation, a conditional least squares adjustment, and a conditional search, see e.g. [Jonge and Tiberius 1996]. Although these elements are clearly kept apart in the

mathematical formulation, they are combined in the numerical algorithm. The result is a solution which achieves a global minimum. The whitening filter aims at a float estimate of the ambiguities which has the smallest possible standard deviation and which is obtained by a 'udu' and 'ldl' factorizations. This estimate is then used to determine the integer solution without a search procedure. The decision on whether or not to consider this solution as the final ambiguity set is based on statistical arguments (Fig. (6.1)). If the hypothesis is rejected, a search procedure is applied. This approach results in a very simple and very fast algorithm for many cases of practical importance, typically for all baselines up to 35-40 km. It is not as rigorous as the LAMBDA method and may occasionally result in a local minimum.

6.3 Precision Implications

For the discussion in this and the next section, two satellites in 2D space case will be considered. In this case, C_e, in general, is a full 2x2 matrix of the form

$$C_e = \begin{bmatrix} \sigma_1^2 & \sigma_{12} \\ \sigma_{12} & \sigma_2^2 \end{bmatrix}. \tag{6.17}$$

The whitening of C_e, as described before and as implemented in Appendix C, results in

$$C_{\bar{e}} = \begin{bmatrix} \sigma_1^2 - \dfrac{\sigma_{12}^2}{\sigma_2^2} & 0 \\ 0 & \sigma_2^2 \end{bmatrix} \text{ and } U = \begin{bmatrix} 1 & \dfrac{\sigma_{12}^2}{\sigma_2^2} \\ 0 & 1 \end{bmatrix}. \tag{6.18}$$

It is clear that the whitening process preserves the volume, i.e. the determinants of the covariance matrices before and after whitening are the same. Moreover, taking the trace of the covariance matrix as a precision measure, one can conclude that the whitened observations are more precise than the original ones if correlation exists in the original observations; the difference in this specific case being equal to $(\sigma_{12}^2 / \sigma_2^2)$.

Another way of looking at this problem is to consider the matrix 'U' as an unknown to be determined. In this case,

$$C_{\bar{e}} = U^{-1} C_e U^{-T} = \begin{bmatrix} 1 & -u \\ 0 & 1 \end{bmatrix} \begin{bmatrix} \sigma_1^2 & \sigma_{12} \\ \sigma_{12} & \sigma_2^3 \end{bmatrix} \begin{bmatrix} 1 & 0 \\ -u & 1 \end{bmatrix} = \begin{bmatrix} d_1 & 0 \\ 0 & d_2 \end{bmatrix} \tag{6.19}$$

where the precision measure after whitening is

$$\Phi = d_1 + d_2 = \sigma_1^2 + \sigma_2^2 - 2u\sigma_{12} - u^2\sigma_2^2. \tag{6.20}$$

The minimization of Φ with respect to 'u' results in

$$\frac{\partial \Phi}{\partial u} = -2\sigma_{12} - 2u\sigma_2^2 = 0 \Rightarrow u = \frac{\sigma_{12}}{\sigma_2^2} \tag{6.21}$$

which is the same result as obtained by the 'udu' factorization.

It is clear that the more the original observations are correlated (larger value of σ_{12}), the more precise the whitened observations become, i.e. the more efficient the whitening process will be. It is also clear that the whitening process is more efficient for large dimensions because more terms will be subtracted from the trace after whitening. These two observations are very important to the problem of integer ambiguity resolution and, in fact, they are the key to the success of this technique.

6.4 Geometric Implications

The whitening process, being a space projection technique, can also be interpreted as a transformation of the original receiver–satellite mutual positional vectors geometry on a non-orthogonal system of axes. For the 2D case, consider only the change in one of

the receiver-satellite vectors. In this case, the spatial position of the satellite after whitening with respect to its original position is computed as follows:

$$\begin{bmatrix} x' \\ y' \end{bmatrix} = \begin{bmatrix} 1 & -u \\ 0 & 1 \end{bmatrix} \begin{bmatrix} x \\ y \end{bmatrix} = \begin{bmatrix} x - uy \\ y \end{bmatrix} \tag{6.22}$$

which is depicted in Fig. (6.3) as a translation of the original space position of the satellite with respect to the receiver along the x-axis.

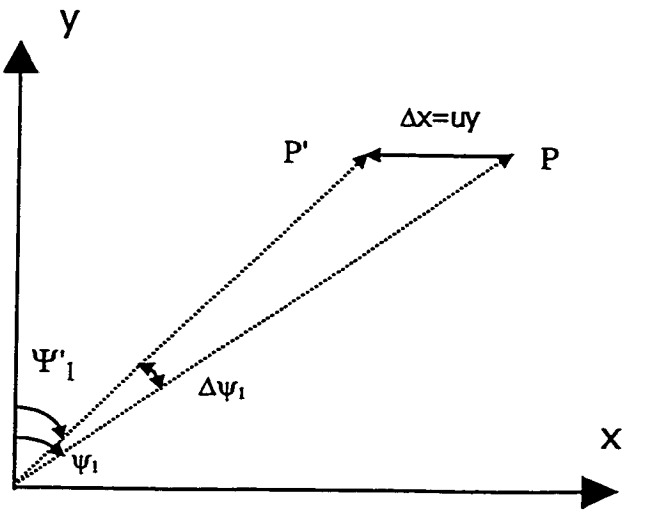

Fig. (6.3) : Relative Change in the Receiver-Satellite Vector due to Whitening

It is clear that the translation

$$\Delta x = y\{\tan(\psi_1) - \tan(\psi'_1)\} \tag{6.23}$$

is a function of the receiver-satellite vector direction cosines before and after whitening. For the case of several satellites, relative positions of satellites change as well.

To describe the receiver-satellite vector change in a collective way, an independent measure of the geometry is needed. Since the baseline geometry matrix 'B' in Eq. (6.1) contains the direction cosines of the different receiver-satellite vectors, the DOP factor based on it gives a measure of the receiver-satellite geometry. This measure is invariant

under orthogonal transformations; i.e. the sum of the diagonals of the cofactor matrix will be invariant under such transformations; that is one reason why the orthogonal transformations do not qualify as ambiguity transformations. The cofactor matrix in the original space is

$$C_{DOP} = (B^T B)^{-1}. \tag{6.24}$$

The pre-multiplication of both sides of Eq. (6.1) by the matrix U^{-1} projects the problem from the original space to the white space. By so doing, the geometry matrix in the white space is

$$\overline{B} = U^{-1}B, \tag{6.25}$$

and the corresponding cofactor matrix is

$$C_{DOP_w} = (\overline{B}^T\overline{B})^{-1} = (B^T U^{-T} U^{-1} B)^{-1}. \tag{6.26}$$

For orthogonal transformations, the product $U^{-T}U^{-1}$ would become the identity and the cofactor matrix would again be given by Eq. (6.24); this is not the case for the whitening transformation, however. By carrying out the DOP calculations, the new DOP factor can be represented in terms of the original DOP as

$$DOP_w = DOP - \Delta DOP, \tag{6.27}$$

where ΔDOP characterizes the change in the DOP factors and hence the change in the receiver-satellite mutual positional vectors geometry after whitening. The last result indicates that there must be a matrix 'U', for which ΔDOP is maximum. For the purpose of this discussion, the case of only two satellites in 2D will again be considered. In this case

$$B = \begin{bmatrix} \cos\Psi_1 & \sin\Psi_1 \\ \cos\Psi_2 & \sin\Psi_2 \end{bmatrix} \text{ and } U = \begin{bmatrix} 1 & u \\ 0 & 1 \end{bmatrix}, \tag{6.28}$$

where Ψ_1 and Ψ_2 are the angles of the receiver-satellite vectors of the two satellites with respect to the first coordinate axis, respectively, and 'u' is an unknown parameter of the matrix 'U'. Substituting 'B' and 'U' above into Eqs. (6.24) and (6.26) and computing the DOP as the trace (as opposed to the square root of the trace) of the cofactor matrix and then simplifying, one gets

$$DOP = 2 / \sin^2(\Delta\Psi), \tag{6.29}$$

and

$$DOP_w = (2 + u^2 - 2u \cos(\Delta\Psi)) / \sin^2(\Delta\Psi). \tag{6.30}$$

By substituting the last two expressions into Eq. (6.27), the DOP change is

$$\Delta DOP = (2u \cos(\Delta\Psi) - u^2) / \sin^2(\Delta\Psi) \tag{6.31}$$

where $\Delta\Psi = \Psi_2 - \Psi_1$ is the angle between the two receiver-satellite vectors. The maximum change in the receiver-satellite geometry, due to maximizing ΔDOP, occurs when

$$u = \cos(\Delta\Psi). \tag{6.32}$$

This choice of 'u' as stated above leads to maximizing (as opposed to minimizing) ΔDOP of Eq. (6.31) because the second derivative of that equation with respect to 'u' is negative. Substitute this last value into Eq. (6.32), the maximum ΔDOP is

$$\Delta DOP_{max} = \cot^2(\Delta\Psi). \tag{6.33}$$

It is clear that for dimensions higher than two, the expression for ΔDOP will be more complicated and will contain a set of angles, instead of one $\Delta\Psi$.

7. TESTS, RESULTS AND ANALYSIS : AMBIGUITY RESOLUTION

Results from three short baseline tests are presented in this chapter to analyze the performance of the developed integer whitening filter in resolving the GPS phase ambiguity. A fourth variable baseline length flight test is also reported to investigate the longest safe baseline with whitening.

7.1 Tests Description

The main objective of the ambiguity resolution tests is to investigate the performance of the whitening filter technique to instantaneously (in one epoch) resolve the ambiguities on the fly (OTF) after loss of lock or cycle slips. In addition, the time required to resolve the first ambiguities will be estimated for the following cases: single frequency (L1-only), dual frequency (wide-lane), and dual/single frequency (wide-lane then L1). In all cases, the reference for the correct ambiguity resolution was obtained by an independent software. In the first test, the threshold of the Fisher test was 1.2 and the validation (or verification) time was set to 10 epochs. In the second and third tests, the validation time was also set to 10 epochs with 1.5 for the Fisher test as threshold to account for the fact that the satellite coverage was not as good as in the first test. Also, in order to check the ability of the whitening technique to recover the integer ambiguity after loss of lock, a number of artificial gaps were introduced in the data by using a specially developed software. The data is then processed and the recovered ambiguity set is compared to the original ones. The fourth test is the gravity flight test described in § 8.1.4. For the purpose of ambiguity resolution testing, GPS only data is processed in kinematic mode for baselines ranging from few kilometers up to 135 km. The purpose of this last test was to investigate the longest safe baseline the OTF integer whitening method can resolve the ambiguity for.

7.1.1 Van test

In this case, the GPS antenna was mounted on top of a moving van used originally to georeference digitally captured images. For the purpose of static initialization, about 20 minutes of static data was first collected. The vehicle then moved for about 40 minutes in an L-shaped trajectory with an average speed of 50 km/h and frequent stops. 8 satellites were available during the test period, with an average PDOP of 1.5. The distance between the vehicle and the master station was 1.6 km during the static period and up to 6 km in kinematic mode. For data collection, Ashtech Z-12 receivers with a special logging software were used. The results of this test are shown in Fig. (7.3) and Fig. (7.4) and Table (7.1) under VA281. The vehicle trajectory is shown in Fig. (7.1) below.

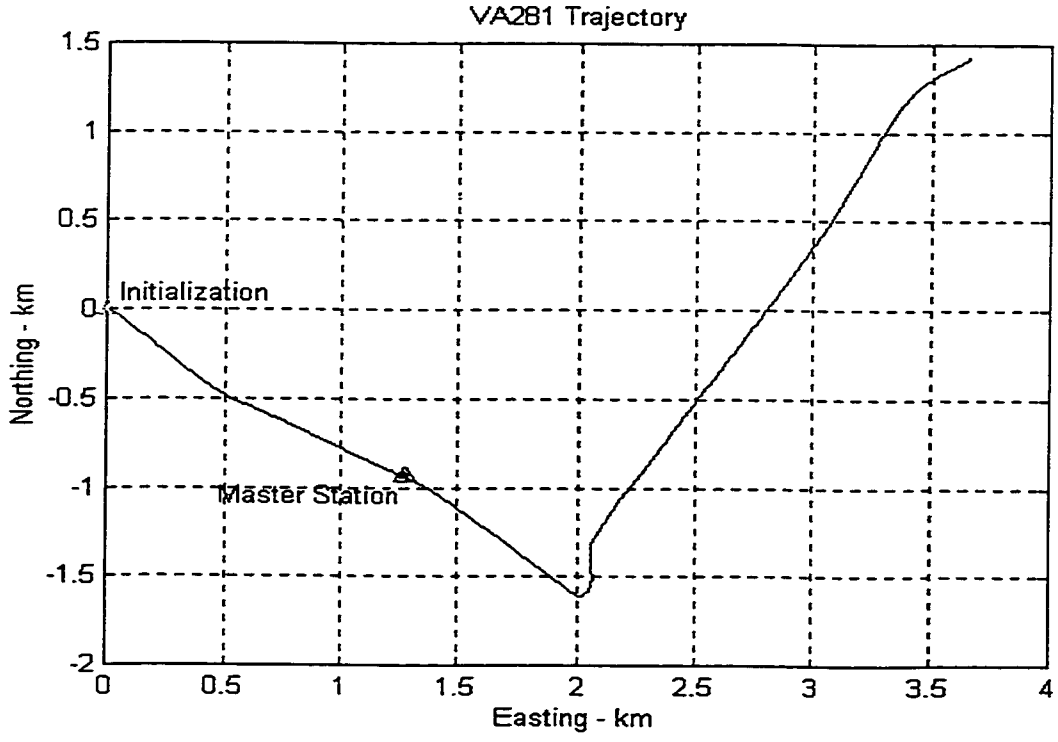

Fig. (7.1) : Trajectory Profile (VA281 Test)

7.1.2 Anorad test

The second and third tests have been conducted in a test field at the University of Calgary. In both tests, the GPS antenna was mounted on top of a platform moving along the Anorad platform described in §8.1.1. Pillar S5 on the roof of the UofC Engineering building was used as a master station. The baseline between the master and remote stations was about 200 m. For the first test, satellite coverage changed from 8 during the static period to 6 during the kinematic period. In the second test, however, only 6 satellites were available in both the static and kinematic periods. The static period, for each of the two cases, was about 20 minutes, and the kinematic period was about 30 minutes for each. Also, Ashtech Z-12 receivers with a special logging software were used to collect the GPS data. The results of the two tests are shown in Fig. (7.3) and Fig. (7.4) and Table (7.1) under 19-Jun and EW11, respectively. When plotted against time, the platform trajectory along the track is sinusoidal. The east-west trajectory, along the track, is straight line as shown in Fig. (7.2) below. The platform was moving with a maximum speed of 0.2 m/s.

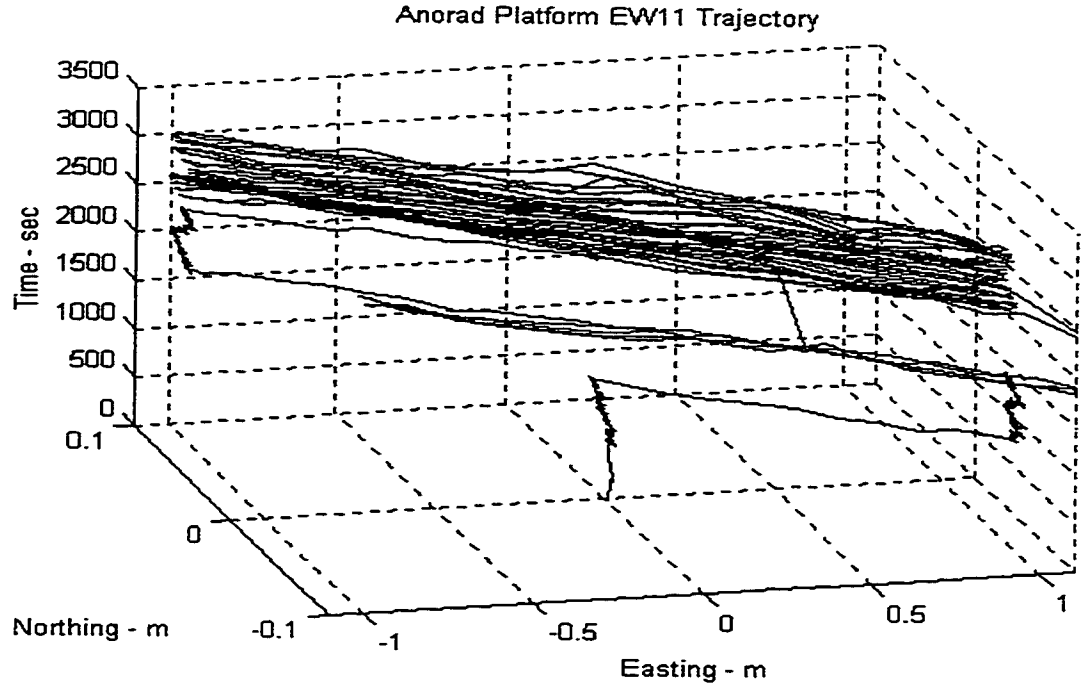

Fig. (7.2) : Anorad Platform Trajectory vs. Time (EW11 Test)

7.2 Ambiguity Resolution Test Results and Analysis

Tests presented in the following are designed to investigate the effectiveness of the integer whitening method in resolving the GPS carrier phase ambiguity on the fly, referred to as OTFWhite method.

7.2.1 Time to fix ambiguity – single frequency (L1 Case)

In this case, only L1 observations are used to resolve the integer ambiguity. Time to fix the first ambiguity is depicted in Fig. (7.3) for the L1 case, and Fig.(7.4) for the WL case, for the three tests. Although the time needed to resolve the integer ambiguity by the whitening technique is less than the one required by the search technique, the differences are not as large as in the widelane case. This is due to the fact that the wavelength of the L1 observation is much shorter than that of the widelane. The short wavelength makes it difficult to get a good float estimate over a short time of observation. The other reason is that the redundancy in the L1 case is less than it in the dual frequency case. Notwithstanding, the whitening technique shows an improvement of almost 50 percent over the search technique; i.e., only half the initialization time required by the search technique is required by the whitening technique in the L1 case to resolve the L1 phase ambiguity.

It is worth mentioning that the validation time for the whitening method was set to 10 epochs. The algorithm of the search method was to reset this time to 30 epochs in order to guarantee enough validation. This philosophy turned out not to be practically useful because of the continuous change of the satellite configuration. The correct ambiguity set could have been reached by the search method in almost the same time as the whitening technique, if the validation time would not have been reset to such a long time. The results shown in Fig. (7.3) and Fig.(7.4) and Table (7.1) below for the search method are without modifying the search algorithm validation philosophy.

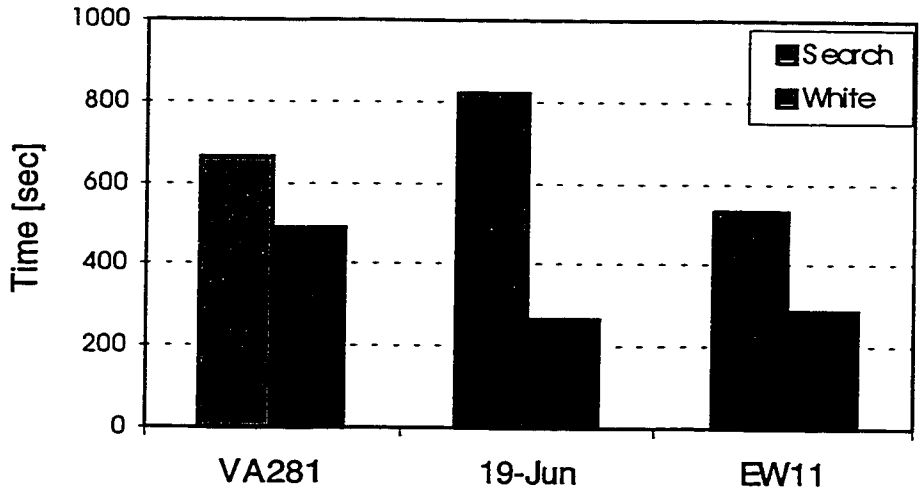

Fig. (7.3) : Time to Fix Integer Ambiguity in seconds (L1 case)

7.2.2 Time to fix ambiguity – dual frequency (widelane case)

Fig. (7.4) shows the result of the three tests for the case when dual frequency observations are available and used. In this case, the data from L1 and L2 observations are used to form the widelane combination. The longer wavelength of the widelane observation makes the whitening process highly efficient. It is also seen that the number of available satellites (number of degrees of freedom or redundancy) plays an important role in the time required to resolve the ambiguity. When 8 satellites were available (VA281 and 19-Jun), the resolution time was very short, while when only 6 satellites were available (EW11), longer resolution time was required for the OTFWhite method. This shows the importance of having good satellite coverage for the OTFWhite technique to be ultimately successful. There was not as much gain in the resolution time for the search method by using the widelane observable; the most likely reason for that is the long validation time required by the search method.

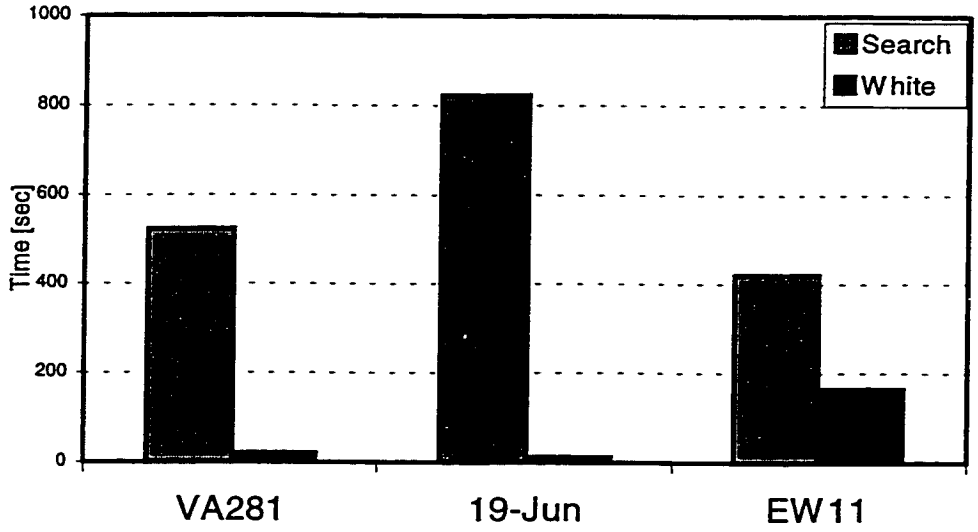

Fig. (7.4) : Time to Fix Integer Ambiguity in seconds (Widelane case)

7.2.3 Time to fix ambiguity (WL/L1 case)

The widelane observable is much noisier than the L1 one. In this respect, positioning accuracy resulting from using the widelane observable is expected to be inferior to that obtained by the L1 observable. It is preferable to resolve the L1 ambiguity after the widelane ambiguity has been resolved. Also, in cases of good satellite coverage, the rewinding of the data and solving for the L1 ambiguity, after the widelane ambiguity is resolved, makes the resolution of the L1 ambiguity much faster than the original one, see Table (7.1) column VA281. The rewinding of data seems not to work correctly with the search method resulting in longer fixing time for L1 or no fix at all.

Table (7.1) : Time to Fix Integer Ambiguity in seconds (WL/L1 Case)

Test / Method	VA281	June19	EW11
Search	522/float	821/NA	422/1216
White	21/12	11/11	165/165

7.2.4 Instantaneous resolution/recovery of ambiguity

In order to check the ability of the whitening technique to recover the integer ambiguity after loss of lock, a number of artificial gaps were introduced in the data of the VA281 test by using a specially developed software. This data is then processed and the recovered ambiguity set is compared to the original one. It was found that in all cases, the instantaneously (using only one epoch) recovered ambiguity sets are exactly the same as the original ones with a 100 percent success rate. At the vehicle stops, the position of the vehicle was known from processing static data. It was found, that the estimated position of the vehicle at stops after recovering the ambiguity is the same as the original ones. This provides a strong indication that the whitening technique is capable of instantaneously recovering the ambiguity after loss of lock.

It is worth mentioning here that the instantaneous recovery of the ambiguity works fine after the first static ambiguity is resolved. It is also worth mentioning, that enough static time at the beginning is needed to make sure that the first resolved ambiguity set is the correct one; the processing of data usually goes smoothly when the first ambiguity set is correct. Fig. (7.5) shows the residual position errors due to loss of phase lock after fixing the ambiguities. The position residual errors are below one half of the L1 wavelength (10 cm) indicating that the ambiguities were resolved to their correct values after loss of lock.

7.2.5 Position accuracy implications

Table (7.2) shows, for all three tests, the difference in position as compared to the reference values at the end of the static periods. In all cases, the L1 results do not differ from the reference values. The widelane-derived position, on the other hand, results in an error of about 35-50 mm. This is due to the higher noise level of the widelane observation when compared to the L1 one. Resolving the L1 ambiguity after the widelane ambiguity has been resolved, however, gives almost the same position result as the original L1 result. However, the requirement for long validation time of the used search method

seems to make it difficult for the method to estimate a better position after the data has been rewound for the WL/L1 case.

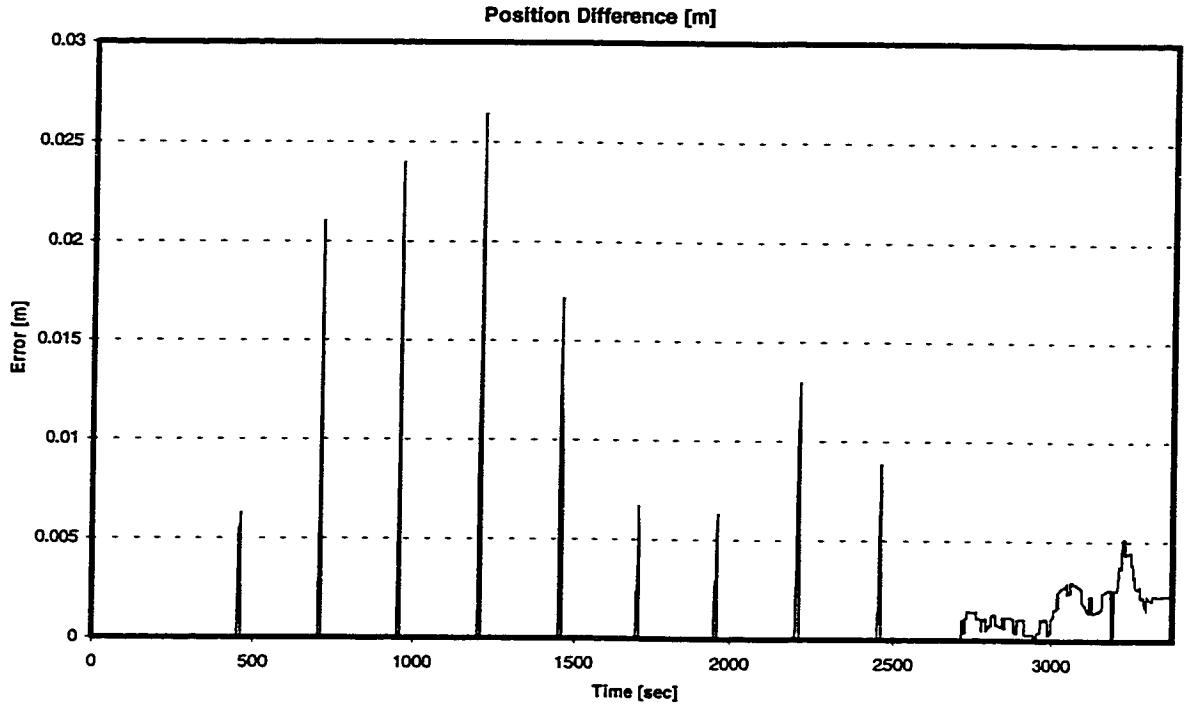

Fig. (7.5): Trajectory Position Residual Errors due to Loss of Phase Lock (VA281 Test)

Table (7.2) : Position Difference after Ambiguity Fix (All Cases) [mm]

Method \ Test		VA281	June19	EW11
Search	WL	40	33	52
	L1	0	3	4
	WL/L1	263	N/A	71
White	WL	20	34	39
	L1	0	4	2
	WL/L1	3	2	5

7.2.6 Baseline length and whitening

The purpose of this test is to investigate the performance of the OTFWhite method with different baseline lengths. One of the profiles of the flight test described in §8.1.4 was used for this purpose. The profile was sliced into chunks of 30 min. data segments, each starting in kinematic mode at different baseline length. Baselines of 10, 30, 40, 70, 95, and 130 km were processed independently under different combinations of the validation time and Fisher discrimination ratio resulting in a total of 444 runs, see [Amlacher 1998] for details. In this test, four different ground master stations were available. The reference to the various runs was obtained by carrying out a network adjustment between the ground master stations. The result of the network adjustment is the calculation of the measurement corrections at these master stations. The reference trajectory is then obtained by applying corrections to the raw measurements at the mobile station (the aircraft) through weighting the corrections from the different master stations by a location covariance function via a statistical method called NetAdjust [Raquet 1998]. The corrected raw data was run once with an independent software and the results of this processing was considered as a reference. Both the ambiguity values and the trajectory position were used to judge the correctness of the obtained solution from the KINWHITE 444 processing.

There were differences between the different solutions and the reference trajectory resulting in different rms for the horizontal and vertical trajectory position. During the period when the ambiguities are not fixed, the position rms values were higher compared to the period after fixing. The OTFWhite method was able to correctly resolve the integer ambiguity at all time in kinematic mode for baselines up to 40 km. Baseline solutions above 40 km were not as reliable as that below the 40 km baseline. Different combinations between the different statistical parameters were investigated. Table (7.3) shows a lookup table for runs with successful resolution of the ambiguity.

In order to investigate the sensitivity of OTFWhite to the number of available satellites, four data subsets with gaps every five minutes were processed. The distance between the master and remote stations was between 30 - 40 km. First, the data were

processed using all 8 visible satellites. Then the number of satellites was reduced one at a time and reprocessed. The ambiguities were resolved to their correct values for the cases where the number of satellites were 6 or more. For the cases below 6 satellites, the ambiguities were incorrectly resolved, see [Amlacher 1998] for details.

Table (7.3) : Lookup Table for OTFWhite

Distance [km]	t_0 [sec]	t [sec]	F
0 - 30	20	10	1.2
30 – 70	20	10	1.5
70 +	50	20	1.75

where,

t_0 : time required for the first ambiguity validation

t : time required for successive ambiguity validation

F : Fisher ratio; discrimination test

8.
TESTS, RESULTS AND ANALYSIS : ADAPTIVE KALMAN FILTER

In this chapter, results from four real-data kinematic tests are presented and analyzed where the performance of the adaptive Kalman filter (AKF) is compared to that of the conventional Kalman filter (CKF). The objectives of the tests are to show the applicability of the developed AKF with real data, test it in a well-controlled operational mode, and analyze its performance with the two most demanding kinematic applications, image direct georeferencing and airborne gravimetry.

8.1 Tests Description

The tests described in this chapter have been designed to analyze the performance of both the conventional Kalman filter (CKF) and the adaptive Kalman filter (AKF) for the integrated INS/GPS system from different perspectives. The first is a test in a controlled environment where reference position and velocity can be obtained with high accuracy and the attitude information can be kept almost constant. It is the most benign test environment, almost free of vibrations and sudden dynamical changes. The second test is part of a flight test, similar to the one simulated and analyzed in Chapter 5. It is used to compare the simulation environment to actual flight scenario, and thus validate the assumptions made in the simulation. The third and fourth are airborne tests, one with a precise attitude reference, the other with an accurate gravity reference. Both of them belong to the most demanding applications of the integrated INS/GPS, direct image georeferencing and airborne gravimetry and are bound to show clearly the differences between the adaptive and the conventional filters.

8.1.1 Anorad test in a controlled environment

The purpose of the test in this section is to investigate the performance of the developed adaptive Kalman filter in operational mode with superior reference values for

position and velocity, but a limited dynamical range. Performance in position, velocity, and attitude will be compared for the two filters. For that purpose, a test along a well-controlled trajectory was carried out where the INS/DGPS was mounted on top of a kinematic measurement base, called Anorad AG12-84, see Appendix D for its technical specifications and Fig. (8.1) for the test setup. While maintaining constant attitude by moving on a level base in constant direction, position and velocity of the platform change according to the computer controlled motion along the 2m track. In this case, the kinematic trajectory is generated by mounting the INS/GPS system on top of the platform which goes back and forth along its track according to a preloaded program to the servo control unit.

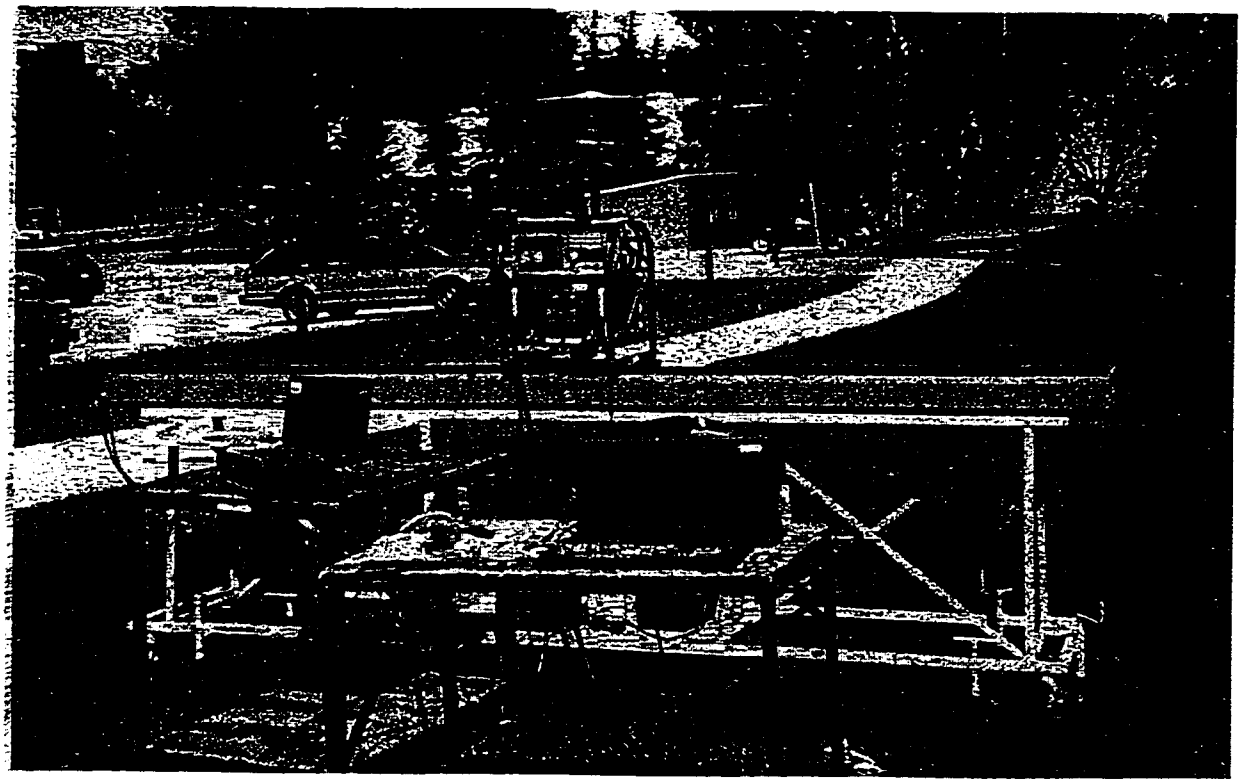

Fig. (8.1) : INS/GPS on Anorad Platform (Anorad Test Setup)

The calibration of the Anorad system which is done by comparing the actual trajectory implemented by the system to the nominal trajectory, has shown that a positional accuracy of the platform of better than 0.1 mm rms can be achieved. Results

can, therefore, be compared to a tenth of a millimeter; this accuracy is more than an order of magnitude better than that expected from the integrated INS/GPS. According to the manufacturer's specifications, the flatness and stability of the base is about 10 μm along the 2 meter track which results in an attitude angle stability of better than 0.1 arcsecond; this stability is sufficient for the test.

The trajectory, generated and used in this study, consists of three static and kinematic periods as depicted in Fig. (8.2). Only one of the kinematic periods of sufficient length has been analyzed in the following. The three static data sets were collected at the center and at both ends of the track for the purpose of resolving the GPS phase ambiguity and orienting the Anorad data, first to the WGS-84 reference system, and then to a local TM coordinate system.

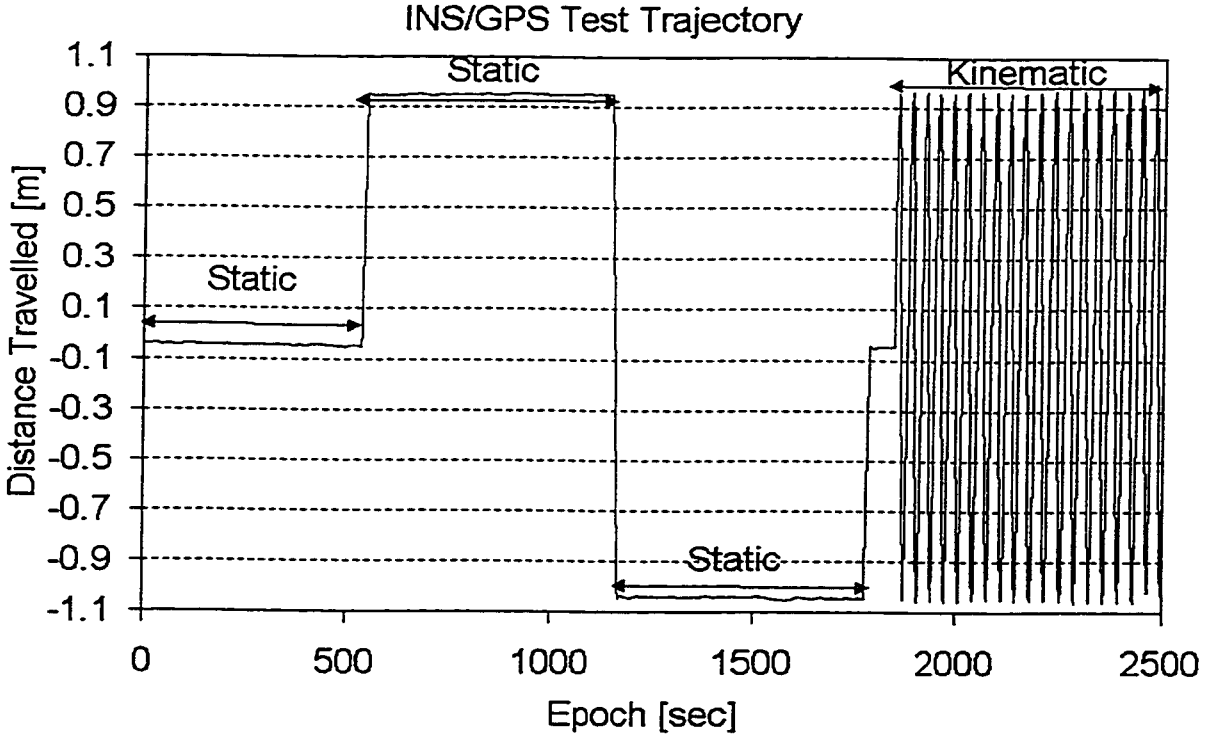

Fig. (8.2): Anorad Test Trajectory

In the test, one complete cycle from a specific point on the track and back takes 35 seconds. A complete cycle along with dynamics of the test are shown in Fig. (8.3). A

complete cycle consists of a sinusoidal wave of 1000 incremental distances. To generate this trajectory, the platform is accelerated and decelerated in a sinusoidal fashion according to the profile shown in the third subplot of Fig. (8.3) with values ranging from zero to a maximum of 0.03 m/s^2. The resulting velocity profile is a co-sinusoidal wave and is shown in the second subplot of Fig. (8.3); its value ranges from zero to a maximum of 0.2 m/s. The first subplot shows the resulting position profile with respect to time. Results from the main kinematic portion of the test will be presented.

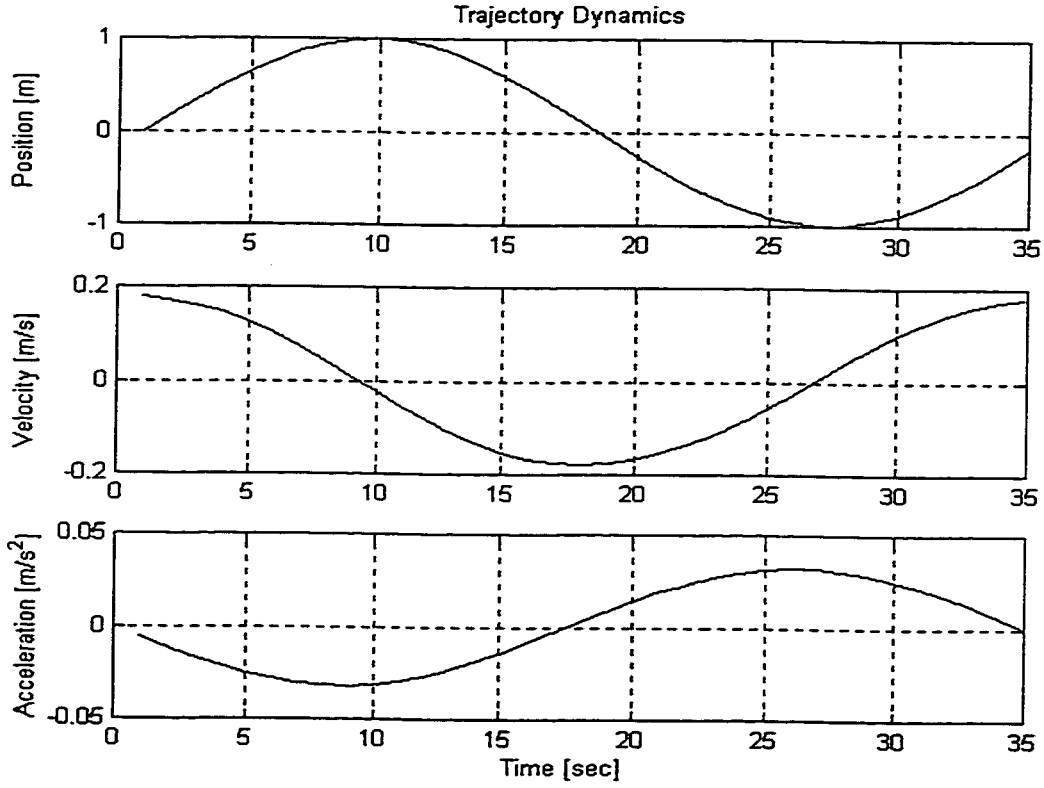

Fig. (8.3) : Trajectory Dynamics over One Cycle (Anorad Test)

8.1.2 Flight test

The purpose of the test in this section is to analyze the performance of both the CKF and the AKF on real data, for a trajectory similar to the one simulated in Chapter

Five. (8.4) shows the trajectory of this test. The segments of this trajectory are similar to the trajectory simulated and described in §5.1. The aircraft starts taxing between A and A1, then takes off between A1 and B. A horizontal maneuver with a change in the roll takes place between B and C, then, between C and D a flight with almost constant height. Another horizontal maneuver takes place at point D. The dynamics of the trajectory is very similar to that described in Table (5.1). Also, the underlying statistical assumptions of the used models are the same as those used in the simulation and described in §5.1.

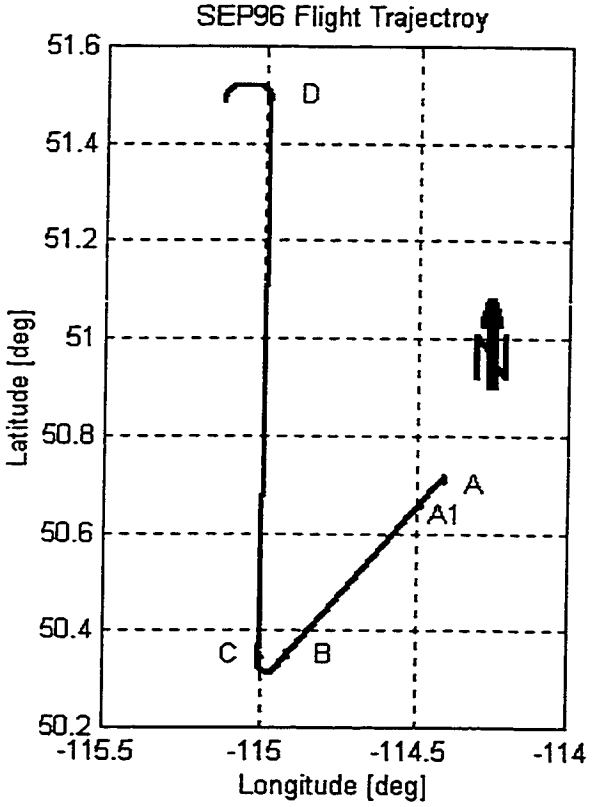

Fig. (8.4) : SEP96 Flight Test Trajectory

8.1.3 Flight test with precise attitude reference

The test described in this section was carried out in Calgary in early July 1994. The purpose of the test was to assess the in-flight orientation (attitude) accuracy of a DGPS/INS. The system consisted of an Ashtech-Z12 GPS receiver at the master station

and a Trimble 4000SSE GPS receiver along with a LTN90-100 strapdown INS in the aircraft. The average flight velocity was 360 km/h at an altitude of 1000 m. The attitude reference was provided by a precise photogrammetric camera (Zeiss LMK) and 17 ground control points along with tens of ground tie points. The attitude accuracy of the photogrammetric reference at the camera perspective center resulting from the bundle adjustment is 3-6 arcsec [Skaloud et al. 1994] for azimuth, pitch and roll. Results from seven flight lines flown over a period of about an hour and a half are presented. The test trajectory is shown in Fig. (8.5) below.

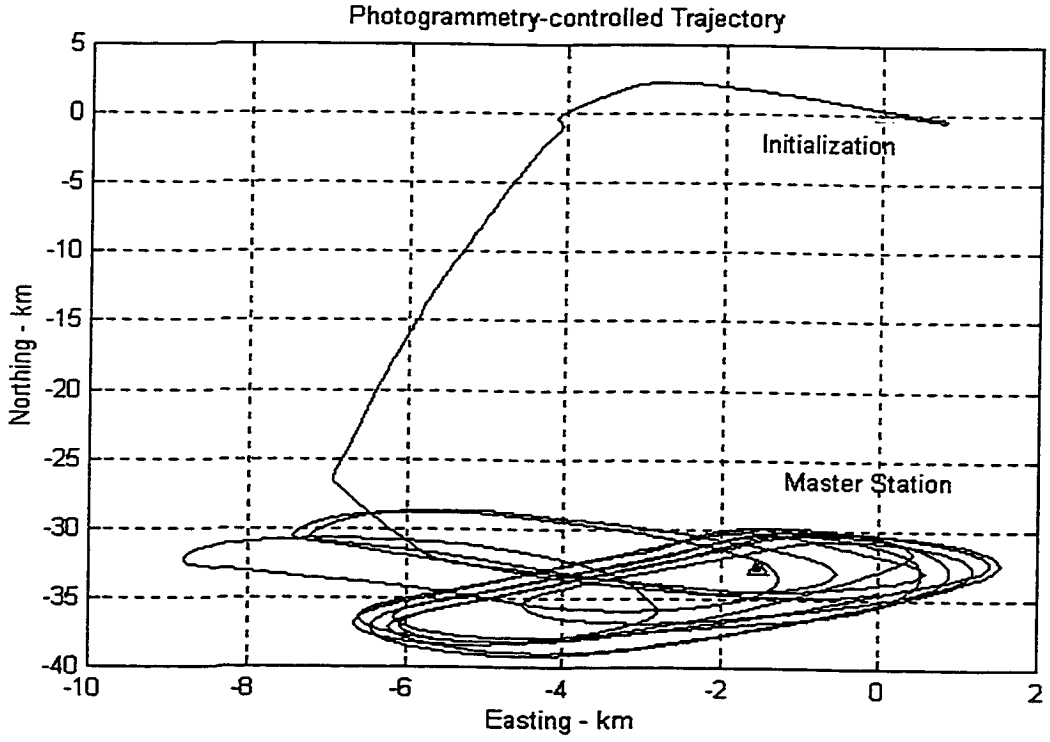

Fig. (8.5) : Attitude Test Trajectory

8.1.4 Flight test with gravity reference

The purpose of this test was to measure airborne gravity by differencing data from DGPS and a strapdown INS. The system was flown over the Rocky Mountain near

Calgary on September 9-11, 1996, see [Glenie and Schwarz 1997] for details of the test. The area flown has dense ground gravity measurements that were upward continued to the flight height to obtain a reference [Argeseanu 1995]. The reference gravity measurements on the ground were regularly distributed with an average spacing of about 8 km and 3 km in the south-east corner of the area flown. The accuracy of the upward continued reference is 1.5-2 mGal [ibid.].

To investigate the performance of the adaptive Kalman filter against the conventional Kalman filter, data from the second day of the flight test was used. Trimble 4000SSI data at the master and aircraft were used along with the Honeywell LRF-III strapdown INS data. The average flight velocity was 360 km/h at an altitude of 4350 m. Approximately 6 hours of data have been used in the following investigation. The trajectory is shown in Fig. (8.6) below.

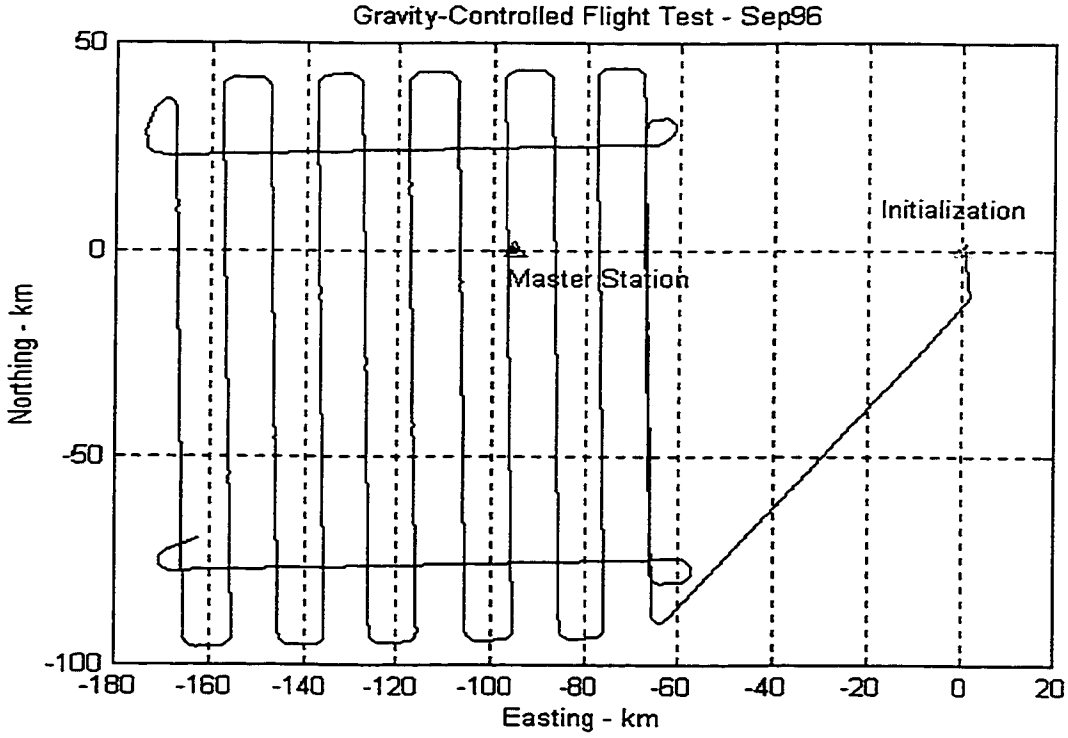

Fig. (8.6) : Gravity Test Trajectory

8.2 Test Results and Analysis

8.2.1 Anorad test

The results presented in this section are those resulting from comparing the INS/GPS KINADA software output with the Anorad logged data. The two data streams were first transformed to a common frame, a local TM coordinate system using the three static points common to the two coordinate systems. Position and velocity errors are computed as follows

$$e_i = X_i^{\text{Anorad}} - X_i^{\text{INS/GPS}} \tag{8.1}$$

where, X_i : position or velocity parameter of element 'i'.

The measure of accuracy used in this case is the root-mean square error and is calculated as follows

$$\text{rmse}_i = \sqrt{\frac{1}{n}\sum_{i=1}^{n} e_i^2}\,. \tag{8.2}$$

where, n : number of observations.

The attitude accuracy obtained from GPS at both ends of the Anorad base was not good enough as a reference for the INS/GPS results; a static GPS position accuracy of 3 mm over the 2 m base gives an attitude accuracy of 5 arcmin. Also, because attitude was assumed constant during the test, attitude results are calculated by removing the mean value as follows:

$$e_i = X_i^{\text{INS/GPS}} - \text{mean}(X_i^{\text{INS/GPS}}), \tag{8.3}$$

and the rmse is calculated in the same way as in Eq. (8.2) above.

Data from the Anorad base are logged at 10 Hz rate. The first task when analyzing the INS/GPS data with the Anorad logged data was to synchronize the two data streams. First, it was important to check the finest synchronization resolution the Anorad base itself can provide. This was done by correlating the Anorad logged data with a nominal sinusoid trajectory. It was found that the base-generated sinusoid has a synchronization error of 70 milliseconds, see Fig. (8.7). This error results in a periodic residual synchronization error with a maximum value of 0.01 m in the position difference sequences. The synchronization error was removed from the results and what remains afterwards represents the actual errors plus a residual synchronization effect.

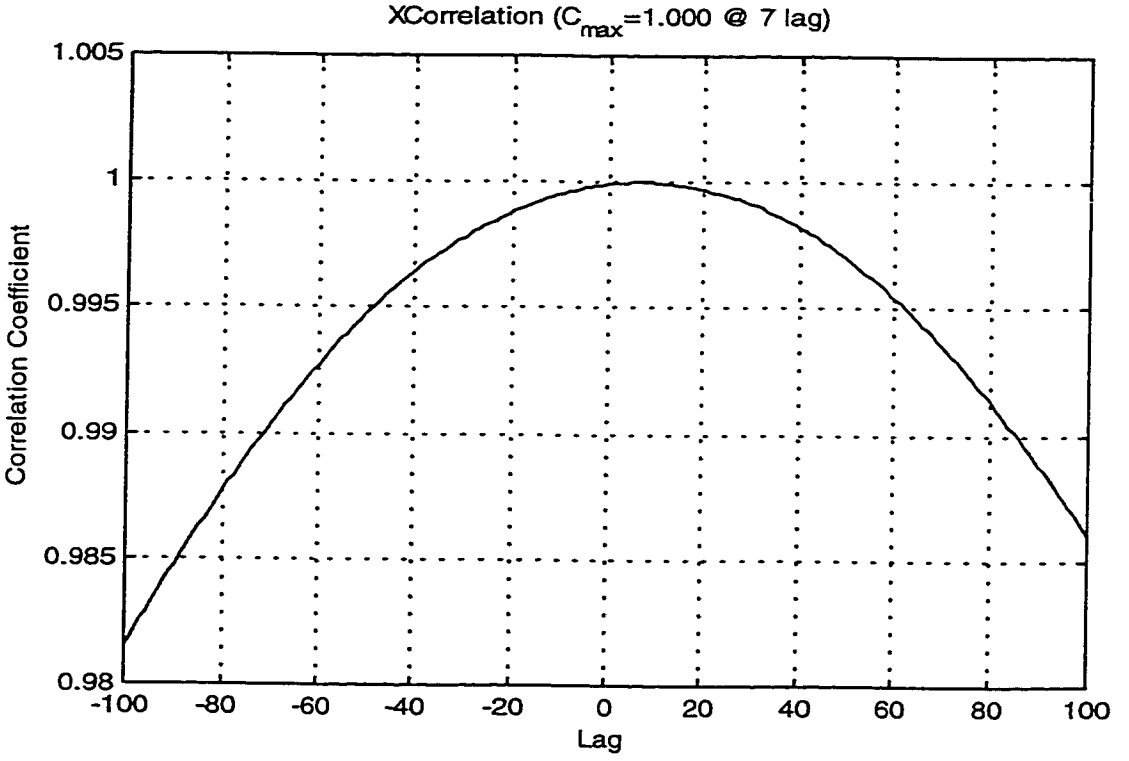

Fig. (8.7) : Synchronization Error between Base Logged Data and Nominal Trajectory (Anorad Test)

The residual synchronization error was treated as a random error with uniform distribution in the region of interest. If T is the synchronization resolution possible, the synchronization error, e_s, should be smaller than one half of T, i.e. $|e_s| < T/2$. The uniform probability density is then 1/T and the resulting rmse can be calculated as

$$\text{rmse}_s = \sqrt{\frac{1}{T}\int_{-T/2}^{T/2} e_s^2 de_s} = \frac{T}{\sqrt{12}}. \tag{8.4}$$

Hence, at a 10 Hz data rate, the expected synchronization rmse is 30 ms which corresponds to a position error of 0.005 m.

Position and Velocity Error Results

To ensure the validity of the GPS update measurements to the INS/GPS master Kalman filter, GPS only data was processed. The spectrum of the GPS-only position results, Fig. (8.8), show a systematic amplitude at the base periodic motion of 35 seconds. It also shows a systematic error of a smaller amplitude of 1 mm at 150 seconds which falls in the spectral range expected for the GPS signal multi-path, see the discussion in §3.1.1.

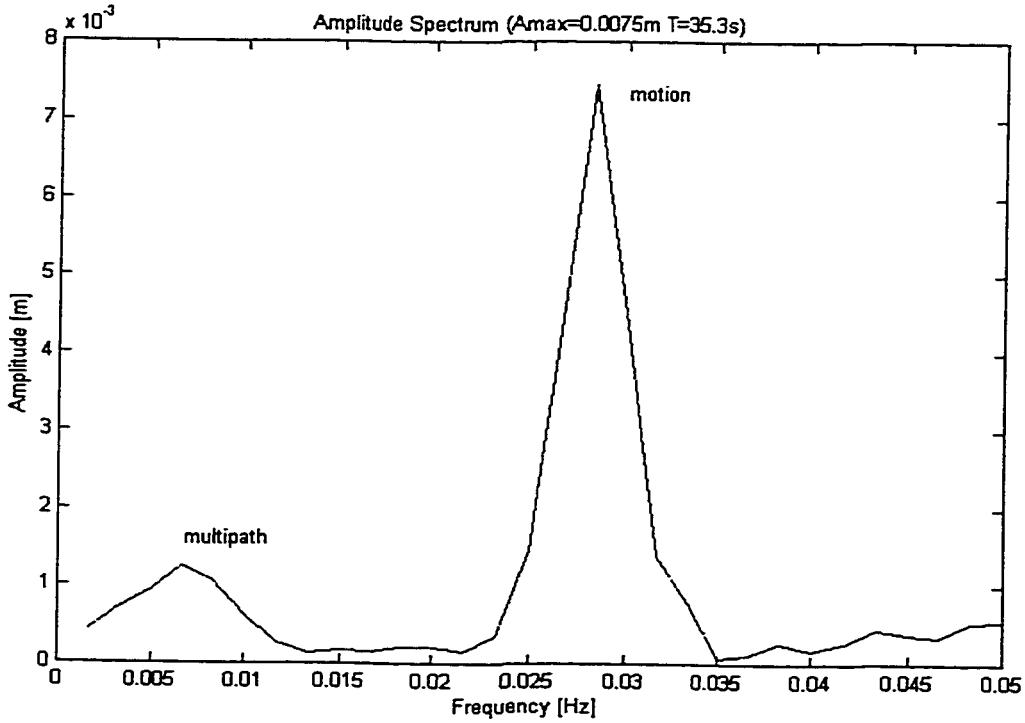

Fig. (8.8) : Amplitude Spectrum of Kinematic GPS Position Error Signal (Anorad Test)

Figs (8.9a) and (8.9b) show the position error of the INS/GPS output as compared to the Anorad output, after being synchronized, in the cases of conventional and adaptive Kalman filters, respectively. Although the error amplitude is not the same, there is a clear effect of the motion systematic period of 35 seconds in both cases. As discussed before, a residual synchronization error of 30 ms is expected at a 10 Hz data rate. However, there is a clear difference between the conventional and adaptive Kalman filter responses to this residual synchronization error. While the conventional filter tends to have a smooth estimate of the position state, the adaptive emphasizes high-frequency changes. The effect of tracing the high-frequency changes is very clear at both ends (turns) of the Anorad trajectory, where the error signal peaks. Position error rms values are 0.016 m and 0.005 m, for the conventional and adaptive cases, respectively, showing that the systematic error has a more pronounced effect in the CKF case.

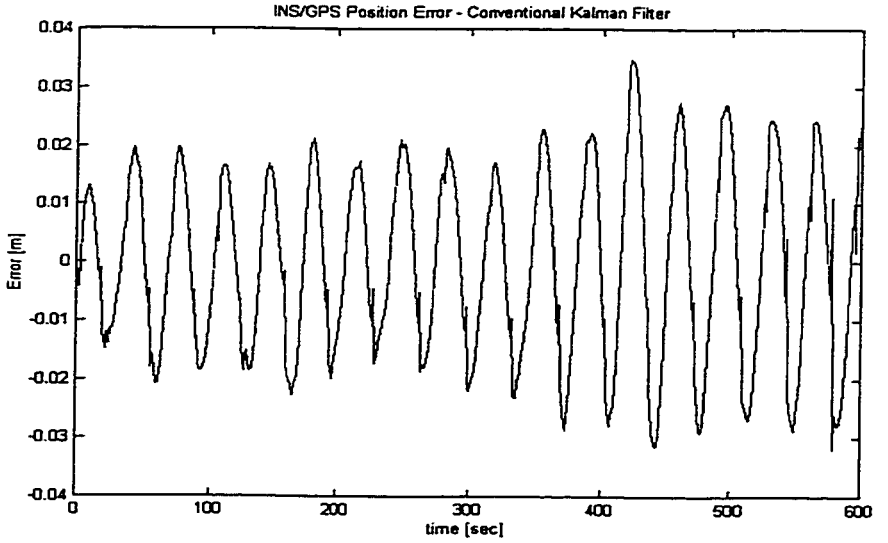

Fig. (8.9a) : INS/GPS Position Error (Anorad Test) - CKF

The spectra of the previous two cases show a spike at a frequency corresponding to the Anorad motion frequency of 35 seconds, see Figs. (8.10a) and (8.10b) below.

In the low-frequency band, both figures show the effect of the GPS multi-path signal around 150 seconds (0.0067 Hz) and the motion effect at 35 second (0.0286 Hz).

In the high-frequency band, the spectrum of the adaptive case, Fig. (8.10b), although almost at the same amplitude level, is flatter than that of the conventional filter. It shows that the adaptive filter response to the systematic effect is less apparent than that of the conventional filter. In the medium frequency band, between 0.05 to 0.15 Hz, there is a clear transition in the spectrum of the conventional filter that does not show up in the adaptive filter. A possible reason for such a phenomenon is the fact that the adaptive filter keeps changing its bandwidth. So, the adaptive filter makes faster transitions of its tracking bandwidth than the conventional filter.

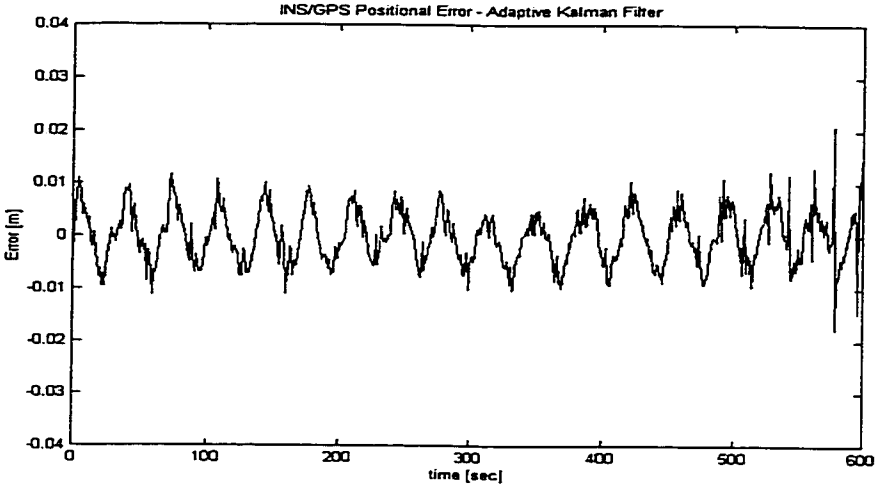

Fig. (8.9b) : INS/GPS Position Error (Anorad Test) - AKF

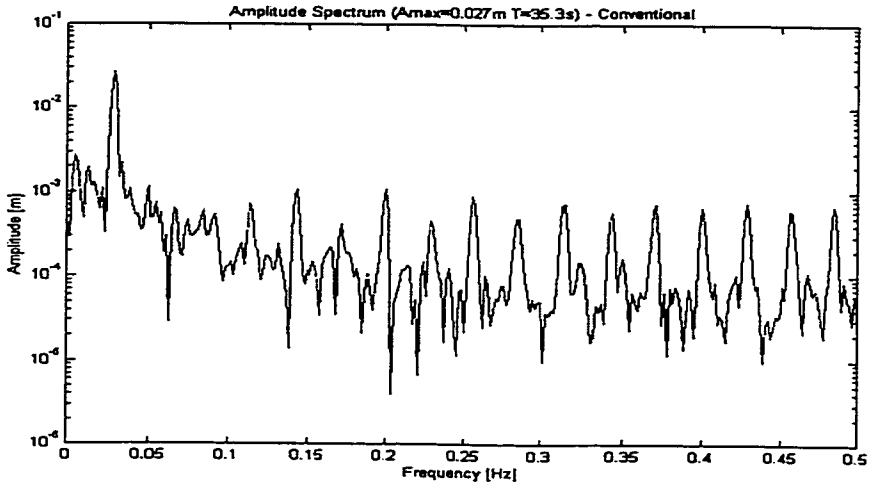

Fig. (8.10a) : INS/GPS Position Error Spectrum (Anorad Test) - CKF

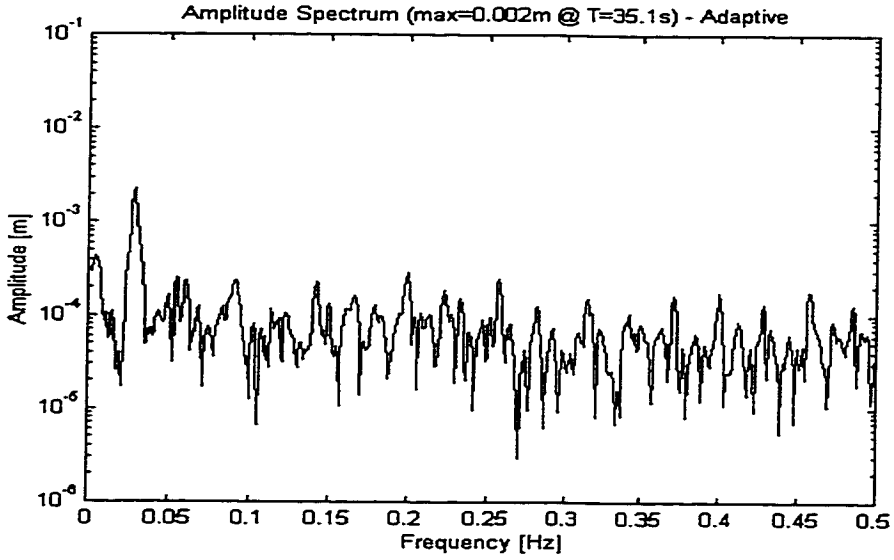

Fig. (8.10b) : INS/GPS Position Error Spectrum (Anorad Test) - AKF

After modeling the motion systematic effect and removing the frequencies at and below it, the noise of the position error is shown in Figs. (8.11a) and (8.11b), for the conventional and adaptive cases, respectively. The noise standard deviation in both cases is the same, 0.002 m. This shows that although the low-frequency effects are emphasized in the conventional filter, its noise level is close to the noise level of the adaptive filter. In other words, both filters performed the same in terms of noise in this test. The reason both noise levels are the same is that the position noise level in this case corresponds to the noise level expected from the position derived from DGPS phase measurements which is common to both AKF and CKF.

Velocity error behavior is more or less the same like position error behavior except that the systematic motion effect is less pronounced in the velocity error spectrum. The obvious reason for that is the fact that velocity is a differential of position in which the low-frequency signal content is less emphasized and the high-frequency component is pronounced. The conclusions drawn from the position error analysis apply to the velocity error, too. In this test, the INS/GPS average velocity error standard deviation was 0.005 m/s in both AKF and CKF cases.

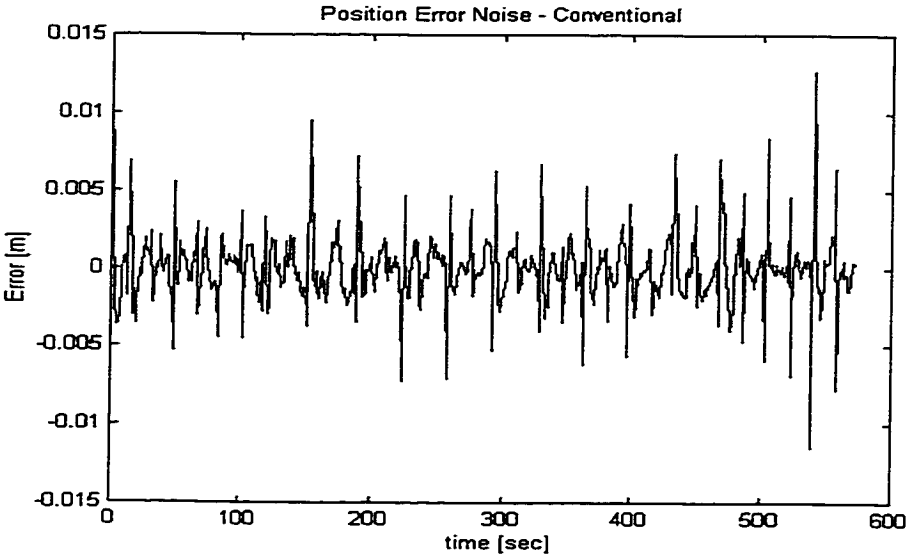

Fig. (8.11a) : INS/GPS Position Error Noise (Anorad Test) - CKF

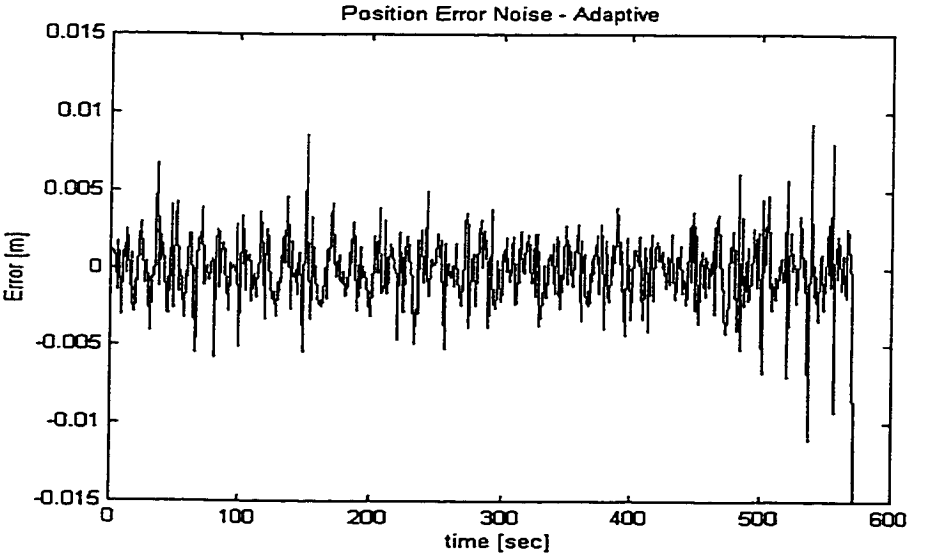

Fig. (8.11b) : INS/GPS Position Error Noise (Anorad Test) - AKF

Leveling and Azimuth Error Results

Figs. (8.12a) and (8.12b) below illustrate the roll error in the conventional and adaptive Kalman filters, respectively; plots for the pitch error are very similar and will not be discussed separately. Due to the nature of the Anorad motion, the roll state in the

Kalman filter was modulated by the motion sinusoid resulting in an equivalent to the motion-shape error pattern. Even after subtracting the mean value of the roll state, the shape of the error pattern did not change. The resulting roll rmse is 8.3 arcmin for both cases, conventional and adaptive. It is clear that this error is mainly due to the periodic motion.

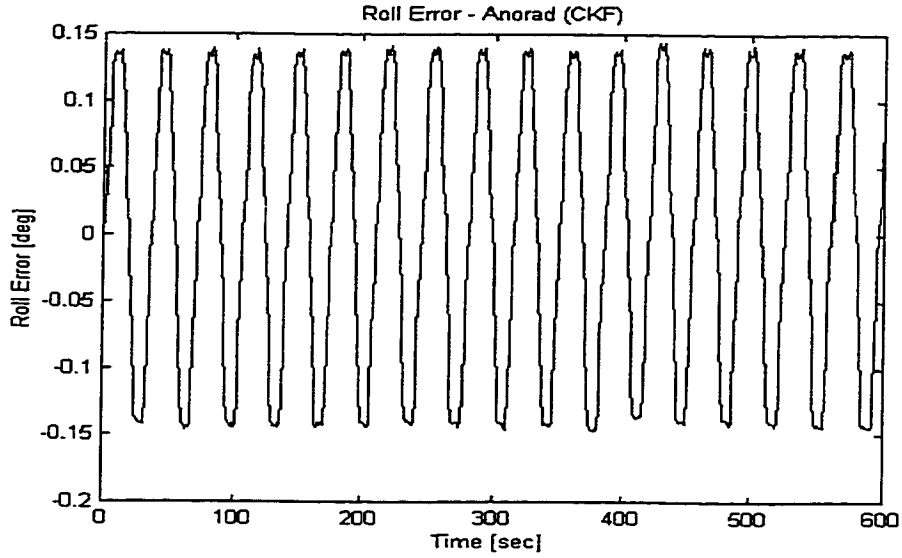

Fig. (8.12a) : INS/GPS Roll Error (Anorad Test) - CKF

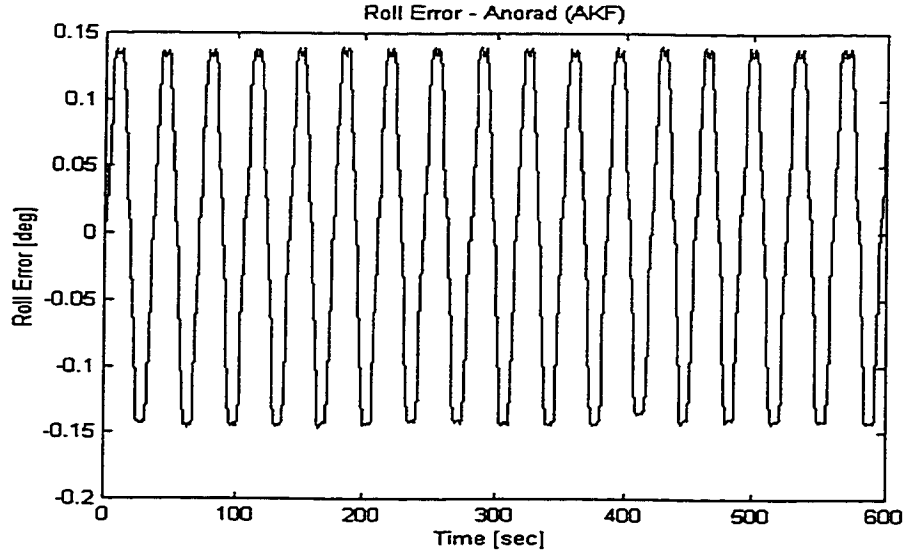

Fig. (8.12b) : INS/GPS Roll Error (Anorad Test) - AKF

After modeling the systematic effect of the periodic motion and removing the frequencies at and below it, the roll noise was reduced to 10.2 arcsec, see Figs. (8.13a) and (8.13b). The accuracy of estimating the leveling error was the same for both filters. The low rotational dynamics of this test is the main reason for this result. The roll estimate in this test has a noise level close to that expected from the attitude sensor (the gyro), see specifications in Appendix D.

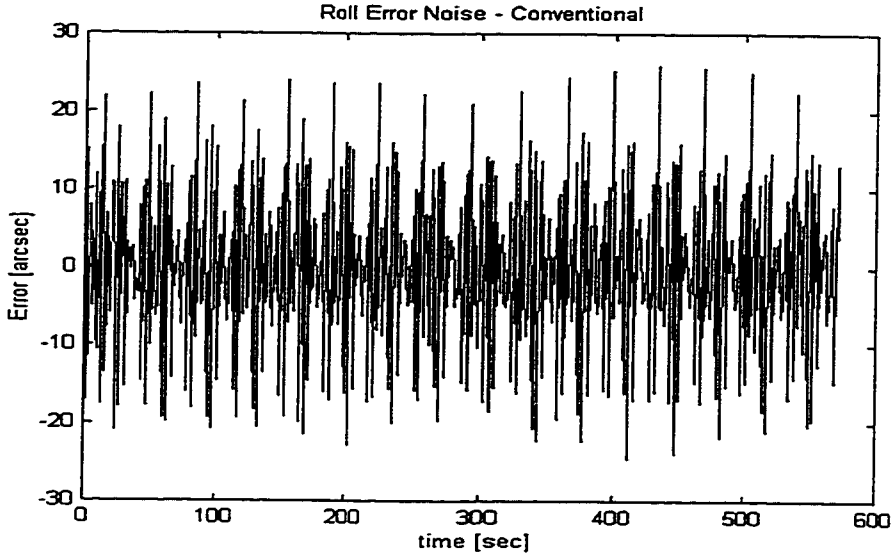

Fig. (8.13a) : INS/GPS Roll Error Noise (Anorad Test) - CKF

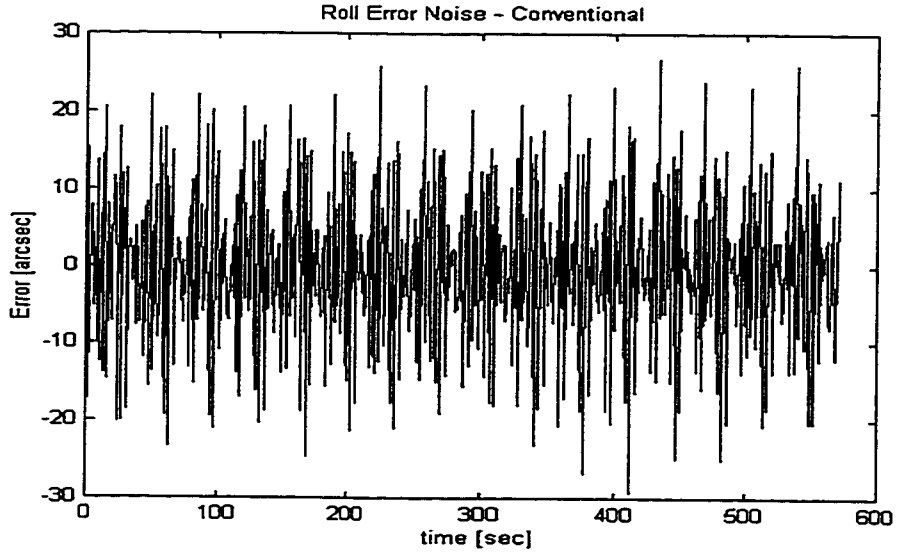

Fig. (8.13b) : INS/GPS Roll Error Noise (Anorad Test) - AKF

The azimuth misalignment state was not as easy to estimate as the leveling error states in this test. One reason for this is the fact that during the test the base goes back and forth under low dynamics and without maneuvers. Maneuvers and dynamics changes help decouple the filter states and consequently get better navigation state estimates. Fig. (8.14) shows the azimuth error in the conventional and adaptive cases. The reason both figures show erroneous starting azimuth is due the fact that the azimuth error is calculated by subtracting the azimuth values from their average value during the whole period.

The conventional Kalman filter shows an almost linear drift of 60' over the 600 seconds, while the adaptive Kalman filter shows a non-linear drift of 6' over the same period. It is worth mentioning that a typical drift of 6" over 600 seconds (0.01°/h) under normal operational procedures is expected from the LTN90-100 system. A possible reason for that is, that the special procedure of going back and forth under benign dynamics and, most importantly, without maneuvers made the decoupling of the gyro drift state and the azimuth state unsuccessful. In other words, what is seen as azimuth error is, in fact, the sum of the azimuth error and the gyro drift error, see the discussion in §5.2.2. A possible reason for the lower drift happening in the adaptive Kalman filter case is the fact that the filter changes its bandwidth to help decouple the azimuth and gyro drift states, and hence estimate the azimuth. Using polynomials to model the long-term drift of the azimuth error and take it out, the short-term noise in the error are 51.2" and 5.2", for the conventional and adaptive cases, respectively, which indicate a better azimuth estimate in AKF case.

Table (8.1) summarizes the results obtained from the Anorad test and the computations and analyses done. The GPS row represents processing GPS data only. The conventional Kalman filter case uses covariance matrices of constant measurement noise and system noise. For the adaptive Kalman filter, four different cases were taken into account. In the R-only case, adaptation of the measurement covariance matrix R is done based on the residual sequence; adaptation based on the innovation sequence led to singularity of the estimated R matrix which made the software to crash and is, therefore, not reported. The Q-only adaptation is done using the full formula, Eq. (4.34). The R&Q

is a simultaneous adaptation of R and Q using adaptation of Q by the formula in Eq. (4.34), and adaptation of R using the residual sequence. The R&QQ is a simultaneous adaptation of R and Q using the simplified formula for Q, Eq. (4.35).

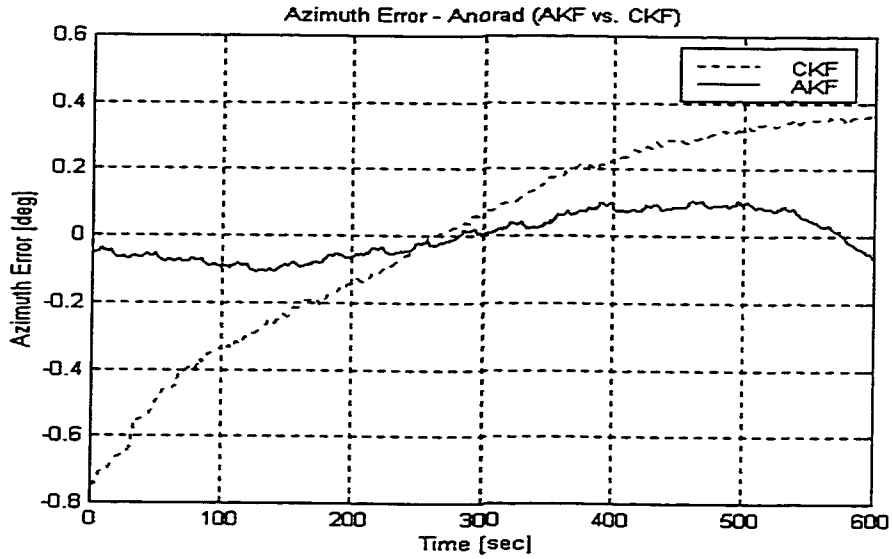

Fig. (8.14) : INS/GPS Azimuth Error (Anorad Test) - AKF vs. CKF

In Table (8.1), the RMS is computed as described in Eq. (8.2) above, without removing the systematic effect, which represents the long-term development of the error. A1 and A2 are the amplitudes of the error signal before and after modeling and removing the motion systematic effect, respectively. The RMS2 is computed using Eq. (8.2) after removing the motion systematic effect. The mean and noise are computed for the error free from the motion systematic effect, which represent the short-term behavior of the error. Since the systematic effect is due to the reference data in this case, the last column, containing the noise values, should be compared. The good GPS position and velocity rms values, 7 mm and 1 cm/s, respectively, are due to the fact that the carrier phase ambiguity was resolved to its correct integer over a very short baseline, 200 m. Also, the low dynamics made a smooth tracking of the Anorad trajectory by GPS possible.

As indicated in Table (8.1), for position and velocity, both cases of R-only and Q-only performed almost the same. This was to be expected because both position and velocity are directly observable components of the Kalman filter. A relative change in R

or Q should result in the same change in the gain and consequently in the same effect of the position and velocity updates. The same also applies to the leveling states where the choice of R-adaptation or Q-adaptation seem not to be critical in this test for them. The azimuth, however, was critical in this test because of the absence of maneuvers. The Q-only case outperformed the conventional and the R-only cases because of the sensitivity of the azimuth state to the dynamics changes and consequently to the Q matrix. Judging by the results of the position, velocity, and attitude errors, the R&Q simultaneous adaptation always performs worse. This result is not surprising and, indeed, was expected. Recall from the discussion in §4.4.5 and §5.2.8, the R&Q simultaneous adaptation leads to a destabilized filtering procedure. The results from the simplified Q formula in the R&QQ case and those from the R-only case are very close which indicate that the Q simplified model in this test results in an almost constant or very slowly changing Q-matrix.

Table (8.1) : Summary Results (Anorad Test)

Kinematic Accuracy		RMS	A1	A2	RMS2	Mean	Noise
Position [m]	GPS	0.0070	0.0060	0.0024	0.0047	0.0000	0.0040
	Conventional	0.0160	0.0213	0.0045	0.0050	0.0000	0.0022
	Adaptive (R-Only)	0.0064	0.0075	0.0050	0.0048	0.0000	0.0024
	Adaptive (Q-Only)	0.0052	0.0058	0.0047	0.0046	0.0000	0.0022
	Adaptive (R&Q)	0.0157	0.0029	0.0032	0.0154	0.0000	0.0140
	Adaptive (R&QQ)	0.0064	0.0075	0.0050	0.0048	0.0000	0.0024
Velocity [m/s]	GPS	0.0098	0.0041	0.0024	0.0095	0.0000	0.0089
	Conventional	0.0060	0.0080	0.0014	0.0019	0.0000	0.0009
	Adaptive (R-Only)	0.0026	0.0029	0.0006	0.0015	0.0000	0.0013
	Adaptive (Q-Only)	0.0035	0.0016	0.0015	0.0033	0.0000	0.0021
	Adaptive (R&Q)	0.0072	0.0014	0.0017	0.0072	0.0000	0.0067
	Adaptive (R&QQ)	0.0026	0.0029	0.0006	0.0015	0.0001	0.0013
Roll/Pitch [arcmin]	Conventional	6.3447	8.8626	0.7553	0.6861	0.0000	10.1
	Adaptive (R-Only)	6.2690	8.7562	0.7488	0.7363	0.0000	10.1
	Adaptive (Q-Only)	6.3626	8.8872	0.7463	0.7364	0.0000	10.2
Noise in [arcsec]	Adaptive (R&Q)	6.3314	8.8383	0.7378	0.7916	0.0000	14.8
	Adaptive (R&QQ)	6.2712	8.7592	0.7491	0.7377	0.0000	10.1
Azimuth [arcmin]	Conventional	18.5074	27.2717	N/A	N/A	0.0000	51.1
	Adaptive (R-Only)	13.0606	19.4280	N/A	N/A	0.0000	49.2
	Adaptive (Q-Only)	4.1386	6.0192	N/A	N/A	0.0000	5.2
Noise in [arcsec]	Adaptive (R&Q)	31.6692	18.3934	N/A	N/A	0.0000	114.0
	Adaptive (R&QQ)	4.8245	6.4788	N/A	N/A	0.0000	18.8

Noise: after HPF; A1:from amplitude spectrum; A2&RMS2:after modeling motion systematic error @ 35s

8.2.2 Flight test

The focus of this section will be to show the difference between the CKF and the AKF filters in estimating the azimuth misalignment and the Z gyro drift states. The difference between the azimuth estimate of each of the two filters characterizes the behavior of each of them with respect to the dynamics changes. As was discussed in Chapter 5, dynamics affects the estimates of each of the CKF and the AKF differently. While the CKF maintains a relatively smooth estimate of the azimuth misalignment state after maneuvers, the AKF changes its bandwidth with dynamics changes resulting in a relatively noisy estimate of the same state, see Figs. (5.3a) and (5.3b). The same is also clear from Fig. (8.15) where the difference of the estimates of the two filters is illustrated. At the time of take-off, a large difference between the estimates of the two filters is most likely due to the change of the AKF estimate due to the change in its bandwidth. At maneuvers, because the AKF traces changes faster than the CKF, there is a clear drift in the difference between the estimates of the two filters. This drift is most likely due to the drift in the CKF estimate. The bias between the two estimates on straight lines is almost constant with little variation (noise); the noise can be contributed to the AKF estimate noise. The bias, however, can be explained in light of the estimate of the Z gyro drift illustrated in Fig. (8.16). It is clear from the figure that the AKF maintains a fixed estimate of the Z gyro drift, while the CKF estimate does change after each turn. The difference between the estimates of the Z gyro drift states in the two filters is responsible for the bias of the estimate of the two states.

Fig. (8.17) shows the gain for both cases the AKF and the CKF, for real data. It is clear that dynamics have very little effect on the gain of the CKF, see the dotted line. The effect of dynamics is more pronounced in the case of the AKF, the solid line in the figure. The change in the gain can be interpreted as a change in the filter bandwidth as discussed in §3.2.6. It can be seen that the changes in the dynamics, that is reflected in the changes in the filter gain, is also reflected in the changes in the estimates of the two filters; compare the pattern of changes in Figs. (8.15) and (8.17).

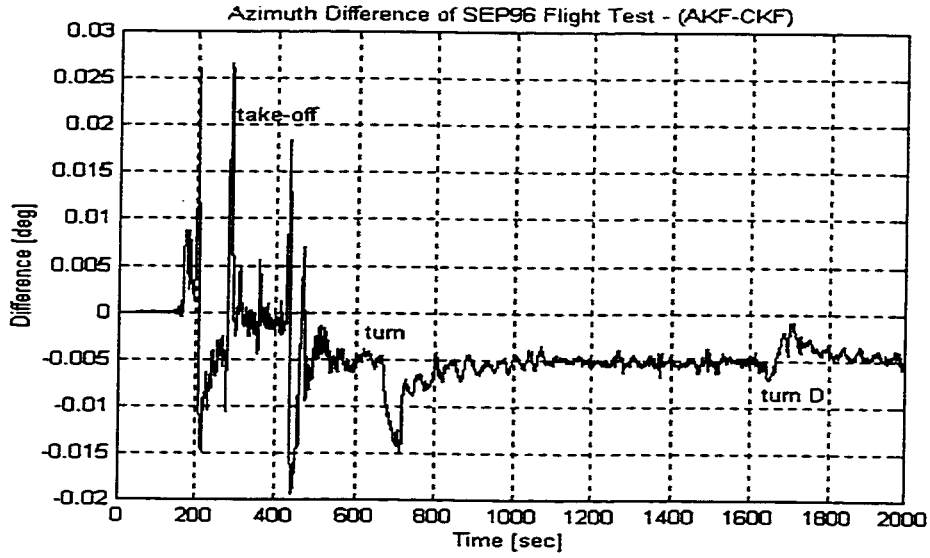

Fig. (8.15) : Azimuth State Estimate Difference (SEP96 Flight Test) - (AKF-CKF)

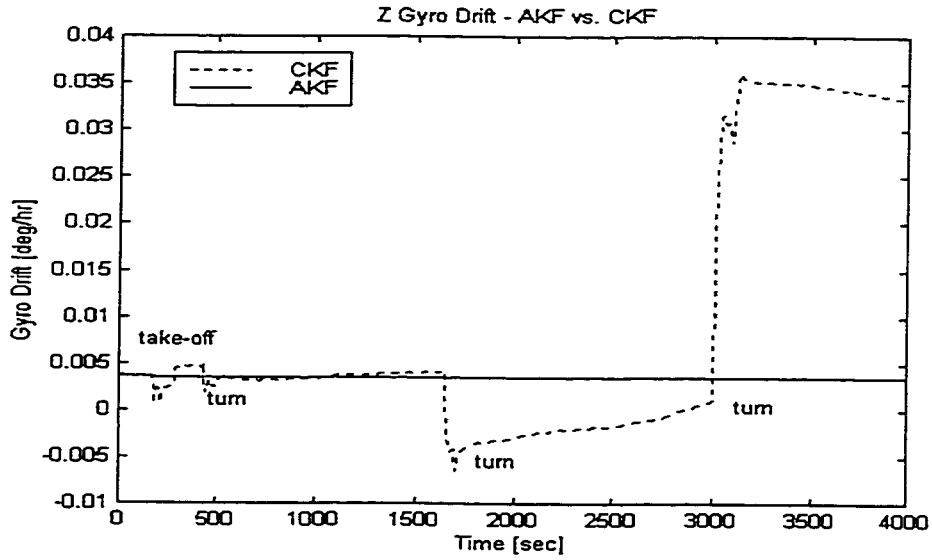

Fig. (8.16) : Z Gyro Drift Estimate (SEP96 Flight Test) - CKF vs. AKF

The results of this section almost match the results in the simulation test. They are the outcome of processing real data indicating that the analysis carried out in the simulation study is valid.

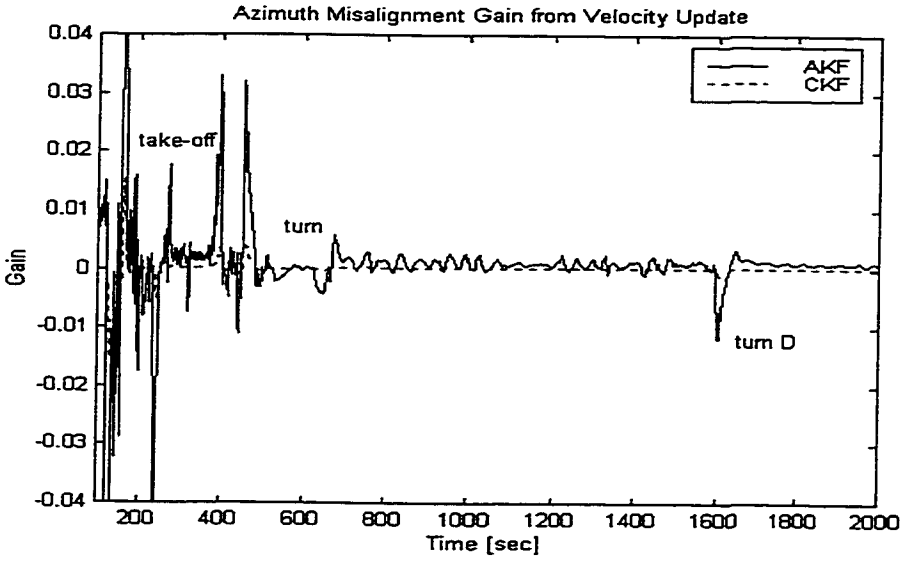

Fig. (8.17) : Kalman Gain of Azimuth Misalignment from Velocity Update (SEP96 Flight Test) - CKF vs. AKF

8.2.3 Attitude reference test

The results presented in this section focus on the precise short-term attitude determination capability of the integrated INS/GPS system comparing again the adaptive Kalman filter to the conventional Kalman filter. The accuracy of the attitude parameters is calculated by comparing the INS/GPS attitude parameters to those obtained by an aerial triangulation bundle adjustment. The bundle adjustment procedure uses GPS camera coordinates in conjunction with ground control points, see [Skaloud et al. 1994] for details. The result of the photogrammetric bundle adjustment is the position of the camera perspective center and the orientation of its axes in a local-level frame, R_c^l. Both of the INS/GPS and the camera are fixed to the body of the aircraft and their relative position and orientation are assumed unchanging during flight. The transformation between the camera coordinate frame and the INS body frame, R_b^c, is usually obtained by field calibration of the system [ibid.]. However, in this test, the first image was used as reference to the rest of the images, i.e. the body-to-camera transformation matrix was calibrated by using the first image. The relative change (error) between the INS-derived

attitude information, R_b^l, and that of the photogrammetrically derived one is calculated as follows

$$\Delta R = R_c^l (R_c^l(2))^{-1} = R_c^l R_l^c(2) = R_c^l (R_b^c R_l^b). \tag{8.5}$$

Because ΔR has only small angles, it can be approximated as follows

$$\Delta R = \begin{pmatrix} 1 & -\varepsilon_u & \varepsilon_r \\ \varepsilon_u & 1 & -\varepsilon_p \\ -\varepsilon_r & \varepsilon_p & 1 \end{pmatrix}, \tag{8.6}$$

where, ε_r, ε_p, ε_u : errors in roll, pitch, and yaw, respectively.

Errors of the camera perspective center position between the INS/GPS derived values and those obtained from the bundle adjustment are simply the algebraic difference between the two after removing the linear offset between the GPS antenna and the IMU center. The results presented here are obtained from a specially designed software. Position and orientation were obtained from the INS/GPS output at 64 Hz and matched with results from the bundle adjustment along the flight lines. Fig. (8.18) shows the errors while Table (8.2) shows the statistics of the results of processing seven flight lines.

The rms of the roll, pitch, and yaw errors are 0.05, 0.05, 0.006 deg, for the conventional filter and 0.05, 0.002, 0.004 deg for the adaptive filter, respectively. It should be noted that these statistics do not include the initial misalignment. Hence, they represent the evolution of the errors with time after alignment. For a navigation-grade INS, such as LTN90-100, the expected short-term attitude accuracy should be in the gyro output resolution range of few arcseconds, e.g. 0.001 deg (4").

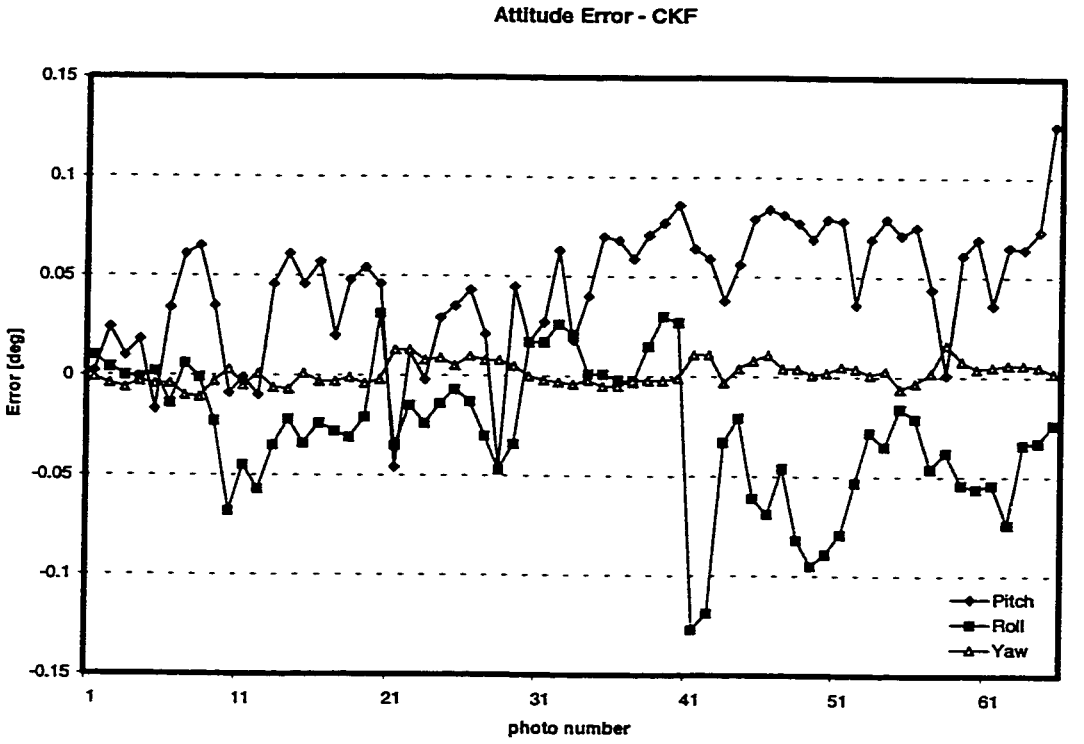

Fig.(8.18a):Attitude Errors at Perspective Center for all Flight Lines (Attitude Test)-CKF

The pitch and azimuth errors, in the adaptive Kalman filter output, is very close to what is expected from this INS. The roll, however, is much poorer and the reason is that due to operational constraints, the INS and the camera were not mounted on the same platform. The mounting of the camera, however, allowed, accidentally, for some movements causing roll errors. There is an improvement of about 35% in the estimate of the azimuth component and a 20 times improvement in the pitch estimate in case of adaptive Kalman filter. The estimation of the pitch in the conventional Kalman filter is a problem for this test. Investigations in [Skaloud 1999] showed that the horizontal gyros had higher noise level than the vertical gyro, for this specific test. Nevertheless, The differences between the output of the two filters are due to the different behavior of each of the two filters, as discussed in Chapter Five.

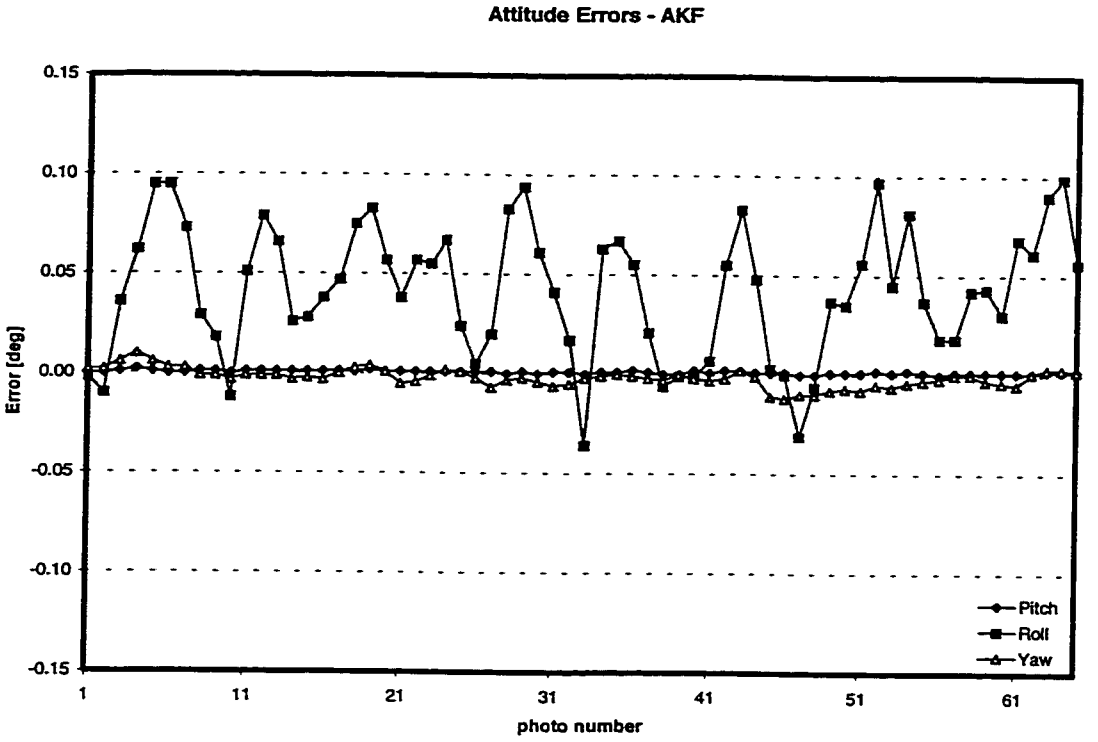

Fig. (8.18b):Attitude Errors at Perspective Center for all Flight Lines (Attitude Test)-AKF

The comparison in Table (8.2) indicates that the results from the R-only, Q-only and R/Q are very close to one another, except for the case in which the height component diverged in the R/Q adaptation. Comparable results show that relative weighting between the R and the Q covariance matrices is the key to the adaptation. The divergence of the height in the R&Q adaptation shows potential negative effects of using the R&Q adaptation. This result supports the discussion in §4.4.5 and §5.2.8. The height results of the R&Q case of this test may be an extreme situation but shows very clearly the negative effect of using the simultaneous R&Q adaptation. In general, results of this test show, clearly, the applicability of the AKF in the application of image direct georeferencing. They also indicated potential improvement of the attitude estimates when applying AKF over the currently used CKF. The large bias in the position results is attributed to the bad geometry and satellite coverage from GPS which result in an incorrect resolved ambiguity set.

Table (8.2):Errors at Perspective Center for all Flight Lines (Attitude Test)-CKF vs. AKF

Case		δE - m	δN - m	δh - m	δs - m	ε_p - deg	ε_r - deg	ε_u - deg
Conventional	STDEV	1.2265	0.2757	1.0313	0.6959	0.0342	0.0331	0.0062
	MEAN	0.4640	1.0520	1.0408	2.0590	0.0491	-0.0254	0.0004
	RMS	1.3125	1.0944	1.4702	2.1865	0.0601	0.0418	0.0062
	MAX	-3.4801	-1.0520	3.2962	2.2968	-0.0949	-0.1526	0.0158
Adaptive R-only	STDEV	0.0180	0.0101	0.1451	0.1298	0.0006	0.0332	0.0041
	MEAN	0.2943	-0.4899	1.1579	1.2930	0.0010	0.0414	-0.0018
	RMS	0.2948	0.4900	1.1670	1.2995	0.0012	0.0531	0.0045
	MAX	0.3355	0.5118	1.4680	1.5755	0.0025	0.0994	0.0122
Adaptive Q-only	STDEV	0.0180	0.0101	0.0869	0.0741	0.0006	0.0332	0.0041
	MEAN	0.2943	-0.4898	0.9867	1.1413	0.0010	0.0414	-0.0018
	RMS	0.2948	0.4899	0.9906	1.1438	0.0011	0.0531	0.0045
	MAX	0.3355	0.5118	1.1270	1.2639	0.0024	0.0994	0.0122
Adaptive R/Q	STDEV	0.0553	0.0791	3651.98	3651.73	0.0296	0.0338	0.0041
	MEAN	0.2379	-0.3966	2930.08	2930.39	0.1155	0.0393	-0.0097
	RMS	0.2443	0.4044	4682.13	4682.13	0.1192	0.0518	0.0105
	MAX	0.3321	0.5292	-11037	11037.8	0.2243	0.0975	0.0193

8.2.4 Gravity reference test

In this case, gravity disturbance in the vertical direction, δg, is calculated from two streams of acceleration information one coming from the INS, the other from GPS [Schwarz and Wei 1994, Schwarz and Li 1996], as follows

$$\delta g = f_u - a_u + E_c - \gamma_u \tag{8.7}$$

where,

f_u : upward component of the specific force obtained from INS,

a_u : upward component of the vehicle acceleration obtained from GPS by differentiating vehicle upward velocity once or by differentiating vehicle upward position twice,

γ_u : upward component of the normal gravity vector at aircraft height,

E_c : Eötvös correction due to Coriolis acceleration and centrifugal accelerations in the horizontal directions, which is computed as follows

$$E_c = 2v_E\omega_e \cos\varphi + \frac{v_E^2}{R_1 + h} + \frac{v_N^2}{R_2 + h} \tag{8.8}$$

where,

ω_e : Earth's rotation rate (15°/h),

v_E, v_N : east and west components of the vehicle velocity obtained from GPS,

ϕ, h : vehicle latitude and ellipsoidal height obtained from GPS,

R_1, R_2 : prime-vertical and meridian radii of curvature (WGS84 ellipsoid).

The processing of the INS and GPS data is done in three main steps. Firstly, both the INS and the GPS data streams are blended in a Kalman filter to allow for the estimation of the navigation parameters as well as the gyro and accelerometer biases. This step is accomplished through the software package KINADA for the conventional and adaptive Kalman filters. Secondly, vehicle kinematic acceleration is determined by differentiating the GPS position twice or differentiating the GPS velocity once. Finally, INS specific force and GPS acceleration are differenced according to Eq. (8.7) above to determine the gravity disturbance in the vertical direction, using specially designed software developed at the University of Calgary. To reduce the effect of measurement noise, and that resulting from the differentiation step, the resultant gravity anomaly is low-pass filtered. Four specific cut-off frequencies, corresponding to the frequency band of interest, are considered which result in filters of 30, 60, 90, and 120 seconds cut-off frequencies. Results from the four filters in the straight part (14 straight lines) as well as results at turns (10 turns), are computed using specially designed software and will be shown. The reason why results from straight lines are separated from the results at turns is that during turns results are consistently poorer than those along straight lines. Also, the adaptive Kalman filter is expected to perform better than the conventional Kalman filter at turns due to its property of tracking fast changes (high-frequency components) at the turns. Results from the INS/GPS processing is then compared to the upward-continued gravity disturbance which was available as a reference.

Figs. (8.19a) and (8.19b) show the difference between the upward-continued gravity disturbance derived from the ground reference data and that derived from the airborne gravity system for 14 straight lines and 10 turns, respectively. The relatively worse results of the 30 sec filter can be explained by the error induced by the phugoid

motion at 45 sec (f_c = 0.022 Hz). Phugoid motion is the natural oscillation of the aircraft at a certain frequency. This oscillation, when coupled with the INS misalignment errors ε^l, induces an error, $F^l\varepsilon^l$, of period [Boedecker and Neumayer 1995]

$$T_{ph} = \sqrt{2}\,\pi v/g \tag{8.9}$$

where, v : vehicle horizontal velocity.

According to Eq. (8.9), with an average gravity acceleration of g = 9.81 m/s^2, and an average horizontal velocity of 100 m/s for this test, the period of the phugoid motion is about 45 seconds. The maximum error induced by the phugoid motion is $2F^l\varepsilon^l$, which corresponds to 1 mGal per arcsec of misalignment error for each 0.1g aircraft horizontal acceleration. For a navigation-grade INS, at a leveling error of 10" under 0.1g acceleration, the induced acceleration error due to the phugoid motion is up to 10 mGal. So, a cut-off frequency of 30 seconds cannot eliminate the effect of this error as it is clear in Fig. (8.19a). The figure shows that filters with cut-off frequencies below the phugoid frequency were well at or below the 5 mGal rms, while the 30 second filter (smaller than the 45 second phugoid period) was 25 mGal rms in average. Hence, for resolutions below 3 km, special attention should be given to the estimation of the INS/GPS filter attitude components.

Fig. (8.19a) also shows that the results from the 90s and the 120s filters, corresponding to 9 km and 12 km resolutions, are very close to one another. It indicates that no possible further improvement may be achieved by low-pass filtering above 120s cut-off. It also indicates the possibility of the existence of an optimal filtering cut-off frequency (or bandwidth) at which the INS/GPS gravity system can provide gravity information, which in our case would be in between 90 and 120 seconds.

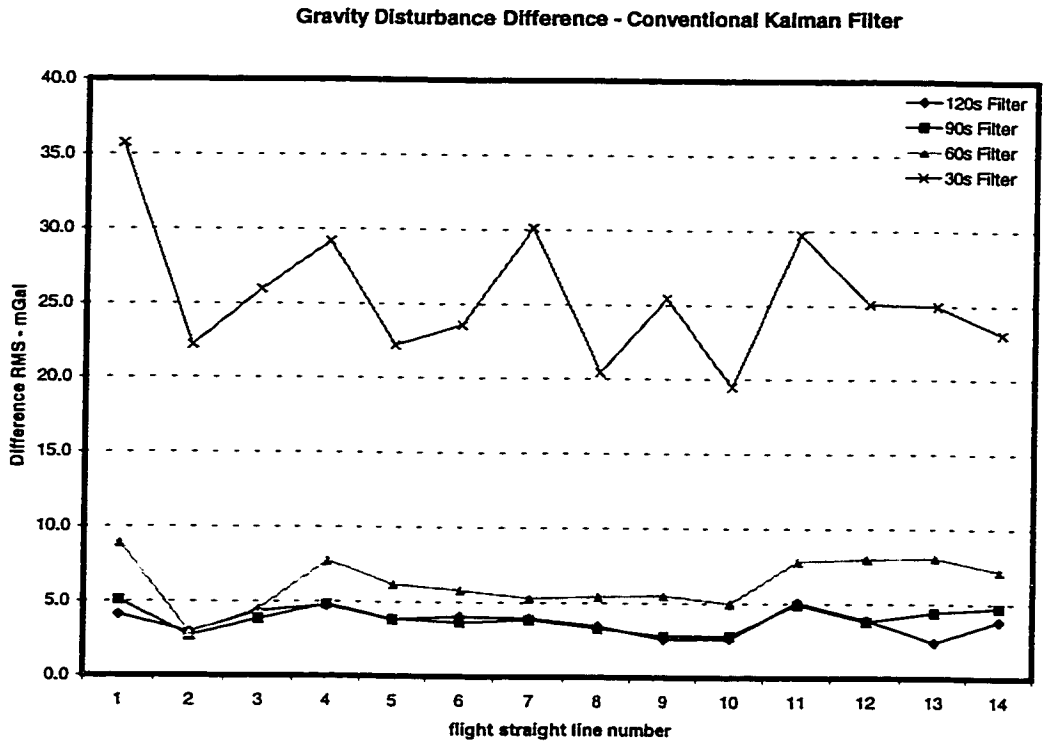

Fig. (8.19a): Gravity Disturbance Difference RMS at Straight Lines (Gravity Test) - CKF

The results at turns, shown in Fig. (8.19b), are worse by a factor of 3-5 when compared to those along straight lines. One possible reason for the worse results at turns is the low sensitivity of the conventional Kalman filter to turns. When the filter starts operating, it is in static mode. It is tuned to steady state during the first few epochs of the first straight flight line. So, the filter is tuned to straight lines and locked onto the straight line gain. It then stops responding to further changes, as for instance those happening at turns. It is intuitive, that filter gains along straight lines are not optimal for turns and new filter gains should be estimated, see the discussion on the filter gain in §5.2.2.

Although there is an improvement of about 5% when using the adaptive Kalman filter; the pattern of the rms errors is almost the same, see Fig. (8.20a). Two facts can be stated here. Firstly, the adaptive filter and the conventional filter performed well in straight lines because the filters had been fine tuned with straight line data. Secondly, most of the benefit gained with the adaptive filter, for the same cut-off frequency, in

tracing high-frequency components of the gravity field was eliminated by the low-pass filtering used to reduce the measurement noise effect.

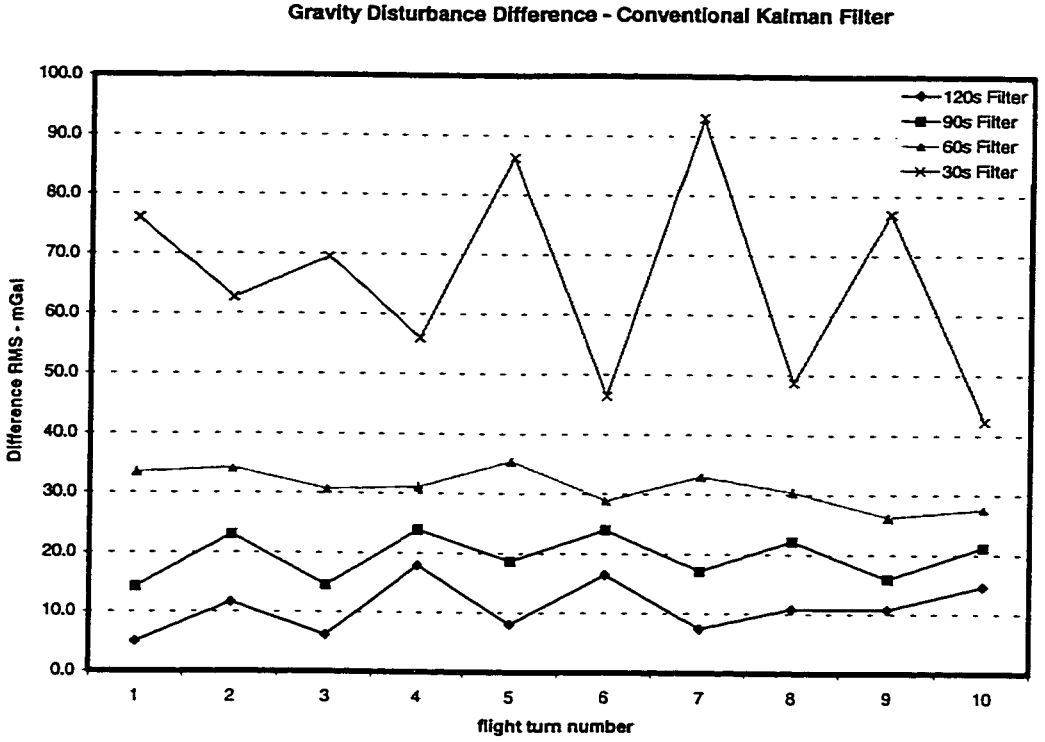

Fig. (8.19b) : Gravity Disturbance Difference RMS at Turns (Gravity Test) - CKF

There is a noticeable improvement in the AKF results vs. the CKF results at turns. It is about 16% for the 90 sec filter as shown in Fig. (8.20b). Adaptive Kalman filter results at turns are consistently better. The most likely reason for the better performance of the adaptive filter is its better tracking of the angular changes at turns. The combined results from straight lines and turns show an improvement of about 16% at the 90 sec filter, when the AKF was used. Figs. (8.21a) and (8.21b) show the difference between the two filters at one of the turns for the 90 sec cut-off frequency. For this specific case, the rms computed for the adaptive Kalman filter is smaller than that of the conventional Kalman filter by about 40%. There is a clear systematic effect on both cases which is more pronounced in the CKF case than the AKF case resulting in amplifying the rms value in the first case.

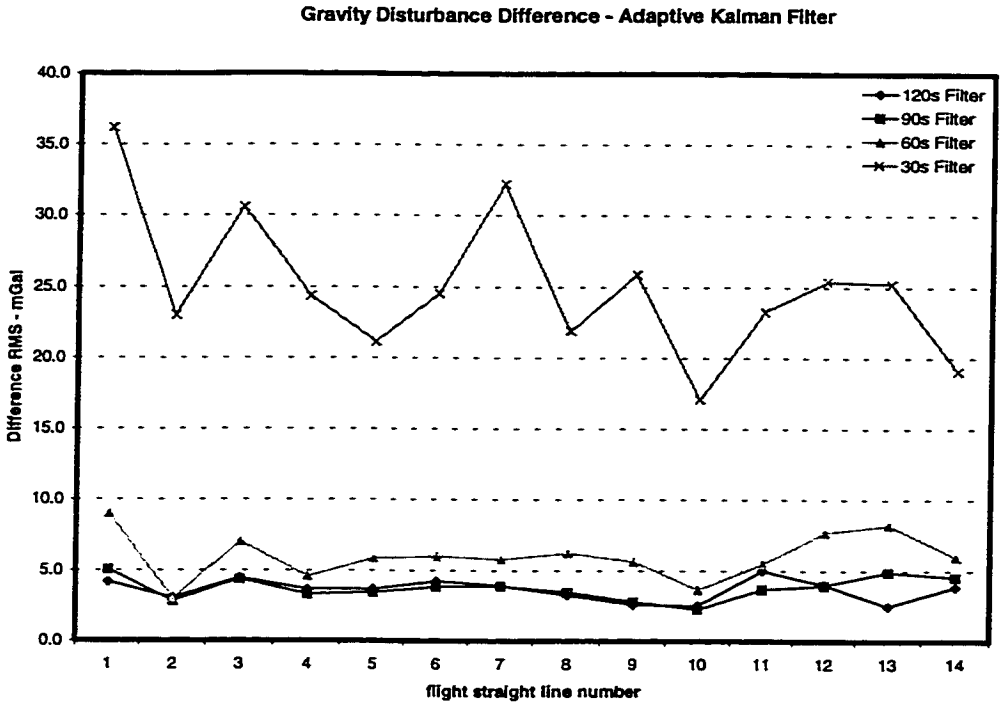

Fig. (8.20a):Gravity Disturbance Difference RMS along Straight Lines (Gravity Test)-AKF

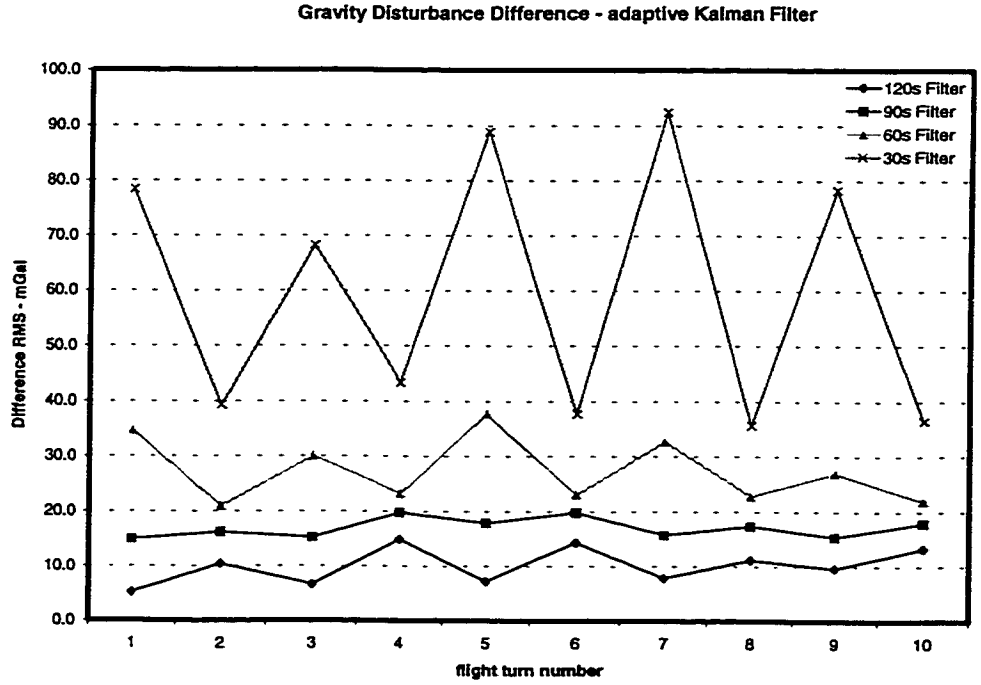

Fig. (8.20b) : Gravity Disturbance Difference RMS at Turns (Gravity Test) - AKF

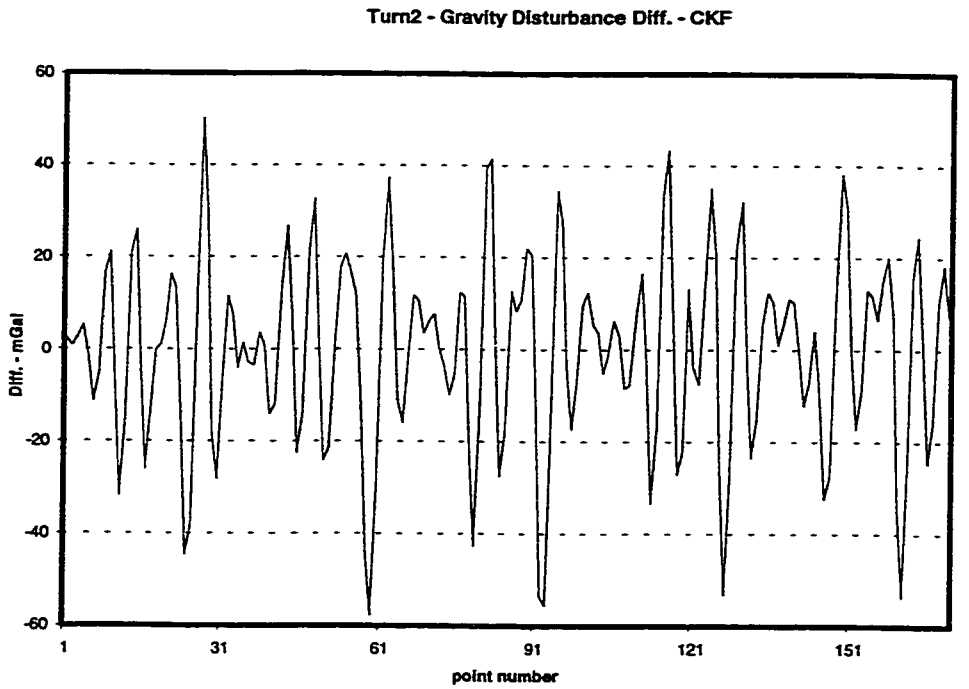

Fig. (8.21a) : Gravity Disturbance Difference at a Turn (Gravity Test) - CKF (90s filter)

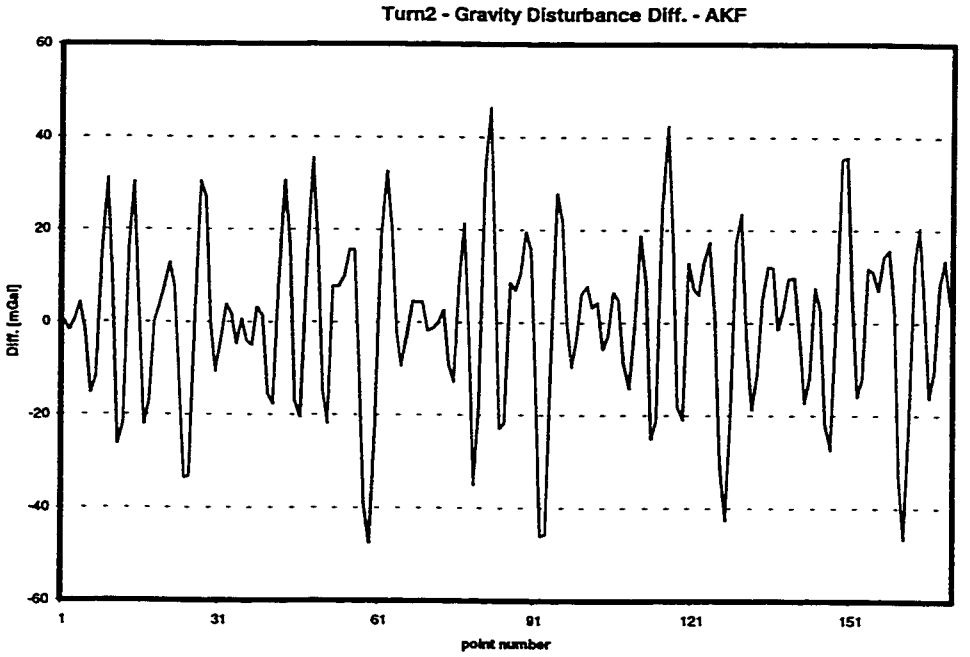

Fig. (8.21b) : Gravity Disturbance Difference at a Turn (Gravity Test) - AKF (90s filter)

Table (8.3) shows summary results from the conventional Kalman filter and the adaptive Kalman filter for the different cut-off frequencies and a linear bias removed. There is no clear difference between the performance of the two filters. The 90 second cut-off filter shows a comparable result to the 120 second filter. The two filters performed well along straight lines and degraded at turns. On average, the performance of the adaptive Kalman filter at turns is better than that of the conventional Kalman filter although even these results are not completely consistent.

Table (8.3) : Gravity Disturbance Difference (Gravity Test) - CKF vs. AKF

	Conventional				Adaptive			
Straight	120s	90s	60s	30s	120s	90s	60s	30s
1	4.1	5.1	8.9	35.8	4.2	5.0	9.0	36.2
2	2.9	2.7	2.8	22.2	3.0	2.8	3.0	23.0
3	4.3	3.8	4.5	25.9	4.5	4.3	7.0	30.6
4	4.7	4.8	7.7	29.2	3.6	3.3	4.6	24.3
5	3.8	3.8	6.1	22.2	3.7	3.4	5.8	21.1
6	4.0	3.6	5.8	23.6	4.2	3.8	6.0	24.5
7	3.9	3.8	5.3	30.1	3.9	3.9	5.8	32.2
8	3.4	3.3	5.4	20.4	3.3	3.5	6.2	21.9
9	2.5	2.8	5.5	25.4	2.6	2.8	5.6	25.8
10	2.6	2.8	5.0	19.5	2.5	2.3	3.6	17.0
11	5.0	4.9	7.8	29.7	5.0	3.7	5.4	23.3
12	3.9	3.8	8.0	25.1	4.0	3.9	7.7	25.4
13	2.4	4.4	8.1	25.0	2.5	4.9	8.2	25.3
14	3.8	4.7	7.1	23.1	3.8	4.5	5.9	19.0
Mean	3.8	4.0	6.5	25.9	3.7	3.8	6.2	25.5
Turn								
1	5.0	14.3	33.5	75.9	5.2	14.9	34.6	78.3
2	11.6	23.0	34.2	62.7	10.4	16.2	20.9	39.2
3	6.1	14.6	30.7	69.5	6.6	15.2	30.0	68.3
4	17.9	23.9	31.1	56.0	14.9	19.8	23.2	43.4
5	8.1	18.7	35.4	86.3	7.3	17.9	37.7	88.9
6	16.5	24.0	28.9	46.4	14.3	19.8	23.0	37.7
7	7.5	17.1	33.0	93.0	7.9	15.7	32.7	92.5
8	10.8	22.2	30.4	48.8	11.2	17.3	22.8	35.6
9	10.8	15.9	26.2	76.9	9.7	15.4	27.0	78.3
10	14.6	21.2	27.5	42.3	13.3	17.9	21.9	36.5
Mean	11.7	19.8	31.2	67.8	10.6	17.1	28.0	63.9
Straight and Turns								
Mean	8.1	13.2	20.8	48.0	7.4	11.4	18.7	45.6

9. SUMMARY, CONCLUSIONS, AND RECOMMENDATIONS

This chapter contains a summary of the research work presented in this dissertation, the conclusions drawn from the theoretical developments and test results, and recommendations for future research and developments in this field.

9.1 Summary

The objective of this research was to optimize the estimation procedures for kinematic applications when using an integrated INS/GPS system. The optimization was done with respect to the integration algorithm and the GPS carrier phase ambiguity resolution algorithm.

The conventional Kalman filter algorithm with which INS and GPS are integrated is replaced by an adaptive Kalman filter algorithm. The approach taken in this research is to adapt the a priori statistical information of the filter, namely, the measurement noise covariance matrix, R, and the system noise covariance matrix, Q. While these matrices are kept constant in the conventional Kalman filter (CKF) algorithm, they take different values in the adaptive Kalman filter (AKF) algorithm based on the filter innovation sequence. The innovation sequence, being a result of the interaction between the filter states and the measurement update, is an efficient representation of the changes happening to the carrier vehicle. The detailed derivation and development of an innovation-based adaptive Kalman filter using the maximum likelihood estimation criterion is described in this dissertation. Testing and analysis of the proposed adaptive Kalman filter showed its appropriateness for INS/GPS kinematic applications, especially the two most demanding ones, image direct georeferencing and airborne gravimetry.

The optimization of the GPS carrier phase ambiguity resolution algorithm is done by using a space projection technique called the whitening filter. The whitening filter uses a matrix factorization to project the ambiguity estimation problem onto another space which is simpler to analyze. Whitening causes the double differenced ambiguities

to decorrelate and their estimate to become more precise. It also causes the mutual receiver-satellite positional vectors to change. These effects are important to efficiently resolve the ambiguity. The whitening technique used in this research proved efficient for short baselines up to 35-40 kilometers. It also proved efficient as an on the fly technique with instantaneous resolution of the ambiguity after loss of phase lock. The development of the integer whitening filter and its use in the GPS carrier phase ambiguity resolution problem is covered in this dissertation.

9.2 Conclusions

The following conclusions can be drawn with respect to the adaptive Kalman filter, developed in this research, and the new whitening algorithm for GPS phase ambiguity resolution.

Adaptive Kalman Filter

1. The replacement of the widely used conventional Kalman filter by the adaptive Kalman filter for INS/GPS kinematic applications should be considered for the following reasons:
   - the filter a priori statistical information is of secondary importance to the AKF algorithm as they are estimated within the estimation algorithm itself, while they are very important to the CKF
   - test results showed that filter bandwidth keeps changing as the trajectory dynamics change in the case of AKF, while it reaches a constant bandwidth, at steady state, in the case of CKF and stops responding to the outside world; this property of the AKF results in a better tractability of the filter state estimates,
   - test results showed that AKF outperformed CKF in various situations
   - numerical complexity added by the AKF to the CKF algorithm is marginal and is acceptable when the gain of the filter performance is considered; on average, an

extra 5% of the time required by the CKF is needed by the AKF for processing the same set of data.

2. Systematic errors affect CKF and AKF differently; while they have a pronounced effect in the case of CKF, they seem not to be as critical with AKF.
3. Estimation problems that may arise in the case of CKF due to wrong a priori statistical information and/or unsuccessful calibration of system errors, have less effect in the case of AKF as the filter allows for continuous changes in the estimation procedure.
4. The separation of the coupled states in the case of CKF is done through dynamics change (e.g. maneuvers), while it is done through changes in the filter bandwidth in the AKF case.
5. Adapting R-only or Q-only in the AKF case seems to result in the same filter performance in cases where benign dynamics or straight lines trajectories are encountered.
6. Adapting Q-only works better than adapting R-only when relatively high dynamics or sudden geometry changes are encountered, because Q has a direct effect on the filter states through the correction vector.
7. It is safe to always use Q-only adaptation. There is no advantage of using Q and R adaptation simultaneously.
8. Results from simultaneous adaptation of R and Q are numerically unstable when using the full formula for Q, while is very close to results arising from adapting R-only when using the simplified formula for Q.
9. In a normal flight environment where attitude information is available, AKF outperformed CKF by 20%, especially in the azimuth misalignment state estimation, while maintaining a better filter state tracking.
10. In airborne gravimetry, AKF can provide slightly better performance with rms improvements of 10%-15% in turns and less than 5% along straight profiles.

11. Float whitening, although theoretically very important, is not critical for kinematic applications with short baselines, as the innovation sequence is almost always white and does not need whitening.

12. The choice of the averaging moving window is critical for the AKF; a window size smaller than the estimated variances (in R or Q) leads to divergent filter estimates. A window size considerably larger than the number of the estimated variances essentially converts the AKF into a CKF. For the system and measurement models used in this research and for the applications discussed, a window size of 20 epochs was found suitable as it provides reasonable results.

OTF Integer Whitening Filter

1. The problem of GPS carrier phase ambiguity resolution for short baselines can be solved without a search algorithm by using a space projection technique and rounding to the nearest floor or ceiling estimate.

2. The OTF integer whitening filter is an efficient technique for solving the ambiguity resolution problem in a simple and economical way.

3. Epoch-by-epoch resolution of ambiguity on the fly using the integer whitening filter is possible over short baselines, thus making it possible to use the integer whitening filter in real-time kinematic (RTK) applications.

4. A reliable OTF resolution can be achieved with the integer whitening filter for baselines up to 40 km; for longer baselines this technique is not reliable, although baselines of up to 130 km have been correctly resolved.

9.3 Recommendations

The adaptive Kalman filter developed and presented in this dissertation should be considered as a first step in the direction of finding a place for adaptive Kalman filter

methods in geomatics applications. In particular, the following recommendations are made for further investigation of the AKF in integrated INS/GPS systems:

1. specializing and adopting the developed adaptive Kalman filter algorithm to specific kinematic applications, like land-based and airborne direct georeferencing, integrated multi-sensor systems, where conventional Kalman is the widely used integration scheme, and further analysis of the performance of the adaptive Kalman filter in an integration scenario, based on the different situations that might occur in the trajectory,
2. investigating the use of the adaptive Kalman filter in solving specific problems, e.g. alignment procedure on the fly,
3. investigating the performance of the AKF against the CKF in case of post-mission processing of data by using forward filtering and backward smoothing,
4. designing optimal procedures for the choice of R-only, Q-only, for different applications and different integration scenarios.

The simplification and ease of the integer whitening filter technique inspired a new way of looking at the ambiguity resolution problem for kinematic applications over short baselines. The work presented in this dissertation should inspire further developments in the same direction. In particular, the following investigations would help to clarify some remaining questions on the OTF integer whitening filter technique:

1. automate the selection of the ambiguity best candidate through the statistical testing criteria using the obtained lookup tables,
2. carry out investigations to find the relationship between the local minimum and the global minimum in the GPS ambiguity resolution problem and hence define the region for further improvements of the OTF whitening technique,
3. address RTK specific problems, such as time latency, and find their effects on the performance of the OTF whitening technique.

BIBLIOGRAPHY

Almgren, K. (1998), "*A New Method for GPS Ambiguity Resolution on-the-fly at Short Baselines*", Doctoral Dissertation, Department of Geodesy and Photogrammetry, Royal Institute of Technology, Stockholm, Sweden.

Amlacher, C. (1998), "*Accuracy of airborne GPS trajectories from multiple ground stations*", Diploma Report, Institute of Physical and mathematical Geodesy at Graz , Austria.

Anorad (1993), "*Anorad I-Series Installation and operation Manual*", Anorad Corporation, New York 11788.

Argeseanu, V. (1995), "*Upward Continuation of Surface Gravity Anomaly Data*", Proceeding of Airborne Gravimetry, IAG Symposium G4, IUGG XXI.

Baarda, W. (1968), "A *Test Procedure For Use in Geodetic Networks*", New Series 2, Netherlands Geodetic Commission, Delft, The Netherlands.

Babbage, G. (1977), "*Operation of the Inertial Survey System: the Manager's View*", a paper presented at First International Symposium on Inertial Technology for Surveying and Geodesy, Can. Inst. Surv., Ottawa, October 12-14.

Benson Jr., D.O. (1975), "*A Comparison of Two Approaches to Pure-inertial and Doppler-inertial Error Analysis*", IEEE Transactions on Aerospace and Electronic Systems, Vol. AES-11, No. 4, July.

Bierman, G.J. (1977), "*Factorization Methods for Discrete Sequential Estimation*", Academic Press Inc., New York.

Blais, J.A.R. (1985), "Least-Squares Filtering and Smoothing using Givens Transformations", Manuscripta Geodetica, 10:pp208-212.

Boedecker, G., H. Neumayer (1995), "*An Efficient Way to Airborne Gravimetry: Integration of strapdown Accelerometer and GPS*", Proceedings of Airborne Gravimetry, IUGG XXI General Assembly, Boulder, CO, pp. 23-28, July 12-14.

Braasch, M. (1998), "*GPS Multipath Characterization and Mitigation*", Lecture Notes, Geomatics Engineering Department, The University of Calgary, July 8.

Britting, K.R. (1971), "*Inertial navigation Systems Analysis*", John Wiley & Sons Inc., New York.

Brown, R.G., P.Y.C. Hwang (1992), "*Introduction to Random Signals and Applied Kalman Filtering*", John Wiley & Sons Inc., New York.

Bruton, A.M. (1997), "*Reduction of GPS Receiver Noise Using Adaptive Filters*", ION Conference Proceedings, Kansas City, MO, September 16-19.

Bruton, A.M., K.P. Schwarz (1997), "*Airborne Gravity Estimation Using Adaptive Filters*", KIS'97 Conference Proceedings, Banff, Canada, June 3-6.

Chaer, W.S., R.H. Bishop, J. Ghogh (1997), "*A Mixture-of-Experts Framework for Adaptive Kalman Filtering*", IEEE Trans. on Systems, Man., and Cybernetics-Part B: Cybernetics, Vol. 27, No. 3, June.

Chen, D. and G. Lachapelle (1994), "*A Comparison of the FASF and Least-Squares Search Algorithm for Ambiguity Resolution On The Fly*", KIS94 Symposium, Banff, Aug. 30-Sep. 2.

Cramér, Harald (1946), "*Mathematical Methods of Statistics*", Princeton University Press, Princeton, New Jersey.

Czompo, J. (1994), "*Airborne Scalar Gravimetry System Errors in the Spectral Domain*", UCSE Report #20067, Department of Geomatics Engineering, The University of Calgary, Canada.

El-Rabbany, A. (1994), "*The Effect of Physical correlation on the Ambiguity Resolution and Accuracy Determination in GPS Differential Positioning*", Technical Report No. 170, Department of Geodesy and Geomatics Engineering, University of New Brunswick, Fredericton, NB, Canada.

El-Rabbany, A. (1996), "*Temporal characteristics of Multipath Errors*", Technical Report No. 1044, Royal Institute of Technology, Department of Geodesy and Photogrammetry, Stockholm, Sweden.

El-Sheimy, N., K.P. Schwarz, M. Wei, M. Lavigne (1995), "*VISAT: A Mobile City Survey System of High Accuracy*", Proceedings of the ION GPS-95, pp. 1307-1315, Palm Springs, CA, Sept. 12-15, 1995.

Frei, E. and G. Beutler (1990), "*Rapid static Positioning Based on the Fast ambiguity Resolution Approach: The Alternative to Kinematic Positioning*", Proceedings of the 2nd International Symposium on Precise Positioning with GPS, Ottawa, Sep. 3-7.

Gao, Y., E.J. Krakiwsky, J.F. McLellan, (1992), "*Experience with the Application of Federated Filter Design to Kinematic GPS Positioning*", IEEE PLANS, Monterey.

Gao, Y. (1992), "*A Robust Quality Control System For GPS Navigation and Kinematic Positioning*", UCGE Report No. 20075, The University of Calgary, Canada.

Gary, R.A., and P.S. Maybeck (1996), "*An Integrated GPS/INS/BARO and RADAR Altimeter System for Aircraft Precision Approach Landings*", *Department of Electrical and Computer Engineering, Air Force Institute of Technology, Ohio.*

Gelb, A. (Editor) (1974), "*Applied Optimal Estimation*", The MIT Press, Cambridge, Massachusetts, and London, England, Tenth Printing 1988.

Genin, F. (1970), "*Further Comments on the Derivation of Kalman Filters, Section II: Gaussian Estimates and Kalman Filtering*", Theory and Applications of Kalman Filtering, AGARDOgraph 139, C.T. Leondes, ed., NATO Advanced Groups for Aerospace R&D.

Girgis, A.A., and R.G. Brown (1985), "*Adaptive Kalman Filtering in Computer Relaying: Fault Classification using Voltage Models*", IEEE Trans. On Power Apparatus and Systems, PAS-104: No. 5, pp. 1168-1177.

Glennie, C. and K.P. Schwarz (1997), "*Airborne Gravity by Strapdown INS/DGPS in a 100 km by 100 km Area of the Rocky Mountains*", KIS97 Symposium, Banff, Canada, June 3 – 6.

Golub, G.H. and C.F.V. Loan (1989), "*Matrix Computations*", Second Edition, The John Hopkins University Press, New York.

Greenspan, R.L. (1995) "*Inertial Navigation Technology from 1970-1995*", NAVIGATION, Journal of The Institute Of Navigation, Vol. 42, No. 1.

Hammada, Y. (1996), "*A Comparison of Filtering Techniques for Airborne Gravimetry*", UCGO report No. 20089, Department of Geomatics Engineering, The University of Calgary, Canada.

Hatch, R. and H. Euler (1994), *Comparison of Several AROF Kinematic Techniques*, Proceedings of ION GPS-94, Salt Lake City, Utah, Sept. 20-23.

Hatch, R. (1990), "*Instantaneous Ambiguity Resolution*", in Schwarz and Lachapelle (eds.), "Kinematic Systems in Geodesy, Surveying, and Remote sensing", Springer-Verlag, Berlin, IAG Symposia 107.

Haykin, S. (1996), "*Adaptive Filter Theory*", Prentice-Hall Information and System Sciences Series, New Jersey.

Hein, G. and W. Werner (1995), "*Comparison of Different On-The-Fly Ambiguity Resolution Techniques*", Proceedings of ION GPS-95, Palm Springs, CA, Sept. 12-15.

Hoffmann-Wellenhof, B., H. Lichtenegger, J. Collins (1992), "*Global Positioning System Theory and Practice*", Springer-Verlag Wien New York.

Jonge P. and C. Tiberius (1996), "*The LAMBDA Method for Integer Ambiguity Estimation: Implementation Aspects*", LGR-Series, Publications of The Delft Geodetic Computing Center.

Kailath, T. (1972), "*A Note on Least Squares Estimation by the Innovation Method*", the Society for Industrial and Applied Mathematics 10(3) 477-486.

Kailath, T. (1974), "*A View of Three Decades of Linear Filtering Theory*"", IEEE Trans. Inf. Theory IT-20(2): 146-181.

Kailath, T. (1981), "*Lectures on Wiener and Kalman Filtering*", CISM Courses and Lectures No. 140, Springer-Verlag.

Kalman, R.E. (1960), "*A New Approach to Linear Filtering and Prediction Problems*", J. Basic Eng. 82: 35-45 (March 1960).

KINGSPAD (1994), "*Documentation for KINGSPAD Version 2.1*", Department of Geomatics Engineering, The University of Calgary, Canada.

Klobuchar, J. (1991), "*Ionospheric Effects on GPS*", GPS World, Volume 2, Number 4.

Knight, T.K. (1996), "*Rapid Development of Tightly-Coupled GPS/INS Systems*", IEEE Plans'96, Atlanta, Georgia, April 22-26, 1996.

Koch, K.R. (1988), "*Parameter estimation and hypothesis testing in linear models*", Springer, Berlin, Germany.

Kubik, K.K. (1983), "*The Danish Method: Experience and Philosophy*", DGK, Reihe A 98, Munich, Germany.

Lachapelle, G. (1998), "*GPS Theory and Applications*", ENGO 625 lecture notes, Department of Geomatics Engineering, The University of Calgary, Canada.

Lachapelle, G., M.E. Cannon, G. Lu, (1992), "*High-precision GPS Navigation with Emphasis on Carrier Phase Ambiguity Resolution*", Marine Geodesy, Vol. 15.

Lachapelle, G., W. Falkenberg, M. Casey (1987), "*Use of Phase Data for Accurate GPS Differential Positioning*", Proceedings of PLANS, Las Vegas, Nov. 5-7.

Langley, R. (1993), *"The GPS Observables"*, GPS World, Volume 4, Number 4.

Lapucha, D. (1990), *"Precise GPS/INS Positioning For A Highway Inventory System"*, UCSE Report #20038, Department of Surveying Engineering, The University of Calgary, Calgary.

Levy, L. J. (1996), *"Advanced Topics in GPS/INS Integration with Kalman Filtering"*, Navtech Seminars Tutorials, Sept. 10, Kansas City, MO.

Li, Zuofa (1995), *"Efficient Ambiguity Search Using Genetics Algorithms"*, Proceedings of ION GPS-95, Palm Springs, CA, Sept. 12-15.

Liu, Z. (1992), *"Comparison of Statistical Methods for the Alignment of Strapdown Inertial Systems"*, UCGO Report No. 20047, Department of Geomatics Engineering, The University of Calgary, Canada.

Magill, D. T. (1965), *"Optimal Adaptive Estimation of Sampled Stochastic Processes"*, IEEE Trans. On Automatic Control, AC-10: No. 4, 434-439 (October 1965).

Maybeck, P.S. (1972), *"Combined Estimation of States and Parameters for On-line Applications"*, (Report T577 Draper laboratories), Ph.D. dissertation, MIT, Cambridge, Massachusetts.

Maybeck, P.S. (1982), *"Stochastic Models, Estimation, and Control"*, Volumes I and II, Academic Press, INC. New York.

Maybeck, P.S. (1989), *"Moving-Bank Multiple Model Adaptive Estimation and Control Algorithms: An Evaluation"*, Control and Dynamic Systems, Vol. 31, Academic Press, INC. New York.

Maybeck, P.S. (1997), *"Stochastic Processes and Estimation"*, Lecture notes, Department of Geomatics Engineering, The University of Calgary, Aug. 4-16.

McBurney, P.W. (1990), *"A Robust Approach to Reliable Real-time Kalman Filtering"*, CH2811-8/90/0000/0549 $1.0 (c) 1990 IEEE, pp. 549-556.

Mehra, R.K. (1970), *"On the Identification of Variance and Adaptive Kalman Filtering"*, IEEE Trans. on Automatic Control, Vol. 4C-15, No. 2, pp. 175-184.

Mehra, R.K. (1971), *"On-line Identification of Linear Dynamic Systems with Applications to Kalman Filtering"*, IEEE Trans. on Automatic Control, Vol. AC-16 No. 1, February.

Mehra, R.K. (1972), *"Approaches to Adaptive Filtering"*, IEEE Trans. on Automatic Control, Vol. AC-16 No. 1.

Merhav, S. (1996), "*Aerospace Sensor Systems and Applications*", Springer, Berlin.

Mikhail, E.M., and F. Ackerman (1976) "*Observations and Least Squares*", University Press of America Inc., Washington D.C.

Miller, R.W. (1971), "*Asymptotic Behavior of the Kalman Filter with Exponential Aging*", AIAA Journal, Vol. 9, No. 3, pp. 537-539.

Mohamed, A.H. (1994) "*Achieving Cm-level Accuracy of GPS/INS Integration*", ENGO 699.26 course report, Geomatics Engineering Dept., The University of Calgary, Canada.

Mohamed, A.H. (1995) "*Optimal Update Intervals for GPS/INS Integration*", ENGO 621 course report, Geomatics Engineering Dept., The University of Calgary, Canada.

Mohamed, A.H. (1996) "*Robust and Reliable Kalman Filtering of GPS Data*", ION 9th International Technical Meeting, Kansas City, MO, Sept. 17-19.

Mohamed, A.H., KP Schwarz (1998) "*A Simple and Economical Algorithm For Ambiguity Resolution OTF Using a Whitening Filter*", NAVIGATION, Journal of The Institute Of Navigation, Vol. 45, No. 3.

Mohamed, A.H., K.P. Schwarz (1999) "*Adaptive Kalman Filtering for INS/GPS*", Accepted for publication in Journal of Geodesy, Journal of the International Association of Geodesy (*in press*).

Papoulis, A. (1965), "*Probability, Random Variables, and Stochastic Processes*", McGraw-Hill, New York.

Parkinson, B.W., J.J. Spilker (editors) (1996), "*Global Positioning System: Theory and Applications*", American Institute of Aeronautics and Astronautics, Inc.

Purcell, E.J. (1972), "*Calculus with analytical Geometry*", second edition, Meredith corporation, New York.

Raquet, J. (1998), "*Development of a Method for Kinematic GPS Carrier-Phase Ambiguity Resolution using Multiple Reference Receivers*", Department of Geomatics Engineering, The University of Calgary, UCGE Report No. 20116.

Rizos, C. and S. Han (1995), "*A New Method for Constructing Multi-satellite Ambiguity Combinations for Improved Ambiguity Resolution*", Proceedings of ION GPS-95, Palm Springs, CA, Sept. 12-15.

Rogers, G.S. (1980), "*Matrix Derivatives*", Lecture Notes in Statistics, Volume 2, Marcel Dekker, Inc., New York.

Salychev, O. S. (1993), *"Wave and Scalar Estimation Approaches for GPS/INS Integration"*, Technical Report No. 20, Institute of Geodesy, University of Stuttgart, ISSN 0933-2839.

Salychev, O. S. (1994), *"Special studies in Dynamic Estimation Procedures with Case Studies in Inertial Surveying"*, ENGO 699.26 Lecture Notes, Department of Geomatics Engineering, The University of Calgary, Canada.

Salychev, O. S., K.P. Schwarz, Y. Hammada (1995), *"An Analysis of the Wave Approach to State Vector Estimation"*, Proceedings of the IAG Symposium on Airborne Gravity Field Determination, Boulder, Colorado, July 2-14, 1995.

Salychev, O.S. (1998), *"Inertial Systems in Navigation and Geophysics"*, Moscow State Technical University, Bauman MSTU Press, Moscow.

Savage, P.G. (1978), *"Strapdown Sensors"* in *"Strapdown Inertial Systems"*, AGARD-LS-95 Lecture series.

Savage, P.G. (1983), *"Introduction of Inertial Navigation systems"*, Supplemental material, Geomatics Engineering Department, The University of Calgary, Canada.

Sayed, A.H., T. Kailath (1994), *"A State-space Approach to Adaptive RLS Filtering"*, IEEE Signal Processing Magazine, Vol. 11, pp. 18-60.

Schmidt, S.F. (1970), *"Computational Techniques in Kalman Filtering"*, *in "Theory and Applications of Kalman Filtering"*, AGARDograph LS 130.

Schwarz, K.P. (1983), *"Inertial Surveying and Geodesy"*, Review of Geophysics and Space Physics, Vol. 21, No. 4, pp. 878-890.

Schwarz, K.P. (1986), *"The Error Model of Inertial Geodesy – a Study in Dynamic System Analysis"*, in H. Sünkel (ed.) "Mathematical and Numerical Techniques in Physical Geodesy", Springer-Verlag, Berlin.

Schwarz, K.P. (1987), *"Kalman Filtering and Optimal Smoothing"*, Papers for The CISM Adjustment and Analysis Seminars, Second Edition.

Schwarz, K.P. (1991), *"Kinematic modeling - Progress and Problems"*, IAG Symposia on Kinematic Systems in Geodesy, Surveying, and Remote Sensing, Springer-Verlag New York, Inc.

Schwarz, K.P, M. Chapman, M.E. Cannon, P. Gong, D. Cosandier (1993a), *"A precise Positioning/Attitude System in Support of Airborne Remote Sensing"*, ISPRS Vol. 30 Part 2, Ottawa 6-10 June 1994.

Schwarz, K.P., H. Martell, N. El-Sheimy, R. Li, M. Chapman, D. Cosandier (1993b), "*VISAT- A Mobile Highway Survey System of High Accuracy*", VNIS Conference'93 Conference, Ottawa, October 12-15, 1993, pp. 476-481.

Schwarz, K.P., M. Gelderen, M. Wei (1993c), "*Integrated MAPS/GPS Performance Study*", Report No. TCN 92224, Department of Geomatics Engineering, The University of Calgary, Canada.

Schwarz, K.P., M. Wei, M. Gelderen (1994), "*Aided Versus Embedded A Comparison of Two Approaches to GPS/INS Integration*", Proceedings of the 1994 IEEE Position Location and Navigation Symposium, Las Vigas, pp. 314-322.

Schwarz, K.P, M. Wei (1994), "*Aided Versus Embedded: A Comparison of Two Approaches to GPS/INS Integration*", Proceedings of the IEEE PLANS, Las Vegas, pp. 314-322.

Schwarz, K.P., G. Zhang (1994), "*Development and Testing of a Low Cost Integrated GPS/INS*", Proceedings of ION GPS-94, Salt Lake city, Utah, Sept. 20-23, pp. 1137-1144.

Schwarz, K.P, M. Wei (1995a), "*Inertial Geodesy and INS/GPS Integration*", partial lecture notes for ENGO 623, Department of Geomatics Engineering, The University of Calgary, Canada.

Schwarz, K.P, M. Wei (1995b), "*Modeling INS/GPS for Attitude and Gravity Applications*", 3rd international workshop on high precision navigation, Stuttgart, Germany, April 3-6.

Schwarz, K.P., Z. Li (1996), "*An Introduction to Airborne Gravimetry and Its Absolute Boundary Value Problem*", Department of Geomatics Engineering, The University of Calgary, Canada.

Seeber, G. (1993), "*Satellite Geodesy, Foundations, Methods, and Applications*", Walter de Gruyter, Berlin, Germany.

Sideris, M. (1984), "*Computation of Gravimetric Terrain Corrections Using Fast Fourier Transform Technique*", UCSE Report #20007, Department of Surveying Engineering, The University of Calgary, Canada.

Skaloud, J., D. Cosandier, K.P. Schwarz, M.A. Chapman (1994), "*GPS/INS Orientation Accuracy Derived from a Medium Scale Photogrammetry Test*", Proceedings of KIS'94, Banff, Canada, Aug. 30 - Sep. 2.

Skaloud, J. (1999), *"Optimizing Georeferencing of Airborne Survey Systems by INS/DGPS"*, Ph.D. thesis (to be published), Department of Geomatics Engineering, The University of Calgary, Canada.

Sorenson, H.W. (1970), *"Least-Squares Estimation: From Gauss to Kalman"*, IEEE Spectrum, July.

Swerling, P. (1971), *"Modern State Estimation Methods from the Viewpoint of the Method of Least Squares"*, IEEE Transaction on Automatic Control, Vol. AC-16, No. 6, December.

Tapley, B.D., B.E. Schutz, (1974), *"A Comparison of Orbit Determination Methods for Geodetic Satellites"*, A Report of the Department of Aerospace Engineering and Engineering Mechanics, The University of Texas at Austin.

Teunissen, P.J. (1990), *"Quality Control in Integrated Navigation Systems"*, PLANS IEEE 1990 pp. 158-165.

Teunissen, P.J.G. (1994), *"A New Method for fast Carrier Phase Ambiguity Estimation"*, Proceedings of the IEEE Position Location and Navigation Symposium PLANS94, Las Vegas, April 11-15.

Toda, N.F., F.H. Schlee, P. Obsharsky, (1967), *"Regions of Kalman Filter Convergence for Several Autonomous Navigation Modes"*, Paper 67-623 at the AIAA Guidance, Control, and Flight Dynamics Conference, Huntsville, Ala., August 14-16.

Wang, Jinling, M. Stewart, and M. Tsakiri (1997), *"Kinematic GPS Positioning with Adaptive Kalman Filtering Techniques"*, Proceedings of the IAG'97, Rio De Janero, September 1997.

Wei, M., D. Lapucha, H. Martell (1990), *"Fault Detection and Estimation in Dynamic Systems"*, IAG Symposium No. 107, Banff, AB, September, pp. 201-217.

Wei, M., K.P. Schwarz (1990a), *"Testing a Decentralized Filter for GPS/INS Integration"*, Proceedings of the IEEE Position Location and Navigation Symposium, Las Vegas, Nevada, March 20-23, pp. 429-435.

Wei, M., K.P. Schwarz (1990b), *"A Strapdown Inertial Algorithm Using an Earth-Fixed Cartesian Frame"*, Navigation: Journal of The Institute Of Navigation, Vol. 37, No. 2, pp. 429-435.

Wei, M., K.P. Schwarz (1995a), *"Fast Ambiguity Resolution Using an Integer Non-Linear Programming Method"*, Proceedings of ION GPS-95, Palm Springs, CA, Sept. 12-15.

Wei, M., K.P. Schwarz (1995b), *"Analysis of GPS-Derived Acceleration From Airborne Tests"*, Proceedings of the IAG Symposium on Airborne Gravity Field Determination, Boulder, Colorado, July 2-14, 1995.

Wells, D.E., N. Beck, D. Delikaraoglou, A. Kleusberg, E.J. Krakiwsky, G. Lachapelle, R.g. Langley, M. Nakibolou, K.P. Schwarz, J.M. Tranquilla, P. Vanicek (1986), *"Guide to GPS Positioning"*, Canadian GPS Associates, Fredericton, New Brunswick.

White, N.A. (1996), *"MMAE Detection of Interference/Jamming and Spoofing in a DGPS-Aided Inertial System", MS Thesis, Department of Electrical and Computer Engineering, Air Force Institute of Technology, Ohio.*

White, N.A., P.S. Maybeck, and S.L. DeVilbiss (1996), *"MMAE Detection of Interference/Jamming and Spoofing in a DGPS-Aided Inertial System", Department of Electrical and Computer Engineering, Air Force Institute of Technology, Ohio.*

Wild, U., G. Beutler, S. Frankhauser, W. Gurtner (1990), *"Stochastic Properties of the Ionosphere Estimated from GPS Observations"*, Proceedings of the International Sysmposium on Precise Positioning with the Global Positioning System, Ottawa, Canada, September 3-7.

Wong, R.V.C. (1982), *"A Kalman Filter-Smoother for an Inertial Survey System of Local Level Type"*, UCSE Report No. 20001, Department of Surveying Engineering, The University of Calgary, Canada.

Wong, R.V.C. (1988), *"Development of a RLG Strapdown Survey System"*, UCSE Report No. 20027, Department of Surveying Engineering, The University of Calgary, Canada.

Yaglom, A.M. (1987), *"Correlation Theory of Stationary and Related Random Functions"*, Springer-Verlag, Berlin.

Zhang, Q. J. (1995), *"Development of a GPS-aided inertial platform for airborne scalar gravimetry system"*, Ph.D. thesis, Department of Geomatics Engineering, The University of Calgary, Canada.

Zhang, Z. (1997), *"Impact of Rubidium Clock Aiding on GPS Augmented Vehicular Navigation"*, UCGO report No. 20112, Department of Geomatics Engineering, The University of Calgary, Canada.

APPENDIX A.
SIMPLIFIED INERTIAL NAVIGATION ERROR MODEL

In a local-level frame, physical in case of platform systems and mathematical in case of strapdown systems, the inertial navigation system has two stable horizontal channels and an unstable vertical channel. For a strapdown system, the state-space representation of *motion* of a vehicle in the gravitational field of the earth, expressed in a local-level frame*, is of the form [Britting 1971, Wong 1982, Schwarz and Wei, 1995, Salychev 1998]

$$\begin{aligned} \dot{p}^l &= v^l \\ \dot{v}^l &= R_b^l f^b - (2\Omega_{ie}^l + \Omega_{el}^l)v^l + g^l, \\ \dot{R}_b^l &= R_b^l(\Omega_{ib}^b - \Omega_{il}^b) \end{aligned} \tag{A.1}$$

where,

superscripts b, l, e : represent body (measurement), local-level (navigation), and earth-fixed frames

p, v, R_b^l : vehicle position, velocity, and attitude

f^b, g : specific force (measured) and gravity acceleration

Ω^b_{ib}, Ω^l_{ie}, Ω^b_{il}, Ω^l_{el} : body (measured), Earth's rotation, local-level-to-inertial, and local-level-to-earth frame rotation rates.

To simplify the above system of equations, the following is assumed:

1. the Coriolis and Earth's rotation effects, $(2\Omega_{ie}^l + \Omega_{el}^l)v^l$, are neglected
2. the attitude matrix, R^l_b, will contain small rotations only
3. the second-order terms will also be neglected
4. the up specific force, f_u, will be assumed constant and equal to the Earth's mean gravity g
5. a spherical Earth's model with mean radius R is used.

---

* For simplicity, when the superscript is omitted, it is assumed to be 'l', the local-level frame.

The state-space representation of the *velocity* is then given by

$$\begin{pmatrix} \dot{v}_E \\ \dot{v}_N \\ \dot{v}_u \end{pmatrix} = \begin{pmatrix} 1 & -\Xi_u & \Xi_N \\ \Xi_u & 1 & -\Xi_E \\ -\Xi_N & \Xi_E & 1 \end{pmatrix} \begin{pmatrix} f_E \\ f_N \\ f_u \end{pmatrix} + \begin{pmatrix} 0 \\ 0 \\ -\gamma \end{pmatrix}$$

which after neglecting the second-order terms and substituting $g = f_u$, yields

$$\begin{aligned} \dot{v}_E &= f_E + g\Xi_N \\ \dot{v}_N &= f_N - g\Xi_E \\ \dot{v}_u &= f_u - \gamma \end{aligned} , \qquad \text{(A.2)}$$

where,
E, N, u : East, North, up axes of the local-level frame,

Ξ_N, Ξ_E, Ξ_u : attitude components in the local-level frame; roll and pitch for the two horizontal channels and azimuth for the vertical channel

γ : normal gravity.

And, the state-space representation of the *attitude* is

$$\begin{pmatrix} \dot{\Xi}_E \\ \dot{\Xi}_N \\ \dot{\Xi}_u \end{pmatrix} = \begin{pmatrix} 1 & -\Xi_u & \Xi_N \\ \Xi_u & 1 & -\Xi_E \\ -\Xi_N & \Xi_E & 1 \end{pmatrix} \begin{pmatrix} \theta_E \\ \theta_N \\ \theta_u \end{pmatrix} - \begin{pmatrix} -v_N/R \\ v_E/R \\ v_E/r \end{pmatrix}$$

which after neglecting the second-order terms yields

$$\begin{aligned} \dot{\Xi}_E &= \frac{v_N}{R} + \theta_E \\ \dot{\Xi}_N &= -\frac{v_E}{R} + \theta_N \\ \dot{\Xi}_u &= -\frac{v_E}{r} + \theta_u \end{aligned} , \qquad \text{(A.3)}$$

where,
θ_E, θ_N, θ_u, : measured body rates represented in the local-level frame

r : tangential distance to the Earth's spin axis from vehicle position; r = R cot(latitude).

A.1 Error Model of a Horizontal Channel

Linearizing Eq.(A.2) and Eq. (A.3) for one of the horizontal channels, say the east channel, the state-space representation of the *error model* is

$$\begin{aligned} \delta\dot{p}_E &= \delta v_E \\ \delta\dot{v}_E &= g\varepsilon_N + b_A \\ \dot{\varepsilon}_N &= -\frac{\delta v_E}{R} + b_G \end{aligned} \tag{A.4}$$

where,

δp_E, δv_E, $\varepsilon_N=\delta\Xi$: position, velocity, and attitude navigation errors

$b_A=\delta f$, $b_G=\delta\theta$: accelerometer bias and gyro drift bias.

Fig. (A.1) illustrates the above system of differential equations in a block diagram, the so-called Schuler loop for a horizontal inertial navigation channel.

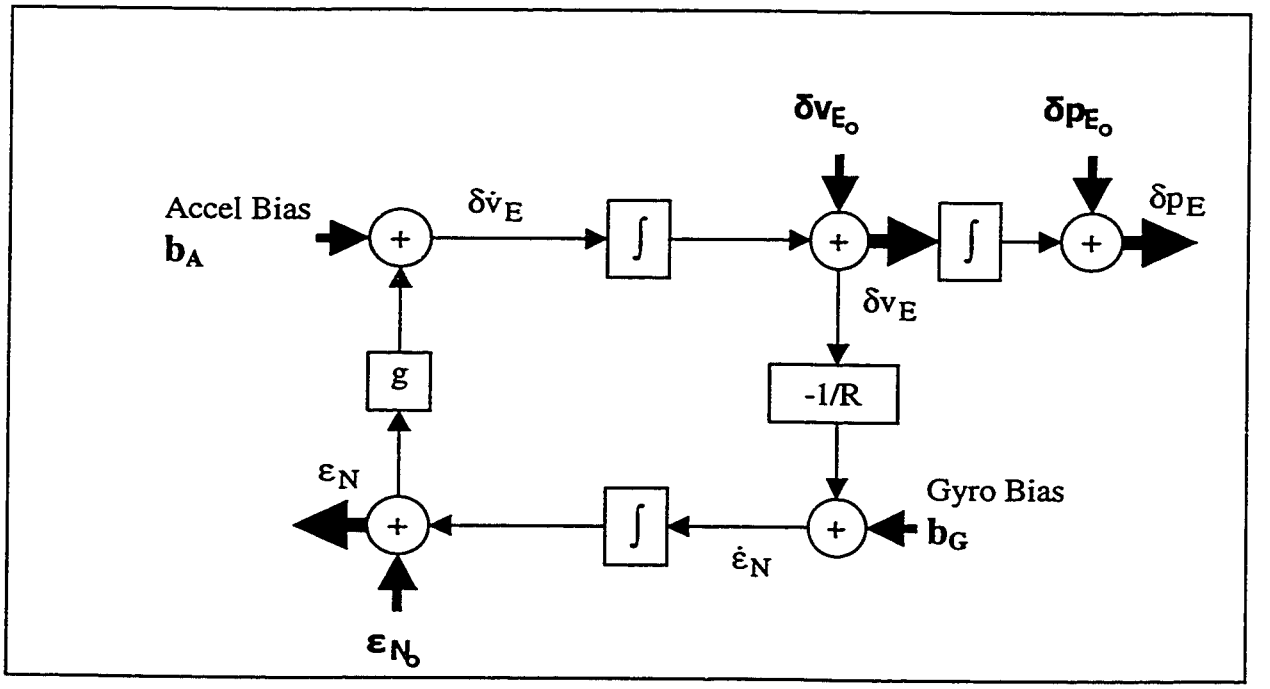

Fig. (A.1) : Schuler Loop of the East Channel

In the above system of equations, differentiating the velocity error equation and substituting the attitude error into it, one gets the following non-homogeneous linear second-order differential equation

$$\ddot{\delta v} + \nu^2 \delta v = \nu^2 R b_G \tag{A.5}$$

where, $\nu = \sqrt{\frac{g}{R}} \approx \frac{1}{806}\text{rad/s} \approx 1.24\text{mrad/s} \approx \frac{1}{5000}\text{Hz} \approx 250^\circ/\text{h}$, corresponding to a time period of 84 minutes, is called Schuler frequency. The frequency-domain representation of Eq. (A.5)

$$s^2 + \nu^2 = 0,$$

where s is the Laplace operator, is the equation for simple harmonic motion with natural frequency, ν, for a Schuler pendulum of length, R, the Earth's radius. The solution of the above differential equation yields [Purcell 1972],

$$\delta v = R b_G + C_1 \sin(\nu t) + C_2 \cos(\nu t) \tag{A.6}$$

where, C_1 and C_2 are constants of integration.

At time t = 0, the initial velocity error is $\delta v = \delta v_0$. Substituting this expression into Eq. (A.6), one gets $C_2 = \delta v_0 - R b_G$ and when substituted back into the same equation, it becomes

$$\delta v = R b_G + C_1 \sin(\nu t) + \delta v_0 \cos(\nu t) - R b_G \cos(\nu t). \tag{A.7}$$

Differentiate Eq. (A.7), to get

$$\dot{\delta v} = C_1 \nu \cos(\nu t) - \delta v_0 \nu \sin(\nu t) + R b_G \nu \sin(\nu t). \tag{A.8}$$

From Eq. (A.8) and Eq. (A.4), it can be shown that

$$\varepsilon = \frac{1}{R\nu} C_1 \cos(\nu t) - \frac{1}{R\nu} \delta v_0 \sin(\nu t) + \frac{b_G}{\nu} \sin(\nu t) - \frac{b_A}{R\nu^2}. \tag{A.9}$$

Now, at t = 0, the initial leveling error (misleveling) is $\varepsilon = \varepsilon_0$. Substituting this value into Eq. (A.9), one gets $C_1 = \frac{b_A}{v} + Rv\varepsilon_0$. Substituting the expression for C_1 into Eq. (A.7), one gets *the velocity error equation*

$$\boxed{\delta v = \delta v_0 \cos(vt) + b_A \frac{1}{v}\sin(vt) + \varepsilon_0 Rv \sin(vt) - b_G R \cos(vt) + b_G R}. \tag{A.10}$$

Substituting this (A.10) in the position error Eq. (A.4) and integrating, one gets

$$\delta p = \frac{\delta v_0}{v}\sin(vt) - b_A \frac{\cos(vt)}{v^2} - \varepsilon_0 R \cos(vt) + b_G R\left(t - \frac{\sin(vt)}{v}\right) + C_3 . \tag{A.11}$$

At t = 0, the initial position error is $\delta p = \delta p_0$. Substituting this value into Eq. (A.11), one gets $C_3 = \delta p_0 + \frac{b_A}{v^2} + \varepsilon_0 R$. Re-substitute the expression for C_3 into Eq. (A.11) to get the equation for the *position error*

$$\boxed{\begin{aligned}\delta p = \delta p_0 + \delta v_0 \frac{1}{v}\sin(vt) + b_A \frac{1}{v^2} - b_A \frac{1}{v^2}\cos(vt) \\ + \varepsilon_0 R - \varepsilon_0 R \cos(vt) - b_G R \frac{1}{v}\sin(vt) + b_G Rt\end{aligned}}. \tag{A.12}$$

Now, to get an expression for the *attitude error* (leveling error in a horizontal channel), substitute the expression for C_1 into Eq. (A.9) and rearrange terms

$$\boxed{\begin{aligned}\varepsilon = \varepsilon_0 \cos(vt) - \delta v_0 \frac{1}{Rv}\sin(vt) - b_A \frac{1}{Rv^2} + b_A \frac{1}{Rv^2}\cos(vt) \\ + b_G \frac{1}{v}\sin(vt)\end{aligned}}. \tag{A.13}$$

Using the previous equations, typical plots of the position, velocity and leveling long-term errors in a horizontal channel of a navigation-grade INS are given in Figs. (A.2) to (A.4) below.

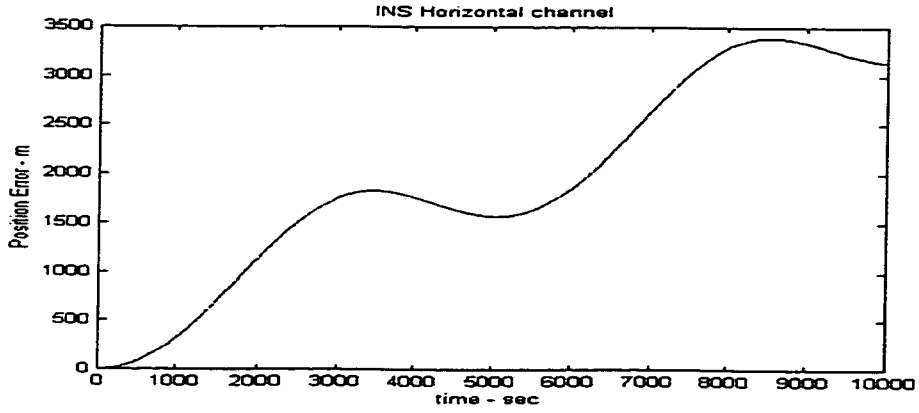

Fig. (A.2) : INS Position Error (Horizontal Channel)

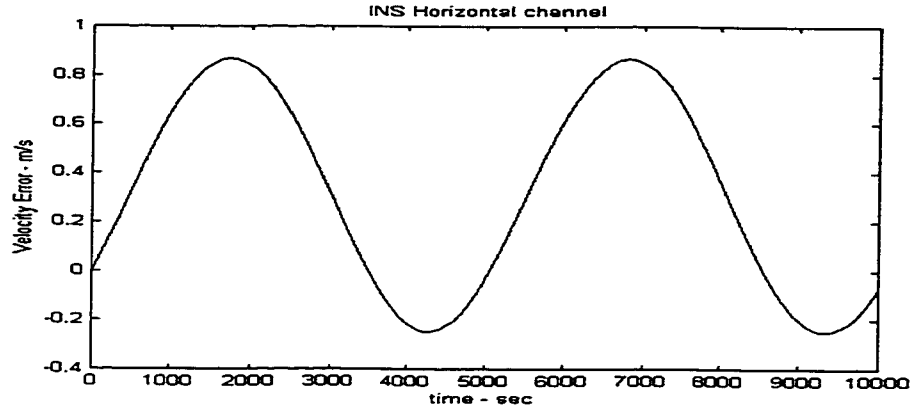

Fig. (A.3) : INS Velocity Error (Horizontal Channel)

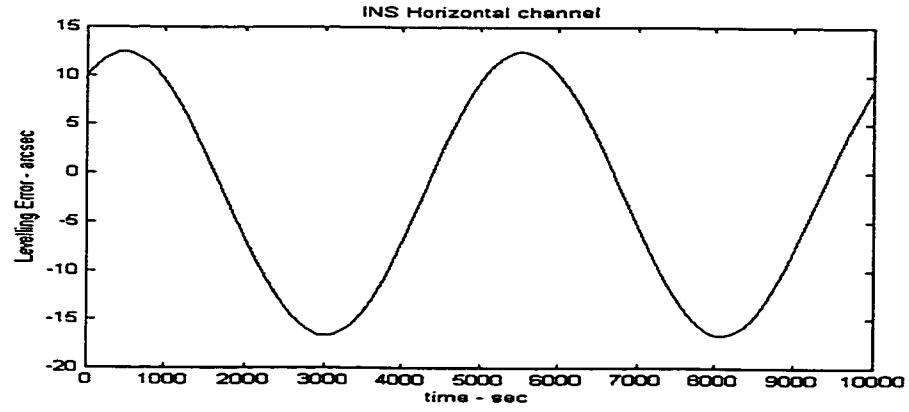

Fig. (A.4) : INS Leveling Error (Horizontal Channel)

A.2 Error Model of the Vertical Channel

Linearizing Eqs. (A.2) and (A.3) for the vertical (up) channel, the *error model* is

$$\begin{aligned}\delta\dot{p}_u &= \delta v_u \\ \delta\dot{v}_u &= b_{Au} \\ \dot{\varepsilon}_u &= -\frac{\delta v_E}{r} + b_{Gu}\end{aligned} \tag{A.14}$$

where, u denotes the vertical (up) channel.

It is clear from Eq. (A.14) that the attitude error of the vertical channel does not affect the velocity and position errors of the same channel. It is also not affected by the errors in the same channels. Consequently, the velocity error can be determined directly by integrating the second equation. In this case, the *up velocity error* takes the form of a freely navigating object in 3D, i.e.

$$\boxed{\delta v_u = \delta v_{u0} + b_A t}, \tag{A.15}$$

where, δv_{u0} is the initial velocity error at time t = 0. Substituting Eq. (A.15) into the position error in Eq. (A.14) and integrating, the *up position error* equation is

$$\boxed{\delta p_u = \delta p_{u0} + \delta v_{u0} t + \frac{1}{2} b_A t^2}. \tag{A.16}$$

The vertical attitude error is, however, a function of the horizontal velocity error. Substitute Eq. (A.10) into the attitude error (azimuth error in this case) of Eq. (A.14), the state-space representation of the azimuth error becomes

$$\dot{\varepsilon}_u = -\delta v_0 \frac{\cos(vt)}{r} - b_A \frac{\sin(vt)}{rv} - \varepsilon_0 \frac{Rv\sin(vt)}{r} - b_G \frac{R(1-\cos(vt))}{r} + b_{Gu}. \tag{A.17}$$

Integrating the above equation from t = 0, where $\varepsilon_u = \varepsilon_{u0}$ is the initial azimuth error (misalignment), to the current time t, the *azimuth error* is

$$\boxed{\begin{aligned}\varepsilon_u = \varepsilon_{u0} - \delta v_0 \frac{1}{rv}\sin(vt) - b_A \frac{1}{rv^2} + b_A \frac{1}{rv^2}\cos(vt) \\ -\varepsilon_0 \frac{R}{r} + \varepsilon_0 \frac{R}{r}\cos(vt) + b_G \frac{R}{rv}\sin(vt) - b_G \frac{R}{r}t + b_{Gu}t\end{aligned}} \qquad (A.18)$$

Using these equations, typical plots of the position, velocity and azimuth errors in the vertical channel can be obtained, see Figs. (A.5) to (A.7), below.

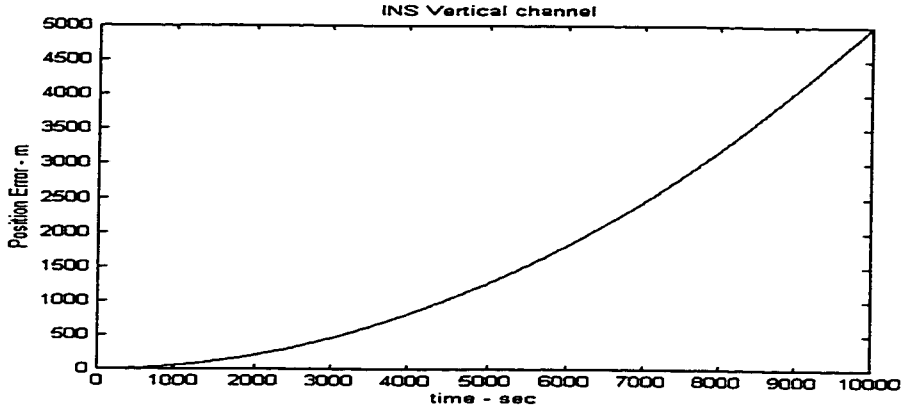

Fig. (A.5) : INS Position Error (Vertical Channel)

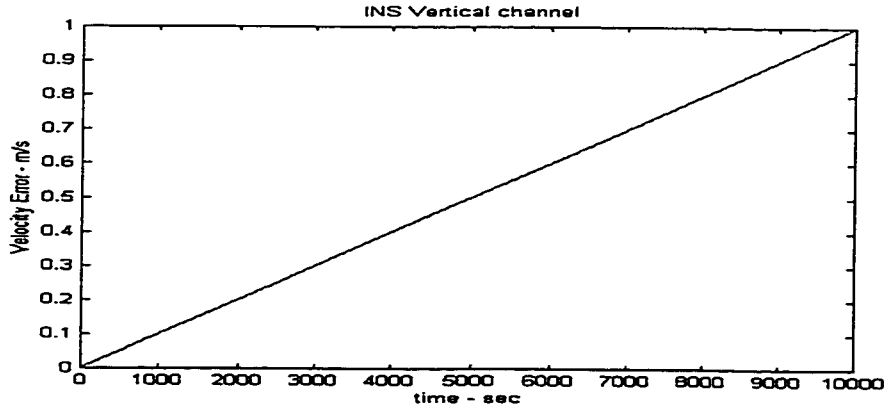

Fig. (A.6) : INS Velocity Error (Vertical Channel)

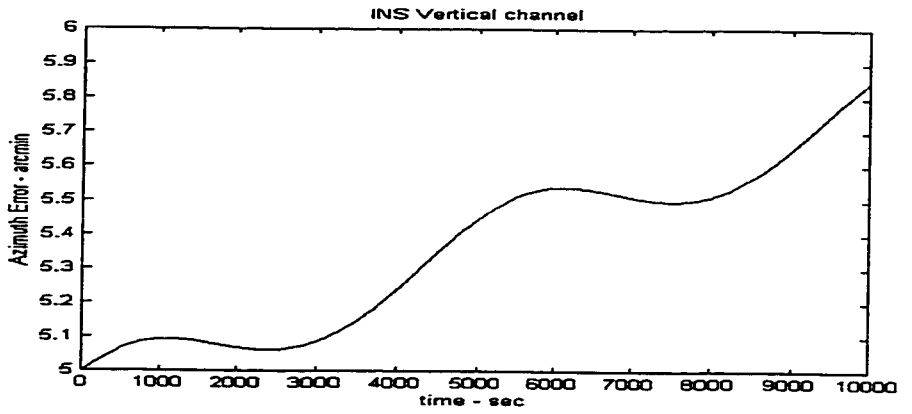

Fig. (A.7) : INS Azimuth Error (Vertical Channel)

For the previous plots, the following specifications have been used to simulate a medium class navigation-grade INS performance [Savage 1978, Schwarz and Wei, 1994, Greenspan 1995, Merhav 1996]:

- constant gyro drift of 0.01°/h; based on $\varepsilon_u = b_G/\omega_e \cos(\phi)$, this bias introduces a 1.06 mrad (~3.6 arcmin) of initial azimuth misalignment
- constant accelerometer bias of 10 mGal; based on $\varepsilon_E = b_A/g$, this bias introduces a 10 μrad (~2") of initial leveling error
- initial leveling error of 10"
- initial azimuth error of 5'
- constant stationary vehicle latitude of 51°
- zero initial position and velocity errors
- R = 6371 km
- ν = 1/806 rad/sec (~ 1/5000 Hz).

The simplified error model discussed above, though provides an insight of the INS long-term error behavior, has limitations. The following are situations where the simplified inertial navigation error model is not recommended and one has to opt for a more complete model:

- high dynamics where the Coriolis has a pronounced effect

- fast trajectory changes, e.g. sharp turns; it invalidates the assumption of small rotations of the R^I_b matrix
- rough topography, e.g. mountainous areas; the assumption of constant vertical acceleration that is equal to the Earth's mean gravity will be violated
- tactical-grade inertial navigation systems where the sensor error characteristics are not as defined as in the case of the navigation-grade systems.

APPENDIX B.
DISCRETE KALMAN FILTER ALGORITHM

The purpose of this Appendix is to provide a hands-on reference to the formulae in the discrete Kalman filtering algorithm. The details of the derivation can be found in [Gelb 1974, Bierman 1977, Maybeck 1982, Brown and Hwang, 1992].

B.1 Measurement and Process Models

The *Measurement Model* is the connection between the measurements, z, and the filter states, x. It describes the geometric or physical relationship between the two through a design (geometric) matrix, H, as follows

$$z_k = H\, x_k + e_{zk}, \tag{B.1}$$

where $e_{zk} = v_k$ is the measurement white noise and its covariance matrix takes the form

$$R_k = C_{ek} = E[v_k v_k^T]. \tag{B.2}$$

The *Dynamics Model*, on the other hand, describes the evolution of the process with time. It relates the filter states to their predecessors through the dynamics matrix, in continuous time, as follows

$$\dot{x} = Fx + w \tag{B.3a}$$

and in discrete time through the process transition matrix Φ as follows

$$x_{k+1} = \Phi\, x_k + e_{xk}, \tag{B.3b}$$

where $e_{xk} = w_k$ is the (system) process white noise with spectral density P, and its covariance matrix is

$$Q_k = C_{wk} = E[w_k w_k^T] = \int_0^T \Phi(T,\tau) P \Phi(T,\tau)^T d\tau . \qquad (B.4)$$

where T is the sampling period. The transition matrix is computed from the process dynamics matrix 'F' as follows

$$\Phi = e^{FT} = I + F\,T, \qquad (B.5)$$

where I is the identity matrix.

Eq. (B.5) is an approximation which is acceptable as long as the sampling interval is chosen small enough so that the higher-order terms can be ignored; for other methods of determining Φ from F, see e.g. [Gelb 1974, Maybeck 1982, 1997, Schwarz 1987, Brown and Hwang, 1992]. Fig. (B.1) below illustrates the Kalman filter process and measurement models.

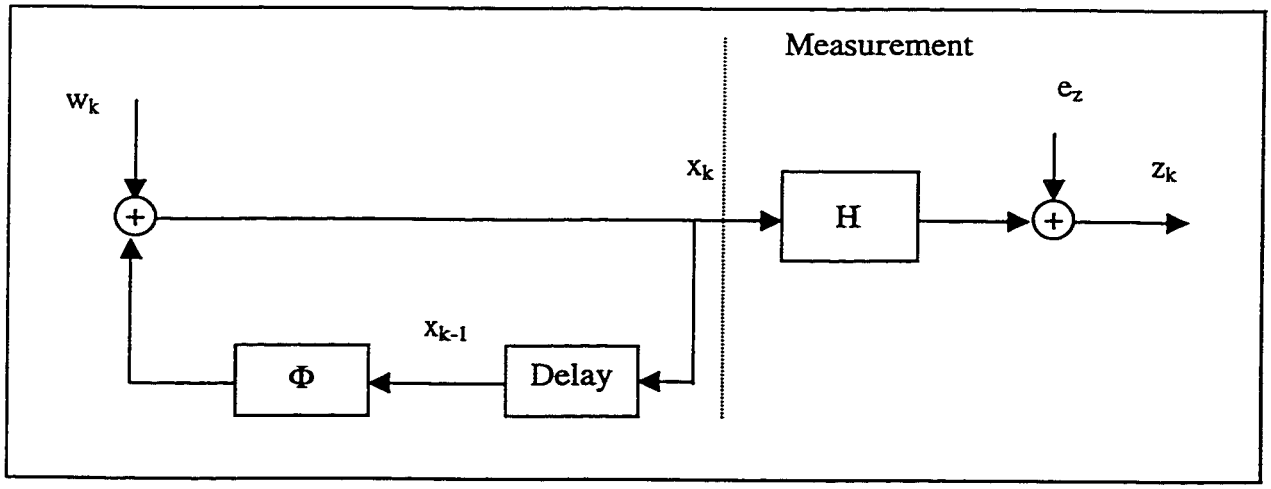

Fig. (B.1) : Kalman Filter Models

B.2 Kalman Filtering Algorithm

For the filter to start off, there must be known a *priori information* or *initial conditions*, x_o, with error covariance matrix

$$P_o = C_{xo} = E[e_{xo}e_{xo}^T]. \tag{B.6}$$

The role of the Kalman filter is, then, to make use of two streams of information, namely, the measurements and the process propagated state information through the process model and come up with the *best* estimate of the state at the current time, i.e.

$$\hat{x}_k(+) = K_1\hat{x}_k(-) + K_2 z_k \ , \tag{B.7}$$

where (+) and (-) represent the state before and after applying the measurement update, and K_1 and K_2 are weighting (or gain) factors. Now, substitute the expressions for the state and measurement to get,

$$x + e_{xk}(+) = K_1(x + e_{xk}(-)) + K_2(Hx + e_{z_k}), \tag{B.8a}$$

which after rearranging becomes,

$$e_{xk}(+) = [K_1 + K_2H - I]x + K_1e_{xk}(-) + K_2e_{zk} \tag{B.8b}$$

where $e_{xk}(+)$ and $e_{xk}(-)$ are the state errors after and before update, assumed white.

For the above estimator to yield an *unbiased estimate*, i.e.

$$E[e_{xk}(+)] = 0, \tag{B.9}$$

the following condition must hold,

$$K_1 = I - K_2H$$

since both the measurement noise and the process noise are assumed zero mean. Denoting K_2 by K_k, the filter estimate is

$$\hat{x}_k(+) = (I - K_k H)\hat{x}_k(-) + K_k z_k \tag{B.10}$$

and its error is

$$e_{xk}(+) = (I - K_k H)e_{xk}(-) + K_k e_{zk} \tag{B.11}$$

and the state error covariance is

$$P_k(+) = E[e_{xk}(+)e_{xk}^T(+)] \tag{B.12}$$

Under the condition that the measurement and process errors are independent, i.e. $E[e_{xk}(-)e_{zk}^T] = E[e_{zk}e_{xk}^T(-)] = 0$, the general form of the state error covariance matrix is

$$P_k(+) = (I - K_k H)P_k(-)(I - K_k H)^T + K_k R_k K_k^T, \tag{B.13}$$

where $P_k(-)$ is the state error covariance matrix before update and K_k is an *arbitrary filter gain.*

Within the class of linear unbiased estimators, the best sought estimate is the one that minimizes the length of the estimation error vector in the L2-norm space. In other words, the best estimate, in this context, is the estimate with the minimum variance or mean-square estimation error, i.e.

$$\frac{\partial tr[P_k(+)]}{\partial K_k} = 0, \tag{B.14}$$

where tr is the matrix trace operator. Using from differential calculus

$$\frac{\partial \mathrm{tr}[\mathrm{ABA}^{\mathrm{T}}]}{\partial \mathrm{A}} = 2\mathrm{AB},$$

and carrying out the differentiation of Eq. (B.14), the *filter optimal gain* is

$$\mathrm{K}_k = \mathrm{P}_k(-)\mathrm{H}_k^{\mathrm{T}}[\mathrm{H}_k\mathrm{P}_k(-)\mathrm{H}_k^{\mathrm{T}} + \mathrm{R}_k]^{-1} \tag{B.15}$$

and the corresponding filter *state error covariance* matrix is

$$\mathrm{P}_k(+) = (\mathrm{I} - \mathrm{K}_k\mathrm{H}_k)\mathrm{P}_k(-). \tag{B.16}$$

The Kalman filter algorithm can then be thought of as consisting of two main steps, namely, time update or prediction and measurement update or filtering. In the time update step, the filter state vector along with its error covariance matrix are projected one epoch in the future as follows

$$\hat{\mathrm{x}}_k(-) = \Phi\hat{\mathrm{x}}_{k-1}(+) \tag{B.17}$$

$$\mathrm{P}_k(-) = \Phi\mathrm{P}_{k-1}\Phi^{\mathrm{T}} + \mathrm{Q}_{k-1}. \tag{B.18}$$

In the update step, however, the measurement information is blended with the prediction information to get an updated estimate of the state. The innovation vector and its covariance matrix are computed first as follows

$$\mathrm{v}_k = \mathrm{e}_{zk}(-) = \mathrm{z}_k - \mathrm{z}_k(-) = \mathrm{z}_k - \mathrm{H}_k\hat{\mathrm{x}}_k(-) \tag{B.19}$$

$$\mathrm{R}_k(-) = \mathrm{C}_{vk} = \mathrm{R}_k + \mathrm{H}_k\mathrm{P}_k(-)\mathrm{H}_k^{\mathrm{T}} \tag{B.20}$$

and their counterparts after the measurement update are called the residual sequence and its respective covariance matrix which are computed as follows:

$$r_k = e_{zk}(+) = z_k - z_k(+) = z_k - H_k\hat{x}_k(+) \tag{B.19a}$$

$$R_k(+) = C_{rk} = R_k - H_k P_k(+) H_k^T. \tag{B.20a}$$

The gain matrix

$$K_k = P_k(-) H_k^T C_{v_k}^{-1} \tag{B.21}$$

and the state error and its covariance matrix

$$\hat{x}_k(+) = \hat{x}_k(-) + K_k v_k \tag{B.22}$$

$$P_k(+) = (I - K_k H_k) P_k(-) \tag{B.23}$$

are then computed; this is known as the covariance Kalman filter formulation. Alternatively, the computation of the gain and the state error covariance matrix can be performed according to the information filter formulation as follows [Gelb 1974, Maybeck 1982]:

$$P_k^{-1}(+) = P_k^{-1}(-) + H_k^T R_k^{-1} H_k \tag{B.24}$$

and

$$K_k = P_k(+) H_k^T R_k^{-1}. \tag{B.25}$$

It is useful to observe that the gain matrix K_k is the ratio between the covariance matrices of the state and the measurements projected onto the state space via the geometry matrix H. The gain can also be interpreted in another way. To see that, expand Eq. (B.19) and substitute z from Eq. (B.1) and $x(-) = x + e_x(-)$, to get

$$v_k = e_{z_k} - H_k e_{x_k}(-). \tag{B.26}$$

Now, substitute this expression into the expression for computing the cross-covariance between the innovation and the states, to get

$$\begin{aligned} R_{xv_k} &= E[e_{x_k}(-)v_k^T] \\ &= E[e_{x_k}(-)e_{z_k}^T] - E[e_{x_k}(-)e_{x_k}^T(-)]H_k^T, \\ &= -P_k(-)H_k^T \end{aligned} \tag{B.27}$$

note that the measurement error and the state errors are assumed uncorrelated. Now substitute Eq. (B.27) into Eq. (B.21), the gain is

$$K_k = -R_{xv_k} R_k^{-1}(-). \tag{B.28}$$

K_k can be seen as a factor that cross-correlates the innovations to the states after weighting them with the inverse of their covariance. This last expression is useful in comparing the Kalman filter algorithm to algorithms like least-squares collocation and stochastic least-squares Wiener filtering. Fig. (B.2) below illustrates the conventional Kalman filter algorithm with its two main steps, namely, prediction and update, in a block diagram and algorithmic fashion. There also exists square-root formulations of the covariance and information Kalman filters, see e.g. [Bierman 1977, Maybeck 1982] for details.

It is worth noting that in the Kalman filter algorithm, there are two models and three different error sources. The two models are the measurement model represented by Eq. (B.1) and the dynamics model represented by Eq. (B.3). The error sources are those associated with the model, the measurement and system parameters before update and the measurement and system parameters after update, respectively. This results in a total of six different error variables. The relations between these error variables play an important role in our development and are therefore given here:

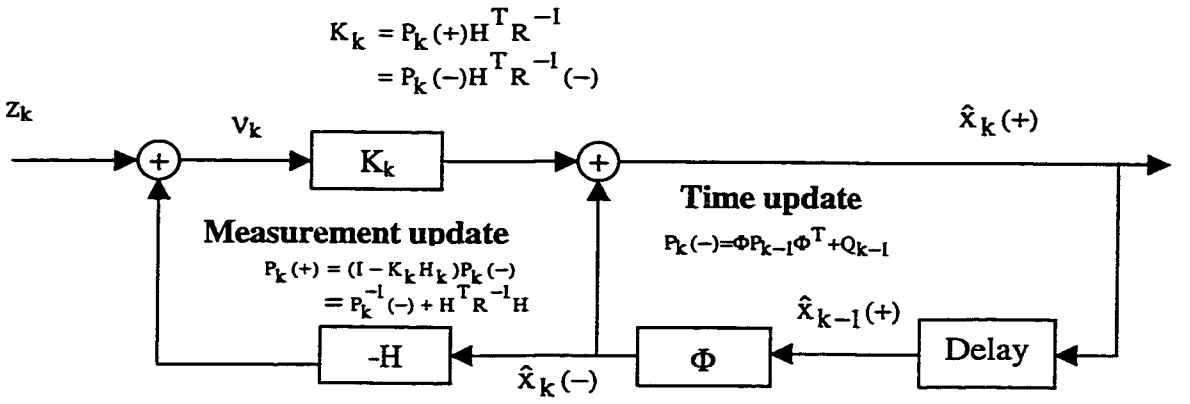

Observation Model

$$z = H x + v; \qquad H, \qquad R = C_v = E[vv^T]$$

Dynamics Model

$$\dot{x} = Fx + w; \qquad \Phi = I + F\,\Delta t, \qquad Q = C_w = E[ww^T],$$

A priori information (*initial conditions*)

$$x_o,\ P_{xo} = E[e_{xo}e_{xo}^T]$$

Time Update (*prediction*)

$$\hat{x}_k(-) = \Phi_{k,k-1}\hat{x}_{k-1}(+) \qquad P_{k(-)} = \Phi_{k,k-1}\,P_{k-1(+)}\Phi^T_{k,k-1} + Q_{k-1}$$

Measurement update (*information filter*)

$$\hat{x}_k(+) = \hat{x}_k(-) + K_k v_k \qquad v_k = z_k - H_k\hat{x}_k(-)$$

$$P_k^{-1}{}_{(+)} = P_k^{-1}{}_{(-)} + H_k^T R^{-1} H_k \qquad K_k = P_{k(+)}H_k^T R^{-1}$$

Fig. (B.2): Kalman Filter Algorithm

$$\left.\begin{aligned} v_k &= e_{zk} - H_k e_{xk}(-) \\ r_k &= e_{zk} - H_k e_{xk}(+) \\ \Delta x &= e_{xk}(+) - e_{xk}(-) = K_k v_k \\ r_k - v_k &= -H_k \Delta x = -H_k K_k v_k \end{aligned}\right\} \qquad (B.29)$$

where e_{zk} and e_{xk} are the measurement noise and the process noise (in models), $v_k = e_{zk(-)}$ and $r_k = e_{zk(+)}$ are the measurement errors before and after update (estimated innovation and residual), and $e_{xk(-)}$ and $e_{xk(+)}$ are the process state errors before and after update.

In an INS/GPS closed-loop error state Kalman filter formulation, the INS is corrected after each measurement update, and thus the predicted error states and measurement differences at the next update time vanish. In other words, $\hat{x}_k(-)$ will always be zero, and thus the above formulation simplifies to the one in Fig. (B.3),

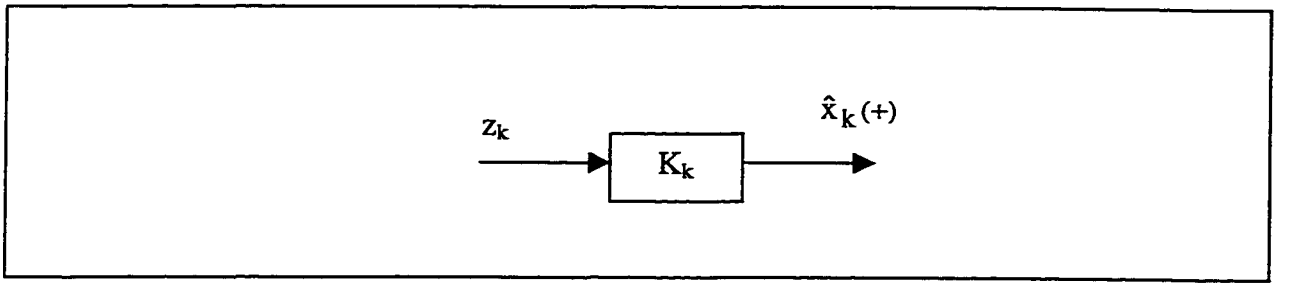

Fig. (B.3) : Closed-loop Error Kalman Filter Algorithm

where,

$$\hat{x}_k(+) = K_k z_k , \tag{B.30}$$

and the update measurements, z_k, are provided by GPS. Therefore, there is no need to propagate the error state vector to the next update time after the INS states have been corrected. In effect, the time update block has disappeared and the measurement update block has reduced to weighting the new measurement with the gain K_k. This clearly shows that Kalman filter does not reset the filter states to the new measurement, instead the filter weighs the measurement according to what it knows about the process and what it knows about the new update information. In other words, although the prediction step has disappeared from the formulation, its effect still exists in the second moment information. It should be noted, however, that the covariance propagation is still needed for both the time and measurement updates as in the original filter. It is interesting to

notice that according to this formulation of the INS/GPS integration, the transition matrix, Φ, is not required for the propagation of the system states (first moment information), but rather needed for the propagation of the system covariance (second moment information). In other words, the deterministic model used to describe the INS error propagation is not used in this formulation to predict the error states deterministically but rather used to get an estimate of their values through the update step based on the covariance stochastic information through the filter gain.

APPENDIX C.
MATLAB® IMPLEMENTATION OF THE INTEGER WHITENING FILTER

This Appendix contains a step-by-step Matlab script of the whitening filter as well as the udu and ldl factorization routines required to resolve the GPS phase ambiguity as implemented in the KINWHITE software.

C.1 Integer Whitening Function

```
function [T,Q] = white(A)

n = size(A,1);
Tp  = eye(n);
Q = A;

do
U  = udu(Q);
U1 = inv(round(U));
Qu = U1*Q*U1';
L  = ldl(Qu);
L1 = inv(round(L));

% Whitened Matrix - Q
Q = L1*Qu*L1';

% Whitening (Transformation) Matrix - T
T= L1*U1*Tp;
Tp = T;

while (L1 ~= eye(n))

return;
```

C.2 Lower-Diagonal-Lower (LDL) Factorization Function

```
function [L,D] = ldl(A)

n = size(A,1);
L = eye(n);
```

```
for j = 1:n-1
d(j) = A(j,j);
L(j+1:n,j) = A(j+1:n,j)/d(j);
for k = j+1:n
A(k:n,k) = A(k:n,k) - A(k,j)*L(k:n,j);
end
end

d(n) = A(n,n);
D = diag(d);

return;
```

C.3 Upper-Diagonal-Upper (UDU) Factorization Function

```
function [U,D] = udu(A)

n = size(A,1);
U = eye(n);

for j = n:-1:2
d(j) = A(j,j);
U(1:j-1,j)  = A(1:j-1,j) / d(j);
for k = 1:j-1
A(1:k,k) = A(1:k,k) - A(k,j) * U(1:k,j);
end
end

d(1) = A(1,1);
D = diag(d);

return;
```

APPENDIX D.
TEST EQUIPMENT TECHNICAL SPECIFICATIONS

This Appendix contains technical specifications for some of the equipment used in the field tests. The purpose of this Appendix is to provide hands-on reference for these specifications.

D.1 Ashtech-Z12 GPS Receiver

Receiver
geodetic-grade GPS receiver with 1 Hz output rate
Channels
12
C/A code and P code signals
full length carrier on L1 and L2 using Z-tracking
Measurement Precision (> 25°) in cm

	10 sec	*5 min*
C/A-code		
carrier phase	0.015 (25 Hz)	0.02 (1 Hz)
pseudo-range	20.00	3.60
P-code A/S off		
L1 carrier phase	0.10	0.02
L2 carrier phase	0.10	0.02
L1 pseudo-range	5.00	0.90
L2 pseudo-range	7.00	1.30
P-code A/S on (z-tracking)		
L1 carrier phase	0.10	0.02
L2 carrier phase	0.10	0.02
L1 pseudo-range	20.00	5.00
L2 pseudo-range	20.00	5.00

D.2 Trimble-4000SSE GPS Receiver

Receiver
geodetic-grade GPS receiver with 1 Hz output rate
Channels
9
C/A code and P code signals
full length carrier on L1 and L2 using cross correlation
Accuracy
Horizontal : 5 mm + 1 ppm

Vertical : 10 mm + 1 ppm
Azimuth: 1 arcsec + 5/b; b: baseline length in km

D.3 LTN90-100 Inertial Navigation System

System
navigation-grade INS with 64 Hz output rate
1 nm/h position error in free inertial mode
Gyro
drift : 0.01 deg/h
scale factor: 5 ppm
misalignment : 2 arcsec
random walk : 0.002 deg/$\sqrt{h}$ (1σ)
Accelerometer
bias : 50 mGal
scale factor : 50 ppm
misalignment : 5 arcsec
random walk : 5 mGal (1σ)

D.4 LRF-III Inertial Navigation System

System
navigation-grade INS with 50 Hz output rate
1 nm/h position error in free inertial mode
Gyro
drift : 0.003 deg/h
scale factor : 1 ppm
misalignment : 2 arcsec
random walk : 0.001 deg/$\sqrt{h}$ (1σ)
Accelerometer
bias : 25 mGal
scale factor : 50 ppm
misalignment : 5 arcsec
random walk : 5 mGal (1σ)

D.5 Anorad AG12-84 Platform

Controller Length : 2 meters
Position resolution : 1 count (16000000 counts/m)
Position Range : ± 999999999 counts
Position accuracy : Within 1 count
Velocity Range : ± 16000000 counts/sec
Acceleration Range : 1000 to 127000000 counts/sec2